Forschungsberichte

aus dem

Institut für Werkstofftechnik
Metallische Werkstoffe

der

UNIKASSEL
VERSITÄT

Herausgeber: Prof. Dr.-Ing. B. Scholtes

Band 7

Patiphan Juijerm

Fatigue behavior and residual stress stability of deep-rolled aluminium alloys AA5083 and AA6110 at elevated temperature

Forschungsberichte aus dem Institut für Werkstofftechnik - Metallische Werkstoffe der Universität Kassel
Band 7

Herausgeber:

Prof. Dr.-Ing. B. Scholtes
Institut für Werkstofftechnik
Metallische Werkstoffe
Universität Kassel
Mönchebergstr. 3
34109 Kassel

Die vorliegende Arbeit wurde vom Fachbereich Maschinenbau der Universität Kassel als Dissertation zur Erlangung des akademischen Grades eines Doktors der Ingenieurwissenschaften (Dr.-Ing.) angenommen.

Erster Gutachter:	Prof. Dr.-Ing. habil. B. Scholtes
Zweiter Gutachter:	Dr.-Ing. Igor Altenberger
Tag der mündlichen Prüfung	19. Juli 2006

Bibliografische Information der Deutschen Nationalbibliothek
Die Deutsche Nationalbibliothek verzeichnet diese Publikation in der Deutschen Nationalbibliografie; detaillierte bibliografische Daten sind im Internet über http://dnb.ddb.de abrufbar

Zugl.: Kassel, Univ., Diss. 2006
ISBN 978-3-89958-260-4
URN urn:nbn:de:0002-2602

Umschlaggestaltung: Melchior von Wallenberg, Nürnberg
Druck und Verarbeitung: Unidruckerei der Universität Kassel
Printed in Germany

Vorwort des Herausgebers

Bei einer zunehmenden Verbreitung elektronischer Medien kommt dem gedruckten Fachbericht auch weiterhin eine große Bedeutung zu. In der vorliegenden Reihe werden deshalb Ergebnisse wichtiger Forchungsarbeiten präsentiert, die am Institut für Werkstofftechnik – Metallische Werkstoffe der Universität Kassel gewonnen wurden. Das Institut kommt damit auch – neben der Publikationstätigkeit in Fachzeitschriften – seiner Verpflichtung nach, über seine Forschungsaktivitäten Rechenschaft abzulegen und die Resultate der interessierten Öffentlichkeit kenntlich und untzbar zu machen.

Allen Institutionen, die duch Sach- und Personalmittel die durchgeführten Forschungsarbeiten unterstützen, sei an dieser Stelle verbindlich gedankt.

Kassel, im November 2003

Prof. Dr.-Ing. habil. B. Scholtes

So far …….. So good

. . . Love, Belief and Effort . . .

Content

Chapter 1

Introduction

Nowadays, automotive as well as aerospace industries have more and more advanced applications involved in high-loading and/or elevated-temperature conditions. In addition, low-weight components are particularly required for environmental, ecological and economical aspects. Therefore, light-weight metals/alloys are frequently mentioned and selected for many applications where low density and high strength to weight ratios are an important consideration. Consequently, improvement and development in the field of light-weight alloys can be seen continuously in automotive as well as aerospace industries. One of the most important light-weight metals is aluminium and its alloys which possess many attractive characteristics including excellent corrosion resistance, reflectivity, high strength and stiffness to weight ratio, good formability, weldability and recycling potential. Certainly, these advantageous properties make them ideal candidates to replace heavier materials (steel or copper) for several industries [1-6].

Therefore, mechanical properties of aluminium alloys become important and investigations about the efficient performance under static and cyclic loading at room and elevated temperature are crucial. Failures occurring in machinery components are almost entirely fatigue failures and thus fatigue properties of structural aluminium alloys are regularly investigated and improved. It is well established that mechanical surface treatments, e.g. shot peening, deep rolling or laser shock peening are effective methods not only to enhance the fatigue behavior but also the wear and corrosion resistance of metallic materials [7-10] due to induced near-surface macroscopic compressive residual stresses and work hardening serve to inhibit or retard fatigue crack initiation as well as crack growth [11-13]. Deep rolling is one of the most well-known mechanical surface treatment methods and exhibits a great depth of work hardening and macroscopic compressive residual stresses in addition to surface smoothening as compared to other mechanical surface treatments. Therefore, recently, deep rolling treatments

are intensively investigated and developed, e.g. deep rolling followed by annealing or ageing [14-19] or high-temperature deep rolling [20-24]. Stability of macroscopic compressive residual stresses, work hardening states and microstructures using the static/dynamic strain ageing as well as precipitation concept are the main objective of these methods. However, the outstanding benefits of the deep rolling treatment are uncertain under high-loading and/or elevated-temperature conditions due to occurring relaxation of near-surface macroscopic compressive residual stresses as well as work hardening states. In this case, a detrimental effect on the fatigue lifetime can be expected, particularly in smooth, soft and mechanically surface treated materials, such as deep-rolled aluminium alloys because their fatigue lifetime depends significantly on the stability of near-surface macroscopic compressive residual stresses as well as work hardening states [24-29]. The stability of macroscopic compressive residual stresses and work hardening states during cyclic loading at room as well as elevated temperature is a very important factor influencing the fatigue lifetime of mechanically surface treated aluminium alloys. However, only rare information systematically cover thermal, mechanical and thermomechanical residual stress relaxation and their effects on the cyclic deformation behavior of mechanically surface treated aluminium alloys. Hence, the stability of near-surface macroscopic compressive residual stresses as well as work hardening states of deep-rolled aluminium alloys under high-loading and/or elevated-temperature conditions and its effects on the cyclic deformation behavior should be systematically investigated and clarified.

For these reasons, the main purpose of this research is to investigate systematically the fatigue behavior and the stability of near-surface residual stresses as well as work hardening of the deep-rolled aluminium alloys at room and elevated temperature. Aluminium alloys AA5083 and AA6110 were investigated in this research representing typical non-precipitation-hardenable and precipitation-hardenable aluminium alloys, respectively. The aluminium alloy AA6110 was investigated entirely for differently aged conditions, namely as-quenched, under-, peak- and over-aged. In addition, to investigate the newly developed and modified deep rolling, high-temperature deep rolling and deep rolling followed by ageing treatments of the as-quenched AA6110 are also systematically investigated and discussed.

Chapter 2

Fatigue of metallic materials

2.1 Introduction and overview

It has been recognized since 1830 that a metallic material subjected to a fluctuating stress can fail at a stress much lower than that required to fracture by a single applied load. Failures occurring under condition of dynamic loading are usually called “fatigue failures” [30]. Fatigue damage in engineering structure or component can be classified into the following different states [31-35].

1) Substructural and microstructural changes within the whole volume of the loaded material leading to cyclic hardening and/or softening.
2) Initiation of microscopic cracks particularly in the surface layer.
3) Growth and coalescence of microscopic flaws to form dominant cracks.
4) Stable propagation of the dominant macroscopic crack.
5) Structural instability or complete failure.

Considerations for microscopic crack initiation and the rate of crack propagation depend strongly on mechanical, microstructural and environmental factors. Under high-loading condition, since the crack initiation life constitutes a major component of the total fatigue lifetime in smooth specimens, the classical stress-based and strain-based methods represent design concepts to calculate fatigue crack initiation. The stresses associated with low cycle fatigue (LCF) are generally high enough to cause significant plastic deformation prior to failure. On the other hand, in the high cycle fatigue (HCF) regime ($N > 10^4$), the material is elastically deformed primarily under low-stress situations. Fig. 2.1 shows an example of a situation, where the short-life approach (as referred to the low cycle fatigue approach) involves the fatigue life for the crack initiation and the subsequent crack growth mechanisms outside the plastic zone. Low cycle fatigue

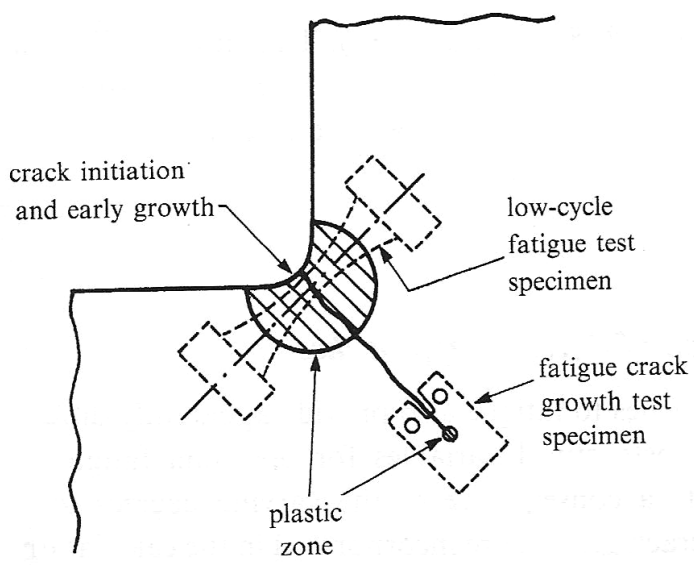

Figure 2.1: A schematic diagram of the various states of fatigue in an engineering component and the approaches used to estimate the fatigue lifetime [32].

and elasto-plastic cyclic behavior of materials represent a considerable interest, since repeated cyclic loading with high stress and strain amplitude can severely limit the useful life of components [36]. At present, the low cycle approach to fatigue design has found particularly widespread use, e.g. in ground-vehicle industries [32].

2.2 Cyclic deformation behavior of metallic materials

It is irrefutable that mechanical properties of metallic materials under cyclic loading relate closely to the microstructures, e.g. crystal structure, dislocations, and precipitates. During cyclic loading, dislocation generation, movement, rearrangement, annihilation and interaction with obstacles, such as other dislocations as well as precipitates are the important keys of the cyclic deformation behavior for almost all metallic materials. These altered microstructures during cyclic loading can be principally interpreted using some important values which can be obtained directly from the hysteresis loop of fatigue tests (see Fig. 2.2), such as plastic strain amplitudes as well as mean strains. Cyclic hardening as well as cyclic softening can be characterized using a plot of plastic strain amplitudes as a function of number of cycles under stress control (see Fig. 2.3). Whereas, a

diagram of mean strains as a function of number cycles under stress control is also helpfully used to analyze cyclic creep especially during cyclic loading at elevated temperature (see Fig. 2.4 as an example).

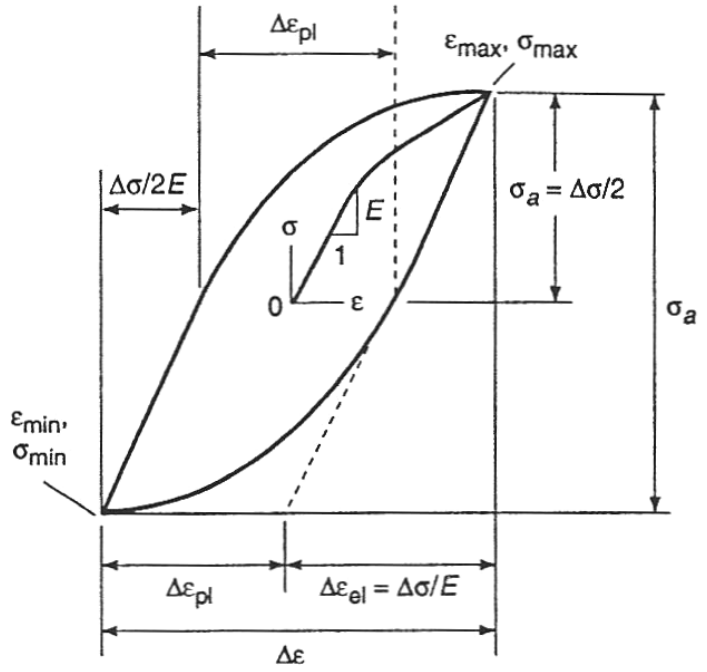

Figure 2.2: A schematic stress-strain hysteresis loop [34].

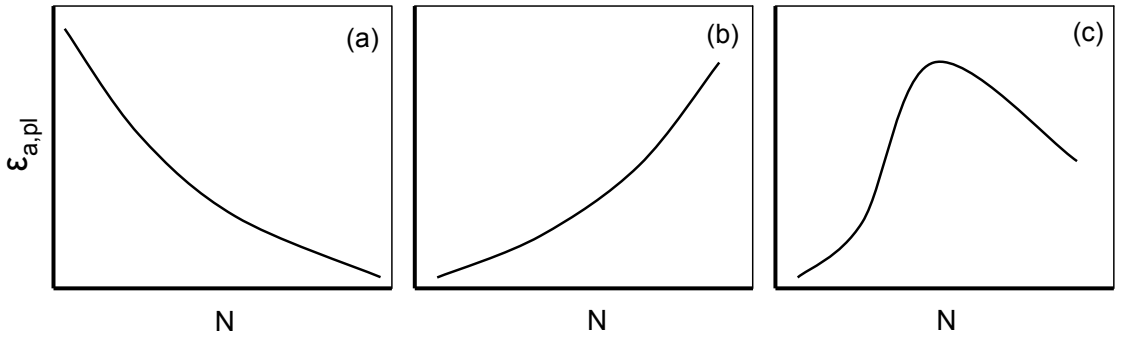

Figure 2.3: Schematic diagrams of characteristic cyclic deformation behavior under stress-controlled fatigue loading, (a) cyclic hardening, (b) cyclic softening and (c) cyclic softening and hardening [37].

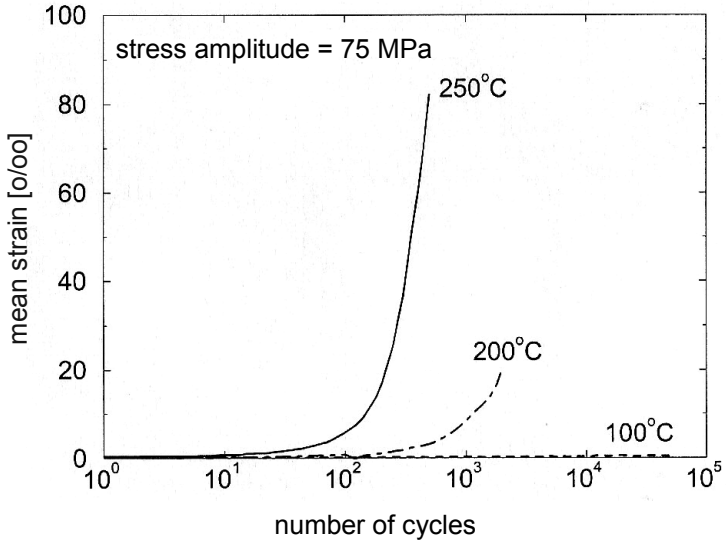

Figure 2.4: An exemplary plot showing positive mean strains due to cyclic creep during cyclic loading of Magnesium AZ31 at elevated temperatures [38,39].

It is well established that fatigue lifetime depends not only on initial microstructure and its alteration during fatigue loading but also strongly on the surface finish and surface treatment, because usually fatigue failures start practically at the surface. For these reasons, if the surface of a material can be modified against crack initiation as well as propagation, fatigue lifetime improvement can be also expected. Therefore, surface treatments for fatigue lifetime improvements are an advanced topic and technologically important. Mechanical surface treatment is one of the most well-known surface treatment methods and serves principally to improve the fatigue lifetime of metallic materials due to induced macroscopic compressive residual stresses as well as work hardening states at the surface and in near-surface regions. Currently, various mechanical surface treatments, e.g. shot peening, deep rolling, ultrasonic shot peening and laser shock peening are provided and intensively investigated with great focus on optimized surface conditions. Thus, details of mechanical surface treatments and their effects on fatigue behavior as well as up-to-date techniques are necessary prerequisites for fatigue design and will be explained in the next section.

2.3 Mechanical surface treatments

2.3.1 Concept and methods

The basic concept of all mechanical surface treatments is a localized (inhomogeneous) near-surface plastic deformation. Several properties as well as microstructures at the surface and in near-surface regions of metallic materials are altered by mechanical surface treatment, e.g. surface topography, plasticity induced phase transformations, increased dislocation densities, induced near-surface macroscopic compressive residual stresses as well as work hardening states [40]. The amount and distribution of these altered near-surface properties depend strongly on the type of mechanical surface treatment as well as the process parameters. An overview of altered near-surface properties, i.e. the induced macroscopic compressive residual stresses as well as work hardening states, microhardness increase, dislocation densities and surface roughness by different selected mechanical surface treatments is given in table 2.1 [24].

Table 2.1: Consequences of selected mechanical surface treatments on near-surface properties of metallic materials [24].

	Amount of residual stress	**Dislocation density**	**Surface microhardness increase**	**Maximum "case" depth**	**Surface roughness**	**Work hardening**
Shot peening	$\cong \sigma_{Yield}$	very high 5-8 x 10^{11} cm^{-2}	150% AISI 304 60% SAE1045	0.3 mm	4-8 µm	5-50%
Laser shock peening	$\cong \sigma_{Yield}$	Medium	40% AA2024 30% AA7075	2 mm	1-5 µm	1-2%
Deep rolling	$\cong \sigma_{Yield}$	10^{11} cm^{-2} or lower	60%	1-3 mm	≤ 1 µm	> 20%

At this time, for several industries, the most well-known method of mechanical surface treatments is shot peening. Due to its flexibility, shot peening can be performed on components of almost any shape, particularly on those possessing a complex geometry [40]. The locally plastically deformed surface layers of the workpiece created by shot peening are a result of the impact of the individual shot particles on the workpiece (see Fig. 2.5 (a)). Fatigue lifetime enhancement of the shot peened workpiece can be expected due to induced macroscopic compressive residual stresses as well as work hardening states at the surface and in near-surface regions. However, it is irrefutable that shot peening usually increases the surface roughness of the workpiece (see table 2.1) [24,41], especially for lower-hardness workpieces [40,42]. The increase of the surface roughness can cause a deterioration of the fatigue lifetime particularly at high stress amplitude as well as in low cycle fatigue regime [43,44].

One of the relatively new methods of mechanical surface treatments is laser-shock peening which uses laser pulses with pulse duration within the nanosecond range to modify the surface layers of workpieces by means of pressure bursts, affecting near-surface region with thicknesses within the millimeter range. The pressure wave causes plastic deformations, when the yield strength is exceeded, developing macroscopic compressive residual stresses at the surface and in near-surface regions of workpiece [40,45]. Fig. 2.5 (b) shows the schematic process of laser-shock peening. Nevertheless, from table 2.1, laser-shock peening affects also the surface roughness of the workpiece [21,24,41].

The mechanical elementary process of deep rolling is the surface pressure created between the workpiece and the spherical device/ball in the contact zone (see Fig. 2.5 (c)). When the yield strength is exceeded, local plastic deformations occur, creating macroscopic compressive residual stresses and the associated microstructural work hardening/softening effects [40,47]. One of the most well-known benefits of deep rolling as compared to other mechanical surface treatments is the great depth of the work hardening states and macroscopic compressive residual stresses. Moreover, surface smoothening is also typical after deep rolling treatments (see table 2.1) [21,24]. From these beneficial effects, deep rolling treatments today are applied in various technical fields, for example for

surgical implants, for components of the steering wheels in the automotive industry as well as for turbine blades in the power plant and aircraft industry [21].

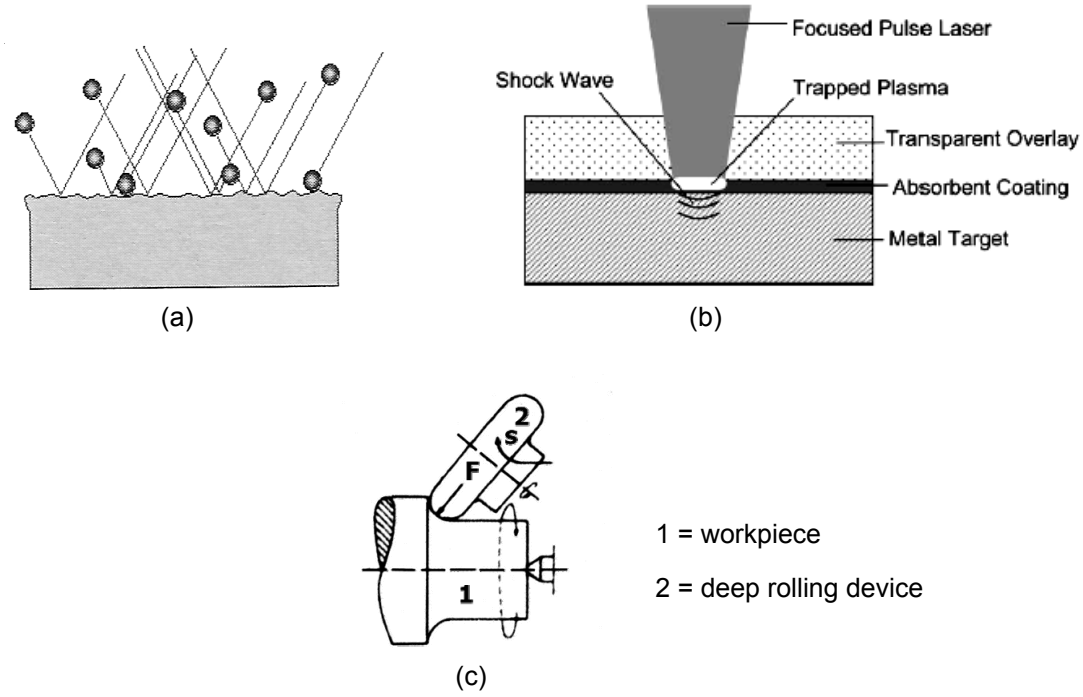

Figure 2.5: Schematic illustrations of selected mechanical surface treatments: (a) shot peening [46], (b) laser-shock peening [45] and (c) deep rolling [41].

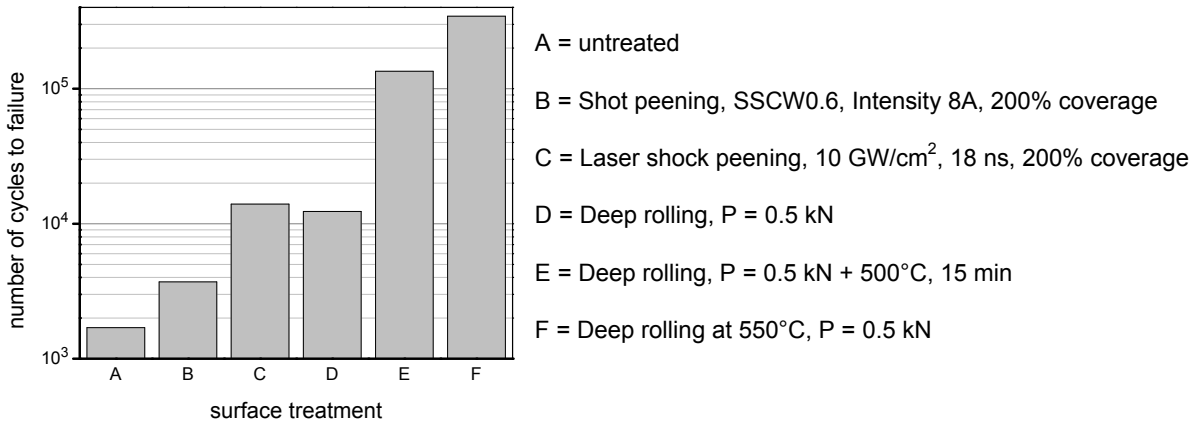

Figure 2.6: Fatigue lifetime improvement for differently surface treated austenitic stainless steel AISI 304 (σ_a = 350 MPa, f = 5 Hz, R = -1) [48].

2.3.2 Effects on cyclic deformation behavior

It is well established that the beneficial effects of mechanical surface treatments, e.g. increased near-surface hardnesses, induced near-surface macroscopic compressive residual stresses, work hardening states as well as surface smoothening (in a case of the deep rolling treatment) serve to inhibit or retard surface fatigue crack initiation as well as fatigue crack growth [11-13]. Moreover, during cyclic loading, lower plastic strain amplitudes of mechanically surface treated condition are generally detected. According to the Coffin-Manson law [49,50], fatigue lifetimes of components can be considerably improved through mechanical surface treatments by lowering the plastic strain amplitude (see Fig. 2.6 as an example).

2.3.3 Residual stress stability

Induced macroscopic compressive residual stresses as well as work hardening states are the most important features for fatigue lifetime improvement of mechanically surface treated metallic materials. Therefore, the stability of residual stresses as well as work hardening states during cyclic loading is very important [35,51]. Unfortunately, however, induced macroscopic compressive residual stresses as well as work hardening states can be reduced or completely relaxed by mechanical and/or thermal energy when the elastic residual strains can be converted into micro plastic strains (dislocation movement as well as rearrangement) by suitable deformation processes [51,52]. Residual stress relaxation phenomena can be principally classified into three groups: mechanical, thermal and thermomechanical residual stress relaxation.

Mechanical residual stress relaxation: Relaxation of macroscopic residual stresses as well as work hardening can occur with increasing applied stress amplitude and number of cycles during cyclic deformation at room temperature as shown in Fig. 2.7 [51,53]. The change of the surface states of mechanically surface treated materials due to cyclic loading can be divided into three phases. Firstly, the near-surface macroscopic compressive residual stresses are strongly reduced in the first cycle (regime I and II in Fig. 2.7) due to quasistatic loading. Secondly, a linear dependence of the residual stresses with the logarithm of

number of cycles occurs according to a logarithmic creep law (regime III in Fig. 2.7):

$$\sigma^{RS} = A(\sigma_a) - m(\sigma_a)\log N \quad (1)$$

where the materials properties *A* and *m* can be determined for *each* stress amplitude from experimental data in the linear section of the curves [51]. Finally, macroscopic compressive residual stresses as well as work hardening states (FWHM-values) decrease drastically after crack initiation (state IV in Fig. 2.7) [51-56]. In addition, there is a threshold stress amplitude below which the near-surface work hardening states are unaltered by cyclic loading indicated by constant FWHM-values, such as for AISI 304, magnesium alloy AZ31 and aluminium alloy AA6110, but where macroscopic compressive residual stress relaxed substantially during fatigue loading [27,28,43].

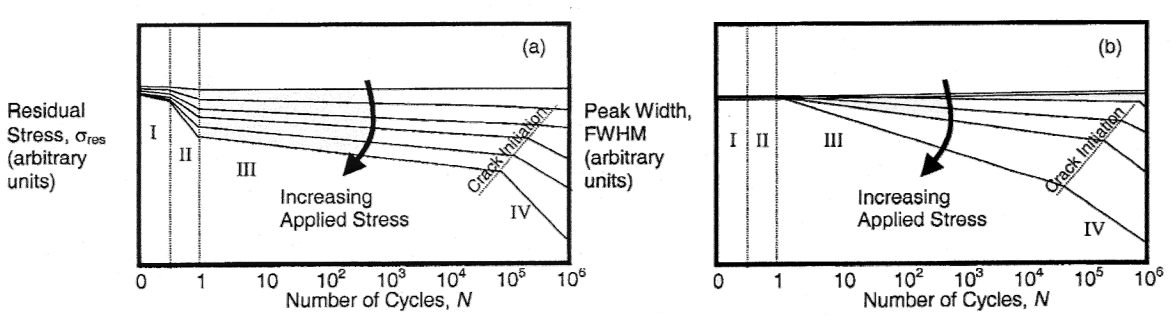

Figure 2.7: Schematic illustrations of the relaxation behavior of (a) residual stresses as well as (b) FWHM-values during fully reversed fatigue tests (R = -1) of shot peened AISI 4140 [53,55].

Thermal residual stress relaxation: Residual stress relaxation at elevated temperature is caused by so-called thermally activated processes. Dislocation movement, rearrangement as well as annihilation occur at elevated temperature and cause the relaxation process [51,52,56]. Thermal relaxation of residual stresses as well as FWHM-values can be described by a Zener-Wert-Avrami function as:

$$\sigma^{RS}/\sigma_0^{RS} = \exp[-(At_a)^m] \tag{2}$$

where m is a numerical parameter dependent on the dominant relaxation mechanism, t_a is the ageing time and A is a function dependent on the material and temperature according to

$$A = B \exp\left(\frac{-\Delta H}{kT_a}\right) \tag{3}$$

where B is a constant, k is the Boltzmann constant, T_a is the ageing temperature and ΔH is the activation enthalpy for the relaxation process. The materials parameters m, B as well as ΔH can be determined using equations (2) and (3) with a plot of the experimental data in Fig. 2.8 [40,51,52,54,56].

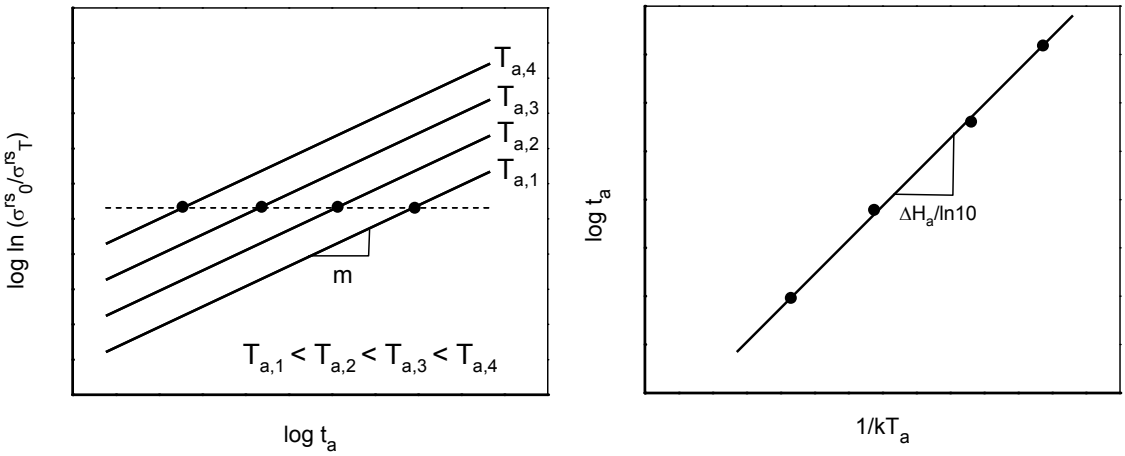

Figure 2.8: Schematic diagrams of the determination of Avrami approach parameters [51].

Thermomechanical residual stress relaxation: Recently, more advanced applications involve cyclic loading at elevated temperature. Thus, during service as well as cyclic loading at elevated temperature, mechanical and thermal residual stress relaxations occur simultaneously. However, at present, only rare information about thermomechanical residual stress relaxation exist [55,57,58]. Some authors reported that under isothermal fatigue loading, thermomechanical residual stress relaxation should be in principle separated into two parts: mechanical and thermal

residual stress relaxation as shown in Fig. 2.9 [58]. Nevertheless, thermomechanical residual stress relaxation phenomena are still completely not clear, hence their intensive and systematic investigation as well as analysis are still necessary.

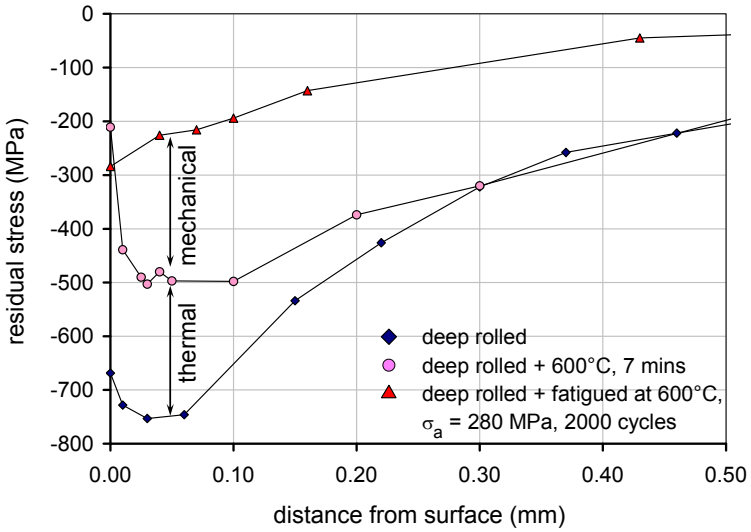

Figure 2.9: Residual stress-depth profiles after thermal and thermomechanical loading of AISI 304 [58].

2.3.4 Modern mechanical surface treatment

Nowadays, many modern mechanical surface treatments are derived from shot peening and deep rolling. At elevated temperatures, the concept of static/dynamic strain ageing is applied to shot peening as well as deep rolling. That means, warm shot peening and high-temperature deep rolling have been established (see Fig. 2.10) particularly for materials having interstitial solute atoms, such as carbon or nitrogen atoms in steels. Superior stability of macroscopic compressive residual stresses as well as work hardening states during cyclic loading can be expected due to dislocation pinning by interstitial solute atoms (so-called Cottrell-clouds) or by very fine carbides [20-23,40,59-62]. Accordingly, superior fatigue lifetimes were observed as compared to conventional mechanical surface treatments (see Fig. 2.6). However, it is still in doubt whether high-temperature mechanical surface treatments can generally enhance the fatigue behavior more significantly than

conventional mechanical surface treatments for materials having substitutional solute atoms, such as aluminium alloys where the full beneficial effects of static/dynamic strain ageing cannot be expected.

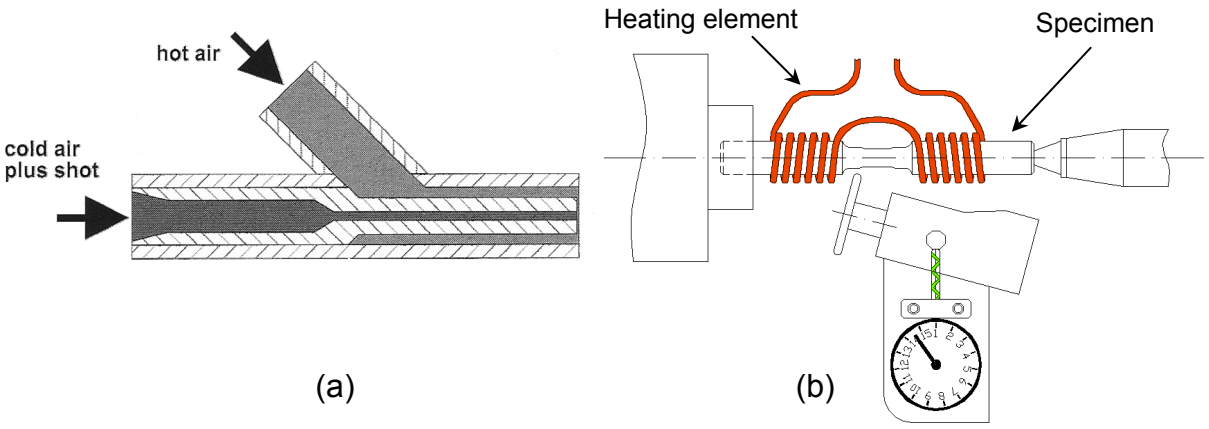

Figure 2.10: Schematic illustrations of modified mechanical surface treatments: (a) warm shot peening [40] and (b) high-temperature deep rolling [63].

Ageing treatments combined with mechanical surface treatments, e.g. shot peening or deep rolling are also methods to enhance the effects of conventional mechanical surface treatments using static/dynamic strain ageing concepts. The fatigue behavior of shot peened or deep-rolled steels can be considerably improved after annealing of optimized temperatures (see Fig. 2.6) [14,62,64]. For precipitation-hardenable materials, such as aluminium and titanium alloys, mechanical surface treatment is normally performed after the ageing treatments to improve the fatigue lifetime. Nevertheless, *in some cases*, mechanical surface treatment is performed on the solution heat treated (as-quenched) condition with subsequent ageing treatments to produce increased hardness by precipitates especially in near-surface regions as shown in Fig. 2.11. Interestingly, fatigue lifetimes can be greater than the conventional method (appreciated/optimized ageing followed by mechanical surface treatment) [17-19,66]. However, on the other hand, induced near-surface macroscopic compressive residual stresses and work hardening states tend to relax during annealing as well as ageing treatments. By the reduction of near-surface macroscopic compressive residual stresses and

work hardening states, a detrimental effect for the fatigue lifetime is expected especially in *smooth*, *soft and mechanically surface treated materials* because their fatigue lifetime depends significantly on the stability of near-surface work hardening states as well as macroscopic compressive residual stresses [24-29]. Thus, presently, it is not fully clear whether mechanical surface treatment followed by ageing treatment is always superior to the conventional method for precipitation-hardenable materials. Therefore, the effects of decreased macroscopic compressive residual stresses as well as work hardening states together with the increased hardnesses by the ageing treatment on the fatigue behavior should be thoroughly and clearly investigated in detail.

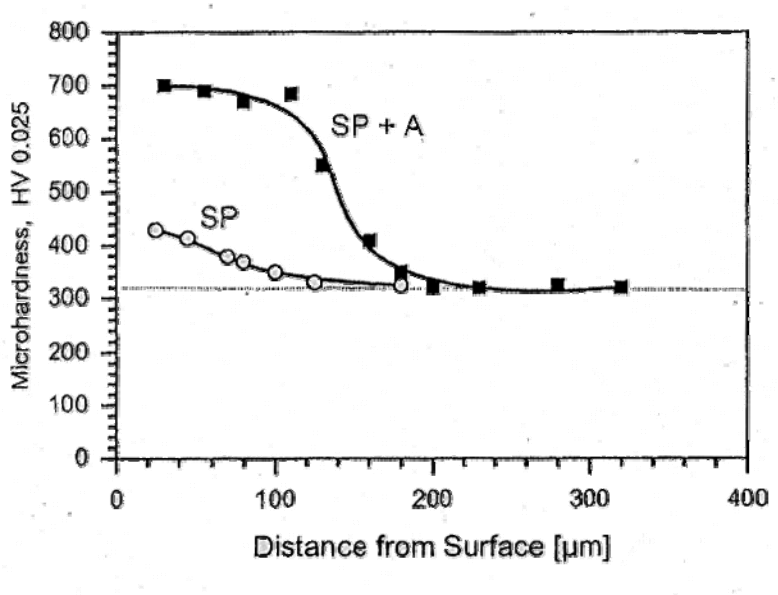

Figure 2.11: Microhardness-depth profile in the as-solutionized β titanium alloy Beta C, after shot peening (SP) and preferential ageing (SP+A) [66].

Chapter 3

Aluminium alloys

3.1 Aluminium and its alloys

Aluminium was a “late comer” and could still be called a “young metal” as compared to other structural materials used today. The process to produce aluminium alloys on an economic basis was developed only about 100 years ago because of the fact that aluminium is difficult to recover from its ore. However, due to their versatilities, e.g. low specific weight, good heat and electrical conductivity, high reflectivity and resistance to corrosion, aluminium is consumed more than all other non-ferrous metals combined including copper and its alloys as well as lead, thin and zinc. As a consequence, the production and consumption of aluminium has increased at a rate of more than 8% per year. Today, aluminium is the second most widely used metal in the world. About 85% of aluminium is used for wrought products, e.g. rolled plate, sheet, foil, extrusions, rod, bar and wire [1-3].

Wrought aluminium alloys can be mainly classified into two groups (see Fig. 3.1): non-precipitation-hardenable and precipitation-hardenable aluminium alloys.

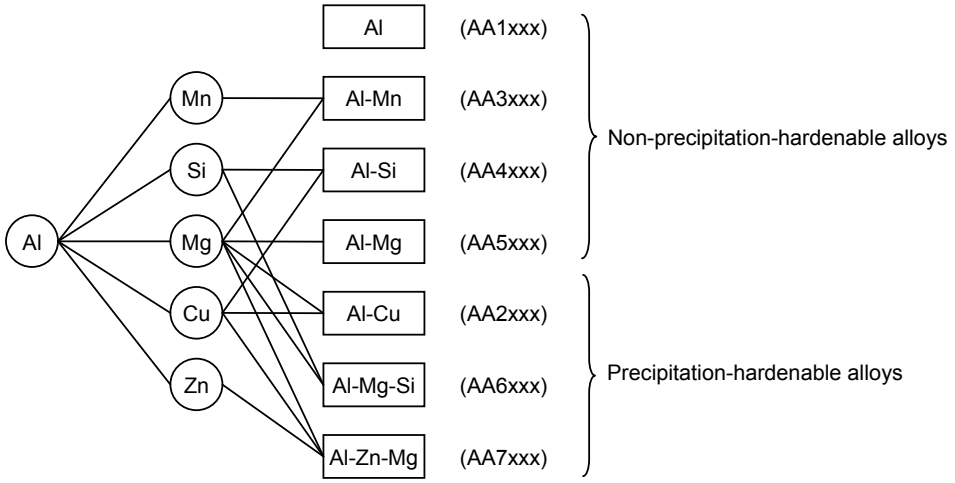

Figure 3.1: Classification of wrought aluminium alloys [1-4].

3.1.1 Non-precipitation-hardenable aluminium alloys

The non-precipitation-hardenable wrought aluminium alloys, e.g. AA3xxx (Al-Mn and Al-Mn-Mg) or AA5xxx (Al-Mg) contain manganese and/or magnesium as the major additions. In these alloys, the increase of strength is principally due to lattice distortion by the atoms in solid solution. When dislocations move on a slip plane, the strain field obstructs movement leading to a pinning effect. Strength can be also developed by work hardening (increasing dislocation density), usually by cold working during fabrication. Dislocations interact with other dislocations and with other barriers to their motion through the lattice [1-4]. Strengthening of aluminium alloys in this group is considerably produced with magnesium in solid solution because of its high solid solubility. The 0.2% yield strengths of AA5xxx alloys may be increased to 300 MPa after cold working. However, these increases are obtained at the expense of ductility and also reduced formability in operations, such as bending and stretch forming [1].

3.1.2 Precipitation-hardenable aluminium alloys

The wrought aluminium alloys which respond to strengthening by precipitation are covered by three series AA2xxx, AA6xxx and AA7xxx (see Fig. 3.1). Precipitation-hardenable aluminium alloys usually contain elements, such as Cu, Mg, Si and Zn which have high solid solubility at high temperature, but rather lower solubility at room temperature. Heat treatment of precipitation-hardenable aluminium alloys generally involves the following states [1-4]:

1) Solid solution treatment at a relative high temperature within the single-phase region to dissolve the alloying elements.
2) Quenching, usually to room temperature, to obtain a supersaturated solid solution (SSSS) of these elements in aluminium.
3) Controlled decomposition of the supersaturated solid solution to form finely dispersed precipitates by the ageing treatment.

The type and sequence of precipitates depend certainly on the alloying elements of each aluminium alloys. Typically, the first stage of precipitation involves local clusters or zones (so-called Guinier-Preston (GP) zones) which usually produce

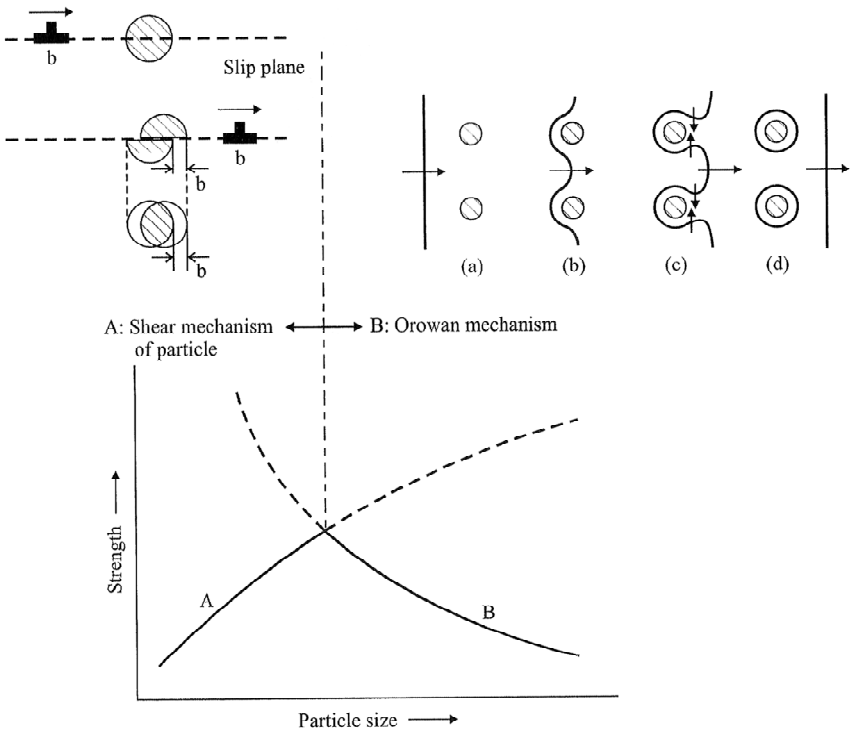

Figure 3.2: Schematic illustration of interactions between dislocations and precipitates and their effect on the contributed strength of precipitation-hardenable aluminium alloys [69,70].

appreciable elastic strains to obstruct dislocation movement. These zones are favored by a low ageing temperature and a high degree of supersaturated solid solution. With additional ageing, the strength of the alloy increases due to the intermediate precipitate which is normally much larger in size than a GP zone and it is formed as a coherent or semi-coherent particle within the matrix. If precipitates are large and widely spaced as in an over-aged condition, they can be readily bypassed by moving dislocation which bow out between them and rejoin by an Orowan mechanism. The yield strength as well as the hardness of the aluminium alloy decrease. This is the situation for the over-aged alloys and the typical age hardening curve in which strength at first increases and then decreases with ageing time associated with a transition from shearing to bypassing of precipitates, as shown schematically in Fig. 3.2 [1-4,30,67-70]. Therefore, it is undeniable that the characteristic of precipitates, e.g. type, structure, morphology, definitely affect the mechanical properties of aluminium alloys. Accordingly, characterization

methods for precipitates of aluminium alloys are essential and have to be considered unavoidably in the next section.

3.1.2.1 Characterization methods

Fortunately, at present, many materials characterization methods have been developed, thus several analytical or test methods are provided to directly or indirectly characterize/identify precipitates in aluminium alloys.

Direct analysis methods: Precipitates of aluminium alloys can be directly seen as well as analyzed, e.g. their phase or crystal structure, phase distribution and morphology using electron optical methods as well as diffraction methods.

- **Electron optical methods:** Electron optical methods, e.g. transmission electron microscopy (TEM) as well as scanning electron microscopy (SEM) are common methods to analyze precipitates in aluminium alloys. However, sufficient background information in understanding the basic principles of these techniques, including the difficult preparation of samples, can limit the analysis of an engineering material [71].
- **Diffraction methods:** X-ray or neutron diffraction (XRD) techniques can be used to identify the phases/compounds present in materials. Nevertheless, the intensity of the diffracted intensity correlates to the volume fraction of the phase/compound. That means, X-ray diffraction method becomes a difficult task when the phases/compounds in materials have relatively small size and low volume fraction [72].

Indirect analysis methods: Mechanical and physical properties of aluminium alloys are altered during ageing treatments due to different type, structure, distribution as well as morphology of precipitates. Therefore, if the alterations of mechanical as well as physical properties during ageing are monitored, from these informations, precipitates of aluminium alloys can be indirectly interpreted, particularly their sequence.

- **Mechanical methods:** Hardness as well as tensile tests are frequently conducted for materials subjected to ageing treatments, due to their simplicity and relatively easy interpretation. Consequently, several

investigations of the precipitation as well as its effects on aluminium alloys using mechanical methods are found.

- **Thermal or electrical analysis methods:** As mentioned above, physical properties of precipitation-hardenable aluminium alloys are altered during ageing treatments, such as heat absorption/release, electrical resistivity as well as conductivity. Therefore, differential scanning calorimetry (DSC) and resistivity/conductivity measurement can also be used to analyze/characterize precipitates of aluminium alloys especially their sequence [73-78].

All in all, it can be summarized that precipitates in aluminium alloys can be efficiently characterized using direct or indirect analysis methods. However, combined methods between direct and indirect analysis methods are always preferred because some problems/questions can not be solved using only direct or indirect analysis methods (see table 3.1). Therefore, numerous investigations about the precipitation reactions in aluminium alloys and its effects on mechanical/physical properties using both direct and indirect analysis methods are found in [79-88].

3.1.2.2 Precipitation of deformed aluminium alloys and its kinetics

Plastic deformation can be a driving force for precipitation. A first important aspect of plastic deformation is the reduction in distance required in a diffusion process. A second aspect is the storage of dislocations by plastic deformations of as-quenched aluminium alloys, which serve as nucleation sites of the subsequent precipitation reaction. Accordingly, kinetics of precipitation of the supersaturated solid solution (as-quenched) aluminium alloys can be principally accelerated by plastic deformation (increased dislocation densities) [88-91]. In many aluminium alloys, the presence of dislocations often changes the precipitation sequence and may also increase mechanical properties as compared to the peak-aged condition as shown in Table 3.2. Therefore, the investigation of rapid kinetics of precipitation in as-quenched aluminium alloys is required particularly for high strength aluminium alloys in the automotive industry, such as AA6110. The basic requirement for automotive sheet is to have a high formability and preferably increase of strength when the part is painted and thus thermally cured. However,

Table 3.1: Characterization ability of selected direct and indirect analysis methods [71-79,81,82].

	Crystal structure	Phase identification	Phase distribution/ morphology	Phase element	Sequence	Property change
TEM	+	+	+	+	+/-	-
SEM/EDS*	-	+/-	+	+	-	-
XRD*	+	+	-	+/-	-	-
DSC	-	-	-	-	+	-
Hardness/ tensile test	-	-	-	-	+/-	$+^{M}$
Resistivity/ conductivity	-	-	-	-	+	$+^{P}$

+ = yes, +/- = possible and - = no
* for the case which the precipitates have sufficient size and/or volume fraction
^{M} for mechanical properties
^{P} for physical properties

Table 3.2: Typical mechanical properties of selected precipitation-hardenable aluminium alloys [92].

	Temper state	0.2% yield strength (MPa)	Ultimate tensile strength (MPa)	Brinell hardness
AA2024	T6	345	427	125
	T8	400	455	128
AA6013	T6	359	386	125
	T8	380	393	130
AA6020	T6	240	262	95
	T8	248	269	100

T6 = solution heat-treated and then artificially aged (as referred to the peak-aged condition)
T8 = solution heat-treated, cold worked and then artificial aged

the holding time in the baking process is usually not long enough to lead to the peak-aged condition for aluminium alloys AA6xxx, so that the potential strength of these alloys can not be fully achieved. Therefore, pre-deformation [93-96] or pre-ageing techniques [93,97-100] are used to increase strength as well as to accelerate the kinetics of precipitation of these alloys in the paint bake hardening process.

3.2 Cyclic deformation behavior of aluminium alloys

As described in section 2.2, dislocation generation, movement, rearrangement and interaction with obstacles, such as other dislocations and/or precipitates during cyclic loading are the important key of the cyclic deformation behavior for almost all metallic materials. Accordingly, it can be claimed that the cyclic deformation behavior/curve of aluminium alloys should be different and strongly dependent on type and characteristic of precipitates, e.g. solute atoms in the supersaturated solid solution (as-quenched) condition, atomic clusters/GP-zones and/or small coherent precipitates in the under-aged condition, coherent and semi-coherent precipitates in the peak-aged condition and semi-coherent and/or incoherent precipitates in the over-aged condition. Differences of the cyclic deformation behaviors/curves of aluminium alloys which contain different precipitates are summarized in table 3.3. The differences between the cyclic deformation curves are assumed to be associated with dislocation-precipitate and dislocation-dislocation interactions during cyclic deformation [101,102].

3.3 Mechanically surface treated aluminium alloys.

Macroscopic compressive residual stresses, work hardening states as well as increased hardnesses at the surface and in near-surface regions of aluminium alloys are normally induced by all mechanical surface treatments, e.g. shot peening [13,17,18,66,103-105], laser-shock peening [106,107] as well as deep rolling [13,16-18,25-29,108,109]. Consequently, fatigue lifetimes of mechanically surface treated aluminium alloys are usually improved especially in the high cycle fatigue regime. For example, Figs 3.3 (a) and (b) show s/n-curves at room temperature of shot peened aluminium alloy AA2024-T3 and -T6 as compared to the polished condition. Fatigue behavior of aluminium alloy AA2024-T3 and -T6 was considerably improved after mechanical surface treatment (shot peening), particularly in the high cycle fatigue regime. Moreover, higher fatigue strength of the shot peened aluminium alloy AA2024-T3 was observed as compared to the shot peened aluminium alloy AA2024-T6 due to higher macroscopic compressive residual stresses of shot peened AA2024-T3 as shown in Fig. 3.4 [13]. However, some investigations indicate that fatigue lifetimes of mechanically surface treated aluminium alloys are lower as compared to the polished/untreated condition at

Table 3.3: Different cyclic deformation behaviors/curves of aluminium alloys which contain different precipitates [25-28,31-34,101,102].

Condition	Characteristic of precipitates	Cyclic deformation behavior/curve	Mechanism
As-quenched/ Non-precipitation-hardenable	solute atoms/atomic clusters	cyclic hardening	Increasing dislocation densities, dislocation-dislocation interactions and dynamic precipitates during cyclic deformation
Under-aged	atomic clusters/small coherent	cyclic hardening	Increasing dislocation densities and dislocation-dislocation interactions during cyclic deformation
Peak-aged	coherent and semi-coherent	cyclic softening	The to-and-fro motion of dislocations through the ordered precipitates causes a mechanical local disordering or scrambling of the atoms in the precipitates. The structure of the precipitates becomes disordered and degraded. The hardening due to ordering is lost.
Over-aged	semi-coherent	cyclic softening	The to-and-fro motion of dislocations through the semi-coherent precipitates during cyclic loading. The structure of the precipitates becomes disordered and degraded. Ordering contribution to hardening of the over-aged condition was lost.

high applied stress amplitudes [16,25-29,44]. Instability of macroscopic compressive residual stresses and work hardening states of mechanically surface treated aluminium alloys is the important reason for this behavior. Notch sensitivity may also play an important role. Nevertheless, only few information on stability of macroscopic compressive residual stresses as well as work hardening states of mechanically surface treated aluminium alloys are found, for example, mechanical residual stress relaxation in [12,27,28,110] and thermal residual stress relaxation in [16,54,56,111]. Moreover, information or details about the thermomechanical residual stress relaxation of mechanically surface treated aluminium alloys are unfortunately not available.

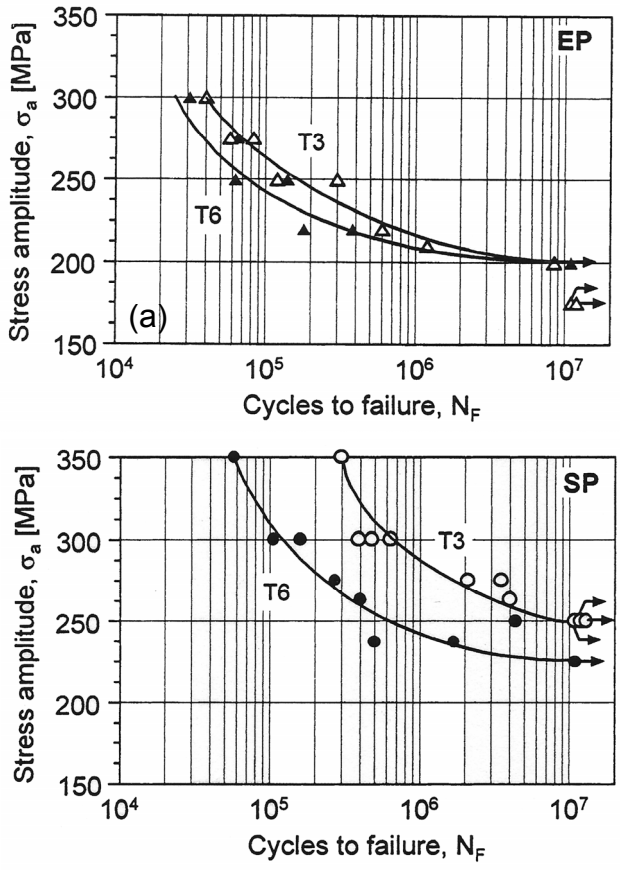

Figure 3.3: S-N curves (*R*= -1) for aluminium alloy AA2024-T3 and -T6 (a) polished condition (b) shot peened condition [13].

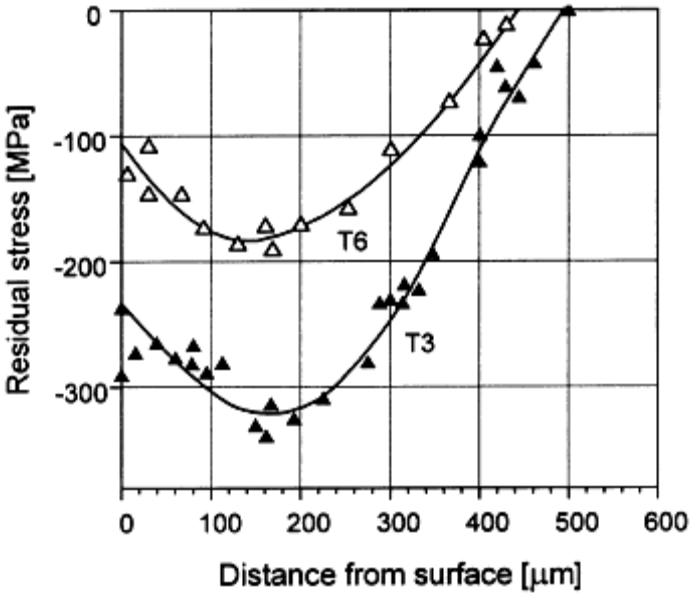

Figure 3.4: Residual stress-depth profiles of shot peened aluminium alloy AA2024-T3 and -T6 [13].

Chapter 4

Materials and experimental procedures

4.1 Materials

Aluminium alloys AA5xxx and AA6xxx are widely used as medium-strength structural alloys in several industries due to their versatilities, e.g. low specific weight, good heat and electrical conductivity, high reflectivity and resistance to corrosion. Furthermore, the advantageous property of aluminium alloys AA5xxx and AA6xxx as compared to high-strength aluminium alloys AA2xxx and AA7xxx is weldability. Accordingly, recently, aluminium alloys AA5xxx and AA6xxx are used mainly in automotive industries [1-4]. Therefore aluminium alloys AA5083 and AA6110 were selected for this research.

4.1.1 Aluminium alloy AA5083

The aluminium alloy AA5083 raw material was delivered as warm rolled sheet with a thickness of 15 mm. The chemical composition of this alloy is shown in table 4.1. Near-surface microstructure of aluminium alloy AA5083 is shown in Fig. 4.1. Due to the severe rolling process the grain structure is no longer visible: intermetallic precipitates are oriented along the rolling direction. Aluminium alloy AA5083 is a non-precipitation-hardenable alloy, thus the specimens were investigated without any further heat treatment.

Table 4.1: The chemical composition of aluminium alloy AA5083 (wt-%).

Element	Si	Fe	Cu	Mn	Mg	Cr	Zn	Ti	Al
wt.%	0.40	0.40	0.10	0.40-1.0	4.5	0.05-0.25	0.25	0.15	Bal.

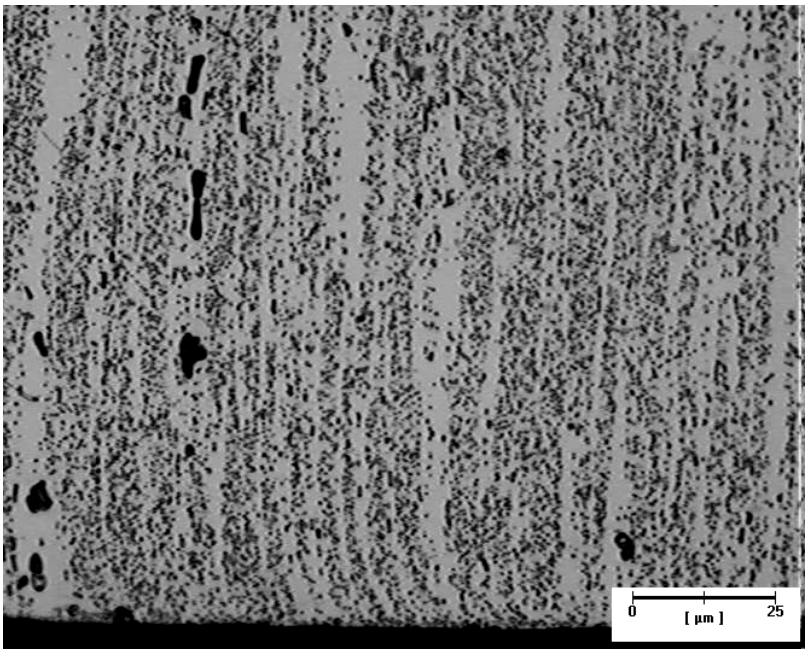

Figure 4.1: Near-surface microstructure of aluminium alloy AA5083.

4.1.2 Aluminium alloy AA6110

The major elements of aluminium alloys AA6xxx are usually magnesium (Mg) and silicon (Si). The precipitation sequence in Al-Mg-Si alloys is generally accepted to initiate with spherical atomic clusters (GP zones), metastable phases, β´´ and β´ leading to the equilibrium β phase Mg_2Si [1-5]. Nowadays higher strength Al-Mg-Si-Cu alloys, i.e. AA6013, AA6110 or AA6111 were developed especially for applications in the automotive industry. The quaternary phase, Q ($Al_5Cu_2Mg_8Si_7$) and its metastable precursor, Q´ is formed and supposed to contribute significantly to mechanical properties of these alloys [1,112,113]. The aluminium wrought alloy AA6110 was delivered from Alcoa Extrusions, Hannover, Germany as extruded bars with a diameter of 34 mm. The chemical composition of this alloy is shown in table 4.2.

Heat treatment: Aluminium alloy AA6110 specimens were solution heat treated in an argon atmosphere furnace at 525°C for 30 minutes followed by water quenching to room temperature. Quenched specimens were aged immediately at 160°C for 1-168 hours to designate the ageing conditions for this research (see Fig. 4.2).

Table 4.2: The chemical composition of aluminium alloy AA6110 (wt-%).

Element	Si	Fe	Cu	Mn	Mg	Cr	Zn	Ti	Al
wt.%	0.86	0.19	0.45	0.46	0.78	0.17	0.02	0.01	Bal.

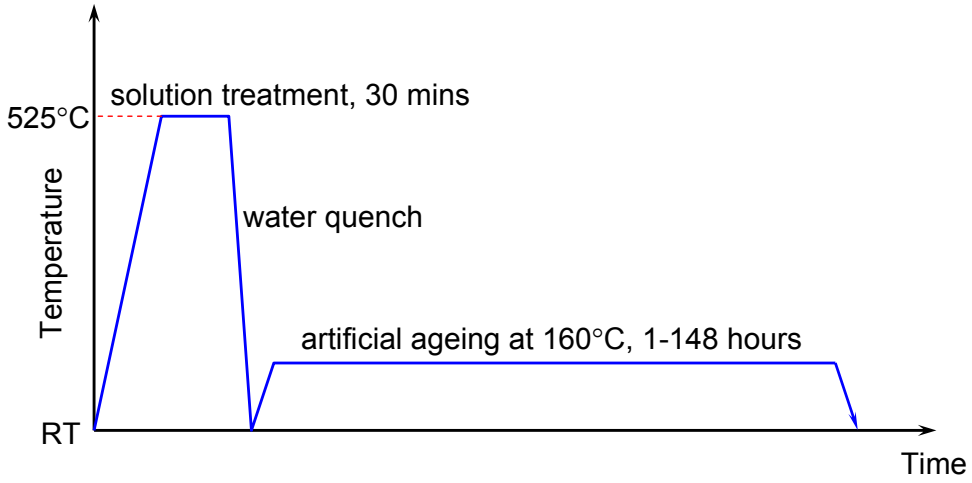

Figure 4.2: Schematic illustration of heat treatment of aluminium alloy AA6110.

Designation of ageing condition: Pre-experiments were carried out to designate the ageing conditions. Differently aged specimens were investigated using microhardness tests with a load of 50 grams as shown in Fig. 4.3. Obviously, after artificial ageing at a temperature of 160°C, the hardness of the as-quenched condition increase continuously with increasing ageing time. Maximum hardness of approximately 140 HV was measured after ageing at a temperature of 160°C for about 12 hours which is designated as the peak-aged condition. Under-, and over-aged conditions were also determined using hardness measurements in Fig. 4.3. Ageing at a temperature of 160°C for about 1 and 168 hours (1 week) were selected for the under- and over-aged conditions, respectively.

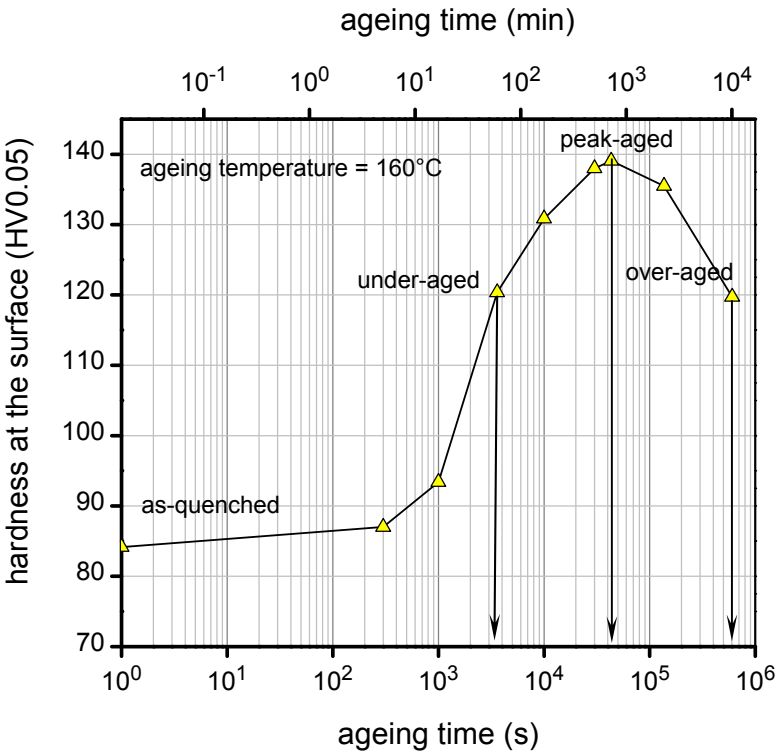

Figure 4.3: Hardnesses at the surface of as-quenched AA6110 as a function of ageing time at an ageing temperature of 160°C.

4.2 Specimen preparation details

Specimen geometry: Cylindrical specimens with a diameter of 7 mm and a gauge length of 15 mm were prepared from the delivered sheets/bars (see Fig. 4.4). The loading direction during tensile/fatigue investigations corresponds to the rolling/extrusion direction of the sheet/bar.

Non-mechanical surface treatment: Non-mechanically surface treated specimens were electrolytically polished in the gauge length leading to a material removal of 100 µm before testing to avoid any influence of prior machining. Electrolyte AC2 of Struers GmbH with current density about 2 A/cm^2 was used for the electrolytic polishing.

Mechanical surface treatment: Deep rolling treatment was performed at room temperature using a hydraulic rolling device with a 6.6 mm spherical rolling element and a pressure of 100 bar (80 bar for the as-quenched AA6110) (see Fig.

4.5 (a)). High-temperature deep rolling was achieved using a pneumatic roller with a diameter of 40 mm. A rolling force of about 0.3 kN (referred to about 80 bar of a hydraulic rolling device) was applied to the as-quenched AA6110 at elevated temperatures up to 250°C. Specimens were heated using induction heating as shown in Fig. 4.5 (b).

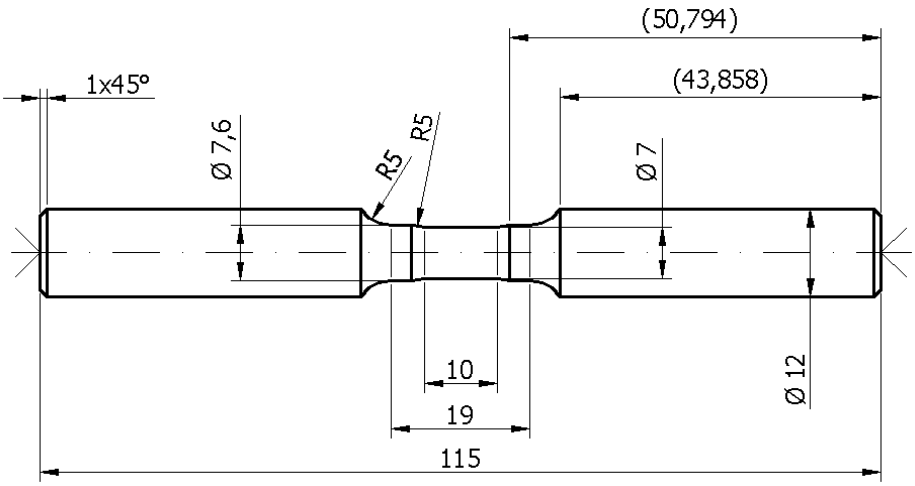

Figure 4.4: Specimen geometry of AA5083 and AA6110 for tensile and fatigue tests.

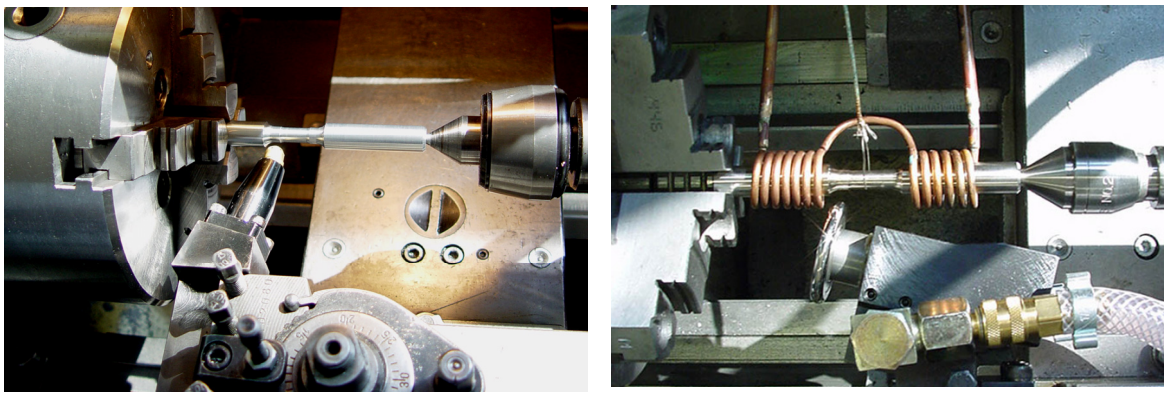

Figure 4.5: Deep rolling devices: (a) hydraulic type for room temperature and (b) pneumatic type including heating element for high temperature deep rolling.

4.3 Characterization methods

4.3.1 Microstructure

Microstructures as well as precipitates of aluminium alloys AA5083 and AA6110 were characterized using light microscopy and transmission electron microscopy (TEM). TEM was carried out using a 200 kV Philips microscope on plan-view samples under two-beam conditions. TEM foils were prepared by twin jet electrolytic polishing.

4.3.2 Differential scanning calorimetry (DSC)

Differential scanning calorimetry (DSC) is a thermal analysis method which measures temperatures and heat flows associated with thermal transitions in a material. For this study, differential scanning calorimetry was performed using a DSC-model Q1000 of TA Instruments in the temperature range 50-350°C with a heating rate of 10°C/minute.

4.3.3 X-Ray diffraction (XRD)

AA5083: Residual stresses and work hardening states of deep-rolled AA5083 were measured using the classical $\sin^2\Psi$-method with CrKα radiation at the {222}-planes and ½ s_2 = 18.56x10^{-5} mm^2/N as elastic constant [114]. Near-surface work hardening was characterized by the full width at half maximum (FWHM) values of the X-ray diffraction peaks.

AA6110: Residual stresses and work hardening states of deep-rolled AA6110 were measured using the classical $\sin^2\Psi$-method with CuKα radiation at the {333}-planes and ½ s_2 = 19.77x10^{-5} mm^2/N as elastic constant [114]. Near-surface work hardening was also characterized by the full width at half maximum (FWHM) values of the X-ray diffraction peaks.

All residual stresses and FWHM-values were measured in longitudinal direction of the specimens. Residual stress- as well as FWHM-value-depth profiles were determined by successive electrolytical material removal. No stress correction was carried out after electrolytical material removal of surface layers.

4.4 Tensile test

Tensile tests were carried out in the temperature range 20-250°C using a universal testing machine type Zwick Z100. All specimens were heated using controlled hot air. In order to minimize thermal gradients, the specimens were held at the test temperature for 10 minutes prior to the start of the actual tests. A strain rate ($d\varepsilon/dt$) of 10^{-3} s^{-1} was used for all investigations.

4.5 Fatigue test

Tension-compression fatigue tests were conducted with a servohydraulical 63 kN-testing machine of Schenck. Stress-controlled fatigue tests without mean stress (R = -1) and with a test frequency of 5 Hz were performed at room and elevated temperature up to 250°C. Strain was measured using capacitative extensometer. For investigations at elevated temperatures, specimens were heated using controlled resistance heating elements and radiant heating for AA5083 and AA6110, respectively (see Figs 4.6 (a) and (b)). In order to minimize thermal gradients, the specimens were also held at the test temperature for 10 minutes prior to the start of the actual fatigue tests.

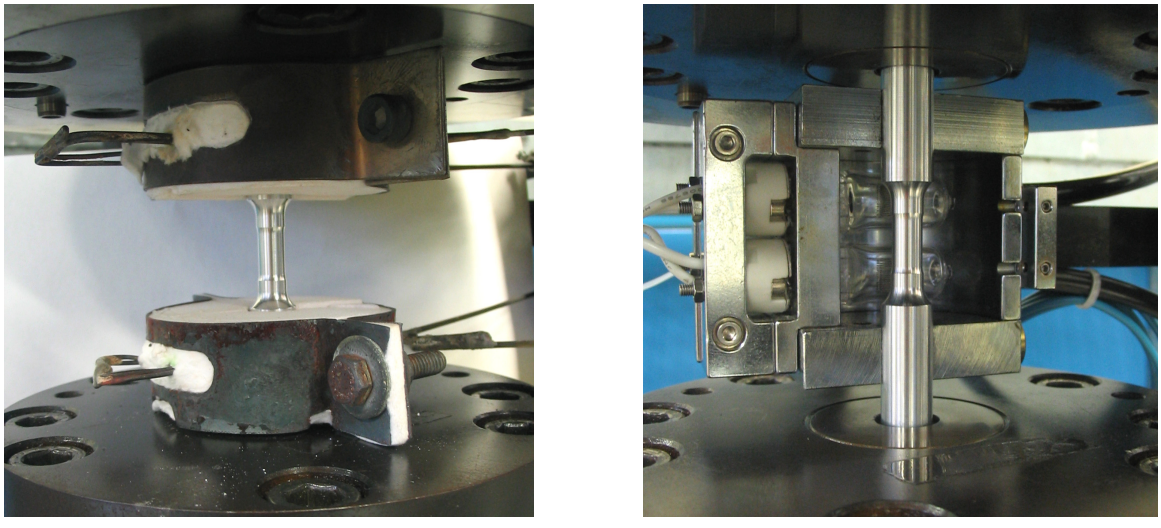

(a) (b)

Figure 4.6: Heating equipments for fatigue tests at elevated temperature: (a) controlled resistance heating elements and (b) radiant heating.

4.6 Overview of the experimental plan

The cyclic deformation behavior of AA5083 and AA6110 was systematically investigated and analyzed. Both aluminium alloys AA5083 and AA6110 in differently aged conditions, namely as-quenched, under-, peak- and over-aged conditions were cyclically deformed at room and elevated temperatures up to 250°C. Cyclic deformation curves and s/n-curves of deep-rolled and polished conditions were measured and compared to analyze the effect of deep rolling on cyclic deformation behavior at room as well as elevated temperatures. The residual stress stability of the deep-rolled condition during cyclic loading at room and elevated temperatures was investigated and presented through residual stress-depth profiles and/or residual stress relaxation as a function of a number of cycles. The chronological order of experiments is summarized in Fig. 4.7. In addition, to study the effect of static/dynamic precipitation of the as-quenched AA6110, deep rolling followed by an ageing treatment as well as high-temperature deep rolling was also investigated. An experimental diagram is shown in Fig. 4.8.

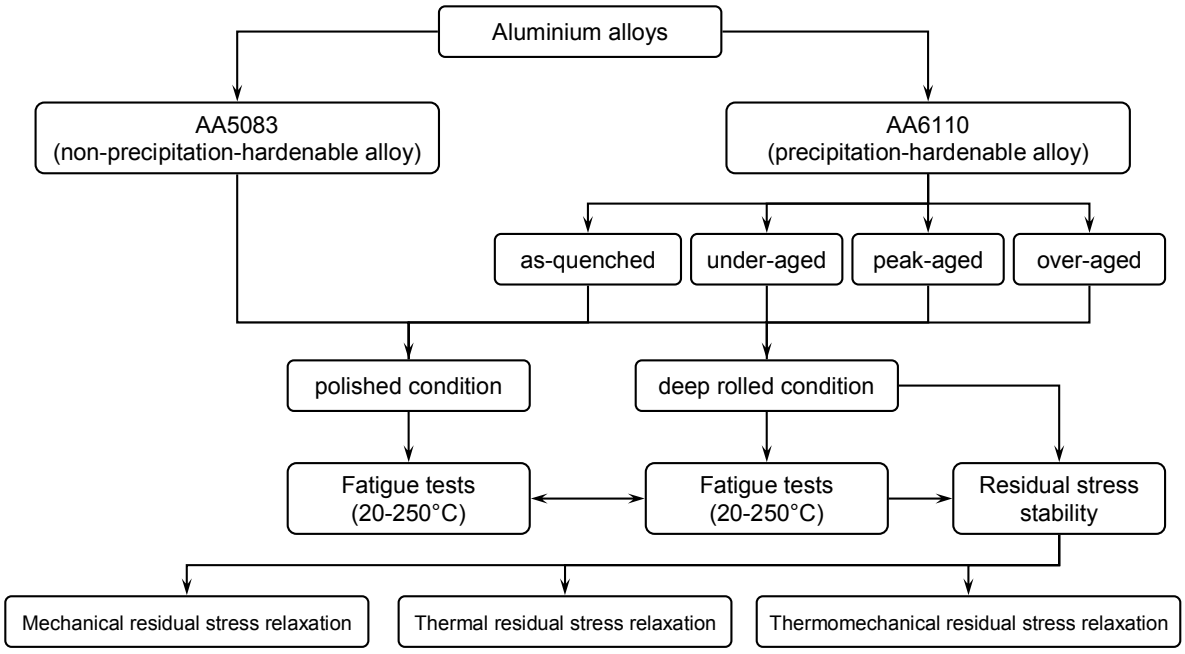

Figure 4.7: Experimental diagram for cyclic deformation behavior investigation of aluminium alloys AA5083 and AA6110.

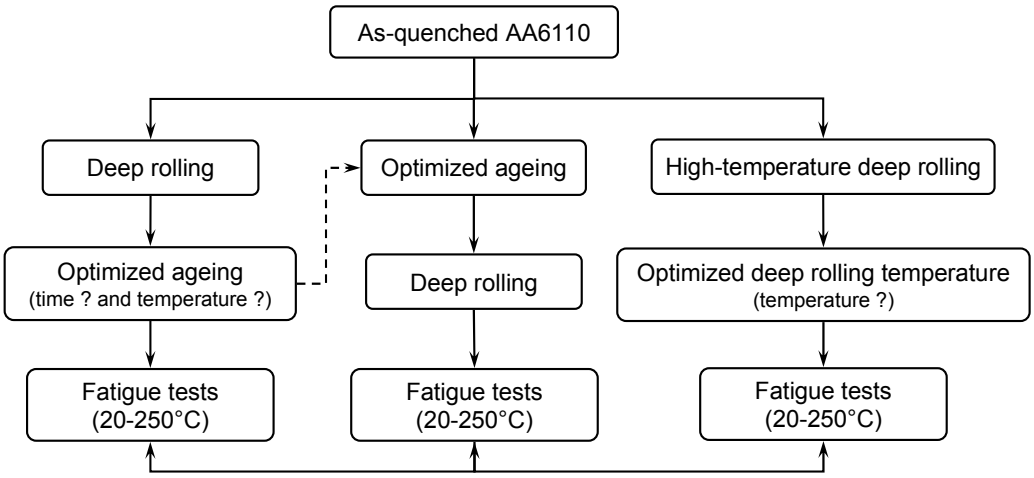

Figure 4.8: Experimental diagram for investigation of modified mechanical surface treatment, deep rolling followed by ageing treatment and high-temperature deep rolling of as-quenched AA6110.

Chapter 5

Experimental results

5.1 Aluminium alloy AA5083

Firstly, the cyclic deformation behavior of the non-precipitation-hardenable aluminium alloy AA5083 was investigated at room and elevated temperatures. Cyclic deformation curves and s/n-curves of polished and deep-rolled AA5083 for different test temperatures are presented. The stabilities of residual stress as well as work hardening state during fatigue tests at room and elevated temperature were observed using the depth profiles of near-surface residual stresses and FWHM-values after fatigue tests at selected test conditions. In addition, results of quasistatic tensile tests of untreated specimens at room and elevated temperatures up to 300°C are also given to reveal the effects of temperature on the mechanical properties of AA5083.

5.1.1 Quasistatic deformation behavior of AA5083

The quasistatic tensile behavior of non-surface treated AA5083 was investigated at room and elevated temperatures up to 300°C. The engineering stress-strain curves for different test temperatures are shown in Fig. 5.1. The effects of temperature on the tensile properties, e.g. the 0.2% yield strength of the aluminium alloy AA5083, can easily be derived from this diagram. For test temperatures of 20 and 100°C, the material showed very small or no differences in the 0.2% yield strengths in tensile tests [2]. However, for test temperatures higher than 100°C, the 0.2% yield strength decreased continuously with increasing temperature, particularly at a temperature of 300°C, the 0.2% yield strength dropped drastically and was only 76 MPa. Moreover, the work hardening rate ($d\sigma/d\varepsilon$) of AA5083 decreased with increasing temperature. Accordingly a flattening out of the stress-strain curves at elevated temperature was also detected in Fig. 5.1 [30].

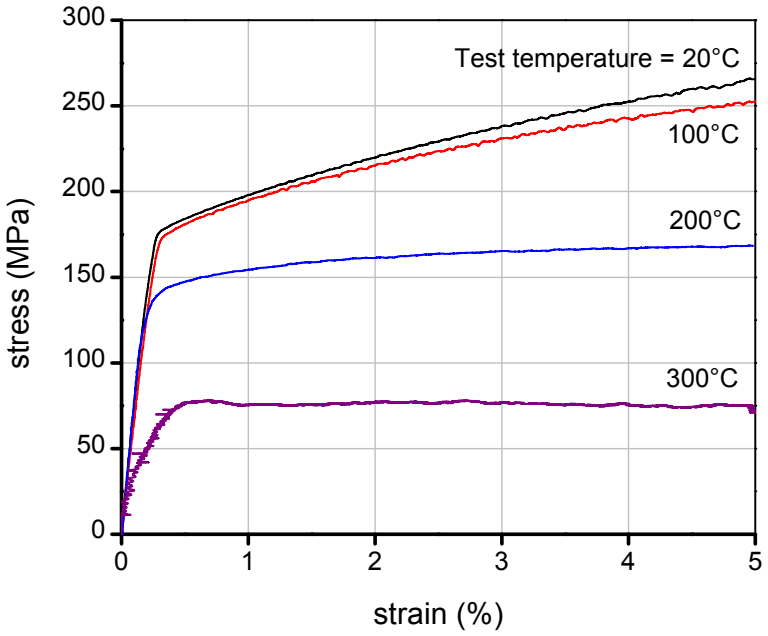

Figure 5.1: Engineering stress-strain diagram of AA5083 for different test temperatures.

5.1.2 Cyclic deformation behavior of polished AA5083

Fatigue lifetime: In general, the fatigue lifetime and strength of metallic materials depends on the applied stress amplitude and temperature. The fatigue lifetime as well as strength normally decrease with increasing stress amplitude and/or temperature, unless pronounced strain ageing effects occur. Non-statistically evaluated s/n-curves of polished condition in the temperature range 20-250°C are presented in Fig. 5.2. From this diagram, the effects of the stress amplitude and temperature on fatigue lifetime are seen clearly. A significant effect of temperature on fatigue strength of AA5083 can be expected because of the influence of temperature on quasistatic tensile strength in Fig. 5.1. The fatigue lifetime at room temperature of polished AA5083 for an applied stress amplitude of 175 MPa is approximately 110,000 cycles, whereas the fatigue lifetime at 250°C for the similar applied stress amplitude is reduced to only roughly 2,800 cycles.

Cyclic deformation curve: At room temperature, the cyclic deformation curves of polished AA5083 exhibit cyclic hardening for all stress amplitudes. However, with increasing temperature, especially above 200°C, the material initially cyclically

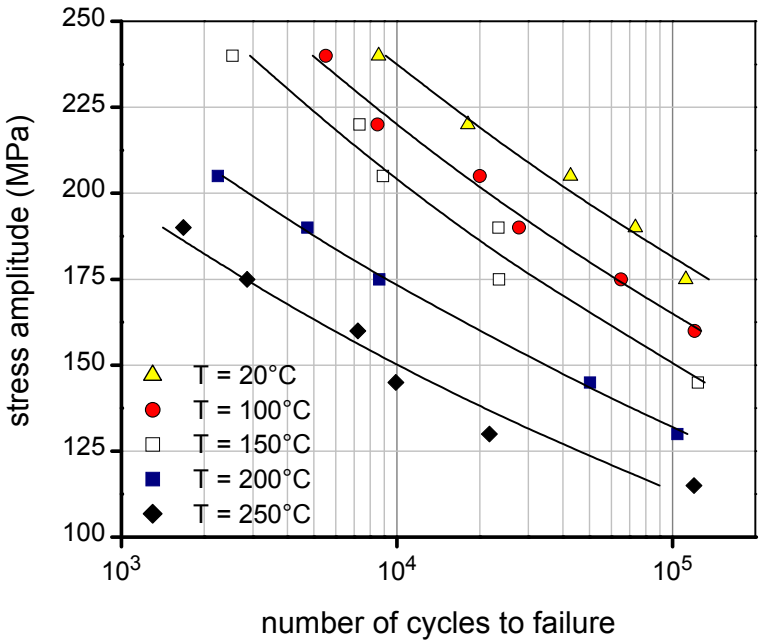

Figure 5.2: Non-statistically evaluated s/n-curves of polished AA5083 in the temperature range 20-250°C.

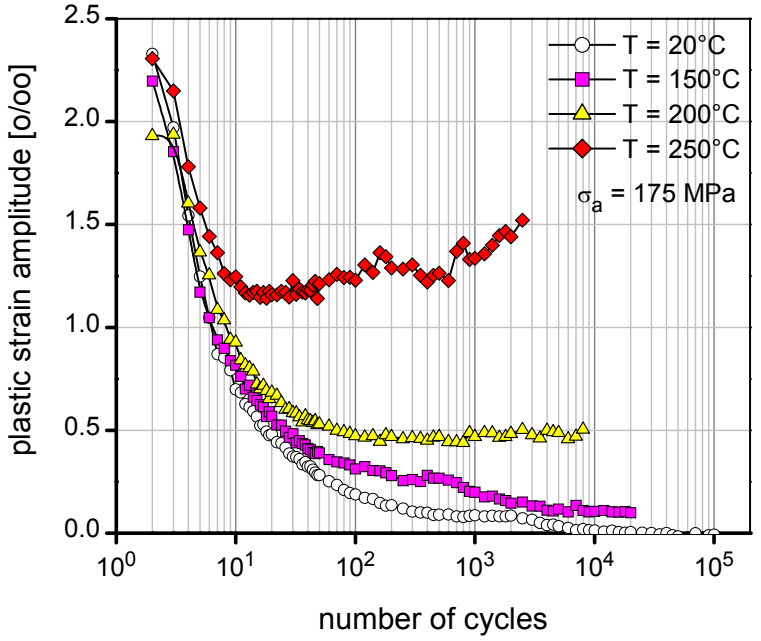

Figure 5.3: Cyclic deformation curves of polished AA5083 at an applied stress amplitude of 175 MPa for different test temperatures.

hardens and then exhibits cyclic softening during fatigue test as shown in Fig. 5.3 which demonstrates the cyclic deformation curves of polished AA5083 at an applied stress amplitude of 175 MPa for different test temperatures.

5.1.3 Cyclic deformation behavior of deep-rolled AA5083

Near-surface properties: After deep rolling (rolling pressure, p = 100 bar), from X-ray diffraction measurements, macroscopic compressive residual stresses as well as work hardening states at the surface and in near-surface regions were detected. Depth profiles of near-surface macroscopic compressive residual stresses and FWHM-values were plotted in Fig. 5.4. Maximum macroscopic compressive residual stresses of approximately -240 MPa in a depth of 30 µm were detected. The FWHM-values in the near-surface regions increase from approximately 1.4° of the bulk to 2.0° at the surface. Deep rolling not only induces near-surface macroscopic compressive residual stresses and work hardening states, but also increased near-surface hardnesses (see Fig 5.5). An increase of near-surface hardness by approximately 25 HV as compared to the bulk was observed after deep rolling.

Fatigue lifetime: Due to beneficial effects of deep rolling, e.g. increased near-surface hardnesses, induced near-surface macroscopic compressive residual stresses and work hardening states, fatigue lifetime enhancement of the deep-rolled condition was expected. Non-statistically evaluated s/n-curves of the deep-rolled AA5083 for different test temperatures were investigated as depicted in Fig. 5.6. At low or intermediate applied stress amplitudes, deep rolling enhances fatigue lifetime of AA5083 considerably as compared to the polished condition (see Fig. 5.2). For example, the fatigue lifetime at room temperature of the polished condition at an applied stress amplitude of 190 MPa is approximately 75,000 cycles whereas the fatigue lifetime of the deep-rolled condition for the same test condition increased dramatically to about 980,000 cycles. However, the beneficial effects of deep rolling were deteriorated during cyclic loading with increasing test temperature (see Fig. 5.7). Finally, deep rolling became ineffective when specimens were cyclically deformed at an applied stress amplitude of 190 MPa with a test temperature of 250°C.

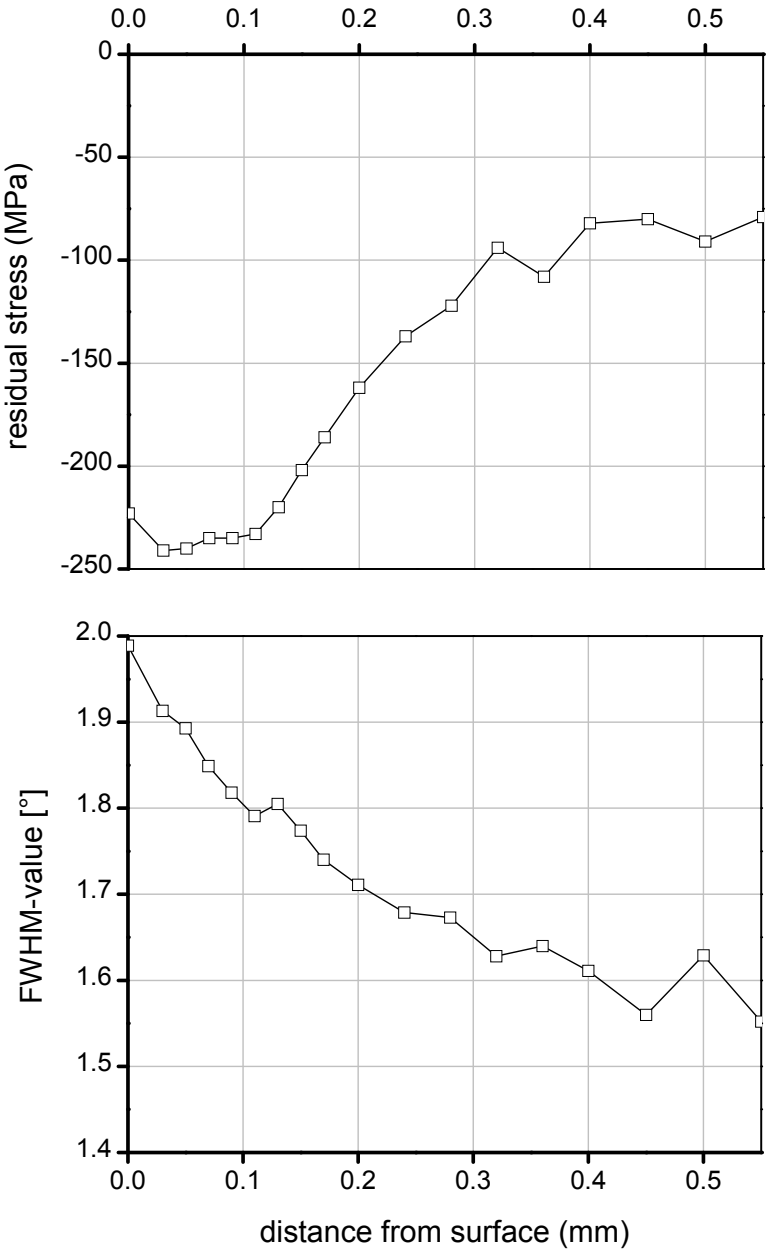

Figure 5.4: Depth profiles of near-surface macroscopic compressive residual stresses and FWHM-values of deep-rolled AA5083.

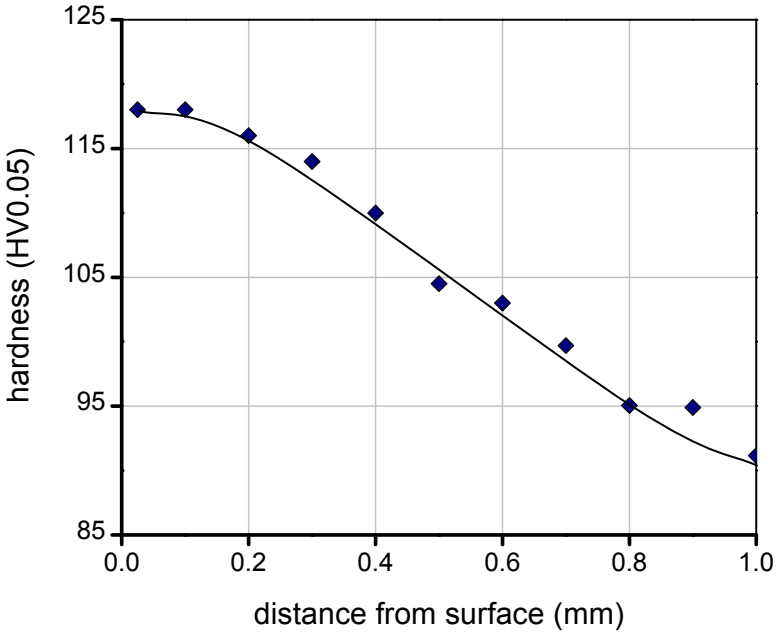

Figure 5.5: Depth profile of near-surface hardnesses of deep-rolled AA5083.

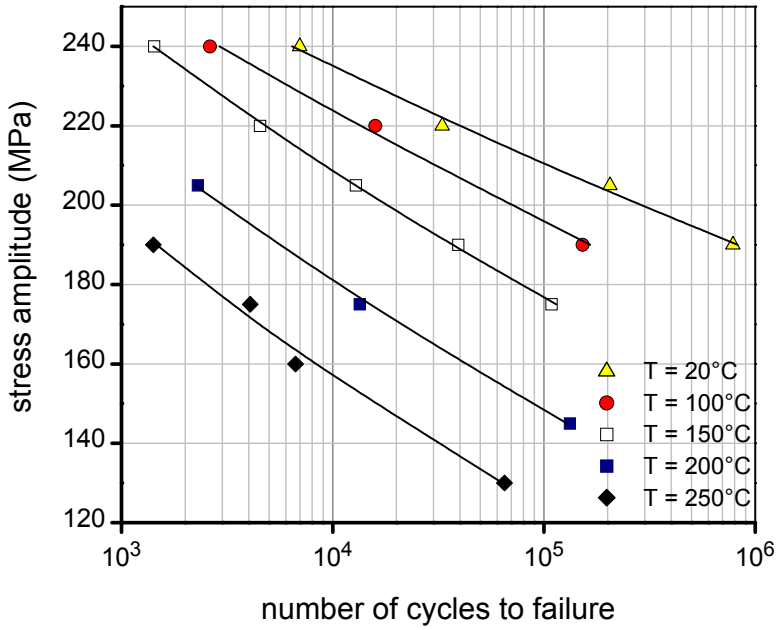

Figure 5.6: Non-statistically evaluated s/n-curves of deep-rolled AA5083 in the temperature range 20-250°C.

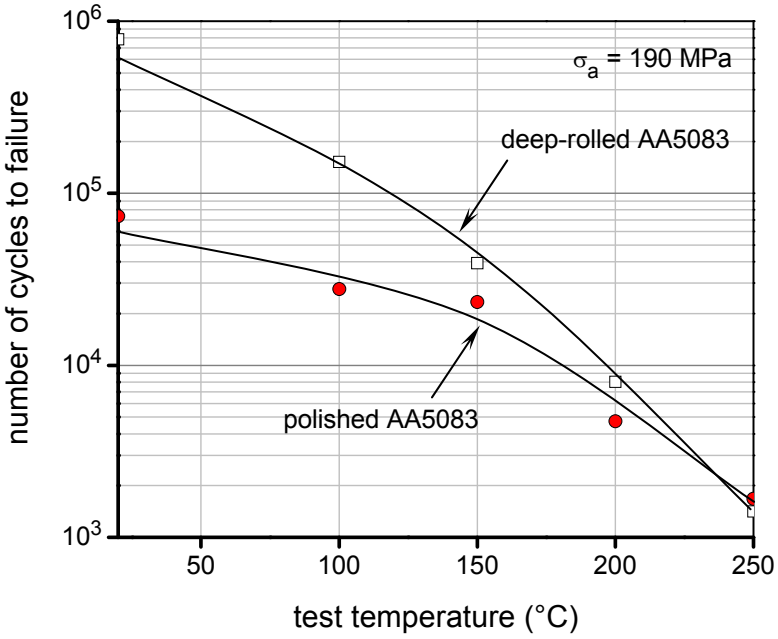

Figure 5.7: Fatigue lifetimes of polished and deep-rolled AA5083 at an applied stress amplitude of 190 MPa for different test temperatures.

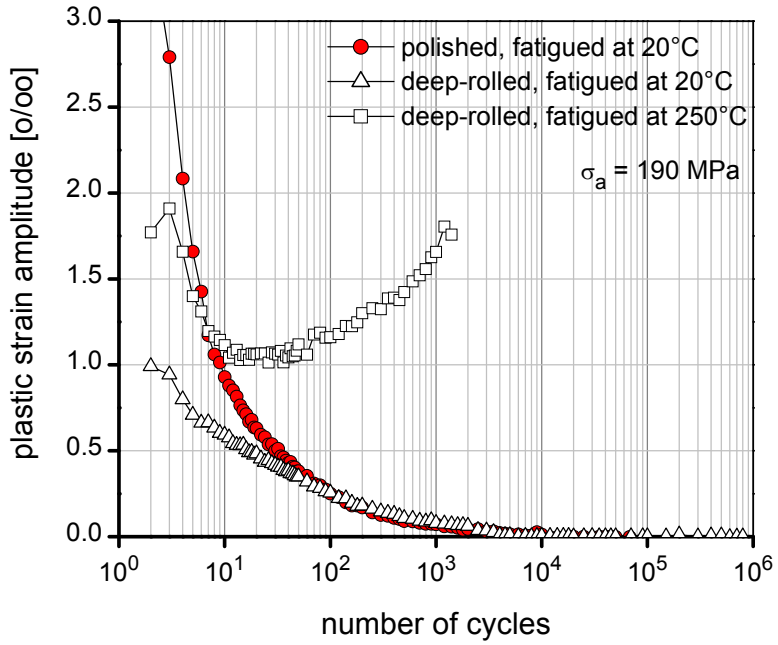

Figure 5.8: Cyclic deformation curves of polished and deep-rolled AA5083 at an applied stress amplitude of 190 MPa for different test temperatures.

Cyclic deformation curve: Similarly to the polished AA5083, the cyclic deformation behavior of the deep-rolled AA5083 exhibits also cyclic hardening for all applied stress amplitudes at room temperature. In all cases where beneficial effects of deep rolling on cyclic lifetime were observed, lower plastic strain amplitudes of the deep-rolled condition were normally detected as compared to the polished condition. Fig. 5.8 shows an example of the reduction of the plastic strain amplitudes of the deep-rolled condition during fatigue tests at an applied stress amplitude of 190 MPa at room temperature. At high test temperatures, a change from initially cyclic hardening to cyclic softening was also detected for the deep rolled condition (see Fig. 5.8).

5.1.4 Residual stress stability of deep-rolled AA5083

It is generally accepted that near-surface residual stress as well as work hardening relaxation occurs in principle during thermal and/or mechanical loading. During cyclic loading at room as well as elevated temperature, near-surface macroscopic compressive residual stresses relax partially or completely due to mechanical as well as thermomechanical relaxation, respectively. To investigate the mechanical residual stress relaxation, specimens were cyclically deformed to half the number of cycles to failure ($N_f/2$) at applied stress amplitudes of 205 and 240 MPa at room temperature. Afterwards, residual stress- and FWHM-value-depth profiles were measured as shown in Fig. 5.9. At an applied stress amplitude of 205 MPa at room temperature, macroscopic compressive residual stress relaxation at the surface and in near-surface regions occurs, whereas work hardening states seemed to be constant at this test condition. Macroscopic compressive residual stresses at the surface and in near-surface regions relaxed also at an applied stress amplitude of 240 MPa at room temperature. In this case instability of work hardening state was detected. For fatigue tests at elevated temperature, thermomechanical residual stress as well as FWHM-value relaxation was observed (Fig. 5.9). Thermomechanical relaxation was more pronounced than only mechanical relaxation due to combined simultaneous relaxation from both mechanical and thermal loading.

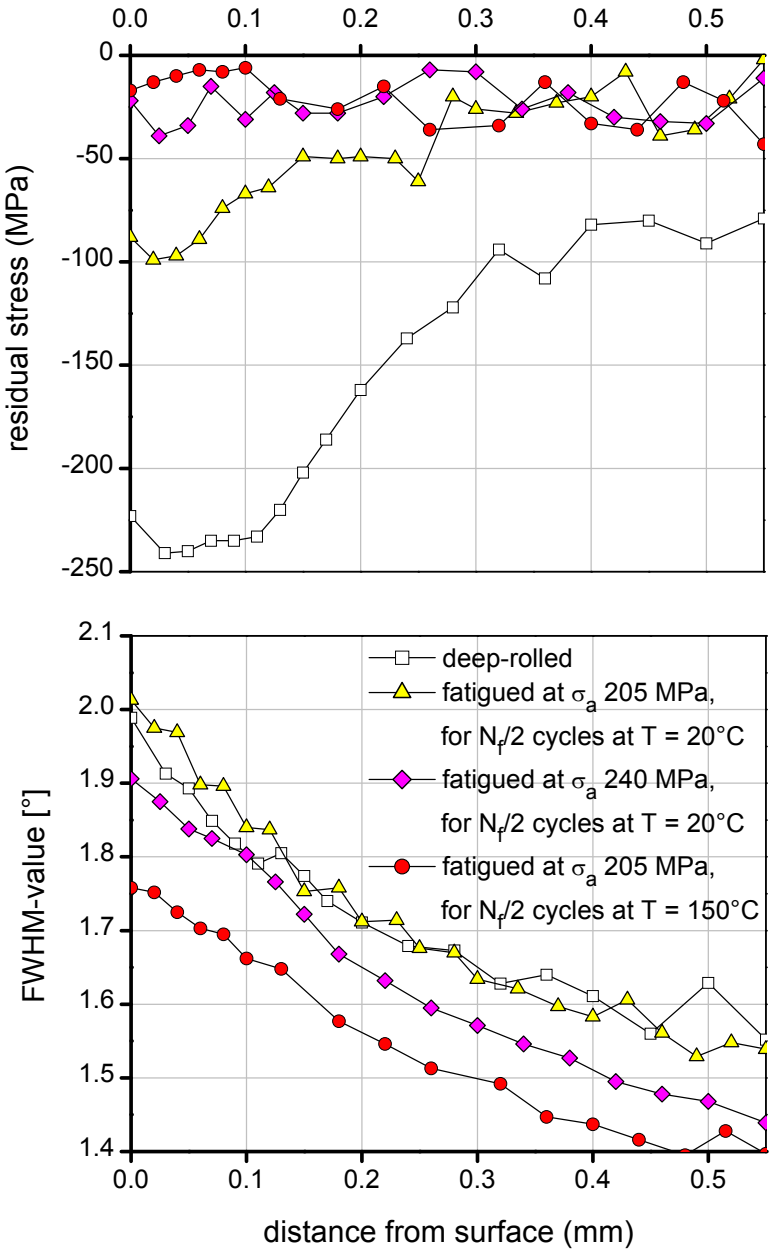

Figure 5.9: Residual stress- and FWHM-value-depth profiles of deep-rolled AA5083 after fatigue tests at half the number of cycles to failure at applied stress amplitudes of 205 MPa and 240 MPa at room and elevated temperatures.

5.2 Aluminium alloy AA6110

In this section, the experimental results on the cyclic deformation behavior of all differently aged conditions, namely as-quenched, under-, peak- and over-aged conditions will be presented (see Fig. 4.7). However, the mechanical properties of this alloy depend certainly on its precipitation characteristics, e.g. type, structure, distribution as well as morphology. Therefore, before studying the cyclic deformation behavior of this alloy, especially at elevated temperature, a detailed characterization of this alloy is carried out firstly and completely discussed in the next section. Afterwards, this information about the microstructure is reused to analyze the cyclic deformation behavior in the following sections.

5.2.1 Material characterization of AA6110

The aluminium alloy AA6110 was characterized using both direct and indirect analysis methods. Firstly, hardness and tensile tests as well as differential scanning calorimetry (DSC), were performed to analyze the precipitation sequence and the change in mechanical properties during ageing treatments. Afterwards, phase compositions and morphology were characterized using X-ray diffraction (XRD) and transmission electron microscopy (TEM).

Hardness test: To indirectly investigate the precipitation sequence as well as its kinetic, as-quenched specimens were aged for different ageing temperatures and times. During artificial ageing treatments, the hardnesses of the as quenched specimens were monitored and plotted in Fig. 5.10. Obviously, for the ageing temperature range 160-250°C, the hardness of the as-quenched condition increased continuously with increasing ageing time until reaching a maximum value. The maximum hardnesses of approximately 140, 132 and 126 HV were measured after ageing at temperature of 160, 200 and 250°C for ageing times of approximately 12, 1 hour(s) and 300 seconds, respectively. The precipitation phases, β´´, β´ as well as Q´ are expected to lead to the increased hardness of copper-containing Al-Mg-Si aluminium alloys after artificial ageing treatments [1,112,113]. It is noteworthy that lower maximum hardness values after high temperature ageing treatments were detected. This might be due to the fact that

precipitates which occurred at a relative high ageing temperature have larger size and relative low volume fraction [1].

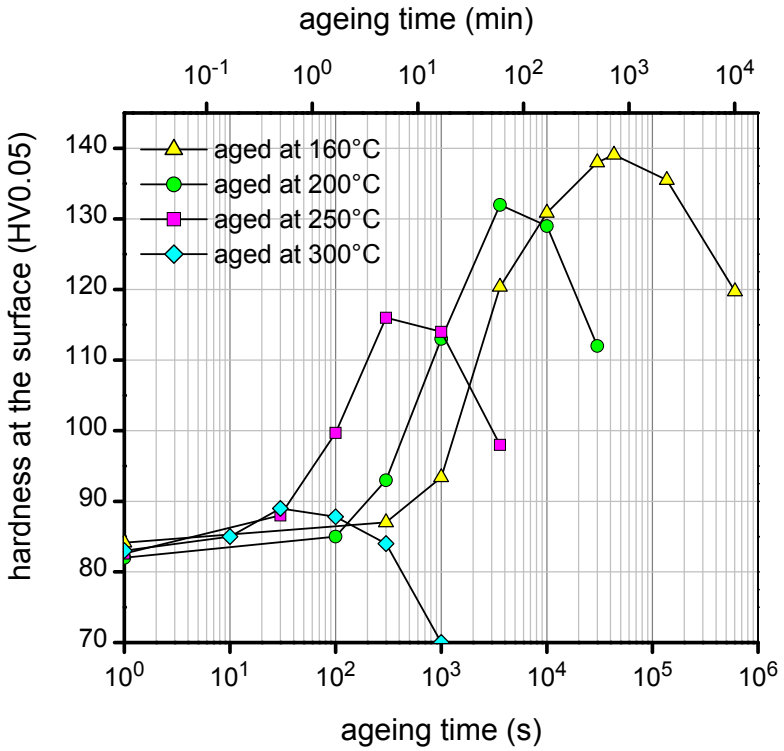

Figure 5.10: Hardnesses of AA6110 as a function of ageing time for different ageing temperatures.

Tensile test: Quasistatic tensile tests were conducted on the as-quenched, under-, peak- and over-aged conditions which were designated in section 4.1.2. Engineering stress-strain curves at room temperature were plotted in Fig. 5.11. Increased 0.2% yield and ultimate tensile strengths were observed after the ageing treatments. It strongly hints that precipitates β´´, β´ as well as Q´ occurred during the ageing treatment at a temperature of 160°C and contributed to the mechanical properties of this alloy. For the peak- and over-aged conditions, a comparatively low work hardening rate ($d\sigma/d\varepsilon$) was detected as compared to the as-quenched and under-aged conditions. It indicates that precipitates in the peak- and over-aged conditions are coherent as well as semi-coherent with the matrix and dislocations move continuously through the precipitates [115,116]. An overview of the tensile and hardness properties of differently aged AA6110 is given in table 5.1.

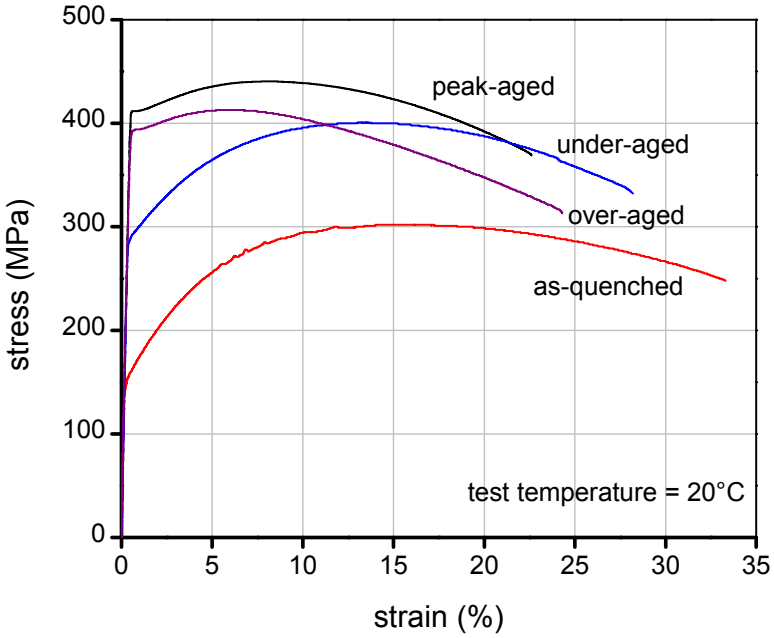

Figure 5.11: Engineering stress-strain curves of differently aged AA6110.

Table 5.1: Hardness and tensile properties of differently aged AA6110.

Condition	Ageing parameter	Hardness [HV0.05]	$\sigma_{0.2}$ [MPa]	UTS [MPa]	Elongation [%]
as-quenched	-	84	155	302	33
under-aged	160°C, 1 hour	120	292	400	28
peak-aged	160°C, 12 hours	139	425	455	22
over-aged	160°C, 168 hours	119	393	413	24

Differential scanning calorimetry (DSC): To investigate precipitation sequences during the ageing treatment, DSC was performed on the as-quenched, under-, peak- and over-aged conditions in the temperature range 50-350°C using heating rates of 10°C/minute. The results are shown in Fig. 5.12. From this diagram, four important peaks of the as-quenched condition were detected:

1) An exothermic peak I in the temperature range 55-125°C was seen. At low temperature, occurring GP-I zones which consist of clusters of Mg and/or Si atoms are probably related with this peak [74,75,79,80].

2) An endothermic peak II occurred in the temperature range of about 125-225°C due to the dissolution of the GP-I zones (clusters of Mg atoms) [79,95,96].

3) A large exothermic peak III, which occurred in the temperature range of approximately 225-260°C, corresponds to the formation of β´´ precipitates of the as-quenched AA6110 [74,75,79-83,85,90,95,96].

4) An exothermic peak IV relates to the precipitation of β´ [74,75,79,81-83,85,95,96] as well as Q´ [80,90].

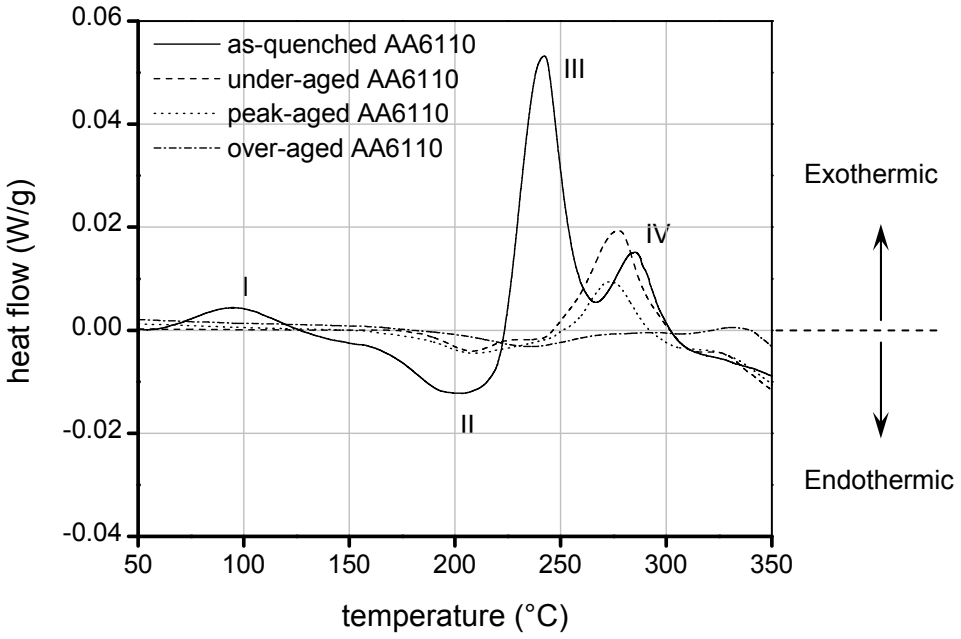

Figure 5.12: DSC thermograms of differently aged AA6110.

For the under- and peak-aged AA6110, the disappearance of the peaks I, II and III were observed. That might be due to the fact that the major precipitates of the AA6110 are β´´ phases and the under- and peak-aged conditions possibly possessed initiated precipitates β´´ before DSC investigation. Therefore, peaks I, II and III of DSC thermogram attributed to formation and dissolution of GP-I zones and occurring of precipitates β´´ were not seen. Moreover, from this diagram, it can be mentioned that precipitates β´´ were formed during ageing at 160°C and precipitates β´ transform from initiated precipitates β´´ of the under- and peak-aged AA6110. Formation of precipitates β´ of the peak-aged condition during DSC test seems to be less pronounced than of the under-aged condition. It can be assumed

that the peak-aged condition possessed already some precipitates β´ in the matrix before DSC investigations. For over-aged conditions, no significant peaks were seen. It is possible that precipitates in this condition are almost semi-coherent precipitates β´.

X-ray diffraction (XRD): It is known that phases/compounds can be analyzed using XRD. However, as mentioned in section 3.1.2.1, XRD becomes a difficult task when the phases/compounds and their volume fraction are relatively small, such as precipitates in aluminium alloys. Accordingly, the β (Mg_2Si) phases were not found by XRD even for the over-aged condition (see Fig. 5.13). A pre-ageing technique [93,97-99] was applied to attempt producing a higher volume fraction of precipitates in the aluminium alloy AA6110. An as-quenched specimen was shortly pre-aged at a temperature of 200°C for 100 seconds followed by secondary ageing at the same ageing temperature of 200°C for 300 seconds. Subsequently, XRD was conducted once more to analyze the precipitates of the aluminium alloy AA6110. Finally, some precipitated phases were detected in the diffraction angle 2θ range between 50-80° as shown in Fig. 5.13. The β (Mg_2Si) phases were found for 2θ = 57.647°, 63.387°, 65.204° and 72.380° after pre-ageing subsequently ageing treatment at temperatures of 200°C. The stable quaternary phases AlFeMnSi were also observed for of 52.425 and 56.400°2θ. Actually, the X-ray diffraction peaks of the AlFeMnSi phases were also observed in the as-quenched and over-aged conditions, but their intensities were not so pronounced (see Fig. 5.13). The stable quaternary phases AlFeMnSi were also found in aluminium alloy AA6013 as documented in [112].

Transmission electron microscopy (TEM): Transmission electron microscopy was also performed to observe the microstructure as well as precipitates of the under-, peak- and over-aged AA6110 as shown in Figs. 5.14 (a), (b) and (c), respectively. Stable quaternary phases AlFeMnSi about 100 nm in size were observed as in aluminium alloy AA6013 [112]. After ageing at 160°C for 1 hour, very fine clusters/precipitates β´´ are embedded within the matrix of the under-aged AA6110. Precipitates β´´ were seen also in the peak-aged condition aged at 160°C for 12 hours. Relative coarsened precipitates β´ were found in the over-aged condition. Results of microstructures in Figs 5.14 (a)-(c) show an excellent

correlation with other direct/indirect characterization methods mentioned above. Characteristic microstructures of AA6110 were summarized in table 5.2.

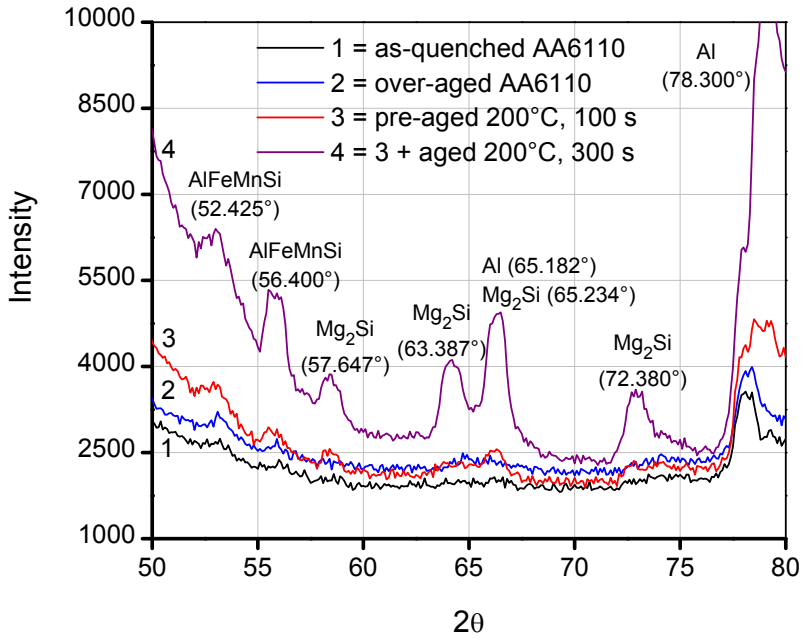

Figure 5.13: Phase analysis of differently aged AA6110 using X-ray diffraction.

Table 5.2: Characteristic microstructures of differently aged AA6110.

Condition	Characteristic microstructures
as-quenched	no effective precipitates β´´ in the matrix described using DSC thermogram
under-aged	DSC and TEM investigations confirm occurring very fine clusters of precipitates β´´
peak-aged	precipitates β´´ are fine and effective in size and structure
over-aged	precipitates change/grow to precipitates β´

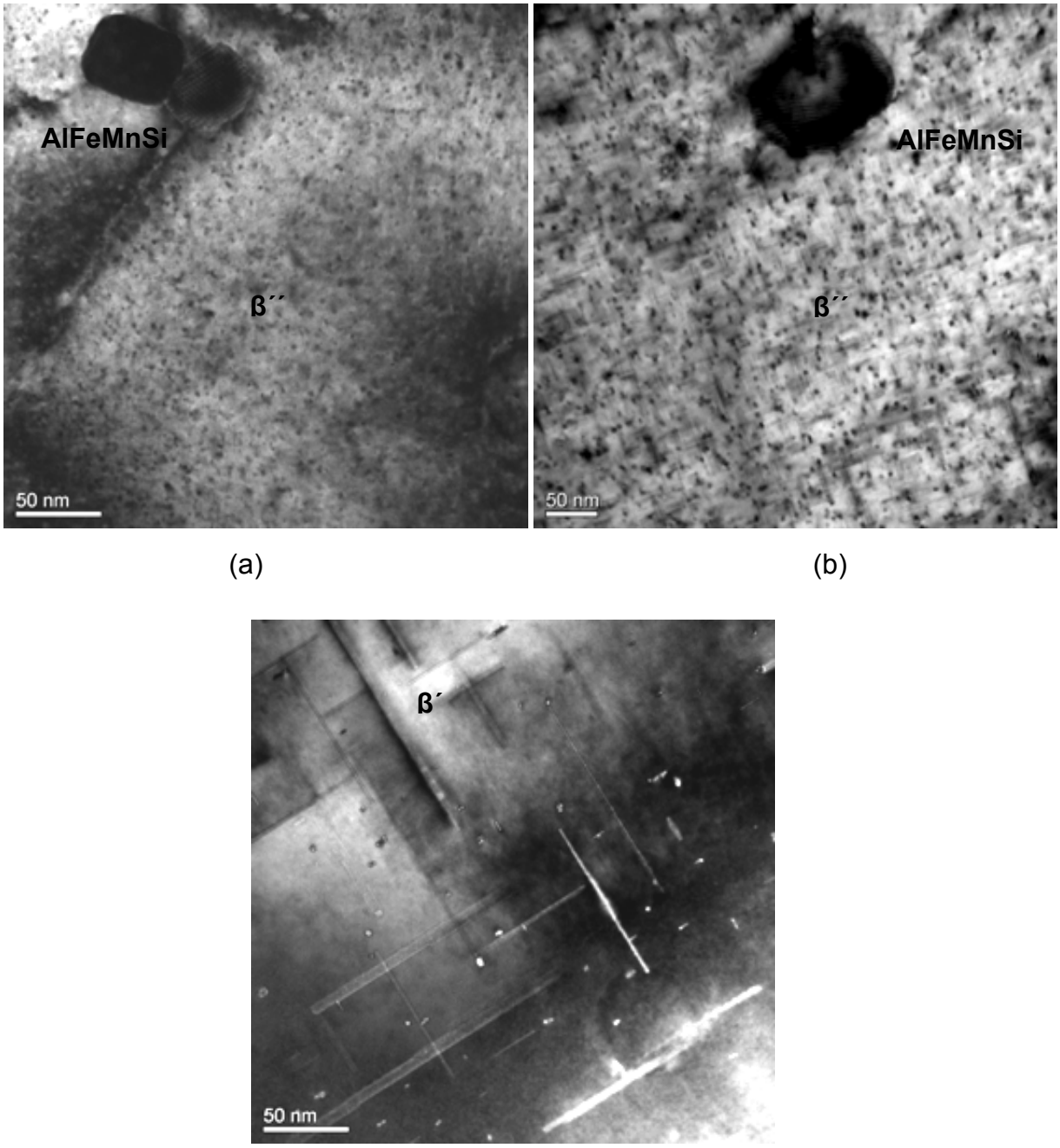

Figure 5.14: Microstructure of (a) under-aged, (b) peak-aged and (c) over-aged AA6110 using transmission electron microscopy.

5.2.2 As-quenched AA6110

Normally, tensile as well as fatigue properties of aluminium alloys decrease at elevated temperatures. However, for the as-quenched condition, static/dynamic precipitation occurs and coherent, semi-coherent and incoherent precipitates alter the mechanical properties continuously during exposure/loading at elevated temperature. Consequently, it can be expected that static/dynamic precipitation contribute significantly to the mechanical properties.

5.2.2.1 Quasistatic deformation behavior of as-quenched AA6110

Engineering stress-strain curves of the as-quenched condition for different test temperatures are shown in Fig. 5.15. As expected, an increase of the 0.2% yield strength of the as-quenched specimen was observed with increasing test temperature. The 0.2% yield strength increased from approximately 155 MPa at room temperature to approximately 245 MPa at a test temperature of 200°C. Subsequently, the 0.2% yield strength decreased at a test temperature of 250°C to approximately 190 MPa. The ultimate tensile strength as well as the work hardening rate decreased continuously with increasing test temperature. Due to

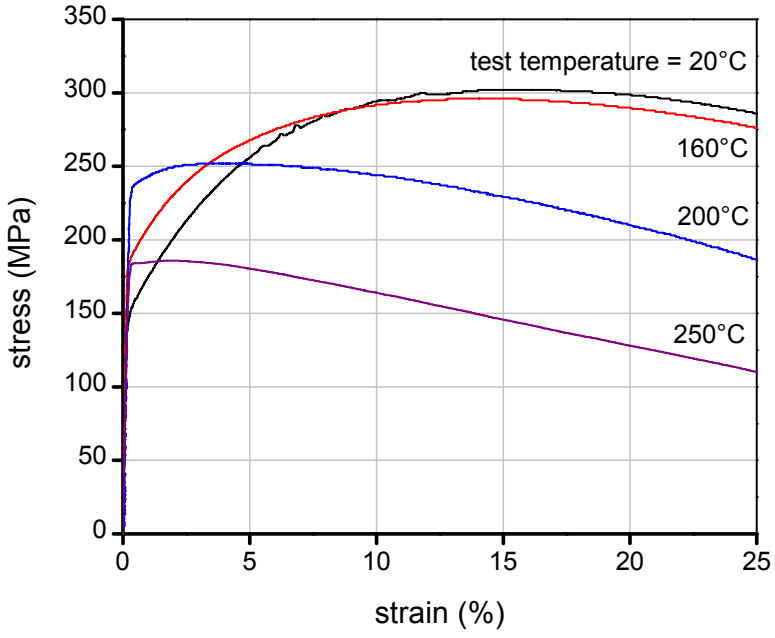

Figure 5.15: Engineering stress-strain diagram of as-quenched AA6110 for different test temperatures.

the influence of temperature on tensile strength in Fig. 5.15, a significant impact of temperature as well as static/dynamic precipitates on the fatigue behavior was expected which is demonstrated in the following results.

5.2.2.2 Cyclic deformation behavior of polished as-quenched AA6110

Fatigue lifetime: Normally, fatigue lifetimes decrease with increasing temperature, however during fatigue tests in the temperature range 100-200°C the static/dynamic precipitation occurs and affects the fatigue lifetimes of the polished as-quenched AA6110 (see Fig. 5.16). For example, the fatigue lifetime at room temperature of the polished as-quenched condition at an applied stress amplitude of 225 MPa is about 30,000 cycles, whereas at a test temperature of 100°C for the same applied stress amplitude, the fatigue lifetime increases to approximately 50,000 cycles. For a test temperature of 250°C, lower fatigue lifetimes of approximately 12,000 cycles were measured.

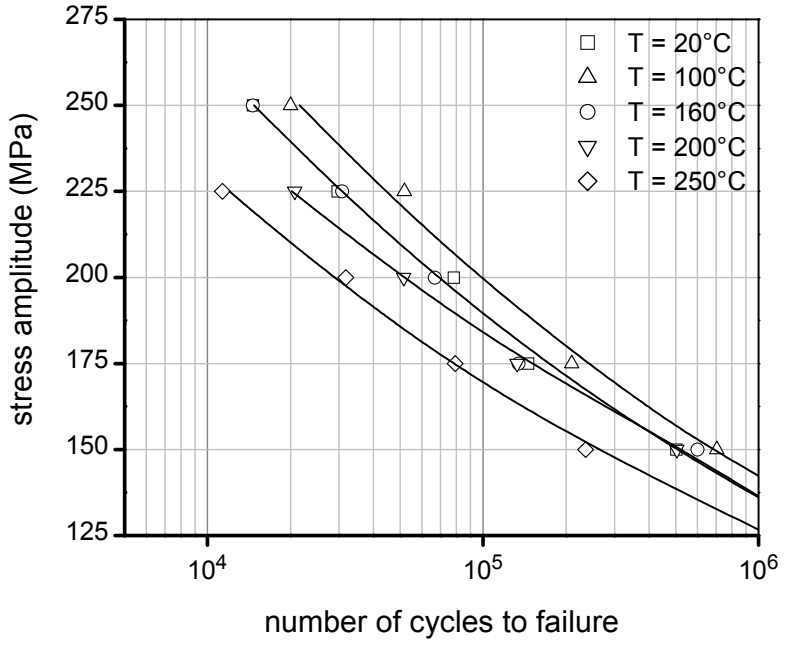

Figure 5.16: Non-statistically evaluated s/n-curves of polished as-quenched AA6110 in the temperature range 20-250°C.

Cyclic deformation curve: At room as well as elevated temperatures up to 250°C, the polished as-quenched condition exhibits cyclic hardening during fatigue tests as shown in Fig. 5.17 presenting the cyclic deformation curves of the polished as-quenched condition at an applied stress amplitude of 225 MPa for different test temperatures. Increasing plastic strain amplitudes with increasing test temperature were normally observed, except for a test temperature of 100°C.

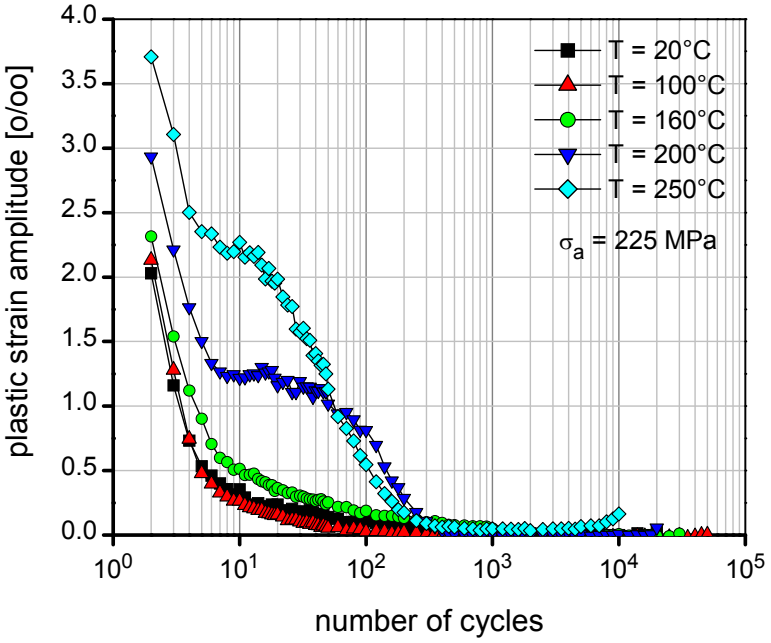

Figure 5.17: Cyclic deformation curves of polished as-quenched AA6110 at an applied stress amplitude of 225 MPa for different test temperatures.

5.2.2.3 Cyclic deformation behavior of deep-rolled as-quenched AA6110

Near surface properties: The near-surface properties of the deep-rolled as-quenched AA6110 were investigated using X-ray diffraction measurements and microhardness tests as shown in Figs. 5.18 and 5.19. Deep rolling induces principally macroscopic compressive residual stresses as well as work hardening states and increased hardnesses at the surface and in near-surface regions. For the chosen deep rolling parameters, the strain hardened layer was about 0.7 mm thick. A maximum macroscopic compressive residual stress value of -266 MPa was measured directly at the surface, while the FWHM-values increased from

approximately 1.1° of the bulk to 2.3° at the surface of the deep-rolled as-quenched condition. An increase of near-surface hardness by approximately 15 HV as compared to the bulk was observed after deep rolling.

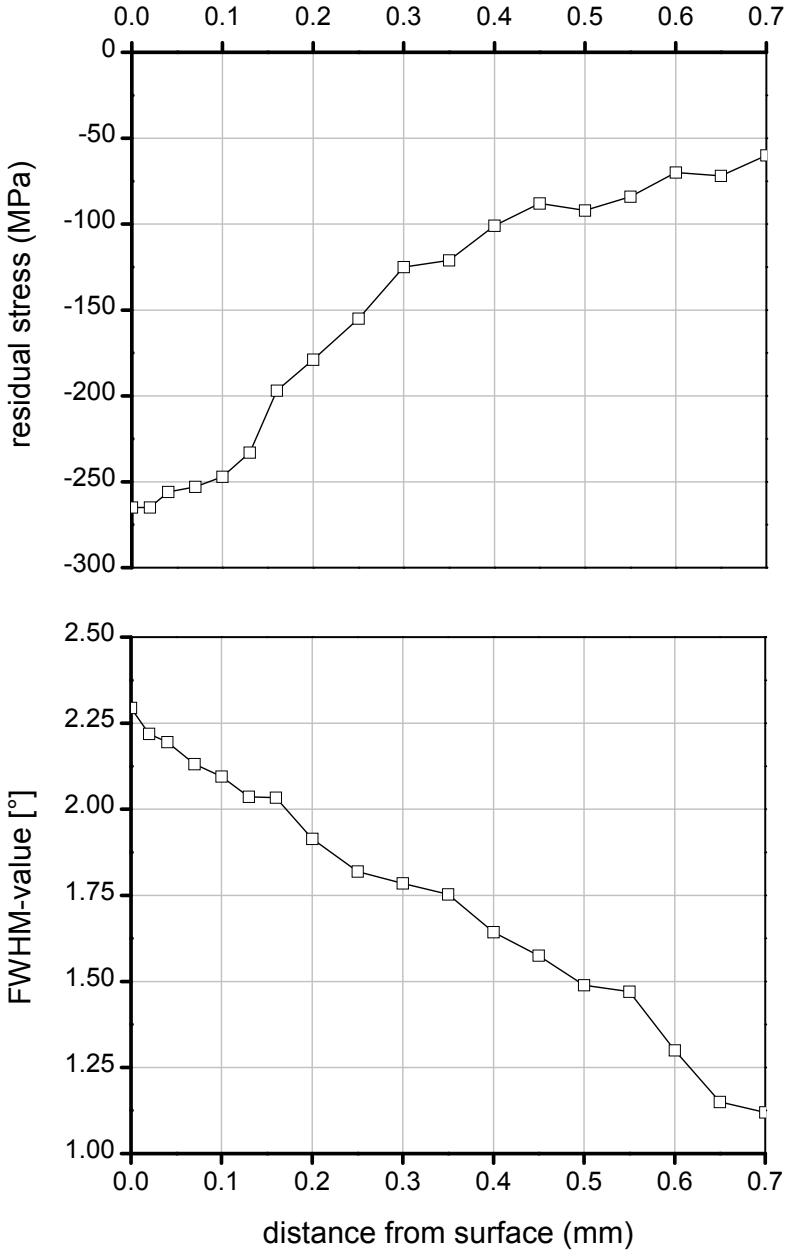

Figure 5.18: Depth profiles of near-surface macroscopic compressive residual stresses and FWHM-values of deep-rolled as-quenched AA6110.

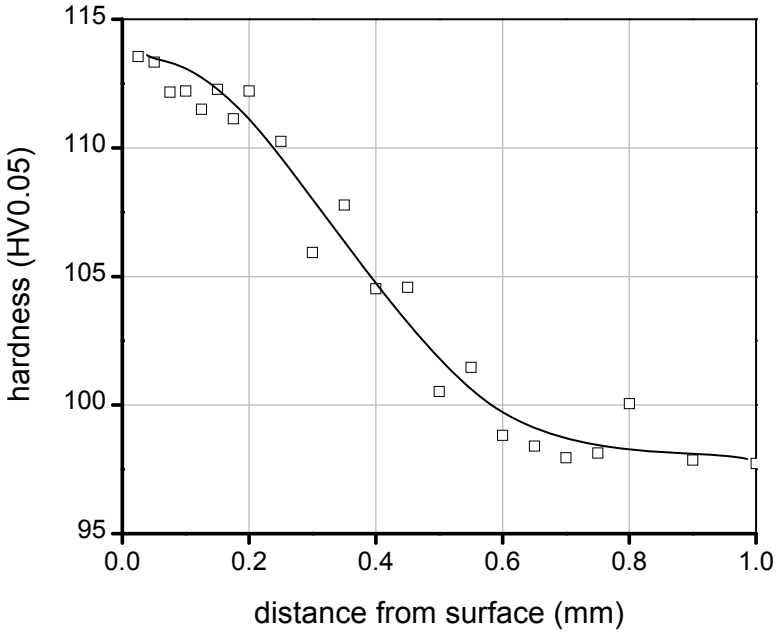

Figure 5.19: Depth profile of near-surface hardnesses of deep-rolled as-quenched AA6110.

Fatigue lifetime: Non-statistically evaluated s/n-curves of the deep-rolled as-quenched AA6110 for different test temperatures are presented in Fig. 5.20. An increase of test temperatures shifts the s/n-curves to lower fatigue lifetime, i.e. the fatigue lifetime of the deep-rolled as-quenched condition at an applied stress amplitude of 175 MPa is about 1,000,000 cycles at room temperature, whereas at a test temperature of 250°C for the same stress amplitude the fatigue lifetime is reduced to roughly 75,000 cycles. However, in most cases a pronounced fatigue lifetime enhancement of the deep-rolled as-quenched condition as compared to the polished as-quenched condition was observed. For example, the fatigue lifetime of the polished as-quenched condition at an applied stress amplitude of 175 MPa at room temperature is only about 150,000 cycles. The beneficial effects of deep rolling decreased during cyclic loading with increasing test temperature (see Fig. 5.21). Finally, deep rolling became ineffective in terms of fatigue lifetime enhancement at a test temperature of 250°C.

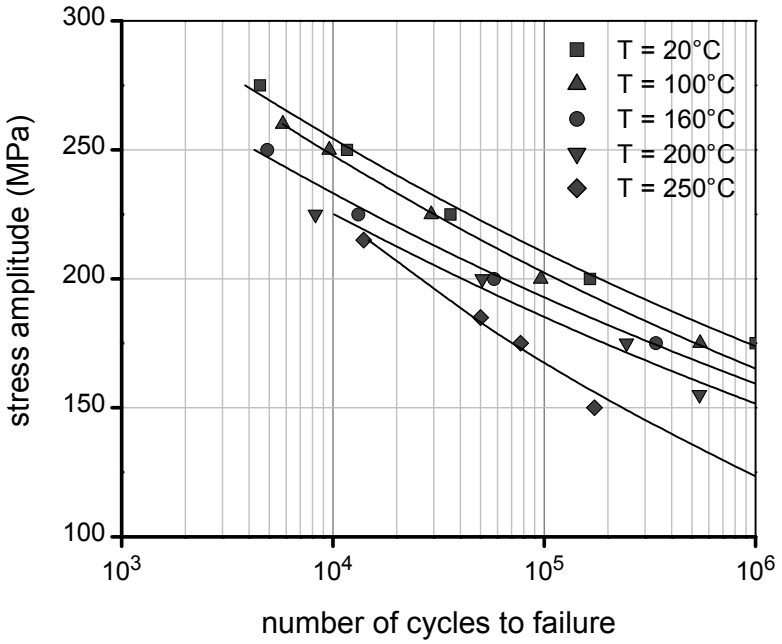

Figure 5.20: Non-statistically evaluated s/n-curves of deep-rolled as-quenched AA6110 in the temperature range 20-250°C.

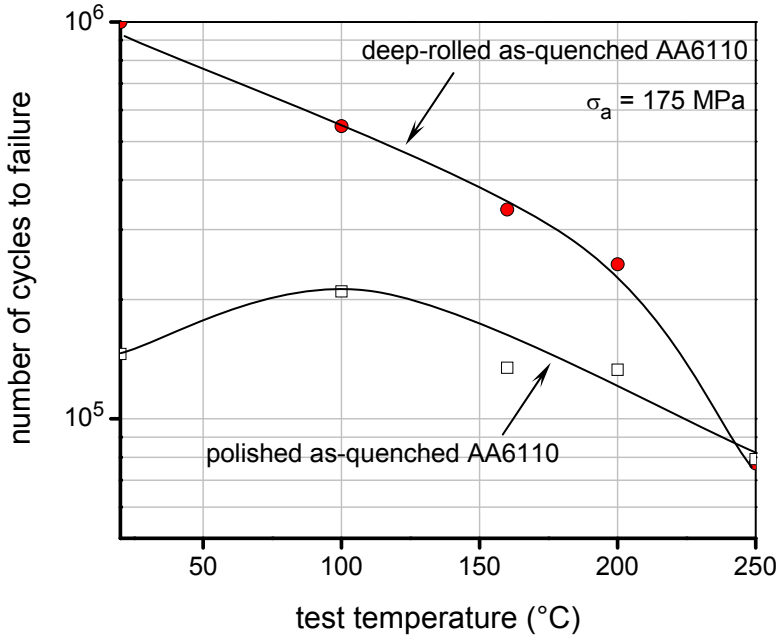

Figure 5.21: Fatigue lifetimes of polished and deep-rolled as-quenched AA6110 at an applied stress amplitude of 175 MPa for different test temperatures.

Cyclic deformation curve: Similarly to the polished as-quenched condition, the deep-rolled as-quenched condition shows also cyclic hardening at room and elevated temperatures. Lower plastic strain amplitudes of the deep-rolled as-quenched condition were generally detected as compared to the polished as-quenched condition as depicted in Fig. 5.22.

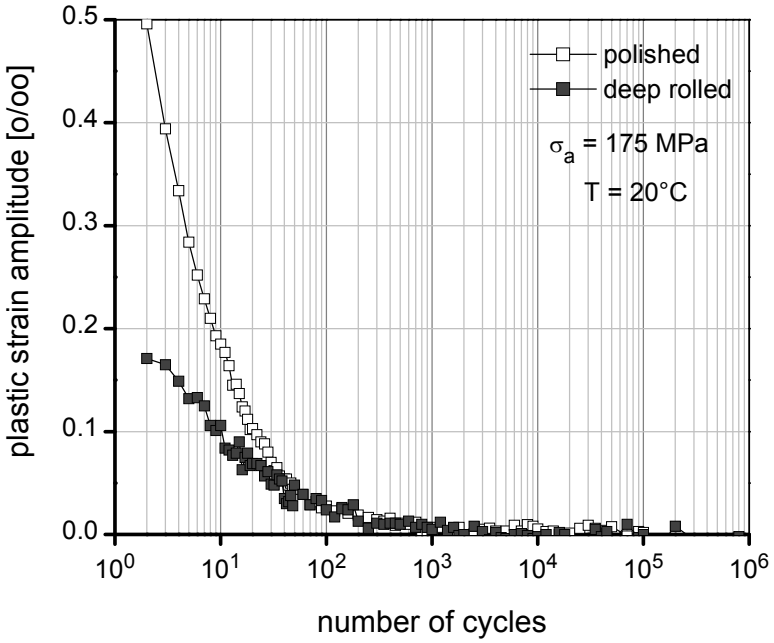

Figure 5.22: Cyclic deformation curves of polished and deep-rolled as-quenched AA6110 at an applied stress amplitude of 175 MPa at room temperature.

5.2.2.4 Residual stress stability of deep-rolled as-quenched AA6110

During cyclic loading or exposure at elevated temperature, mechanical or thermal residual stress relaxation occurs. However, residual stress relaxation during cyclic deformation at elevated temperature is more complicated because mechanical and thermal residual stress relaxations occur at the same time. As a simple approximation, the separate assessment of mechanical and thermal residual stress relaxation might be helpful to analyze the thermomechanical residual stress relaxation of the deep-rolled condition. Therefore, mechanical as well as thermal residual stress relaxation should be firstly investigated. However, mechanical

properties of the as-quenched AA6110 can be more or less altered during exposure at room temperature due to occurring precipitates as well as GP-zones. Accordingly, mechanical residual stress relaxation of the deep-rolled as-quenched AA6110 was not investigated. Nevertheless, thermal residual stress relaxation of the deep-rolled as-quenched AA6110 was intensively investigated and analyzed. Thermomechanical residual stress relaxation was investigated and analyzed through the residual stress- and FWHM-value-depth profiles of the selected fatigued specimens.

Thermal residual stress relaxation: The deep-rolled as-quenched specimens were heated in the temperature range 50-300°C with exposure times up to approximately 1 week to investigate residual stress as well as work hardening relaxation. Thermal residual stress relaxation can be described using a Zener-Wert-Avrami function in equations (2) and (3). Fig 5.23 depicts an experimental verification in the diagram of $\log \ln(\sigma_0^{RS} / \sigma^{RS})$ as a function of log t_a for a constant ageing temperature T_a. The measured data are fitted by a straight line of slope m = 0.17. The activation enthalpy can be also estimated by a slope of the diagram of log t_a versus $1/kT_a$ in Fig. 5.24. The activation enthalpy for the 50% residual stress relaxation process ΔH_{RS} = 1.63 eV and B_{RS} = 4.53 x 10^{15} min^{-1} were determined. Quantitative indications about the near-surface work hardening states can be obtained directly from measurements of the full width at half maximum (FWHM) values of the X-ray diffraction peaks. It seems likely that the temperature and time dependence of the FWHM-value decrease is related to the residual stress relaxation. Indeed, the reductions of the FWHM-values are quite similar to the relaxation of the residual stresses. The Zener-Wert-Avrami function was used once more to describe the FWHM-value decrease. The difference between the FWHM-values after ageing and the initial FWHM-value of 1.1° of the polished as-quenched specimen substitutes the ratio $\sigma^{RS} / \sigma_0^{RS}$ in equation (2). Table 5.2 exhibits the material constants, i.e. m, ΔH and B for the 50% FWHM-value as well as residual stress relaxation which are determined using the experimental data. The calculated curves of the residual stress as well as FWHM-value relaxation using the respective constants are shown in Fig. 5.25 as solid lines.

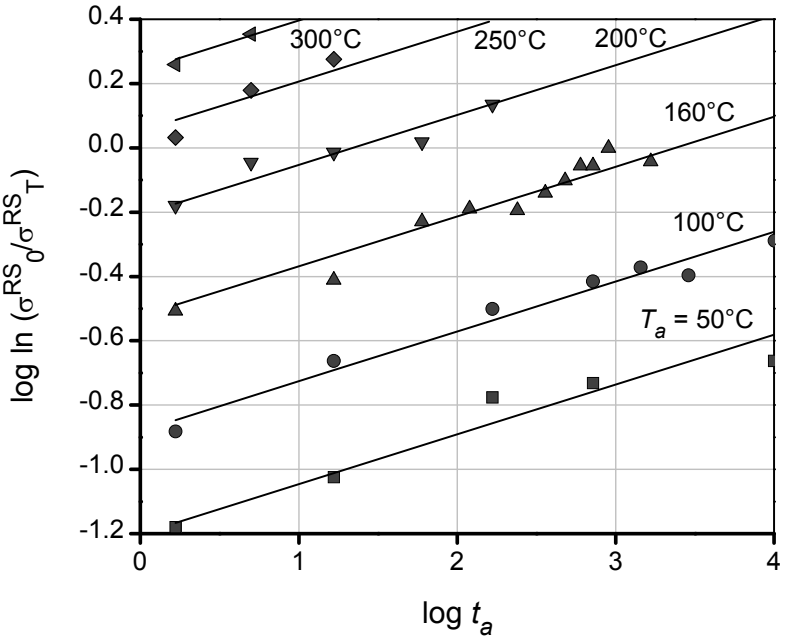

Figure 5.23: Influence of ageing time and temperature on surface residual stress of deep-rolled as-quenched AA6110 in a $\log \ln\left(\sigma_0^{RS}/\sigma_T^{RS}\right)$ versus log t_a diagram.

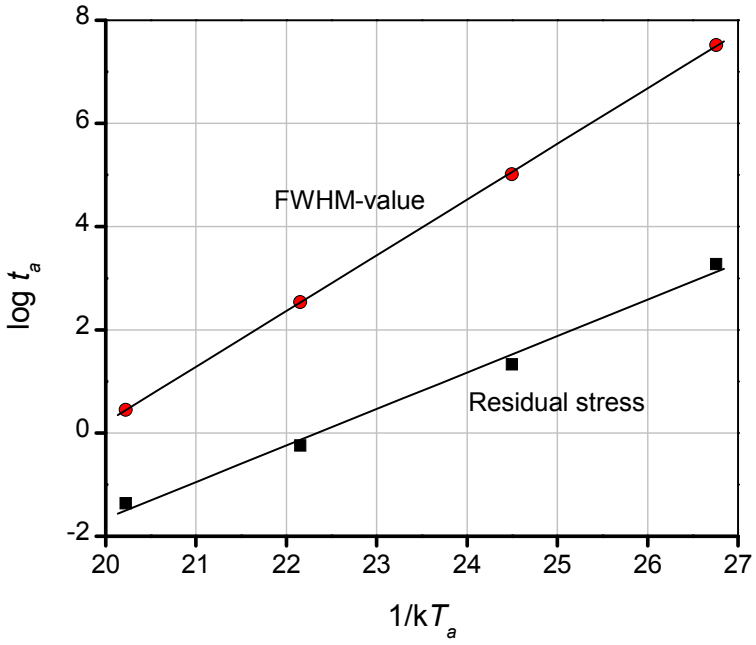

Figure 5.24: Plot of log t_a versus 1/kT_a for the determination of Avrami approach parameters of deep-rolled as-quenched AA6110 for 50% residual stress as well as FWHM-value relaxation.

Table 5.2: Determined materials constants of thermal residual stress and FWHM-value relaxation of deep-rolled as-quenched AA6110.

As-quenched AA6110	*m*	Δ*H* (eV)	*B* (min^{-1})
Residual stress relaxation	0.17	1.63	4.53×10^{15}
FWHM-value relaxation	0.12	2.48	2.13×10^{21}

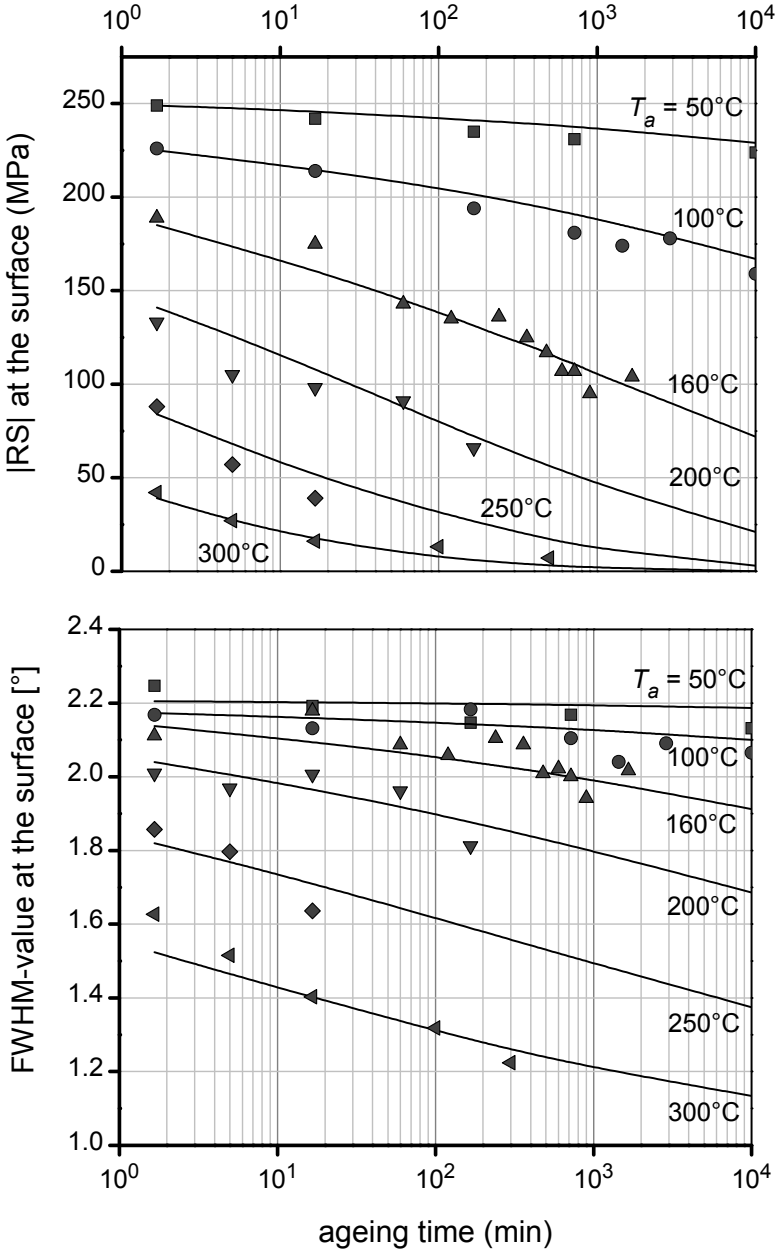

Figure 5.25: Influence of ageing time and temperature on the absolute values of residual stresses and FWHM-values at the surface and their description by the Avrami approach for deep-rolled as-quenched AA6110.

Thermomechanical residual stress relaxation: Three conditions of fatigue tests at elevated temperature were selected to analyze the thermomechanical residual stress as well as FWHM-value relaxation: firstly, the deep-rolled as-quenched condition was heated at a temperature of 160°C for 10 minutes without any applied stress amplitude to obtain a reference state; secondly and thirdly, the deep-rolled as-quenched specimens were fatigued at stress amplitudes of 150 and 250 MPa at 160°C for 1,000 cycles, respectively. Residual stress and FWHM-value-depth profiles of these three selected conditions were measured as compared to the deep-rolled as-quenched condition before heating and loading as shown in Fig. 5.26. Residual stress as well as FWHM-value relaxation at the surface and in near-surface regions can be seen after exposure at a temperature of 160°C for 10 minutes due to thermal relaxation which can be described by applying the Zener-Wert-Avrami function. Thermomechanical residual stress relaxation was also detected after fatigue tests at applied stress amplitudes of 150 and 250 MPa at a test temperature of 160°C for 1,000 cycles. However, near-surface work hardening states (FWHM-values) of the specimen which was fatigued at a stress amplitude of 150 MPa at a test temperature of 160°C for 1,000 cycles appear to be stable as compared to a reference. Moreover for this testing condition, deep rolling can enhance the fatigue lifetime. In contrast, instability of near-surface work-hardening states of the specimen which was fatigued at stress amplitude of 250 MPa at a test temperature of 160°C for 1,000 cycles is obvious. For this test condition (see Figs. 5.16 and 5.20), deep rolling was ineffective for fatigue lifetime enhancement.

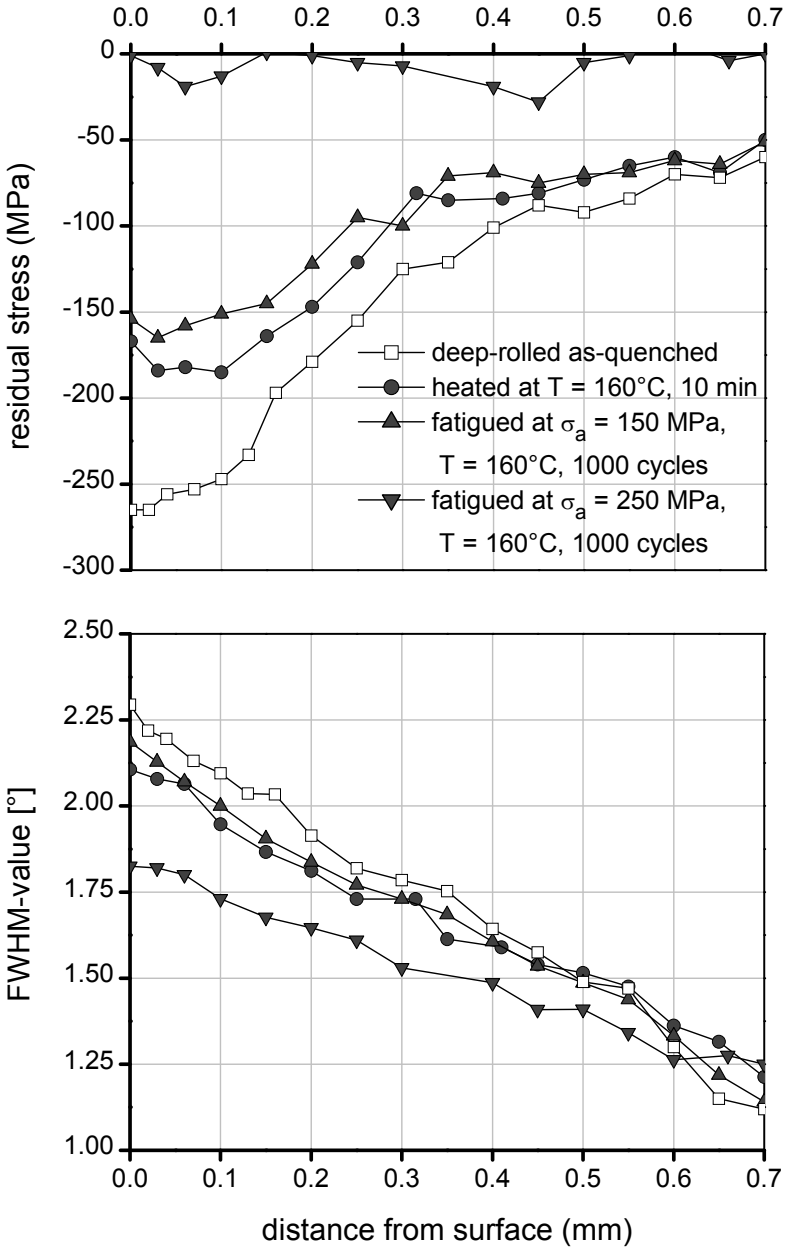

Figure 5.26: Residual stress- and FWHM-value-depth profiles of fatigued as well as heated specimens of deep-rolled as-quenched AA6110.

5.2.3 Under-aged AA6110

The as-quenched aluminium alloy AA6110 was aged at a temperature of 160°C for only 1 hour to simulate the under-aged condition. Precipitates of the under-aged condition can still be altered and then contribute to the mechanical properties during tensile or fatigue tests at elevated temperatures, similarly as in the as-quenched condition. However, the degree of the change of precipitates in the under-aged condition should be less than the as-quenched condition. It is known that fatigue lifetimes of the deep-rolled condition depend strongly on the near-surface properties which can change during cyclic loading at room as well as elevated temperature. This determines the mechanical properties due to static/dynamic precipitation and decreased near-surface macroscopic residual stresses and work hardening through the relaxation process. Therefore, the effects of decreased macroscopic compressive residual stresses, work hardening states and altered precipitates on the fatigue lifetime and cyclic deformation behavior of the under-aged condition shall be investigated.

5.2.3.1 Quasistatic deformation behavior of under-aged AA6110

The engineering stress-strain tensile curves of the non-surfaced-treated under-aged AA6110 in the temperature range 20-250°C are shown in Fig. 5.27. From this diagram, the 0.2% yield as well as ultimate tensile strengths decreased continuously with increasing test temperature although precipitates can still be altered during the test and contribute to the mechanical properties. At room temperature, the 0.2% yield strength is approximately 290 MPa, whereas at temperatures of 160, 200 and 250°C, the 0.2% yield strengths are reduced to about 280, 275 and 180 MPa, respectively. It indicates that the 0.2% yield as well as the ultimate tensile strengths can not be fully recovered by altered static/dynamic precipitation during tensile tests at elevated temperatures. This might be due to the fact that the precipitation process requires not only suitable ageing temperature but also sufficient exposure times to contribute significantly to the mechanical properties.

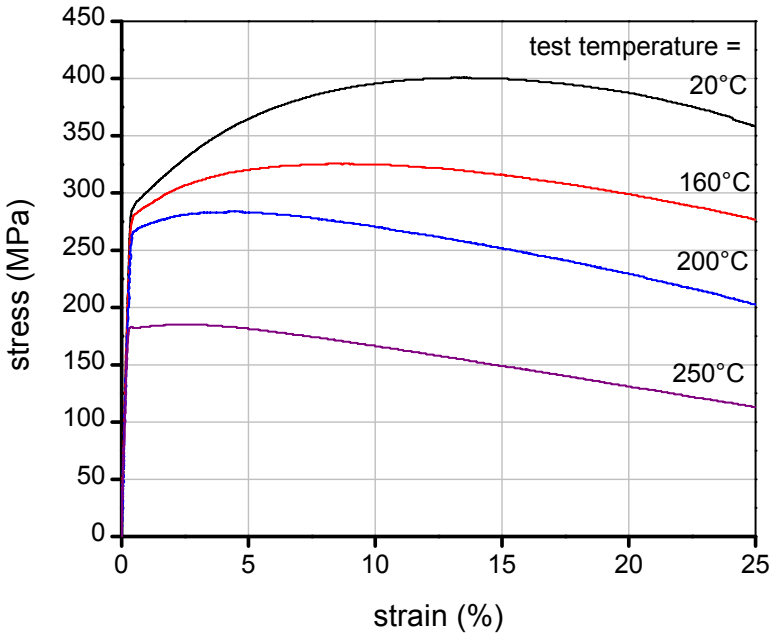

Figure 5.27: Engineering stress-strain diagram of under-aged AA6110 for different test temperatures.

5.2.3.2 Cyclic deformation behavior of polished under-aged AA6110

Fatigue lifetime: Fig. 5.28 depicts non-statistically evaluated s/n-curves of the polished under-aged AA6110 for different test temperatures. An increase in test temperature shifts the s/n-curves to lower fatigue lifetimes, i.e. the fatigue lifetime of the polished condition at room temperature at an applied stress amplitude of 200 MPa is about 255,000 cycles, whereas at a test temperature of 250°C for the same applied stress amplitude the fatigue lifetime is reduced to only roughly 10,000 cycles. Obviously, the altered static/dynamic precipitation show insignificant effects on the shape of the s/n-curves in the low cycle fatigue regime. However, the effect of altered static/dynamic precipitation seems to be beneficial for fatigue lifetime in the high cycle fatigue regime, especially in the temperature range 160-200°C (see Fig. 5.28).

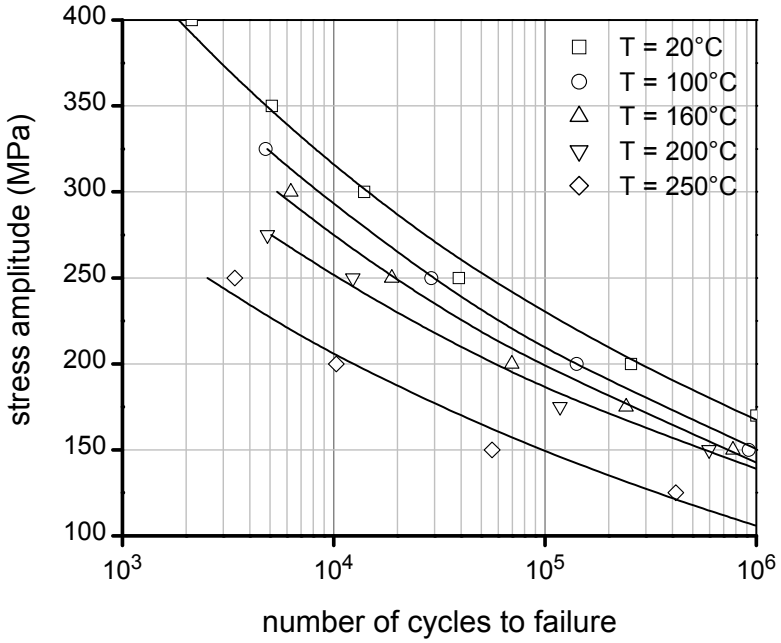

Figure 5.28: Non-statistically evaluated s/n-curves of polished under-aged AA6110 in the temperature range 20-250°C.

Cyclic deformation curve: Plastic strain amplitudes were measured during fatigue tests. Cyclic hardening was detected at room and elevated test temperatures up to 200°C as presented in Fig. 5.29. An increase of the plastic strain amplitude was observed with increasing test temperatures. However, the plastic strain amplitude at a test temperature of 200°C tends to decrease as compared to a test temperature of 160°C. At test temperatures above 200°C, the cyclic deformation behavior switches from cyclic hardening to cyclic softening as shown in Fig. 5.30 which shows the plastic strain amplitudes during fatigue tests of the polished under-aged AA6110 at a test temperature of 250°C for different applied stress amplitudes.

5.2.3.3 Cyclic deformation behavior of deep-rolled under-aged AA6110

Near-surface properties: Deep rolling induced macroscopic compressive residual stresses as well as work hardening states at the surface and in near-surface regions up to a depth of approximately 0.7 mm of the deep-rolled under-aged AA6110 (see Fig. 5.31). Maximum macroscopic compressive residual stresses of -380 MPa were measured at a depth of 40 µm. FWHM-values in near-surface

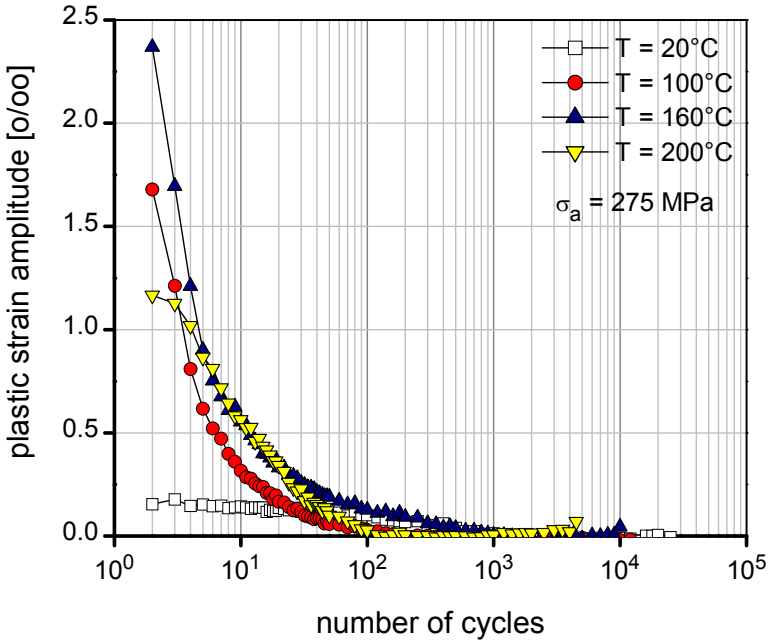

Figure 5.29: Cyclic deformation curves of polished under-aged AA6110 at an applied stress amplitude of 275 MPa for different test temperatures.

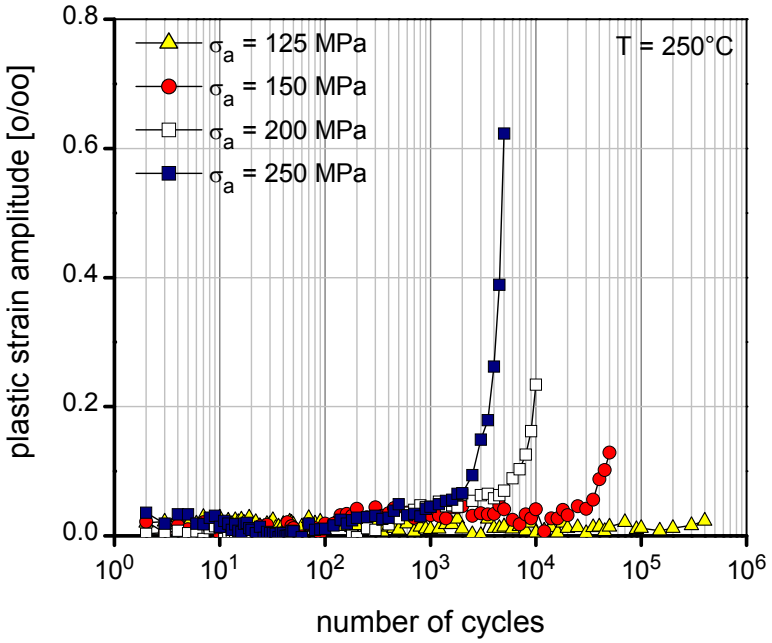

Figure 5.30: Cyclic deformation curves of polished under-aged AA6110 at a test temperature of 250°C for different applied stress amplitudes.

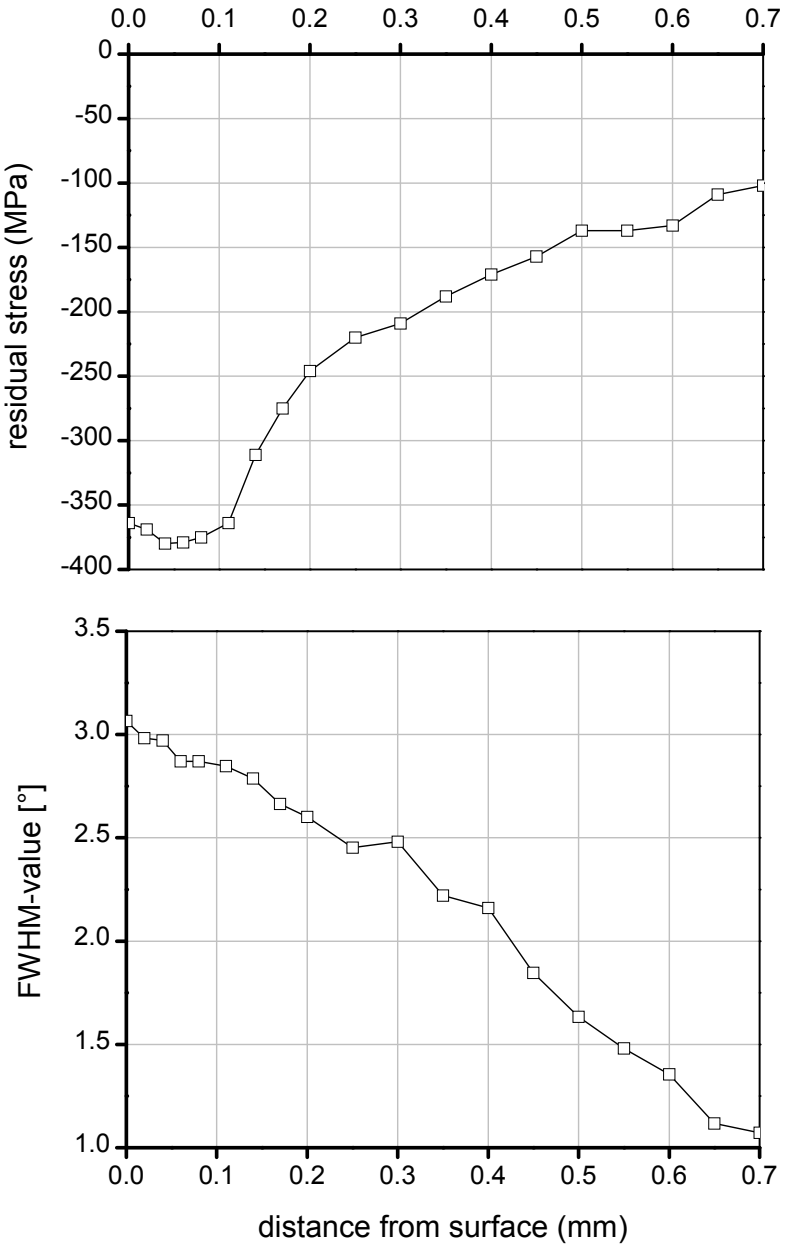

Figure 5.31: Depth profiles of near-surface macroscopic compressive residual stresses and FWHM-values of deep-rolled under-aged AA6110.

regions of the deep-rolled under-aged AA6110 increase from approximately 1.1° of the bulk to 3.1° at the surface. Deep rolling induced also an increase of near-surface hardness by approximately 35 HV as compared to the bulk as shown in Fig. 5.32.

Fatigue lifetime: Non-statistically evaluated s/n-curves of the deep-rolled under-aged AA6110 for different test temperatures are presented in Fig. 5.33. Obviously,

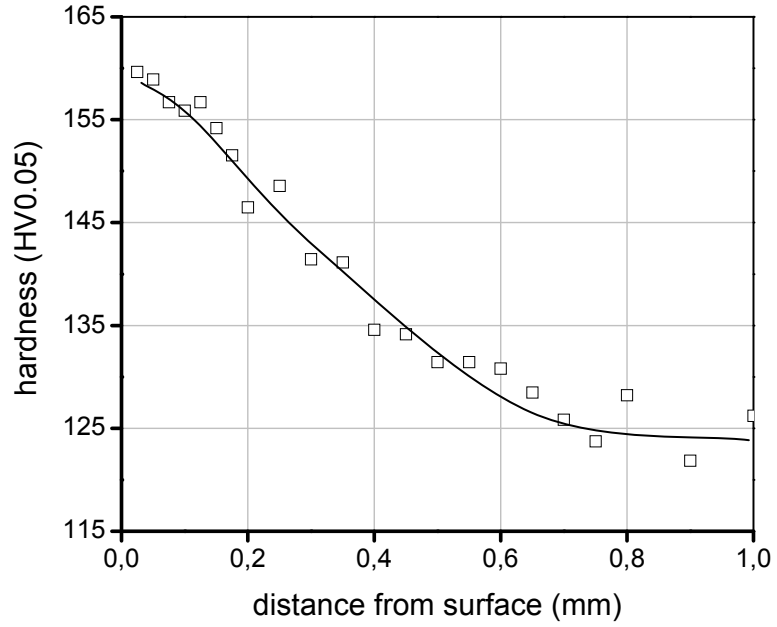

Figure 5.32: Depth profile of near-surface hardnesses of deep-rolled under-aged AA6110.

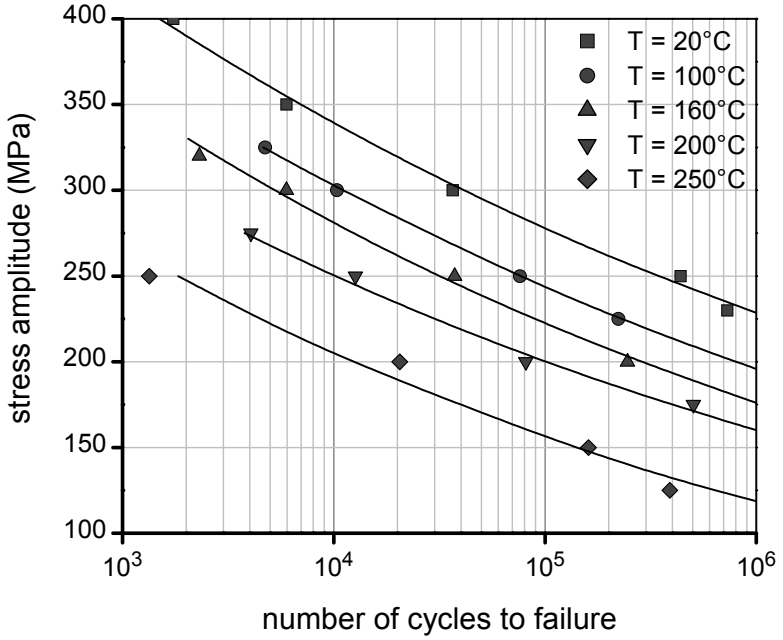

Figure 5.33: Non-statistically evaluated s/n-curves of deep-rolled under-aged AA6110 in the temperature range 20-250°C.

fatigue lifetimes decrease with increasing test temperature as well as applied stress amplitude. For example, the fatigue lifetime of the deep-rolled under-aged condition at room temperature at an applied stress amplitude of 250 MPa is about 440,000 cycles, whereas at a test temperature of 250°C for the same applied stress amplitude the fatigue lifetime is reduced to only roughly 1,500 cycles. Furthermore, the static/dynamic precipitation affected only insignificantly the s/n-curves of the deep-rolled under-aged condition at elevated test temperatures. A fatigue lifetime enhancement of the deep-rolled under-aged condition was observed as compared to the polished under-aged condition (see Figs. 5.28 and 5.33). However, the beneficial effects of deep rolling decreased with increasing test temperature as shown in Fig. 5.34. Finally, deep rolling is ineffective for the fatigue lifetime of the under-aged AA6110 at an applied stress amplitude of 250 MPa at a test temperature of 250°C.

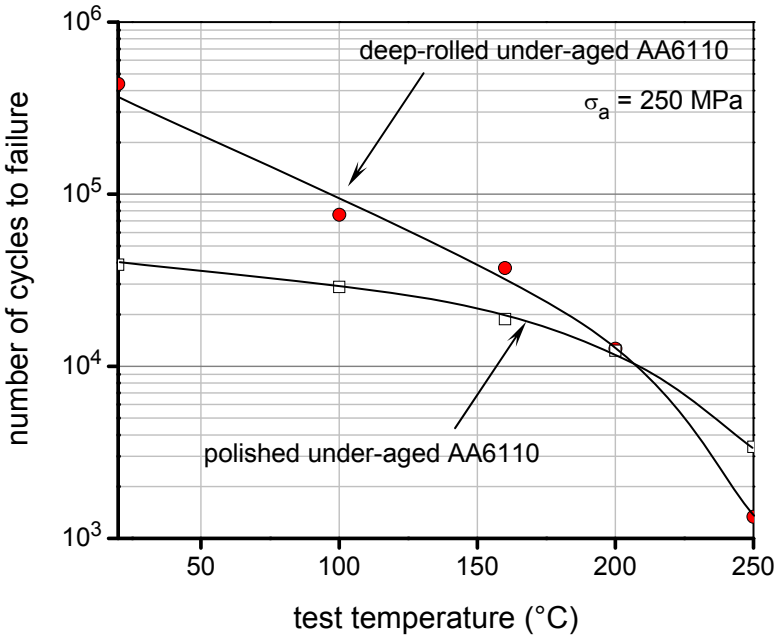

Figure 5.34: Fatigue lifetimes of polished and deep-rolled under-aged AA6110 at an applied stress amplitude of 250 MPa for different test temperatures.

Cyclic deformation curve: At elevated temperatures up to 200°C, the deep-rolled under-aged condition exhibits cyclic hardening. Cyclic softening was observed at a test temperature of 250°C similar to the polished under-aged condition. Plastic

strain amplitudes of the deep-rolled condition are normally lower than the polished under-aged condition if the beneficial effects of deep rolling prevail. In contrast, in a case where deep rolling is ineffective, higher plastic strain amplitudes of the deep-rolled condition were detected. For example, Fig 5.35 shows plastic strain amplitudes during fatigue tests at stress amplitude of 250 MPa for test temperatures of 160 and 250°C. At a test temperature of 160°C, deep rolling enhanced the fatigue lifetime at an applied stress amplitude of 250 MPa whereas at a test temperature of 250°C, deep rolling became ineffective (see Fig. 5.34).

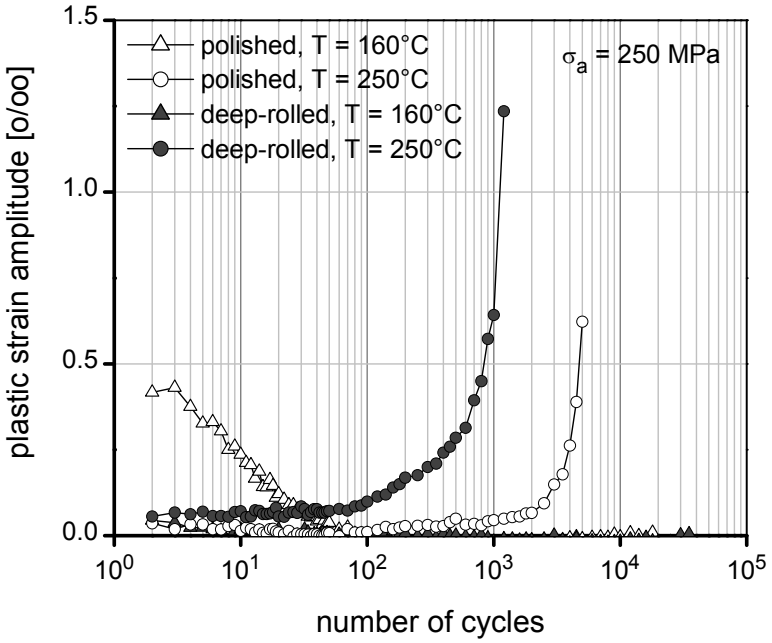

Figure 5.35: Cyclic deformation curves of polished under-aged AA6110 at a stress amplitude of 250 MPa for test temperatures of 160 and 250°C.

5.2.3.4 Residual stress stability of deep-rolled under-aged AA6110

From the results of AA5083 and as-quenched AA6110, it was expected that the stability of near-surface macroscopic compressive residual stresses as well as particularly work hardening states of the deep-rolled condition significantly affect the fatigue lifetime as well as strength at room and elevated temperatures. Therefore, the stability of macroscopic compressive residual stresses as well as

work hardening states of the deep-rolled under-aged AA6110 during fatigue tests at room and elevated temperature were investigated. Moreover, thermal residual stress relaxation was also investigated and will be presented in the following section.

Mechanical residual stress relaxation: Fig. 5.36 shows mechanical residual stress as well as FWHM-value reduction of the deep-rolled under-aged AA6110 during fatigue tests at room temperature for different applied stress amplitudes. The macroscopic compressive residual stresses at the surface of the deep-rolled under-aged condition decreased with increasing applied stress amplitude and number of cycles, particularly in the first cycle of fatigue tests. Subsequently, a linear decrease of macroscopic compressive residual stresses with the logarithm of number of cycles was observed. The work hardening states appear to be stable up to applied stress amplitudes of approximately 350 MPa. For an applied stress amplitude of 400 MPa, the FWHM-values at the surface of the deep-rolled under-aged condition are unstable during fatigue tests at room temperature.

Thermal residual stress relaxation: A Zener-Wert-Avrami function was used to describe thermal residual stress relaxation. The materials constant m_{RS} = 0.21 was determined by plotting of $\log\ln(\sigma_0^{RS}/\sigma^{RS})$ as a function log t_a for a constant ageing temperature T_a in Fig. 5.37. Subsequently, the activation enthalpy for the relaxation process was estimated by determining the slope of the log t_a versus $1/kT_a$ plot as shown in Fig. 5.38. The activation enthalpy of the relaxation process ΔH_{RS} = 1.51 eV and B_{RS} = 4.42 x 10^{13} min^{-1} were determined for the deep-rolled under-aged AA6110. The Zener-Wert-Avrami function was also used to describe the FWHM-value decrease. The difference between the FWHM-values after ageing and the initial FWHM-value of 1.1° of the polished under-aged specimen substitutes the ratio $\sigma^{RS}/\sigma_0^{RS}$ in equation (2). Table 5.3 exhibits the determined materials constants of the FWHM-value and residual stress relaxation of the deep-rolled under-aged AA6110. The calculated decrease of FWHM-values as well as residual stresses as a function of ageing time and temperature using the respective materials constants in table 5.3 were constructed as shown in Fig. 5.39 as solid lines.

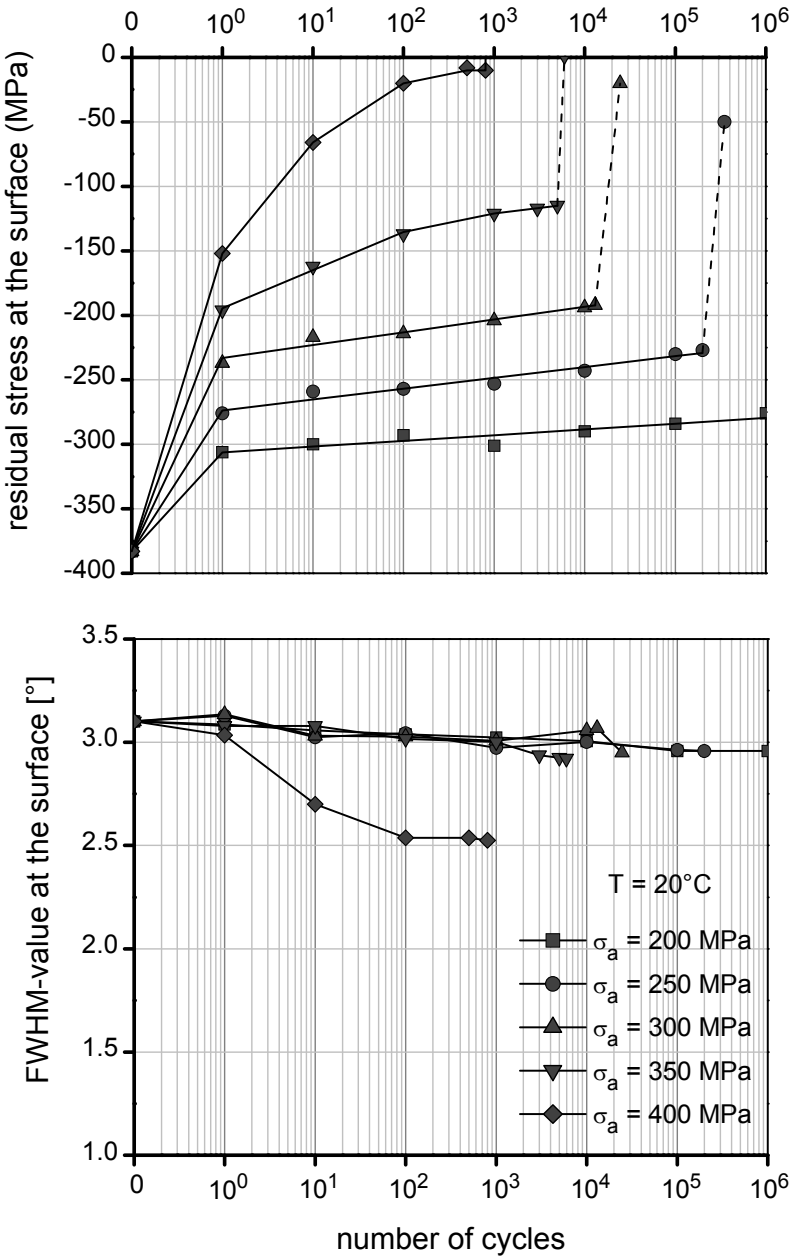

Figure 5.36: Residual stress and FWHM-value relaxation at the surface of deep-rolled under-aged AA6110 during stress controlled fatigue at room temperature for different stress amplitudes.

Thermomechanical residual stress relaxation: Fatigue tests were performed for different stress amplitudes at a given temperature to investigate thermomechanical residual stress relaxation of near-surface macroscopic compressive residual stresses as well as work hardening states of the deep-rolled under-aged AA6110. Depth profiles of near-surface macroscopic compressive residual stresses and

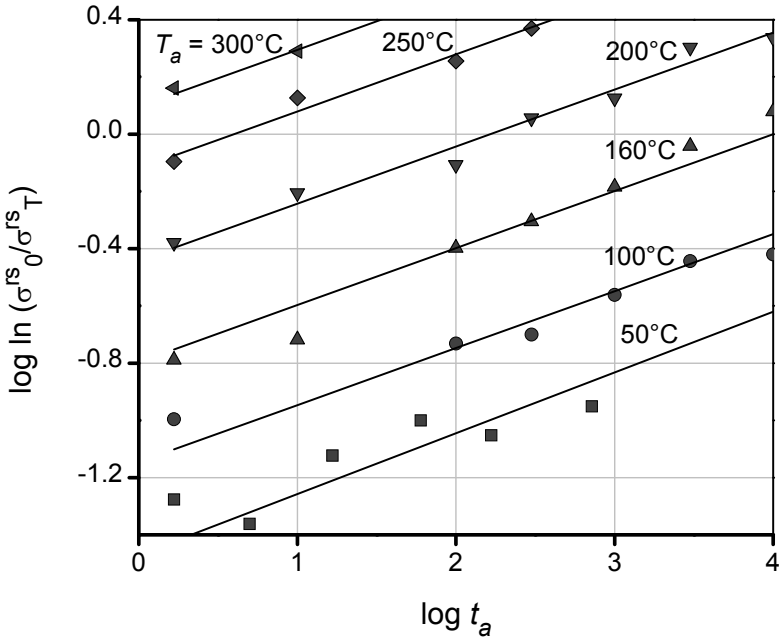

Figure 5.37: Influence of ageing time and temperature on surface residual stress of deep-rolled under-aged AA6110 in a $\log \ln\left(\sigma_0^{RS}/\sigma_T^{RS}\right)$ versus log t_a diagram.

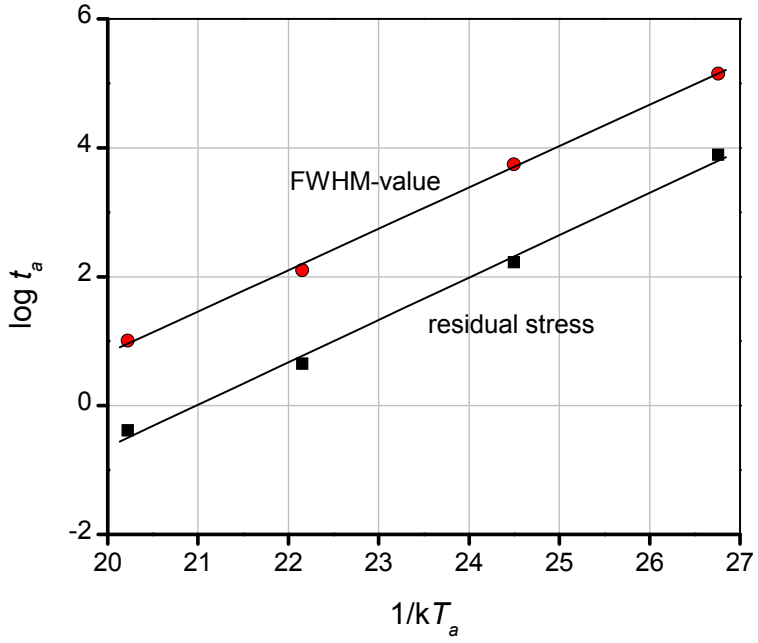

Figure 5.38: Plot of log t_a versus 1/kT_a for the determination of Avrami approach parameters of deep-rolled under-aged AA6110 for 50% residual stress as well as FWHM-value relaxation.

Table 5.3: Determined materials constants of thermal residual stress and FWHM-value relaxation of deep-rolled under-aged AA6110.

Under-aged AA6110	***m***	**Δ*H* (eV)**	***B* (min^{-1})**
Residual stress relaxation	0.21	1.51	4.42×10^{13}
FWHM-value relaxation	0.20	1.48	9.67×10^{11}

FWHM-values were investigated (see Fig. 5.40) for three selected conditions: firstly, the deep-rolled specimen was heated at 200°C for 10 minutes without any applied stress amplitude, thus giving a reference state: secondly and thirdly, the deep-rolled specimens were cyclically deformed at a test temperature of 200°C for given number of cycles of 1,000 cycles at stress amplitudes of 175 and 300 MPa, respectively. Near-surface macroscopic compressive residual stresses decreased after fatigue tests at stress amplitudes 175 and 300 MPa at a test temperature of 200°C for 1,000 cycles. Particularly, at an applied stress amplitude of 300 MPa for a test temperature of 200°C, macroscopic compressive residual stresses relaxed completely. Moreover, instability of near-surface work hardening states of the deep-rolled under-aged specimen for this test condition was detected as compared to the near-surface work hardening of the thermal relaxation at 200°C for 10 minutes as a reference, whereas near-surface work hardening states after the fatigue test at stress amplitudes 175 MPa and at a test temperature of 200°C for 1,000 cycles are fairly stable.

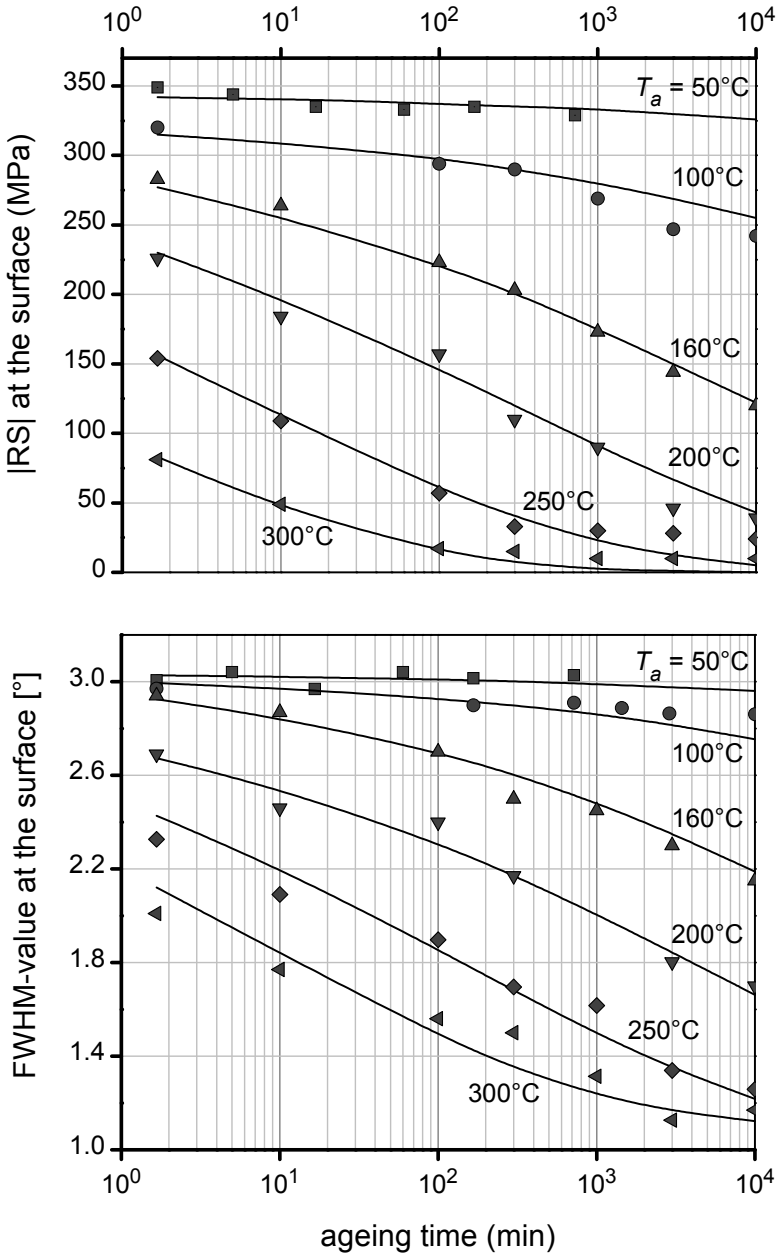

Figure 5.39: Influence of ageing time and temperature on the absolute values of residual stresses and FWHM-values at the surface and their description by the Avrami approach for deep-rolled under-aged AA6110.

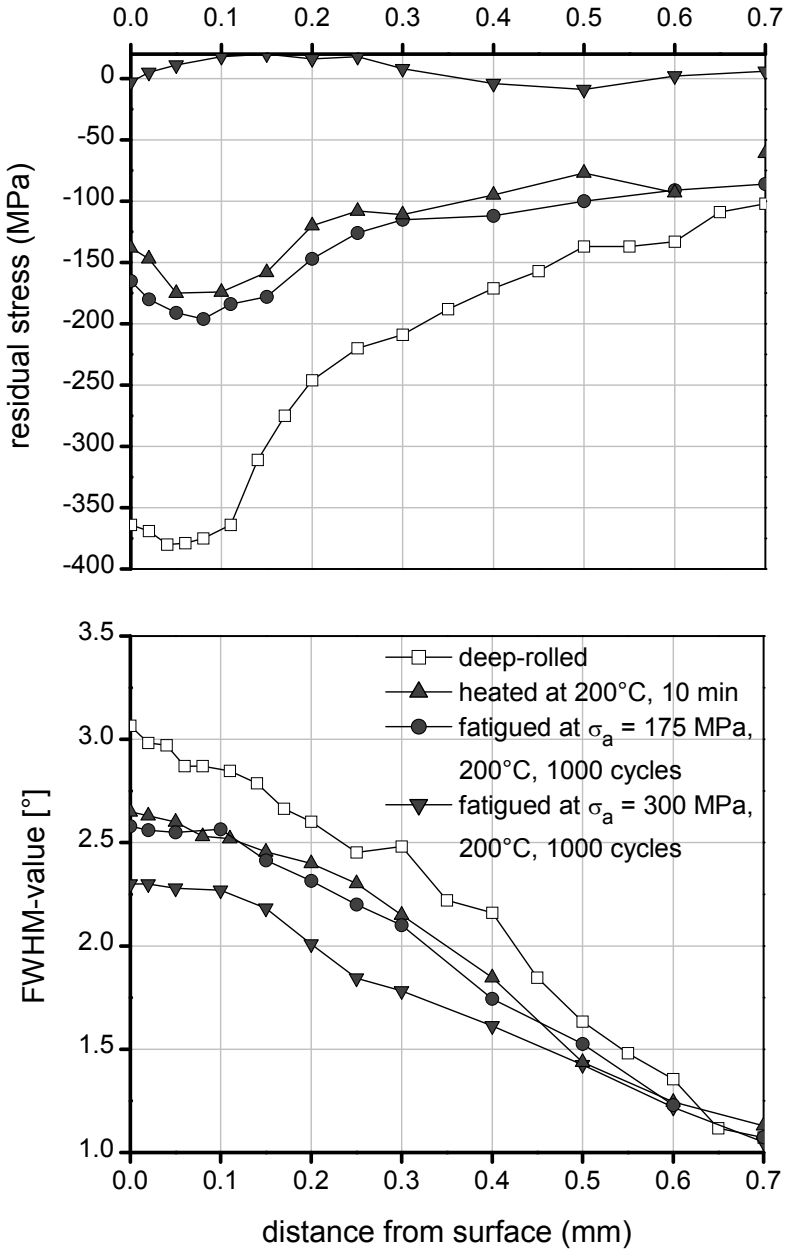

Figure 5.40: Residual stress- and FWHM-value-depth profiles of fatigued as well as heated specimens of deep-rolled under-aged AA6110.

5.2.4 Peak-aged AA6110

The aluminium alloy AA6110 in the peak-aged condition is widely used in automobile industries because of a very attractive strength level and a good surface finishing. However, during loading/exposure at elevated temperature, the metastable phases, β´´ and Q´ may coarsen into equilibrium phases, β (Mg_2Si) and Q ($Al_5Cu_2Mg_8Si_7$), respectively. Consequently, a deterioration of mechanical properties can be more or less expected. In addition, for the deep-rolled condition, the induced near-surface macroscopic compressive residual stresses as well as work hardening states decrease under high-loading and/or elevated-temperature condition due to mechanical, thermal as well as thermomechanical residual stress relaxation. Therefore, the stability of macroscopic compressive residual stresses as well as work hardening states during cyclic loading at room and elevated temperature and its effects on the fatigue behavior of the deep-rolled peak-aged AA6110 shall be intensively investigated.

5.2.4.1 Quasistatic deformation behavior of peak-aged AA6110

Results of quasistatic tensile tests of non-surface-treated peak-aged AA6110 in the temperature range 20-250°C are shown in Fig. 5.41. The engineering stress-strain curves of the peak-aged condition show a low work hardening rate ($d\sigma/d\varepsilon$) during tensile tests at room and elevated temperatures. The 0.2% yield and ultimate tensile strengths decreased continuously and drastically with increasing test temperature, i.e. at room temperature, a 0.2% yield strength of approximately 425 MPa was measured, whereas at a test temperature of 250°C, only approximately 185 MPa was measured.

5.2.4.2 Cyclic deformation behavior of polished peak-aged AA6110

Fatigue lifetime: Non-statistically evaluated s/n-curves of polished peak-aged specimens for different test temperatures are presented in Fig. 5.42. An increasing test temperature shifts s/n-curves to lower fatigue strength as well as lifetime. The fatigue lifetime of the polished peak-aged condition at room temperature at a stress amplitude of 250 MPa is about 42,500 cycles, whereas for the same stress amplitude at a temperature of 250°C, it is reduced to only roughly 5,500 cycles.

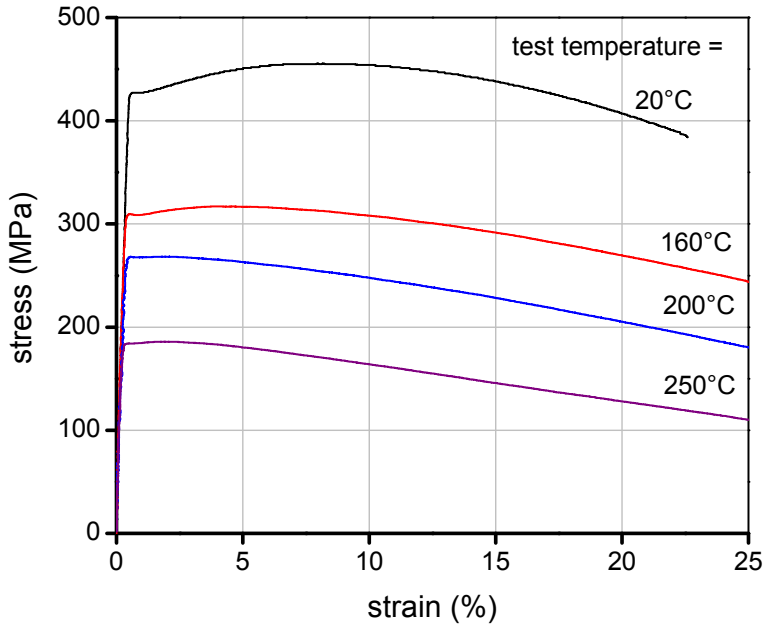

Figure 5.41: Engineering stress-strain diagram of peak-aged AA6110 for different test temperatures.

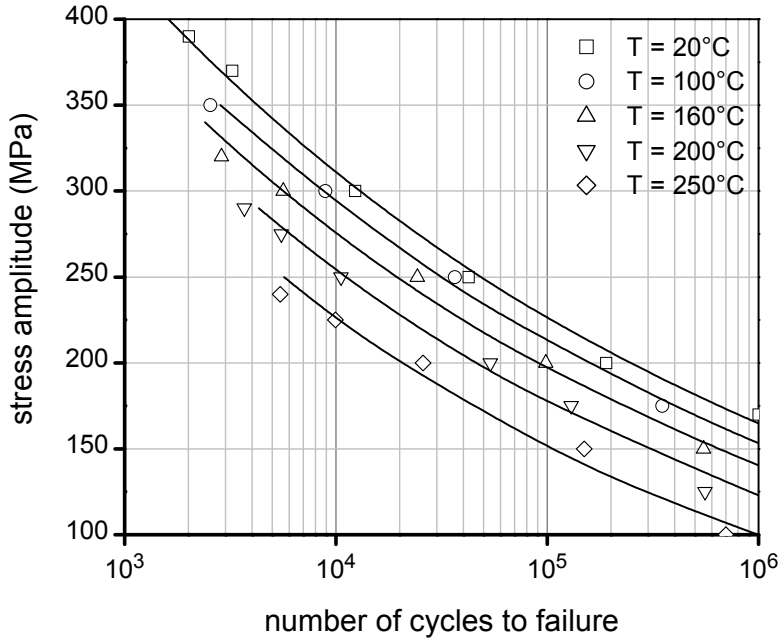

Figure 5.42: Non-statistically evaluated s/n-curves of polished peak-aged AA6110 in the temperature range 20-250°C.

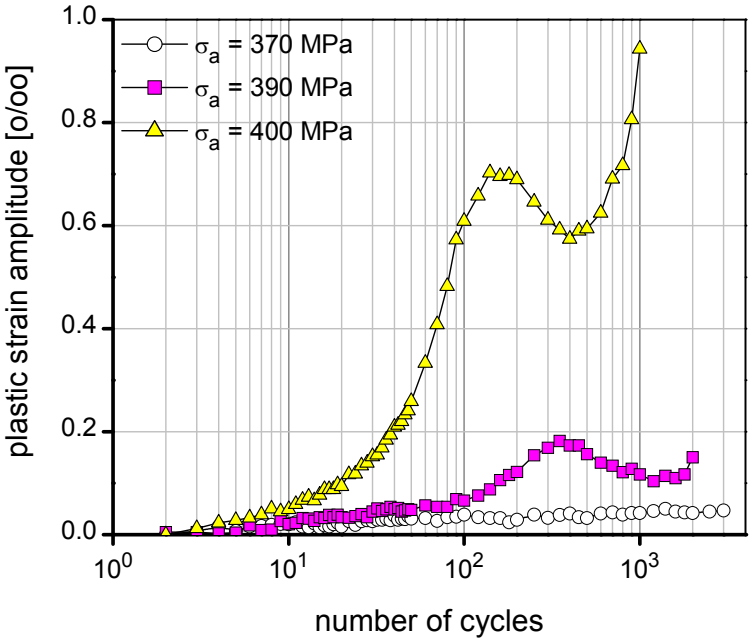

Figure 5.43: Cyclic deformation curves of polished peak-aged AA6110 at room temperature for different stress amplitudes.

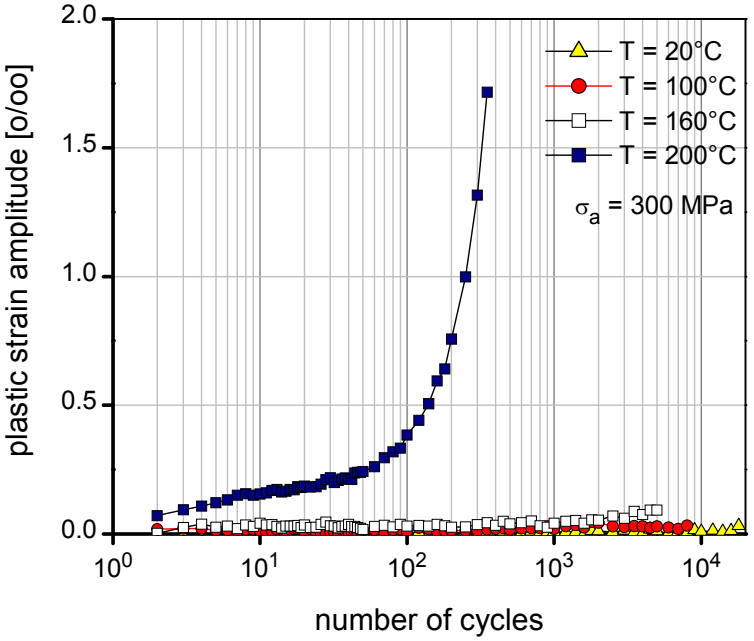

Figure 5.44: Cyclic deformation curves of polished peak-aged AA6110 at an applied stress amplitude of 300 MPa for different test temperatures.

Cyclic deformation curve: During fatigue tests, plastic strain amplitudes were measured to characterize the cyclic deformation behavior of the polished peak-aged condition. At room as well as elevated temperatures, the polished peak-aged AA6110 exhibits mostly cyclic softening during fatigue tests as depicted in Figs. 5.43 and 5.44. Moreover, from these diagrams, an increase of plastic strain amplitudes was also observed with increasing stress amplitude and/or test temperature.

5.2.4.3 Cyclic deformation behavior of deep-rolled peak-aged AA6110

Near-surface properties: Near-surface macroscopic compressive residual stresses as well as work hardening states were detected after deep rolling. Depth profiles of near-surface macroscopic compressive residual stresses and work hardening states of the deep-rolled peak-aged AA6110 are shown in Fig. 5.45. A maximum macroscopic compressive residual stress of -295 MPa was measured at a depth of 20 µm of the deep-rolled peak-aged condition. The FWHM-values in the near-surface regions increase from approximately 1.1° of the bulk to 3.1° at the surface. Increased hardnesses in near-surface regions from approximately 140 HV of the bulk to 162 HV in a depth of 25 µm under the surface were also observed (Fig. 5.46).

Fatigue lifetime: Non-statistically evaluated s/n-curves of the deep-rolled peak-aged condition for different test temperatures are presented in Fig. 5.47. Increased stress amplitudes and/or temperatures shift the s/n-curves to lower fatigue strength as well as lifetime. However, due to beneficial effects of deep rolling, fatigue lifetime enhancement was observed at low and intermediate stress amplitudes as compared to the polished peak-aged condition (see Fig. 5.42). For example, the fatigue lifetime at room temperature of the polished peak-aged condition at an applied stress amplitude of 250 MPa is about 42,500 cycles, whereas the fatigue lifetime of deep-rolled peak-aged condition for the same test condition increased considerably to about 360,000 cycles. Nonetheless, the beneficial effects of deep rolling declined during cyclic loading with increasing test temperature (see Fig. 5.48). Finally, deep rolling became ineffective if the specimens were cyclically deformed at an applied stress amplitude of 250 MPa at a test temperature of 250°C.

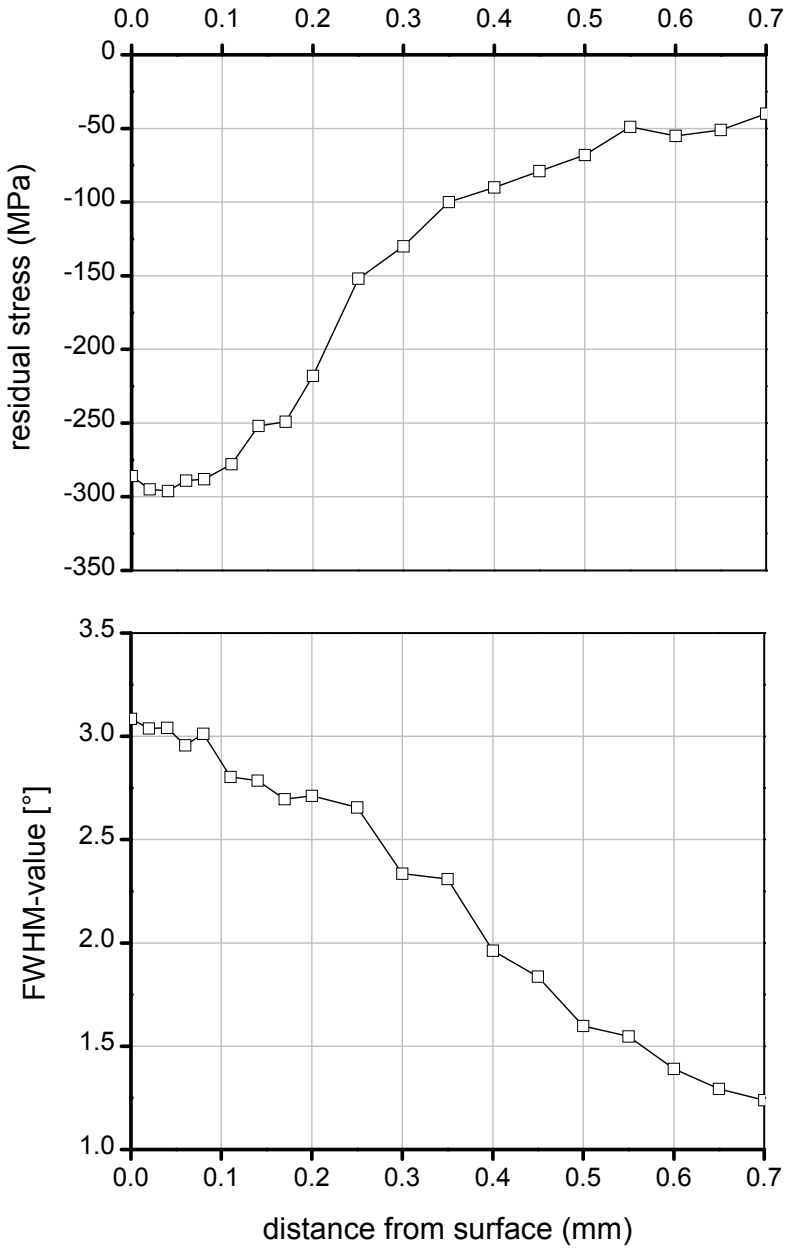

Figure 5.45: Depth profiles of near-surface macroscopic compressive residual stresses and FWHM-values of deep-rolled peak-aged AA6110.

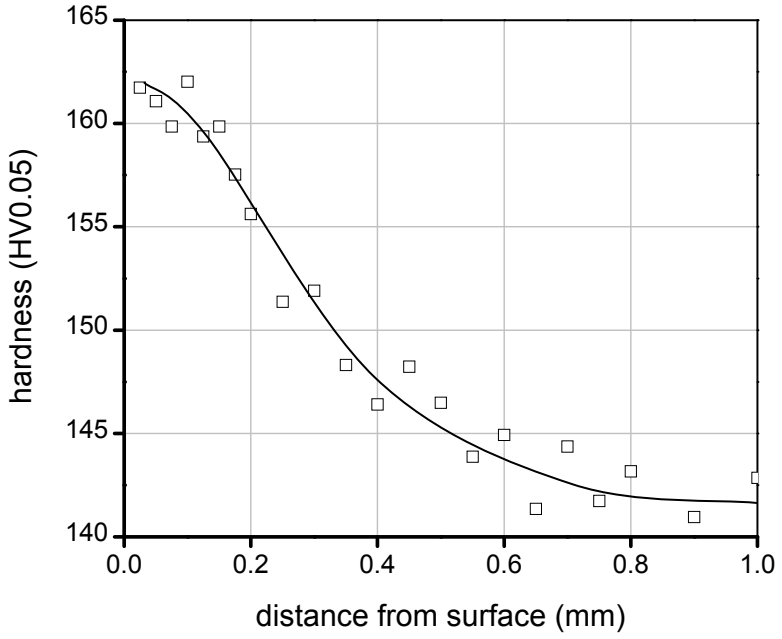

Figure 5.46: Depth profile of near-surface hardnesses of deep-rolled peak-aged AA6110.

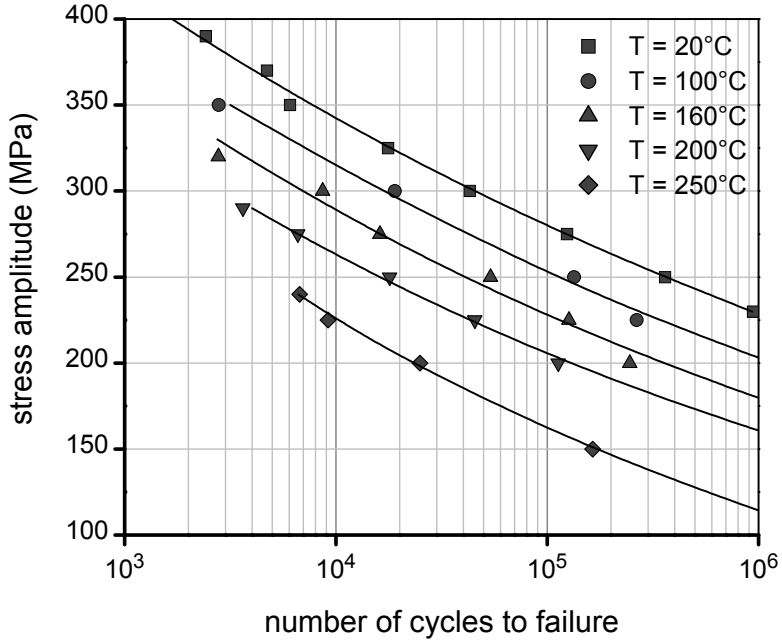

Figure 5.47: Non-statistically evaluated s/n-curves of deep-rolled peak-aged AA6110 in the temperature range 20-250°C.

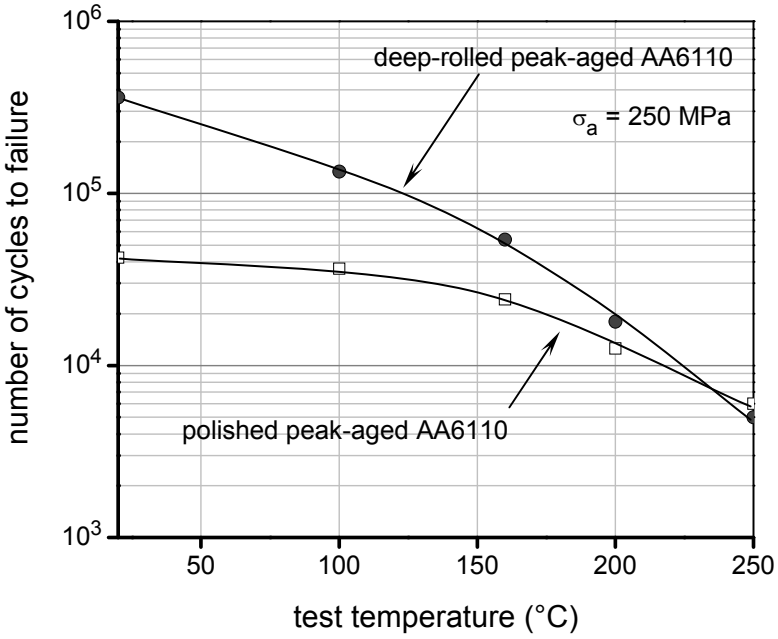

Figure 5.48: Fatigue lifetimes of polished and deep-rolled peak-aged AA6110 at an applied stress amplitude of 250 MPa for different test temperatures.

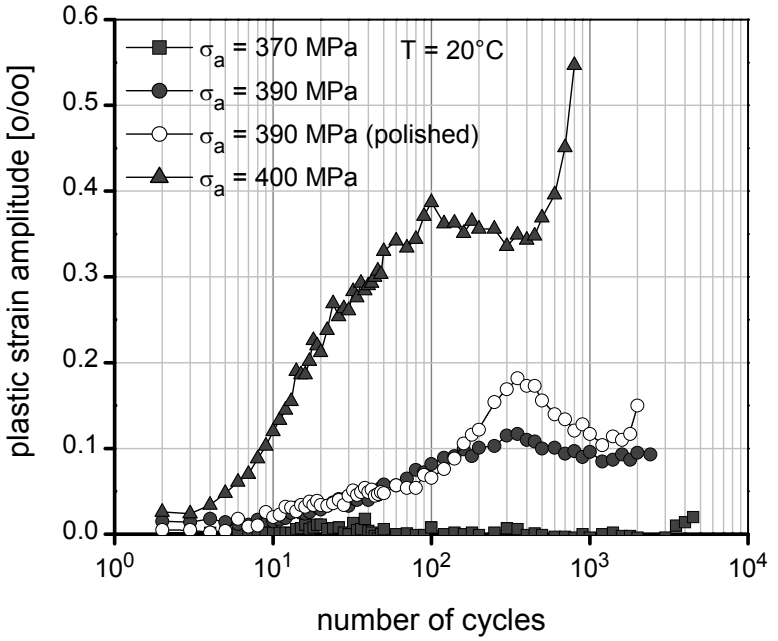

Figure 5.49: Cyclic deformation curves of deep-rolled (as well as polished) peak-aged AA6110 at room temperature for different stress amplitudes.

Cyclic deformation curve: The deep-rolled peak-aged AA6110 exhibits cyclic softening during fatigue tests at room and elevated temperatures similarly to the polished peak-aged condition. With increasing stress amplitude and/or test temperature, plastic strain amplitudes during fatigue tests increased, consequently fatigue lifetimes of the deep-rolled peak-aged condition decreased (see Fig. 5.49). Lower plastic strain amplitudes during fatigue tests of the deep-rolled peak-aged condition were normally measured as compared to the polished peak-aged condition. Thus, in general, deep rolling enhanced the fatigue lifetimes as compared to the polished condition (see Fig. 5.49).

5.2.4.4 Residual stress stability of deep-rolled peak-aged AA6110

The residual stress as well as work hardening state stability of the deep-rolled as-quenched and under-aged conditions were investigated already in sections 5.2.2.4 and 5.2.3.4. However, to assess the thermomechanical residual stress relaxation for all heat treatment conditions, for the deep-rolled peak-aged condition, residual stresses as well as FWHM-values during fatigue tests at different test temperatures and number of cycles were measured to clarify the thermomechanical residual stress relaxation behavior. Furthermore, results of solely mechanical and thermal residual stress relaxation are also presented in this section.

Mechanical residual stress relaxation: Similarly as the under-aged AA6110, relaxation of macroscopic compressive residual stresses as well as work hardening states occurs during cyclic loading at room temperature. With increasing stress amplitude and number of cycles, macroscopic compressive residual stresses decreased. Near-surface macroscopic compressive residual stresses decreased strongly in the first cycle. Afterwards, a linear dependence of the macroscopic compressive residual stresses with the logarithm of number of cycles occurred as shown in Fig. 5.50. The FWHM-values during the fatigue tests appear to be stable at stress amplitudes up to 350 MPa. However, at an applied stress amplitude of 400 MPa, the FWHM-values at the surface of the deep-rolled peak-aged condition were unstable.

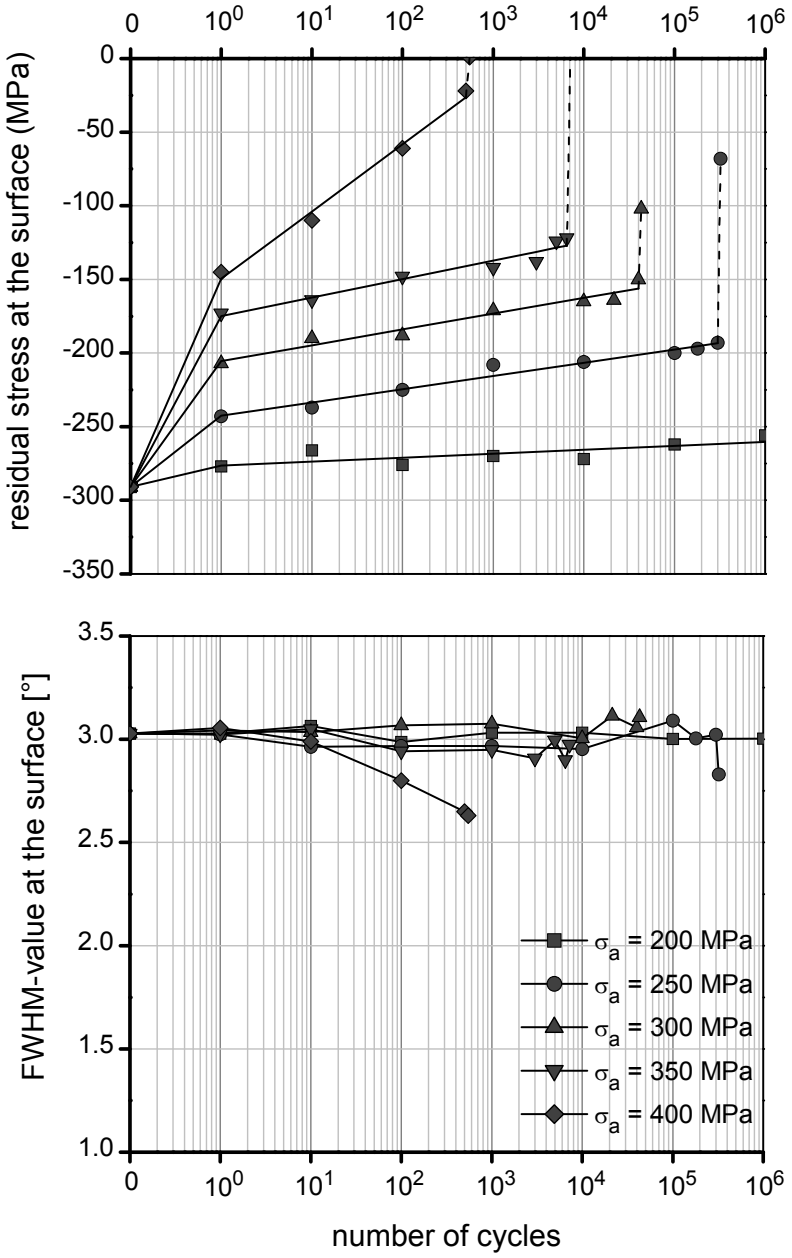

Figure 5.50: Residual stress and FWHM-value relaxation at the surface of deep-rolled peak-aged AA6110 during stress controlled fatigue tests at room temperature for different stress amplitudes.

Thermal residual stress relaxation: A Zener-Wert-Avrami function was used again to describe thermal relaxation of residual stresses as well as FWHM-values. A diagram of $\log \ln(\sigma_0^{RS} / \sigma^{RS})$ as a function of log t_a for a constant ageing temperature T_a in Fig. 5.51 gives a straight line of slope m = 0.22. The activation enthalpy for the relaxation process is determined using the slope of log t_a versus

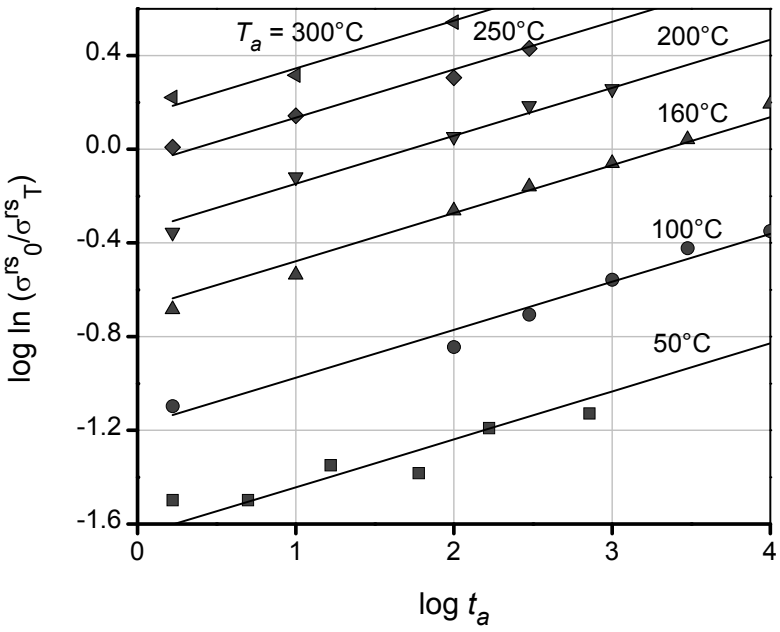

Figure 5.51: Influence of ageing time and temperature on surface residual stress of deep-rolled peak-aged AA6110 in a $\log \ln\left(\sigma_0^{RS}/\sigma_T^{RS}\right)$ versus log t_a diagram.

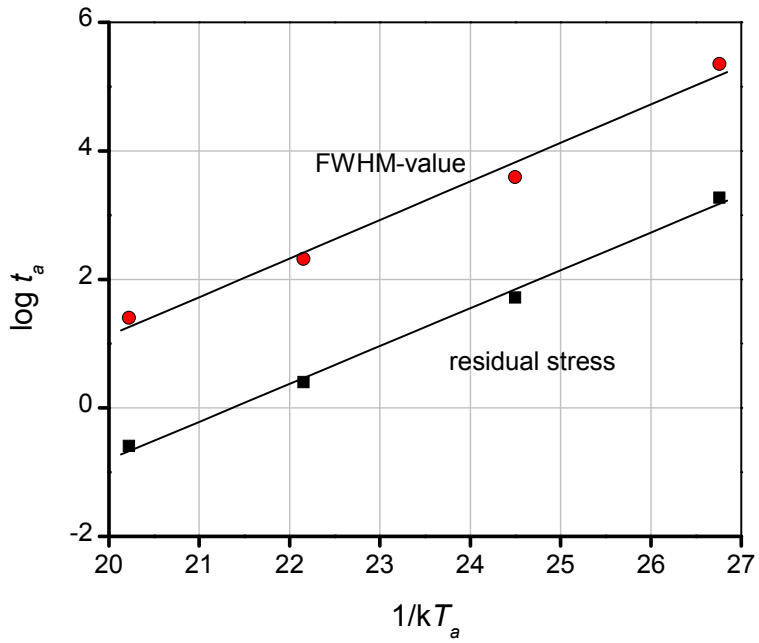

Figure 5.52: Plot of log t_a versus 1/kT_a for the determination of Avrami approach parameters of deep-rolled peak-aged AA6110 for 50% residual stress as well as FWHM-value relaxation.

1/k*Ta* in Fig. 5.52. The activation enthalpy of the relaxation process ΔH_{RS} = 1.35 eV and B_{RS} = 3.06 x 10^{12} min^{-1} were determined for the deep-rolled peak-aged AA6110. The FWHM-value decrease is related to the residual stress relaxation and can be also determined using the Zener-Wert-Avrami function. The difference between the FWHM-values after ageing and the initial FWHM-value of 1.1° of the polished peak-aged specimen substitutes the ratio in equation (2). Table 5.4 shows the determined materials constants of the FWHM-value as well as residual stress relaxation. The calculated decrease of FWHM-values and residual stresses as a function of ageing time and temperature using the respective materials constants in table 5.4 were determined as presented in Fig. 5.53 as solid lines.

Table 5.4: Determined materials constants of thermal residual stress and FWHM-value relaxation of deep-rolled peak-aged AA6110.

Peak-aged AA6110	***m***	**Δ*H* (eV)**	***B*** **(min^{-1})**
Residual stress relaxation	0.22	1.35	3.06 x 10^{12}
FWHM-value relaxation	0.22	1.38	5.21 x 10^{10}

Thermomechanical residual stress relaxation: Residual stresses as well as FWHM-values at the surface were measured during fatigue tests at elevated temperatures. Firstly, the effect of stress amplitude on the thermomechanical relaxation was investigated at a constant test temperature of 160°C for different applied stress amplitudes of 200, 300 and 350 MPa as shown in Fig. 5.54. Residual stresses as well as FWHM-values relaxed from the initial value during holding at a given temperature for 10 minutes prior to the start of the actual fatigue tests. Obviously, after a strong reduction in the first cycle, residual stresses decreased continuously and linearly with the logarithm of number of cycles similarly as in solely mechanical residual stress relaxation until approximately 1,000 cycles. Above 1,000 cycles, a non-linear residual stress relaxation was observed. In contrast, the FWHM-values appear to be stable during fatigue tests up to about 1,000 cycles at stress amplitudes of 200 and 300 MPa for a test

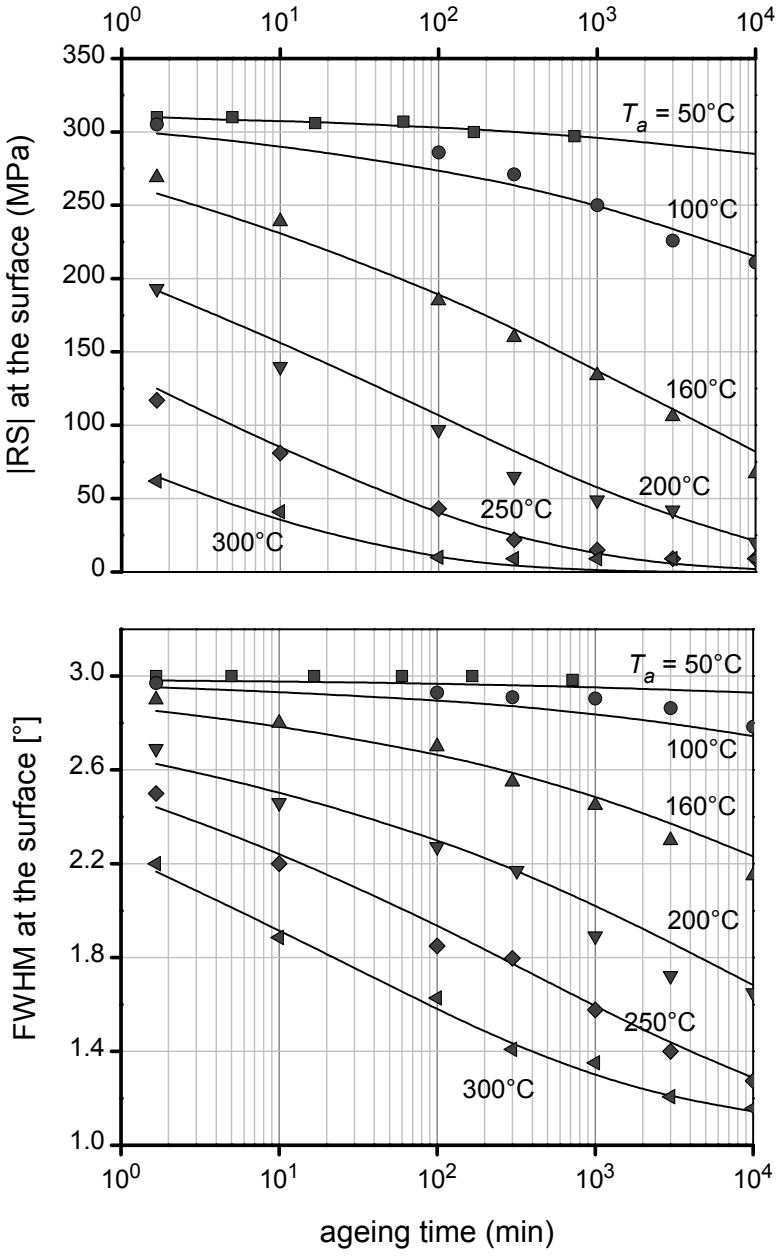

Figure 5.53: Influence of ageing time and temperature on the absolute values of residual stresses and FWHM-values at the surface and their description by the Avrami approach for deep-rolled peak-aged AA6110.

temperature of 160°C. Instability of FWHM-values at less than 1,000 cycles was observed during fatigue test at an applied stress amplitude of 350 MPa at a test temperature of 160°C. Secondly, a constant applied stress amplitude of 300 MPa for different test temperatures of 20, 160 and 200°C was chosen to investigate the effect of test temperature on residual stress as well as FWHM-value relaxation as

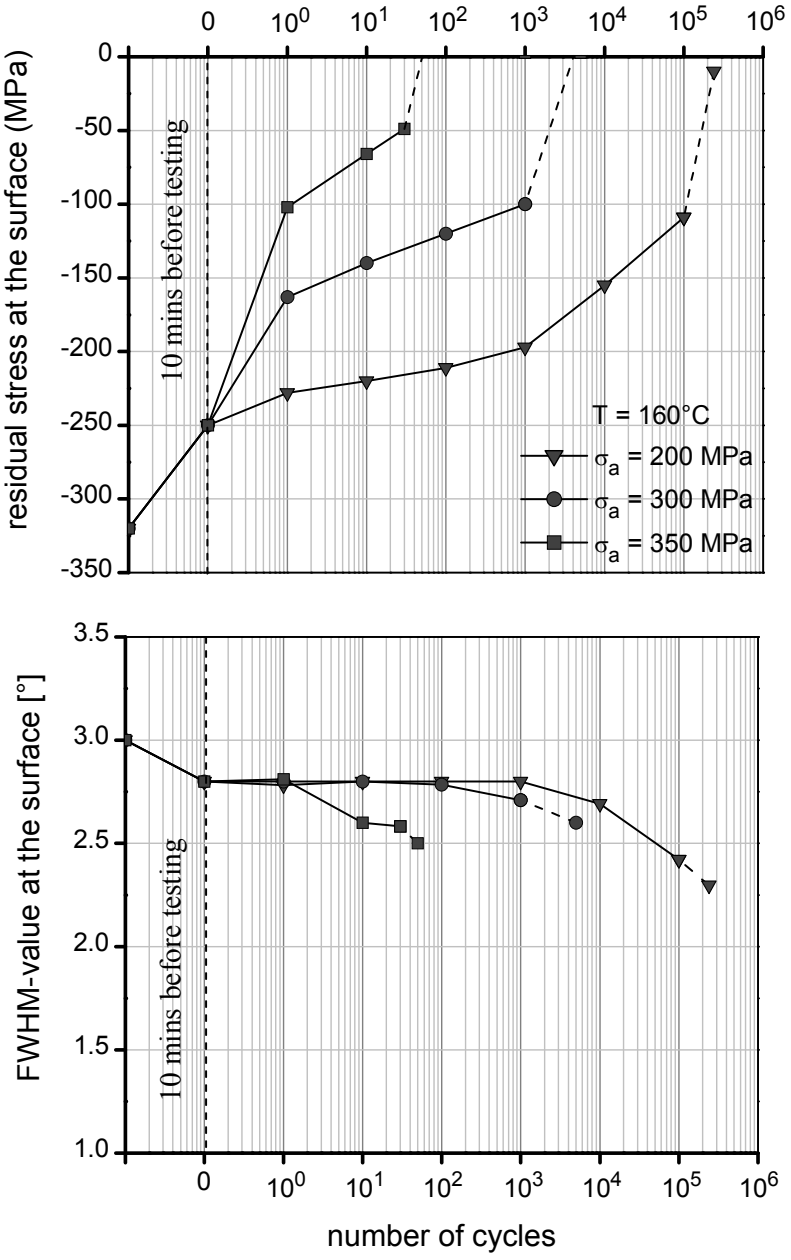

Figure 5.54: Relaxation of residual stresses and FWHM-values at the surface of deep-rolled peak-aged AA6110 during stress controlled fatigue at a temperature of 160°C for different applied stress amplitudes.

depicted in Fig. 5.55. Macroscopic compressive residual stresses decreased with increasing test temperature. Instability of FWHM-values at a number of cycles less than 1,000 cycles was also observed during fatigue tests at an applied stress amplitude of 300 MPa at a test temperature of 200°C. The stability of residual stresses and work hardening states of the deep-rolled peak-aged AA6110 during

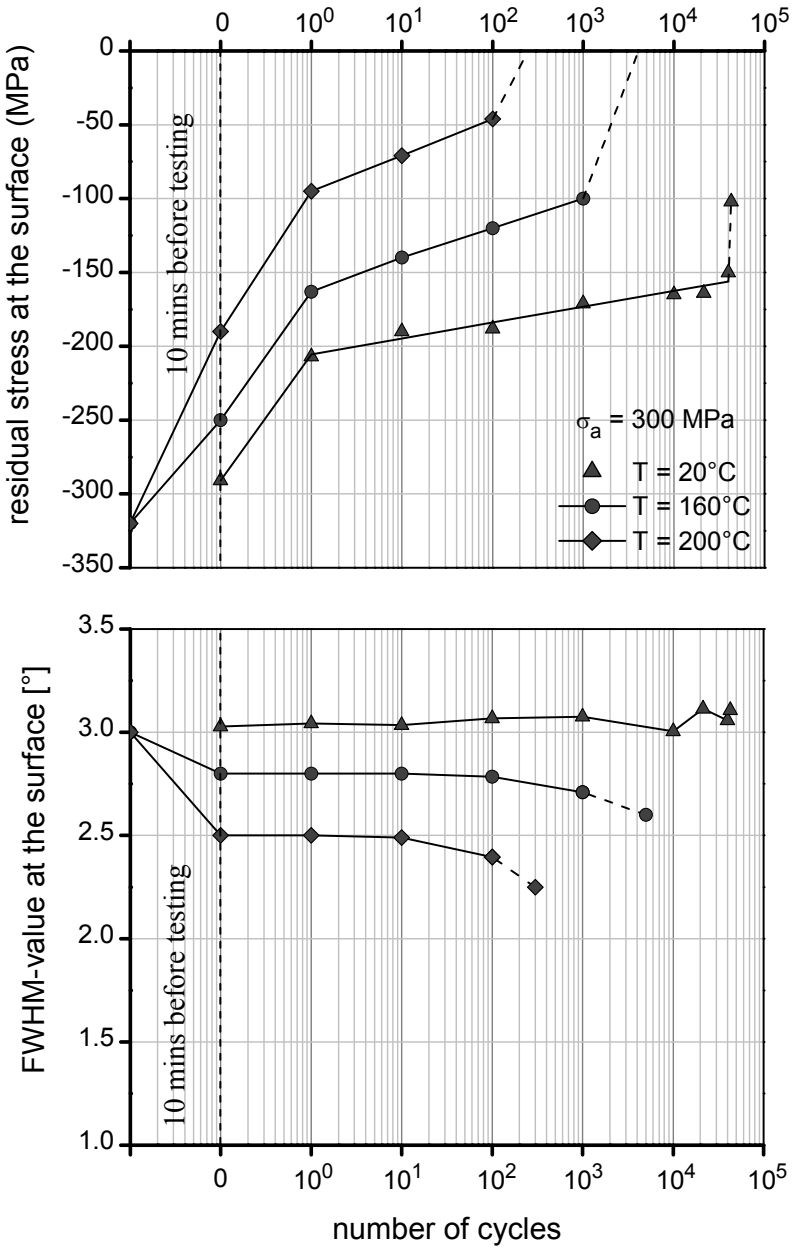

Figure 5.55: Relaxation of residual stresses and FWHM-values at the surface of deep-rolled peak-aged AA6110 during stress controlled fatigue for different test temperatures at an applied stress amplitude of 300 MPa.

fatigue tests at elevated temperatures was confirmed also through residual stress- and FWHM-value-depth profiles. Some selected conditions of fatigue tests at elevated temperature were investigated residual stress- and FWHM-value-depth profiles; firstly, the deep-rolled peak-aged specimen was heated at a temperature of 160°C for 10 minutes without any applied stress amplitude to produce a

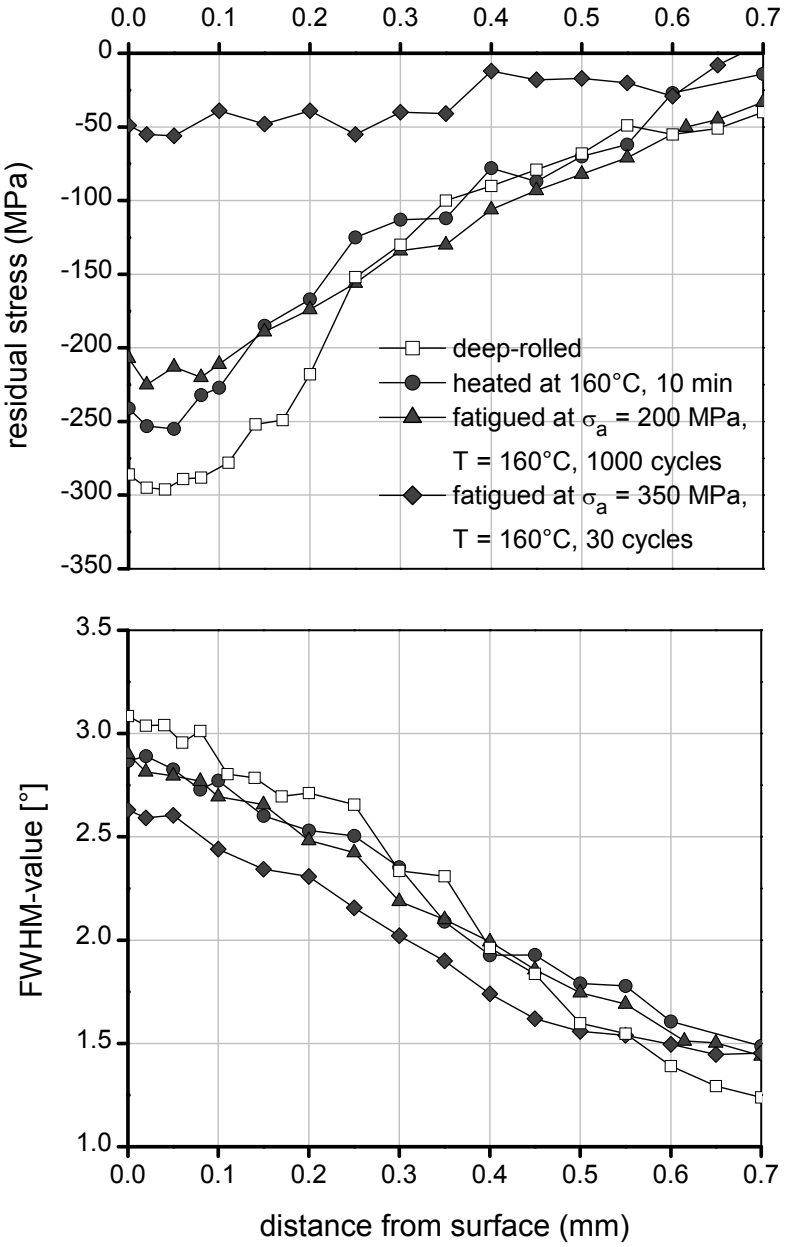

Figure 5.56: Residual stress- and FWHM-value-depth profiles of fatigued as well as heated specimens of deep-rolled peak-aged AA6110.

reference state. Secondly, the deep-rolled peak-aged specimen was cyclically deformed at a test temperature of 160°C for 1,000 cycles at an applied stress amplitude of 200 MPa and thirdly, the deep-rolled peak-aged specimen was cyclically deformed at a test temperature of 160°C for 30 cycles at an applied stress amplitude of 350 MPa. Residual stress- as well as FWHM-value-depth profiles were measured as compared to the deep-rolled peak-aged condition (Fig.

5.56). Significant thermomechanical residual stress relaxation was found after fatigue tests at stress amplitudes 200 and 350 MPa at a test temperature of 160°C for 1,000 and 30 cycles, respectively. Nevertheless, the near-surface work hardening states after fatigue tests at an applied stress amplitude of 200 MPa at a test temperature of 160°C appear to be stable as compared to the reference after 1,000 cycles. On the other hand, instability of near-surface work hardening states of the specimen was detected when the deep-rolled peak-aged specimen was cyclically deformed at an applied stress amplitude of 350 MPa at a test temperature of 160°C for only 30 cycles.

5.2.5 Over-aged AA6110

The as-quenched aluminium alloy AA6110 was transformed into the over-aged condition by ageing at a temperature of 160°C for about 1 week. From the practical point of view, for this condition, some degree of strength as well as hardness is sometimes scarified to improve one or more other characteristic properties, such as dimensional stability, especially in components intended for service at elevated temperatures or lower residual stresses in order to reduce distortion in machining. Hence, the mechanical properties, e.g. the tensile strength, fatigue strength as well as lifetime at elevated temperature of non-mechanically and mechanically surface treated (deep-rolled) over-aged condition were investigated and will be presented in this next section.

5.2.5.1 Quasistatic deformation behavior of over-aged AA6110

Quasistatic tensile tests of non-surface treated over-aged AA6110 were performed in the temperature range 20-250°C as shown in Fig. 5.57. The engineering stress strain curves of the over-aged condition show low a work hardening rate ($d\sigma/d\varepsilon$) similarly to the peak-aged condition. The 0.2% yield and ultimate tensile strengths decreased continuously with increasing test temperature. At room temperature, a 0.2% yield strength was of approximately 393 MPa was measured, whereas at a test temperature of 250°C, the 0.2% yield strength was only about 174 MPa.

5.2.5.2 Cyclic deformation behavior of polished over-aged AA6110

Fatigue lifetime: A clear effect of temperature on the cyclic deformation behavior was expected due to the strong effects of temperature on the tensile properties in Fig. 5.57. Non-statistically evaluated s/n-curves of polished over-aged specimens for different test temperatures are presented in Fig. 5.58. With increasing test temperature as well as stress amplitude, the s/n-curves are shifted to lower fatigue strength as well as lifetime. The fatigue lifetime of the polished over-aged condition at room temperature at an applied stress amplitude of 200 MPa is about 250,000 cycles, whereas the fatigue lifetime is reduced to only about 15,000 cycles at a test temperature of 250°C for the same stress amplitude.

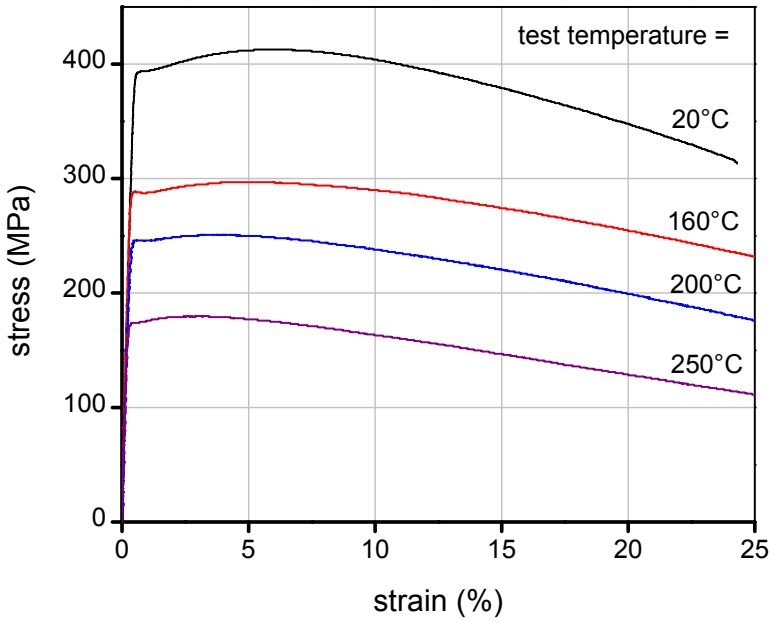

Figure 5.57: Engineering stress-strain diagram of over-aged AA6110 for different test temperatures.

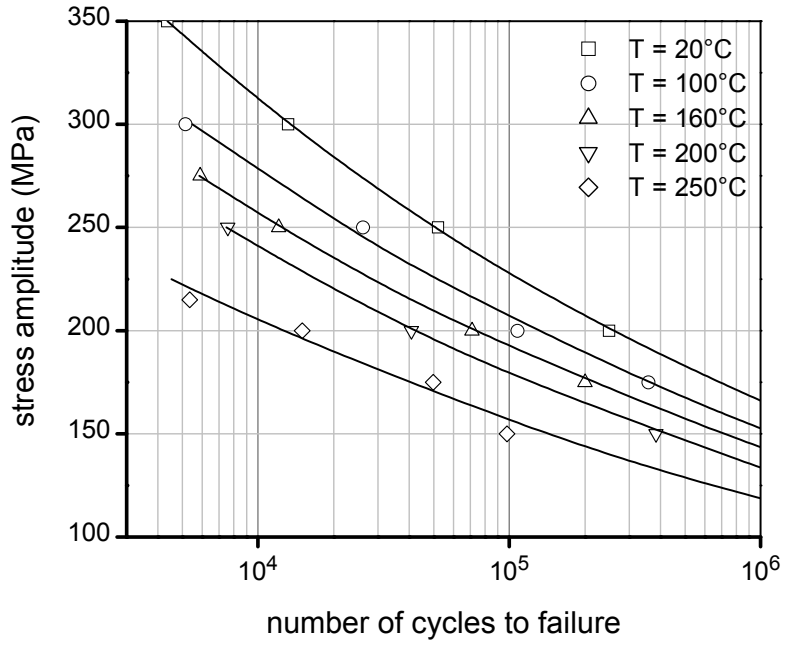

Figure 5.58: Non-statistically evaluated s/n-curves of polished over-aged AA6110 in the temperature range 20-250°C.

Cyclic deformation curve: Plastic strain amplitudes were measured during fatigue tests at room and elevated temperatures as depicted in Figs. 5.59 and 5.60. The polished over-aged AA6110 exhibits cyclic softening during fatigue test at room and elevated temperatures. Additionally, plastic strain amplitudes increased with increasing stress amplitude as well as test temperature.

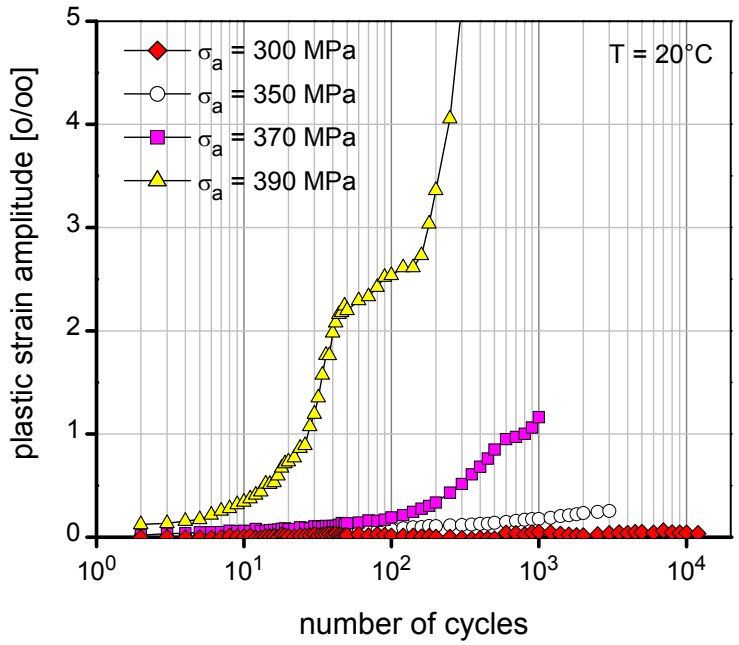

Figure 5.59: Cyclic deformation curves of polished over-aged AA6110 at room temperature for different stress amplitudes.

5.2.5.3 Cyclic deformation behavior of deep-rolled over-aged AA6110

Near-surface properties: From X-ray diffraction measurements, after deep rolling, near-surface macroscopic compressive residual stresses as well as work hardening states were detected. Depth profiles of near-surface macroscopic compressive residual stresses and work hardening states of the deep-rolled over-aged condition are shown in Fig. 5.61. A maximum macroscopic compressive residual stress of -292 MPa was measured at a depth of 20 µm of the deep-rolled over-aged AA6110. While the FWHM-values in the near-surface regions increase from approximately 1.1° of the bulk to 3.1° at the surface. Deep rolling induced

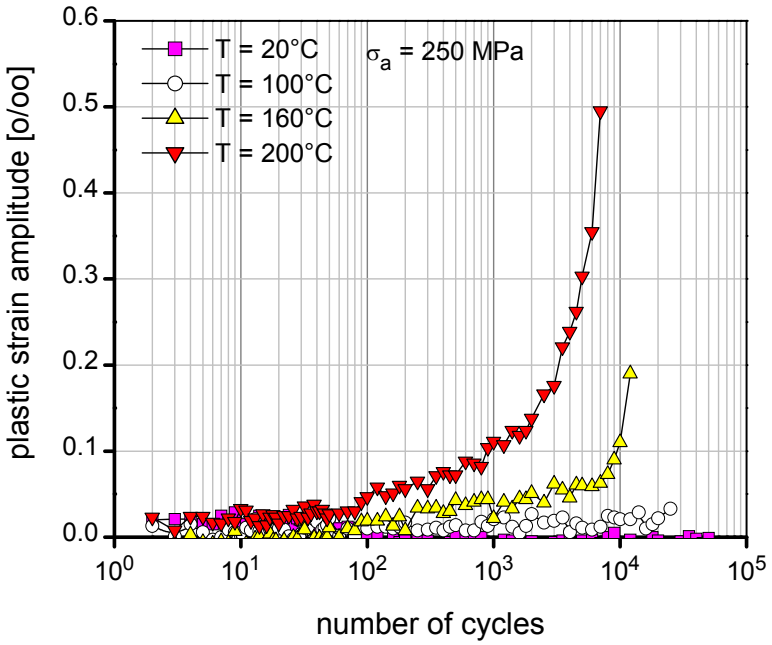

Figure 5.60: Cyclic deformation curves of polished over-aged AA6110 at an applied stress amplitude of 250 MPa for different test temperatures.

also increased hardnesses at the surface and in near-surface regions. A Hardness increase from approximately 123 HV of the bulk to 138 HV in a depth of 25 µm under the surface was detected (Fig. 5.62).

Fatigue lifetime: Non-statistically evaluated s/n-curves of the deep-rolled over-aged condition were measured for different test temperatures as shown in Fig. 5.63. Similarly to the polished over-aged condition, fatigue lifetimes decreased with increasing stress amplitude and/or test temperature. Nevertheless, deep rolling enhances fatigue lifetimes of the over-aged AA6110 particularly at low and intermediate stress amplitudes. At room temperature, the fatigue lifetime of the polished over-aged condition at an applied stress amplitude of 250 MPa is about 50,000 cycles, whereas the fatigue lifetime of the deep-rolled over-aged condition at the same test condition increased to approximately 120,000 cycles. However, the beneficial effects of deep rolling decreased with increasing test temperature as shown in Fig. 5.64. According to this diagram, deep rolling became ineffective at an applied stress amplitude of 200 MPa at a test temperature of 250°C.

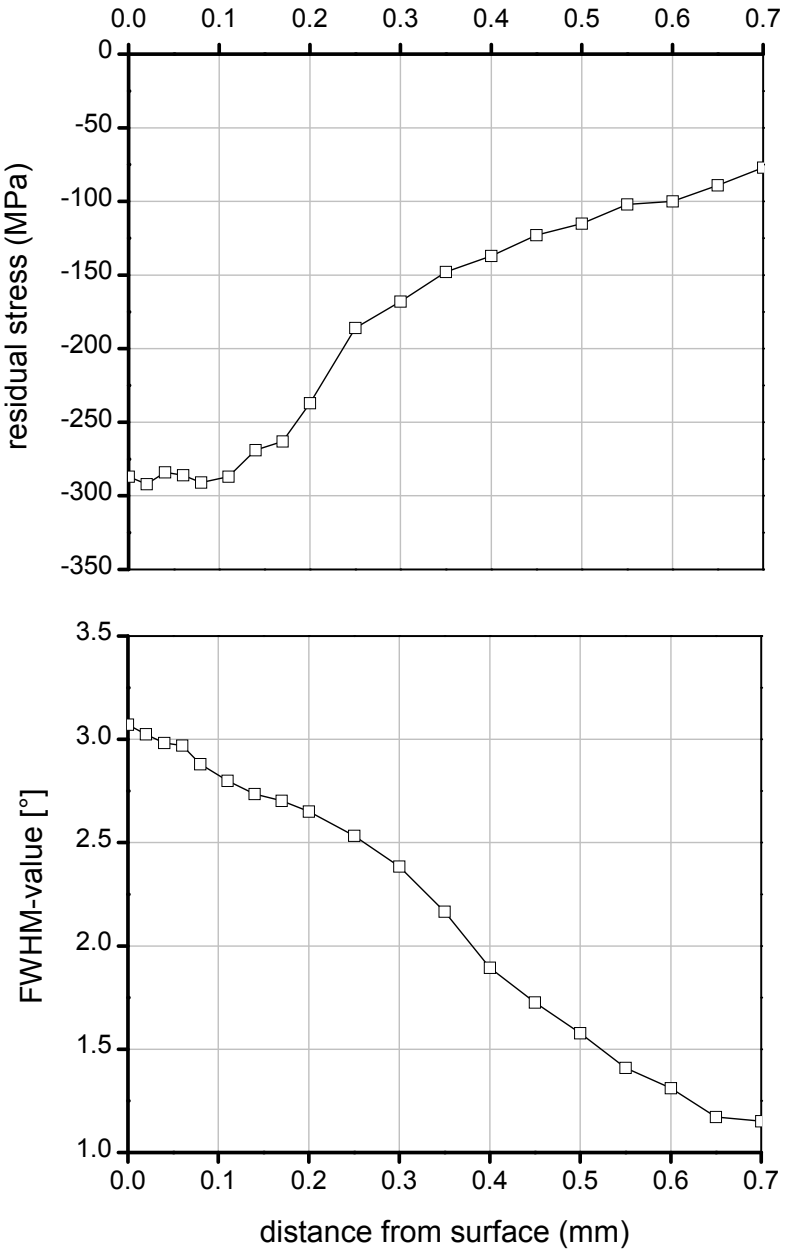

Figure 5.61: Depth profiles of near-surface macroscopic compressive residual stresses and FWHM-values of deep-rolled over-aged AA6110.

Cyclic deformation curve: Cyclic softening during fatigue tests at room and elevated temperatures was also detected for the deep-rolled over-aged condition similar to the polished over-aged condition. Fig. 5.65 exhibits plastic strain amplitudes as a function of number of cycles of the deep-rolled (as well as polished) over-aged condition at a test temperature of 160°C for different applied stress amplitudes. Obviously, cyclic softening as well as the magnitude of plastic

strain amplitudes during fatigue tests increase more and more with increasing applied stress amplitude and/or test temperature. Consequently fatigue lifetimes of the deep-rolled over-aged condition decreased (see Fig. 5.63). Lower plastic strain amplitudes during fatigue tests of the deep-rolled over-aged condition were normally detected as compared to the polished over-aged condition (see Fig. 5.65). Thus deep rolling generally enhances the fatigue lifetimes of the over-aged AA6110.

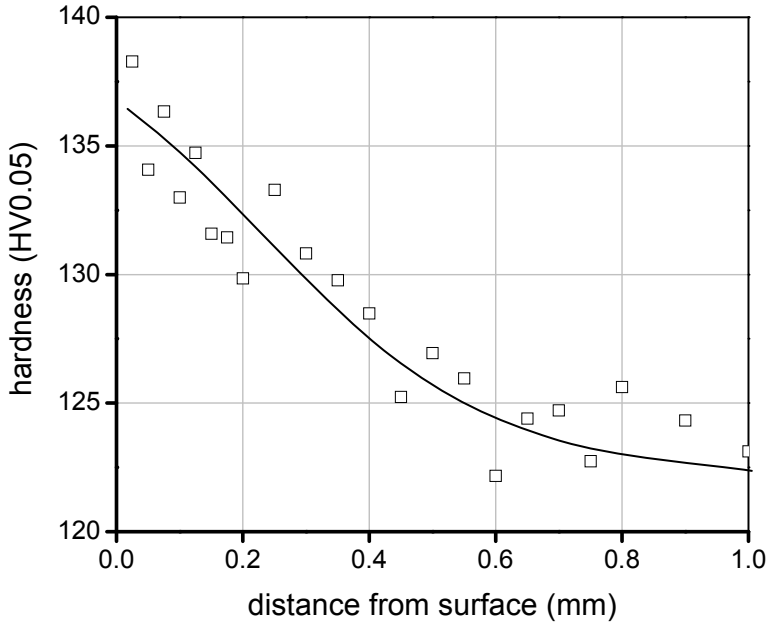

Figure 5.62: Depth profile of near-surface hardnesses of deep-rolled over-aged AA6110.

5.2.5.4 Residual stress stability of deep-rolled over-aged AA6110

Hitherto, residual stress stabilities of the deep-rolled as-quenched, under-aged, peak-aged AA6110 as well as AA5083 were systematically investigated. Mechanical, thermal as well as thermomechanical residual stress relaxation were manifested in decreased residual stresses as a function of number of cycle and/or

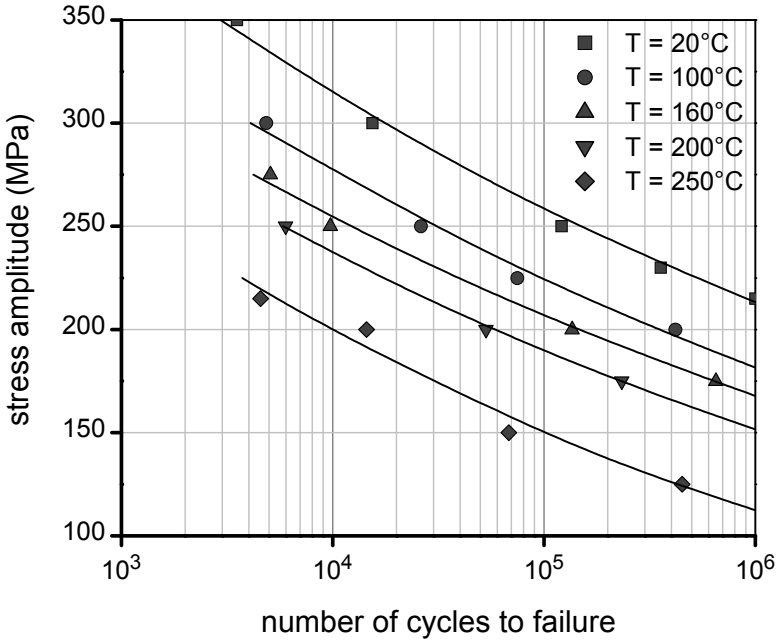

Figure 5.63: Non-statistically evaluated s/n-curves of deep-rolled over-aged AA6110 in the temperature range 20-250°C.

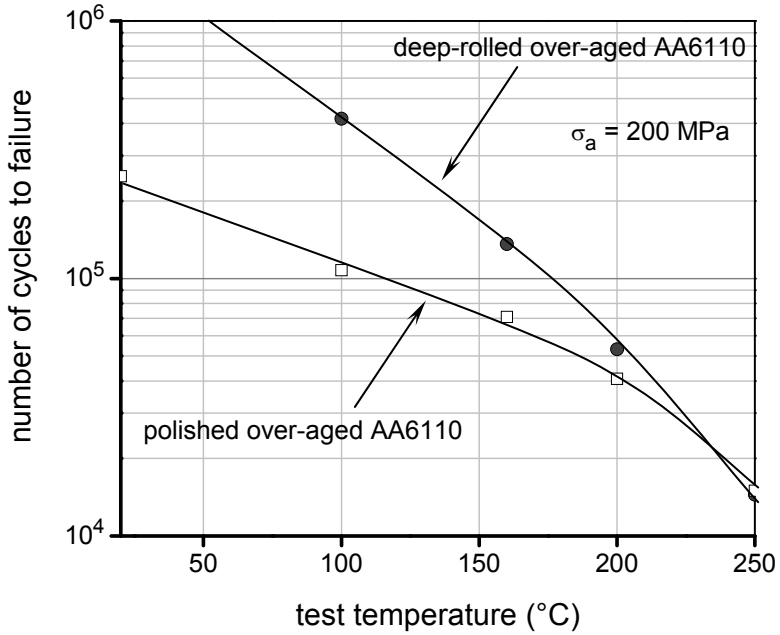

Figure 5.64: Fatigue lifetimes of polished and deep-rolled over-aged AA6110 at an applied stress amplitude of 200 MPa for different test temperatures.

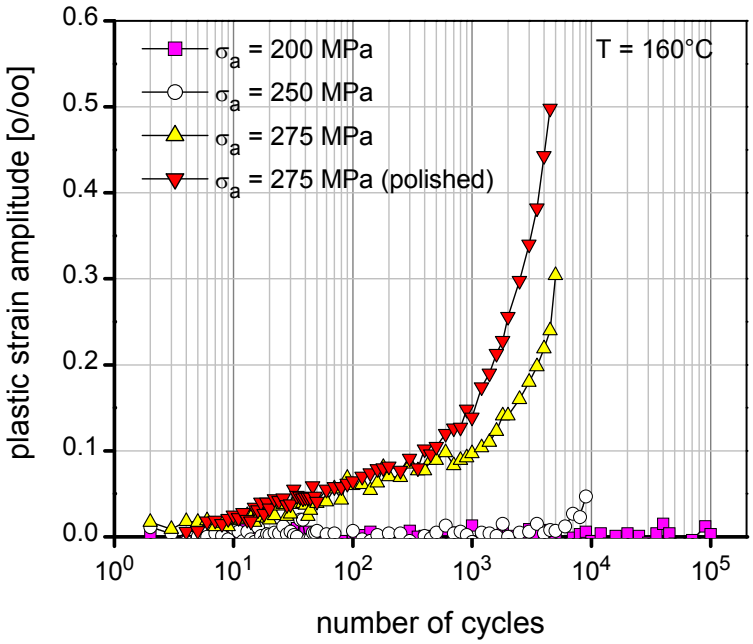

Figure 5.65: Cyclic deformation curves of deep-rolled (as well as polished) over-aged AA6110 at a test temperature of 160°C for different stress amplitudes.

residual stress-depth profiles. The residual stress relaxation of the deep-rolled over-aged AA6110 was also investigated in the same direction. The reduction of residual stresses at the surface during cyclic loading at room temperature for different stress amplitudes will be presented for mechanical residual stress relaxation. Thermal residual stress relaxation will be also analyzed using a Zener-Wert-Avrami function. Residual stress relaxation during fatigue tests at elevated temperature (thermomechanical residual stress relaxation) will be presented through residual stress-depth profiles.

Mechanical residual stress relaxation: Fig. 5.66 shows the mechanical residual stress as well as FWHM-value relaxation of the deep-rolled over-aged condition during fatigue tests at room temperature for different stress amplitudes. The macroscopic compressive residual stresses at the surface of the deep-rolled over-aged condition decreased with increasing applied stress amplitude and number of cycles, particularly in the first cycle of fatigue tests. A linear decrease of macroscopic compressive residual stresses with the logarithm of number of cycles was subsequently observed. At applied stress amplitudes of 350 and 400 MPa or

higher, the near-surface work hardening state became unstable, as can be easily seen in the decay of FWHM-values.

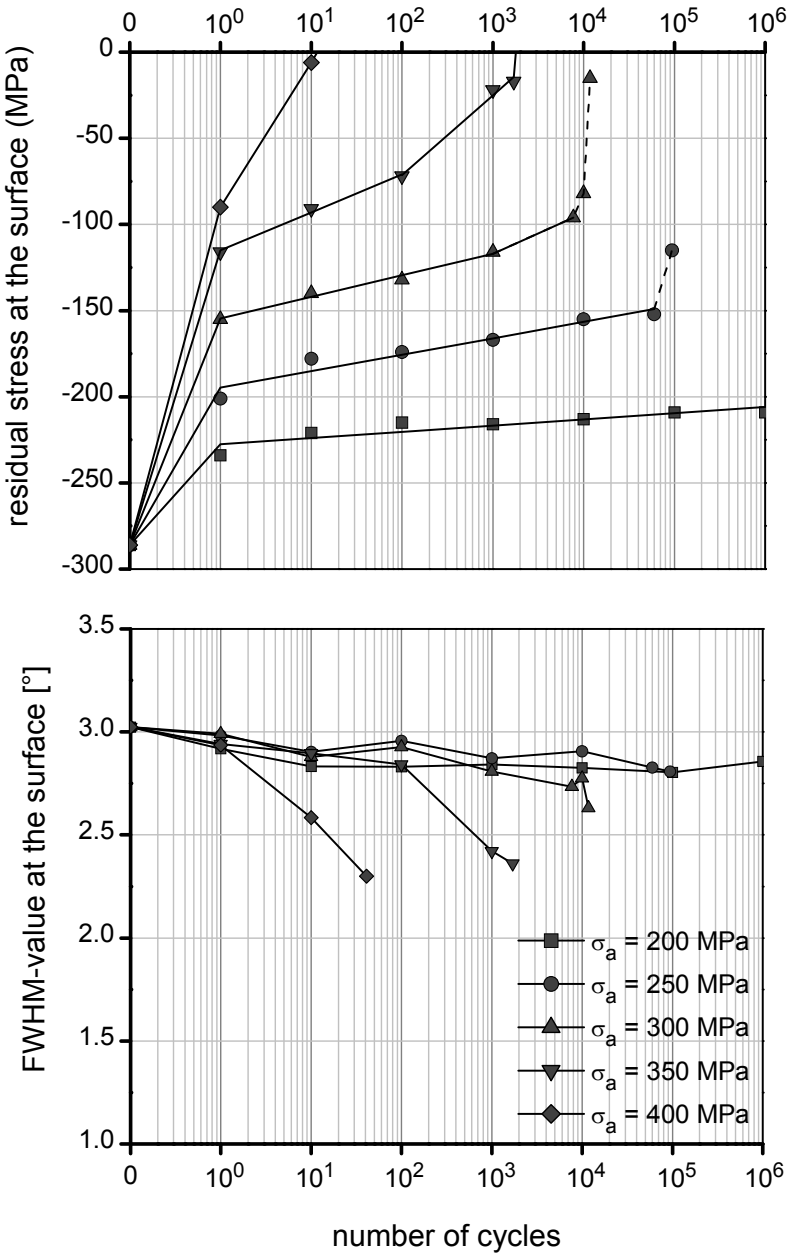

Figure 5.66: Residual stress and FWHM-value relaxation at the surface of deep-rolled over-aged AA6110 during stress controlled fatigue tests at room temperature for different stress amplitudes.

Thermal residual stress relaxation: Reduced residual stresses as well as FWHM-values due to thermal loading were described using a Zener-Wert-Avrami function in equations (2) and (3). A diagram of $\log \ln(\sigma_0^{RS} / \sigma^{RS})$ as a function of log t_a for a constant ageing temperature T_a in Fig. 5.67 gives a straight line of slope m = 0.21. The activation enthalpy for the relaxation process is determined using the slope of the log *ta* versus 1/k*Ta* in Fig. 5.68. The activation enthalpy of the relaxation process ΔH_{RS} = 1.23 eV and B_{RS} = 8.45 x 10^{10} min^{-1} were determined for the deep-rolled over-aged AA6110. The FWHM-value decrease appears to be related to the residual stress relaxation and can also be determined by using the Zener-Wert-Avrami function. The difference between the FWHM-values after ageing and the initial FWHM-value of 1.1° of the polished over-aged specimen substitutes the ratio in equation (2). Table 5.5 shows the determined materials constants of the FWHM-value as well as residual stress relaxation of the deep-rolled over-aged AA6110. The calculated decrease of FWHM-values and residual stresses as a function of ageing time and temperature using the respective materials constants in table 5.5 were constructed as presented in Fig. 5.69 as solid lines.

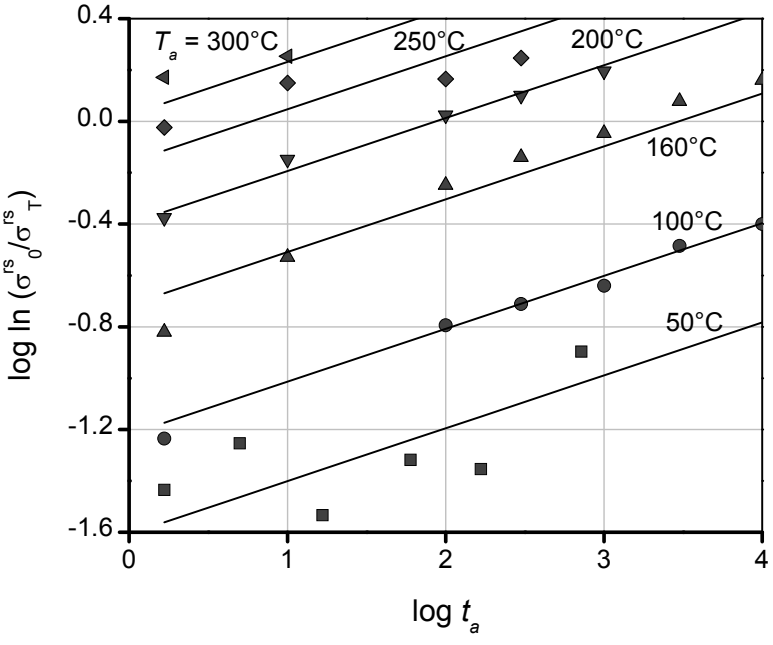

Figure 5.67: Influence of ageing time and temperature on surface residual stress of deep-rolled over-aged AA6110 in $\log \ln\left(\sigma_0^{RS} / \sigma_T^{RS}\right)$ versus log t_a diagram.

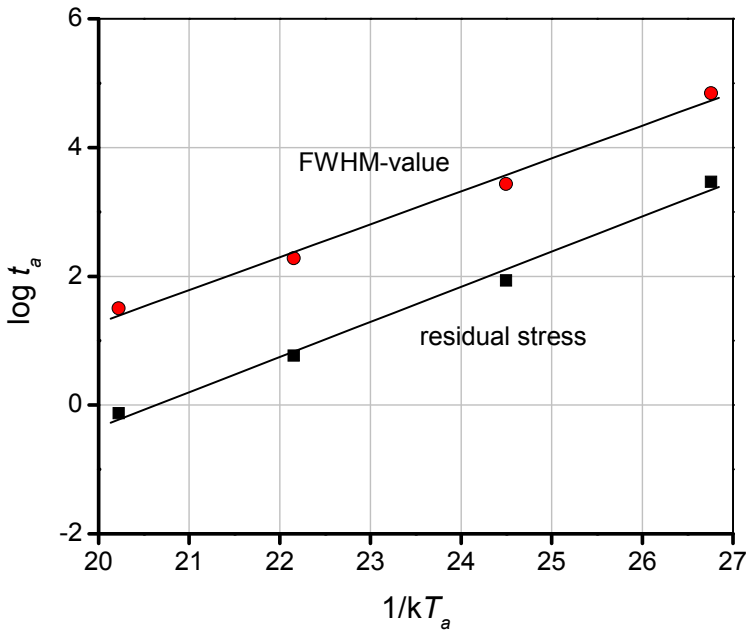

Figure 5.68: Plot of log t_a versus 1/kT_a for the determination of Avrami approach parameters of deep-rolled over-aged AA6110 for 50% residual stress as well as FWHM-value relaxation.

Table 5.5: Determined materials constants of thermal residual stress and FWHM-value relaxation of deep-rolled over-aged AA6110.

Over-aged AA6110	***m***	**Δ*H* (eV)**	***B*** **(min^{-1})**
Residual stress relaxation	0.20	1.23	8.45 x 10^{10}
FWHM-value relaxation	0.22	1.18	7.29 x 10^{8}

Thermomechanical residual stress relaxation: Fatigue tests at elevated temperature were performed to investigate thermomechanical residual stress relaxation and stability of near-surface macroscopic compressive residual stresses as well as work hardening states of the deep-rolled over-aged condition. The depth profiles of near-surface macroscopic compressive residual stresses and FWHM-values of three selected conditions were measured in Fig. 5.70; firstly, the deep-rolled specimen was heated at 160°C for 10 minutes without any applied stress amplitude to obtain a reference state: secondly and thirdly, the deep-rolled

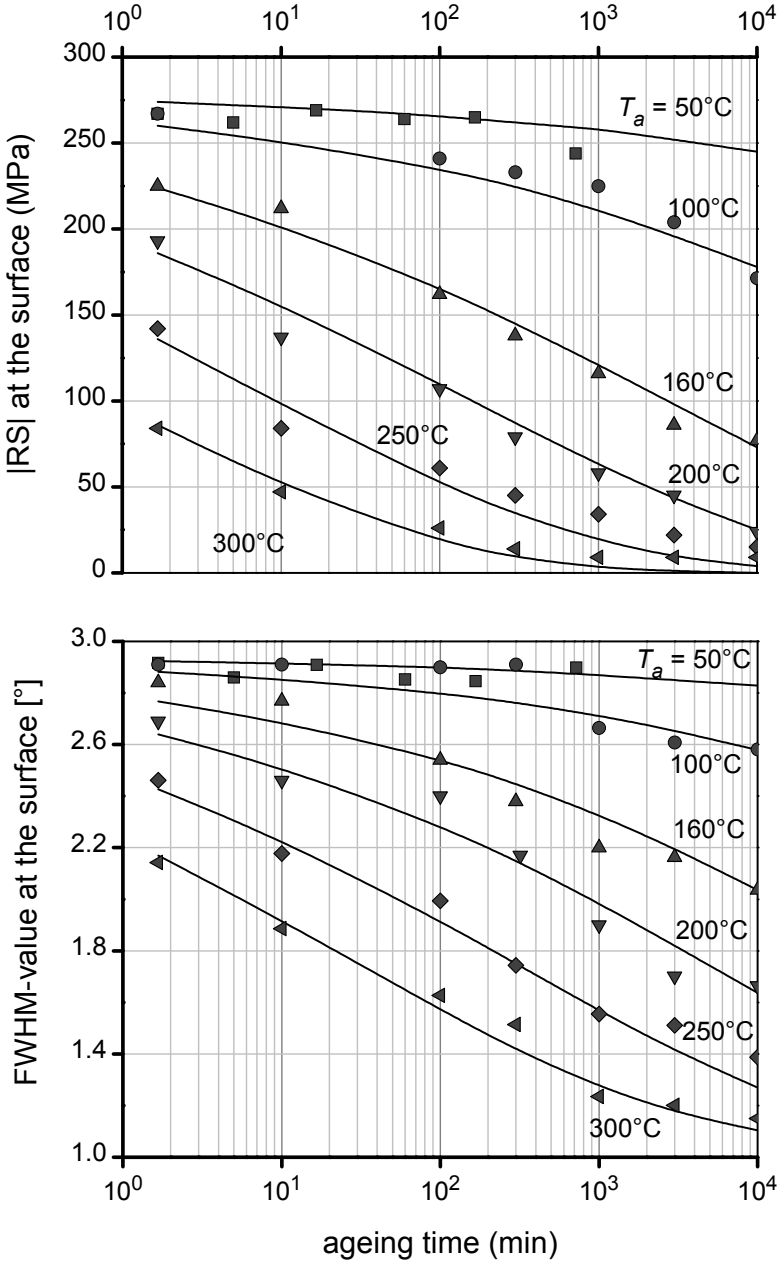

Figure 5.69: Influence of ageing time and temperature on the absolute values of residual stresses and FWHM-values at the surface and their description by the Avrami approach for deep-rolled over-aged AA6110.

over-aged specimens were cyclically deformed at a test temperature of 160°C for 1,000 cycles at applied stress amplitudes of 200 and 290 MPa, respectively. Near-surface macroscopic compressive residual stresses decreased after fatigue tests at applied stress amplitudes of 200 and 290 MPa at a test temperature of 160°C for 1,000 cycles. Particularly, at an applied stress amplitude of 290 MPa or higher,

macroscopic compressive residual stresses relaxed completely. Moreover, instability of near-surface work hardening states for this test condition was also detected as compared to the reference condition, whereas the near-surface work hardening after fatigue tests at an applied stress amplitude of 200 MPa at a test temperature of 160°C appears to be stable after 1,000 cycles.

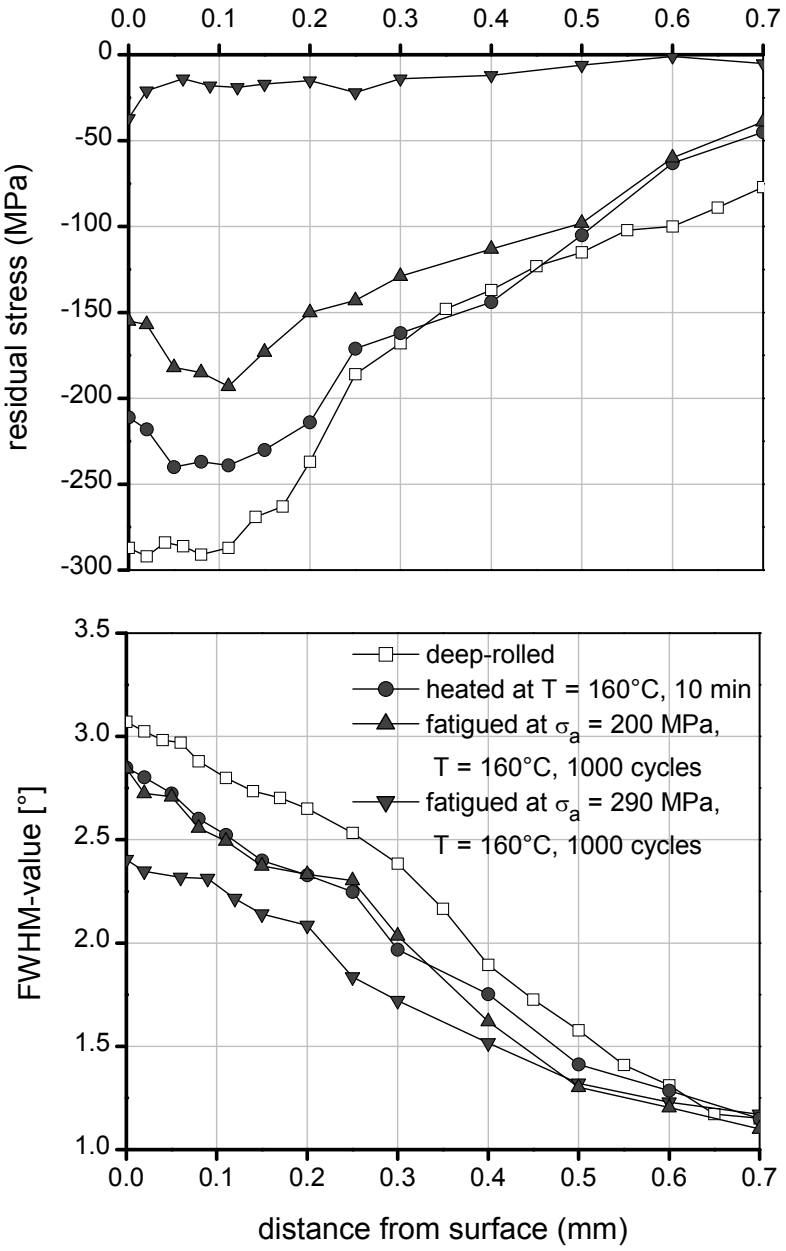

Figure 5.70: Residual stress- and FWHM-value-depth profiles of fatigued as well as heated specimens of deep-rolled over-aged AA6110.

5.2.6 Deep rolling followed by ageing treatment

In the previous sections, the fatigue behavior and residual stability of the differently aged AA6110 in non-mechanically and mechanically surface treated conditions have been systematically investigated. However, modern mechanical surface treatments progress continuously and combination methods of mechanical and thermal treatments have been introduced to achieve optimized surface conditions. For precipitation-hardenable materials, ageing treatments combined with shot peening or deep rolling are perhaps suitable alternative methods to enhance the effects of conventional mechanical surface treatments, i.e. combined methods are known to improve the fatigue behavior of steels [14]. Normally, for precipitation-hardenable materials, such as aluminium and titanium alloys, mechanical surface treatment is performed after ageing treatments for fatigue lifetime enhancement. However, in some cases, mechanical surface treatment is performed on solution heat treated (as-quenched) conditions with subsequent ageing treatments to produce increased hardness by precipitates especially in near-surface regions [17-19,66]. However, on the other hand, at the same time, near-surface macroscopic compressive residual stresses and work hardening states induced by mechanical surface treatments decrease during ageing treatments due to thermal residual stress relaxation. By the reduction of near-surface macroscopic compressive residual stresses and work hardening states, a detrimental effect for the fatigue lifetime can be expected. Therefore, the effects of decreased residual stresses as well as work hardening states together with increased hardnesses by the ageing treatment on the fatigue behavior should be thoroughly investigated and closely monitored in the following sections.

5.2.6.1 Optimization of the ageing treatment

Deep-rolled as-quenched specimens were aged for different temperatures between 50-300°C and times up to approximately 1 week. Afterwards, microhardness and fatigue tests were performed to find the optimized condition.

Near-surface properties: Fig. 5.71 shows the hardnesses at the surface of the deep-rolled as-quenched condition after ageing treatments as a function of ageing times and temperatures. After ageing treatments in the temperature range 160-

250°C, the hardness at the surface increased continuously with increasing ageing time until reaching a maximum value. Maximum hardnesses of approximately 140, 133 and 123 HV were measured after ageing at temperatures of 160, 200 and 250°C for ageing times of approximately 12 hours, 1,000 and 100 seconds, respectively. For an ageing temperature of 300°C, increased hardnesses at the surface were not observed.

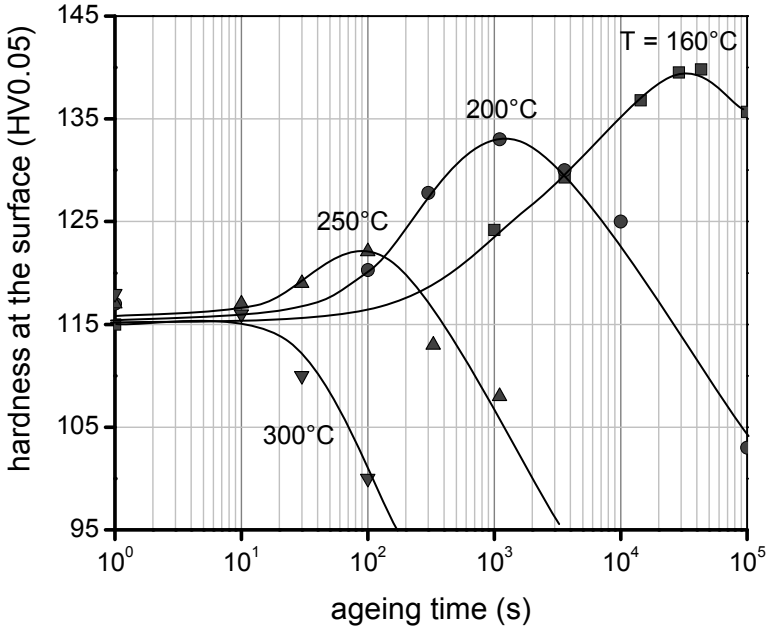

Figure 5.71: Change of the hardness at the surface of deep-rolled as-quenched AA6110 during different ageing treatments.

Fatigue lifetime: Fatigue tests were also performed to evaluate the optimized fatigue lifetime. For this purpose, the relation between ageing time, temperature and fatigue lifetime was established at an applied stress amplitude of 250 MPa as shown in Fig. 5.72. After ageing treatments in the temperature range 160-250°C, the fatigue lifetimes increased continuously with increasing ageing time until reaching a maximum lifetime. The optimized fatigue lifetime of the deep-rolled as-quenched AA6110 was found after an ageing treatment at a temperature of 160°C for about 12 hours.

Cyclic deformation curve: Cyclic hardening was observed in the deep-rolled as-quenched condition (see Fig. 5.17). After ageing treatments at elevated temperatures lower than 300°C, lower plastic strain amplitudes were observed as compared to the deep-rolled as-quenched condition. On the other hand, for ageing treatments at 300°C, increased plastic strain amplitudes was detected as shown in Fig. 5.73. A conversion from cyclic hardening to cyclic softening were observed if deep-rolled as-quenched specimens were aged at relatively high ageing temperature, e.g. at temperatures of 200 and 250°C for ageing times of 28 hours and 1,000 seconds, respectively (see Fig. 5.74).

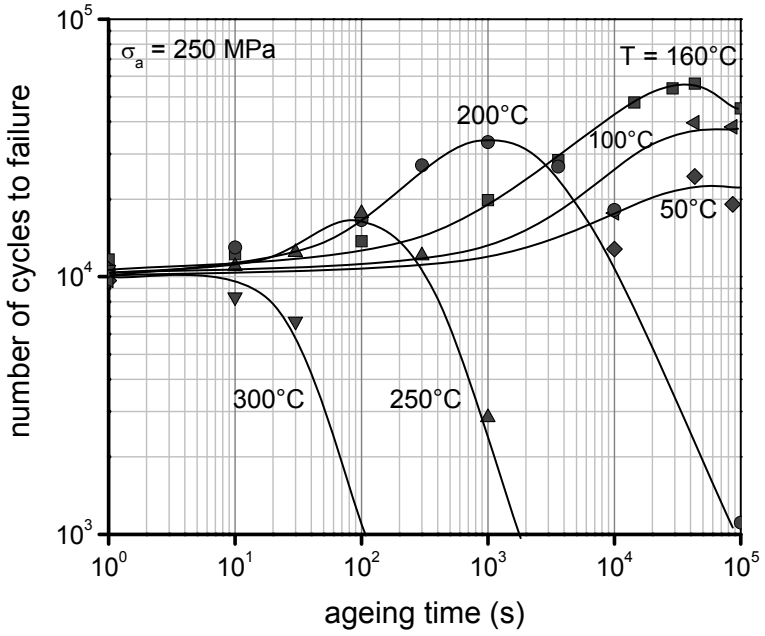

Figure 5.72: Fatigue lifetimes as a function of ageing time and temperature at an applied stress amplitude of 250 MPa.

5.2.6.2 Cyclic deformation behavior of the optimized condition

According to section 5.2.6.1, the maximum hardness as well as fatigue lifetime was observed after an ageing treatment at 160°C for approximately 12 hours. This condition will consequently be named the *optimized ageing parameter/treatment*. The cyclic deformation behavior of the optimized condition will be investigated at

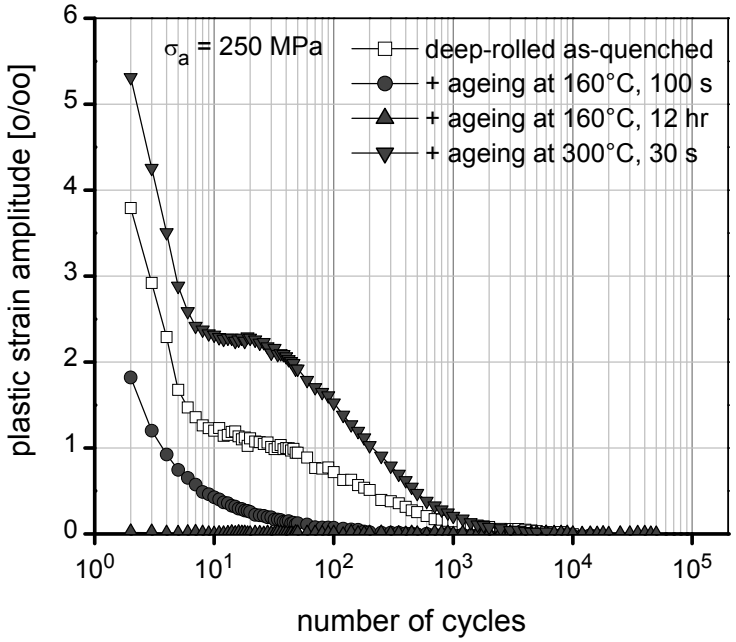

Figure 5.73: Cyclic deformation curves of deep-rolled as-quenched AA6110 after ageing treatments at temperatures of 160 and 300°C for different ageing times at an applied stress amplitude of 250 MPa.

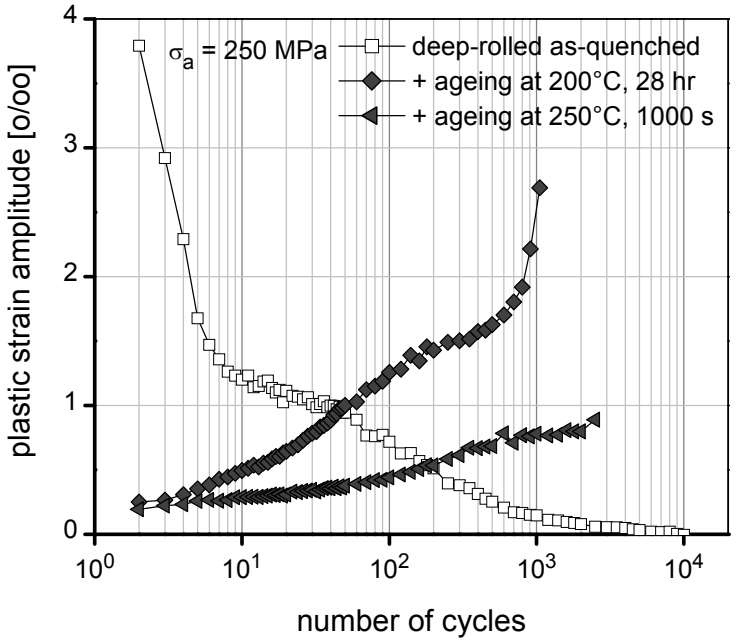

Figure 5.74: Cyclic softening during fatigue tests at an applied stress amplitude of 250 MPa of deep-rolled as-quenched AA6110 after long time exposure at temperatures of 200 and 250°C.

room and elevated temperatures. Depth profiles of near-surface residual stresses, work hardening states and hardnesses, s/n-curves and fatigue lifetimes at elevated temperatures will be presented in this section.

Near-surface properties: The hardness of the deep-rolled as-quenched specimen increased significantly after the optimized ageing treatment as compared to the deep-rolled as-quenched condition as shown in Fig. 5.75. At the meantime, the residual stresses and FWHM-values decreased due to the relaxation as well as recovery processes. Residual stress and FWHM-values at the surface were reduced from -265 to -100 MPa and from 2.3° to 2.0°, respectively. Because residual stress relaxation immediately at the surface is stronger than in subsurface layers, after ageing, a subsurface compressive residual stress maximum is formed as shown in Fig. 5.76.

Fatigue lifetime: Non-statistically evaluated s/n-curve of the deep-rolled as-quenched state after the optimized ageing treatment is shown as compared to the deep-rolled as-quenched condition in Fig. 5.77. At room temperature, the ageing treatment after mechanical surface treatment can enhance the fatigue lifetime especially in low cycle fatigue regime. However, in the high cycle fatigue regime,

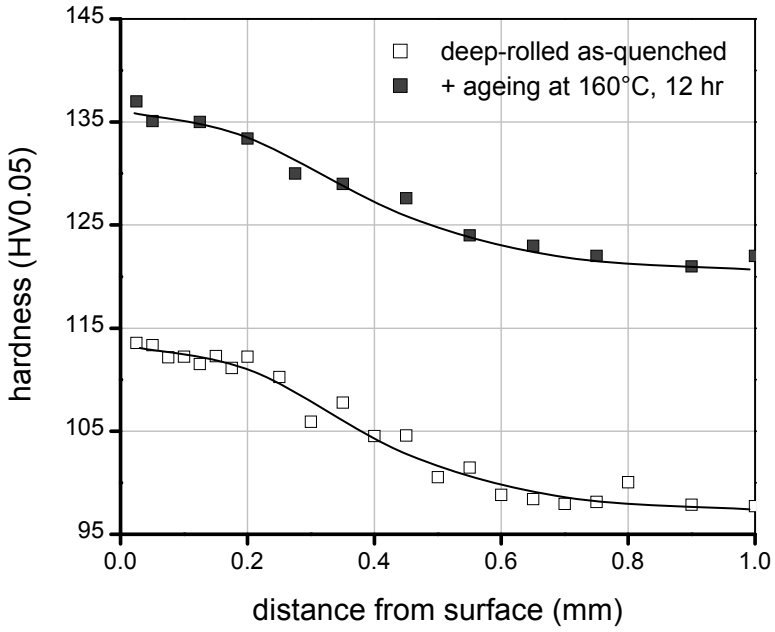

Figure 5.75: Hardness-depth profiles of deep-rolled as-quenched AA6110 before and after the optimized ageing treatment.

the difference in fatigue lifetimes was almost negligible. For elevated test temperature, the optimized-aged deep-rolled condition exhibits also greater fatigue lifetimes as compared to the deep-rolled as-quenched condition. Fig. 5.78 shows a comparison of fatigue lifetimes of the optimized-aged deep-rolled and deep-rolled as-quenched condition as a function of test temperature at an applied stress amplitude of 225 MPa. With increasing test temperature, fatigue lifetimes of the optimized-aged deep-rolled condition decrease continuously.

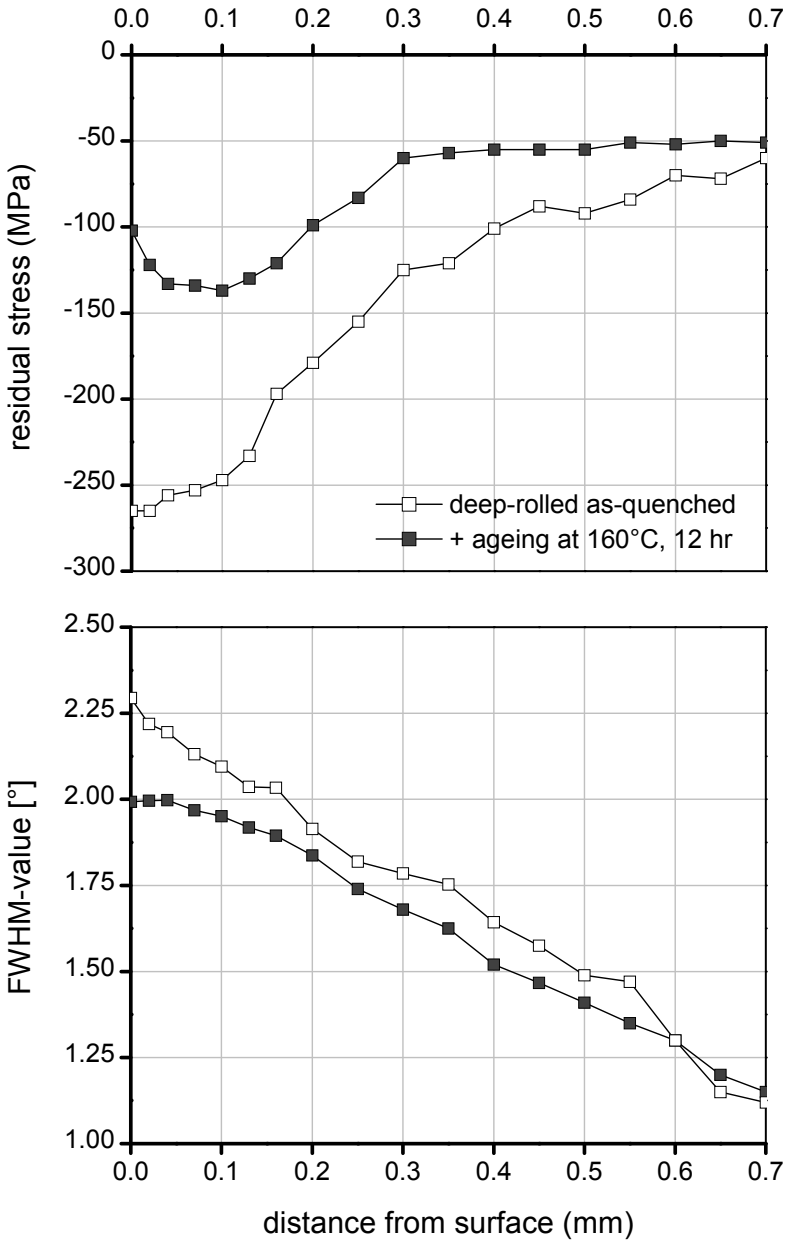

Figure 5.76: Residual stress- and FWHM-value-depth profiles of deep-rolled as-quenched AA6110 before and after the optimized ageing treatment.

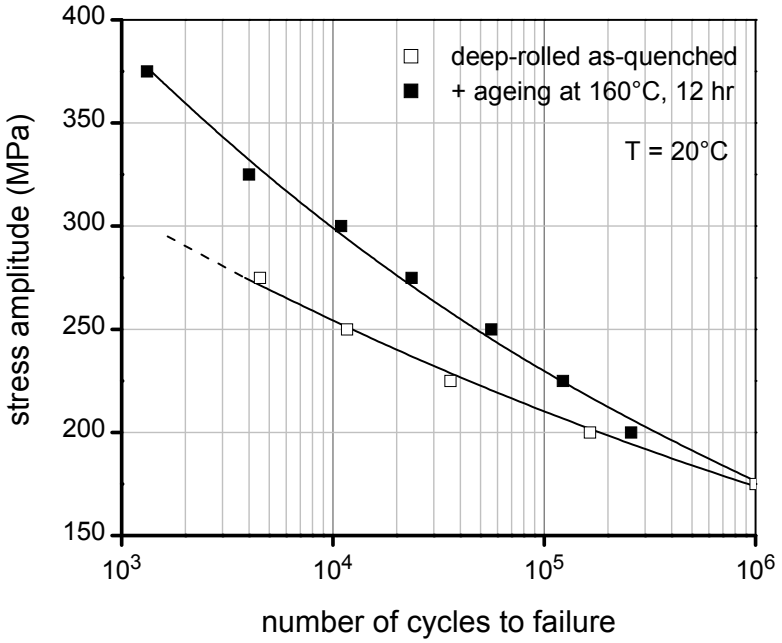

Figure 5.77: Non-statistically evaluated s/n-curves at room temperature of deep-rolled as-quenched specimens before and after the optimized ageing treatment.

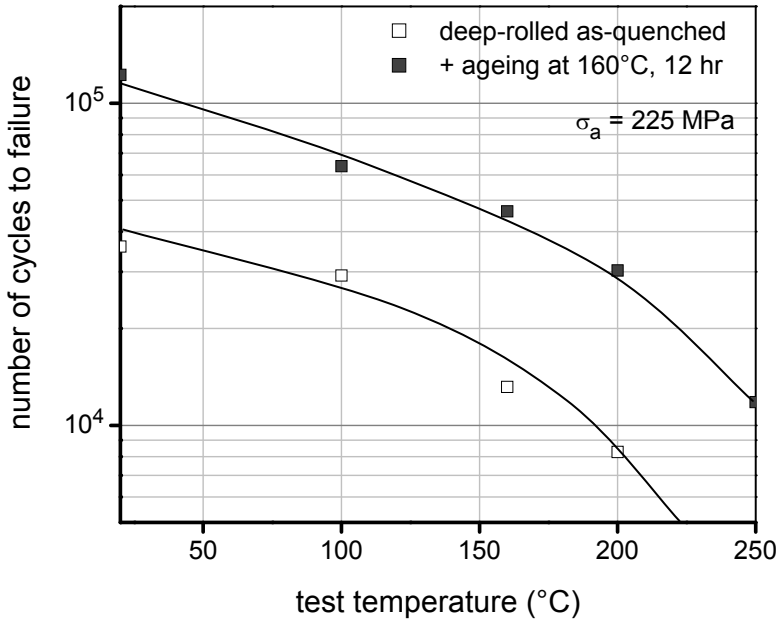

Figure 5.78: Fatigue lifetimes of deep-rolled as-quenched AA6110 before and after the optimized ageing treatment at an applied stress amplitude of 225 MPa for different test temperatures.

5.2.7 Deep rolling at elevated temperature

In the archival literature, high-temperature deep rolling has been successfully investigated for SAE 1045 as well as AISI 304 [20-24]. The fatigue behavior of these steels can be enhanced considerably due to static/dynamic strain ageing and together with very fine carbides at the surface and in near-surface regions [20-24]. Nevertheless, for aluminium alloys, it is still doubtful whether thermomechanical surface treatments can enhance the fatigue behavior more significantly than conventional mechanical surface treatments because aluminium alloys have mainly substitutional solute atoms. Thus, the fully beneficial effects of static/dynamic strain ageing can not be expected. However, static/dynamic precipitation during mechanical surface treatment at elevated temperature may contribute to mechanical properties of the surface as well as the bulk particularly for the as-quenched condition. Therefore, high-temperature deep rolling on the as-quenched aluminium alloy AA6110 was investigated. As-quenched specimens were deep rolled at different elevated temperatures of 160, 200 and 250°C. Afterwards, near-surface properties and cyclic deformation behavior were investigated and presented in this section.

Near-surface properties: After deep rolling at elevated temperatures, near-surface residual stress-, work hardening- and hardness-depth profiles were measured as compared to the room-temperature deep-rolled state as shown in Figs. 5.79 and 5.80. Obviously, macroscopic compressive residual stresses tend to decrease with increasing deep rolling temperature. Maximum macroscopic compressive residual stresses of -181, -152 and -59 MPa were measured at a depth of 20 µm after deep rolling at temperatures of 160, 200 and 250°C, respectively. In contrast, after deep rolling at room temperature, a maximum macroscopic compressive residual stress value of -266 MPa was measured directly at the surface (see section 5.2.2.3). After deep rolling at a temperature of 160°C an approximately FWHM-value of 2.3° was measured which was identical to the one observed after room-temperature deep rolling. However, FWHM-values tend to decrease at high temperature with increasing deep rolling temperature. The FWHM-values about 2.1 and 1.6° were detected after deep rolling at temperatures of 200 and 250°C, respectively. In addition, the case depth of work hardening after deep rolling at elevated temperatures seems to be greater

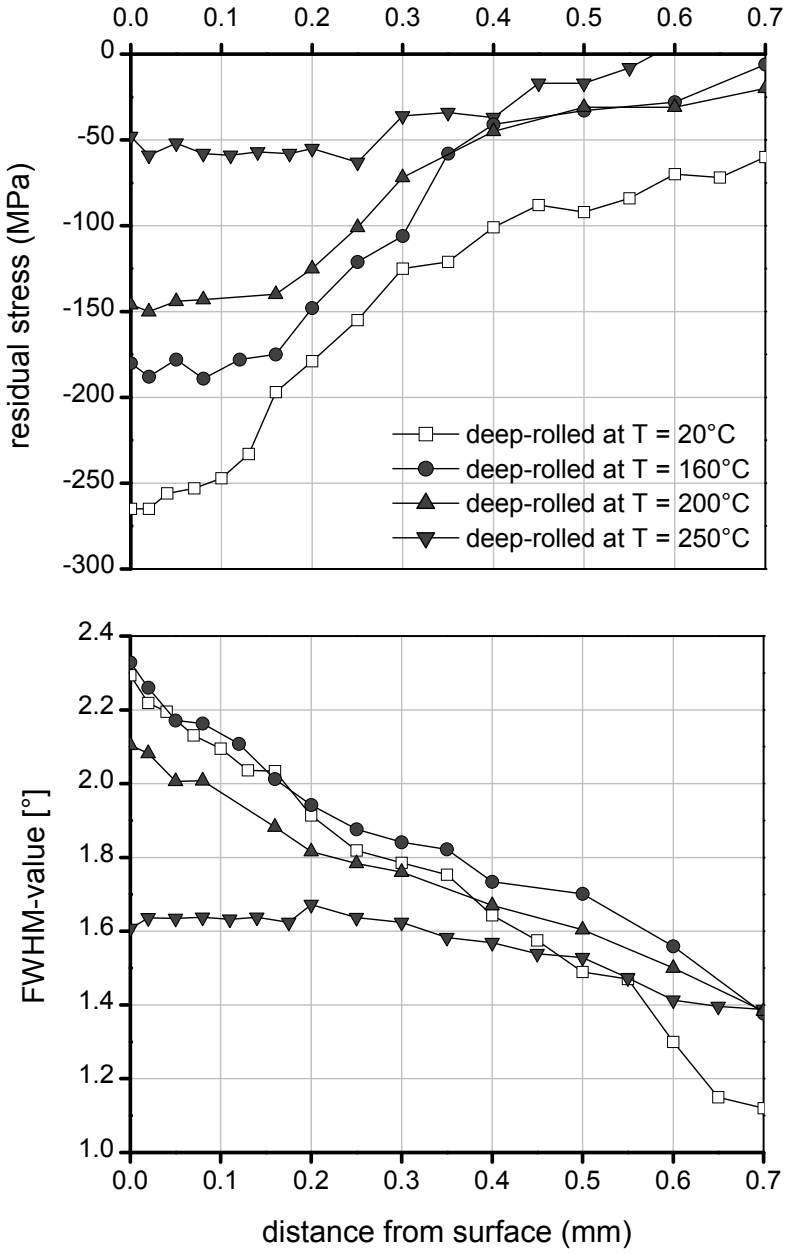

Figure 5.79: Depth profiles of near-surface macroscopic compressive residual stresses and FWHM-values of high-temperature deep-rolled as-quenched AA6110 for different deep rolling temperatures.

than after room-temperature deep rolling. Near-surface hardnesses, however, increased with increasing deep rolling temperature up to 200°C as compared to deep rolling at room temperature. Hardnesses in a depth of 25 µm of about 125 and 134.5 HV were measured after deep rolling at temperatures of 160 and

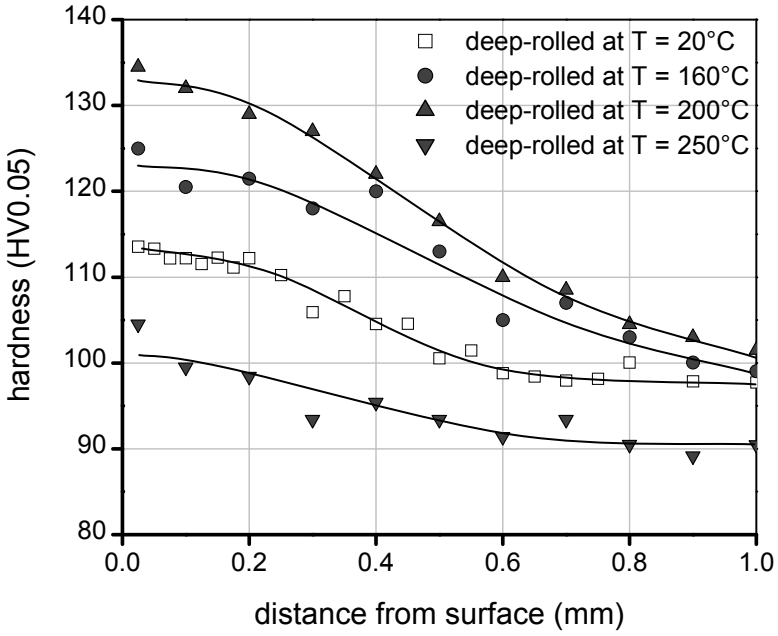

Figure 5.80: Depth profiles of near-surface hardnesses of high-temperature deep-rolled as-quenched AA6110 for different deep rolling temperatures.

200°C, respectively, whereas after deep rolling at room temperature, the hardness in a depth of 25 µm was approximately 113 HV. Conversely, after deep rolling at a temperature of 250°C, a hardness in a depth of 25 µm of only about 104 HV was observed.

Fatigue lifetime: Non-statistically evaluated s/n-curves of the differently high-temperature deep-rolled as-quenched conditions at room temperature are presented as compared to the room-temperature deep-rolled as-quenched condition in Fig. 5.81. The difference fatigue lifetimes for deep rolling treatments at temperatures between room temperature and 200°C were insignificant. In the low cycle fatigue regime, fatigue lifetimes of as-quenched specimens deep-rolled at a temperature of 200°C seem to be slightly better than of the room-temperature deep-rolled as-quenched condition, however in the high cycle fatigue regime, a contrary behavior was seen. Although in room-temperature fatigue tests, the high-temperature deep rolling enhance fatigue lifetimes only insignificantly. However, for fatigue lifetimes in the temperature range of 100-200°C, high-temperature deep rolling shows clearly more positive effects on the fatigue lifetimes as shown in

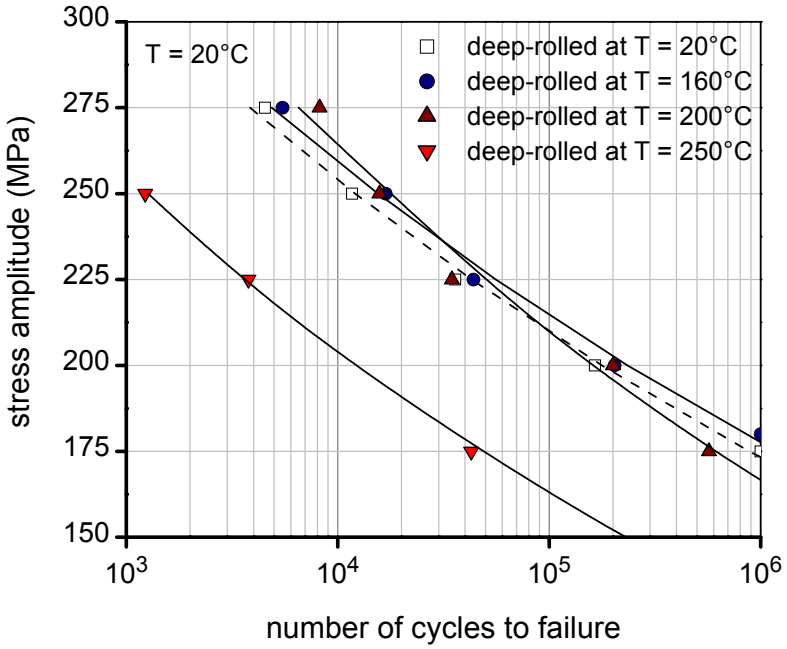

Figure 5.81: Non-statistically evaluated s/n-curves of high-temperature deep-rolled as-quenched AA6110 for different deep rolling temperatures.

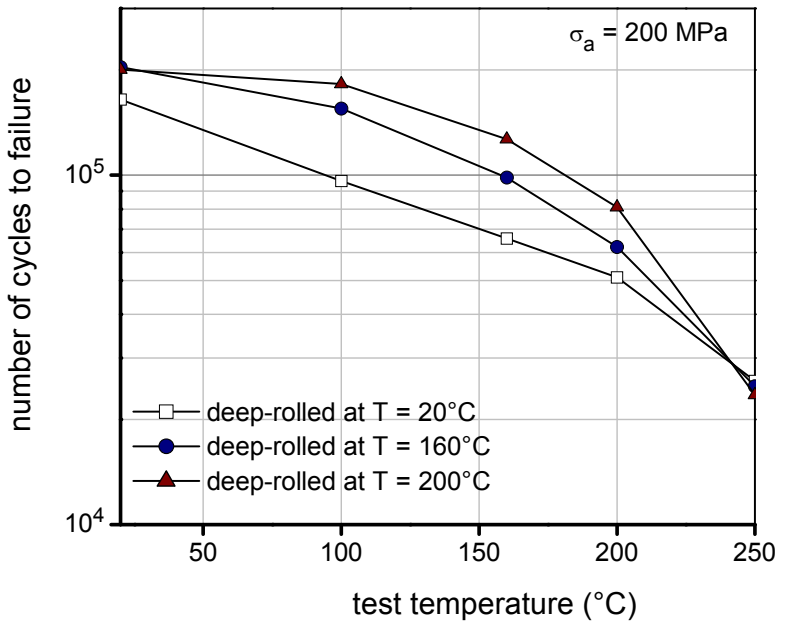

Figure 5.82: Fatigue lifetimes of differently high-temperature deep-rolled as-quenched AA6110 at an applied stress amplitude of 200 MPa for different test temperatures.

Fig. 5.82. For deep rolling at a temperature of 250°C, the fatigue lifetimes at room temperature decreased strongly. At room-temperature fatigue tests, the fatigue lifetime of the room-temperature deep-rolled as-quenched condition at an applied stress amplitude of 250 MPa is about 12,000 cycles whereas the fatigue lifetime of the as-quenched specimen deep-rolled at a temperature of 250°C decreased to approximately 1,200 cycles for the same test condition.

Cyclic deformation curve: During room-temperature fatigue tests, specimens deep-rolled at temperatures up to 200°C exhibited cyclic hardening. Plastic strain amplitudes decreased with increasing deep rolling temperature up to 200°C as shown in Fig. 5.83 which depicts the cyclic deformation curves of the differently high-temperature deep-rolled as-quenched conditions at an applied stress amplitude of 250 MPa at room temperature. Cyclic softening was detected during room-temperature fatigue tests when specimens were deep rolled at a temperature of 250°C.

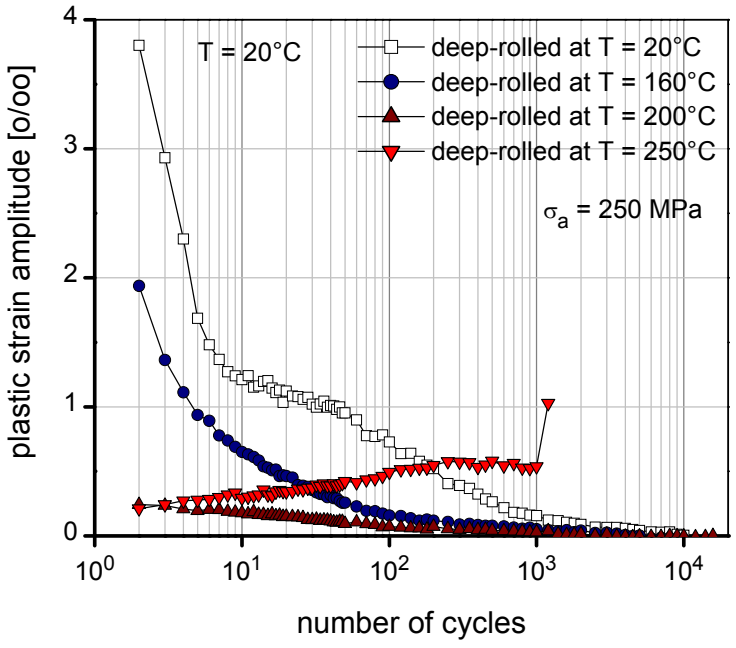

Figure 5.83: Cyclic deformation curves of high-temperature deep-rolled as-quenched AA6110 at an applied stress amplitude of 250 MPa for different deep rolling temperatures.

Chapter 6

Discussion

6.1 Overview/outline

In this section, all results of the previous chapter will be intensively analyzed and discussed. The aluminium alloys AA5083 and AA6110 will be together discussed for all sections, e.g. their quasistatic and cyclic deformation behavior. The quasistatic deformation behavior in the next section, the influence of precipitation as well as temperature on the 0.2% yield and ultimate tensile strengths and work hardening rate will be discussed as a guideline of materials behavior at room and elevated temperatures. The cyclic deformation behavior in the following section (§ 6.3) was separately discussed into six subsections: firstly, the polished condition was discussed in section 6.3.1 where the influence of precipitation, stress amplitude, temperature on the fatigue lifetimes and cyclic deformation curves of the polished AA5083 and differently aged AA6110 will be presented. Secondly, in the section of the deep-rolled condition (§ 6.3.2), experimental results of the only deep-rolled condition will be analyzed and discussed with the same direction/methods as in the polished section. Afterwards, in section 6.3.3 named comparison of the polished and deep-rolled condition, the influence of deep rolling on fatigue lifetime as well as cyclic deformation curve will be discussed as compared to the polished condition using the information from sections 6.3.1 and 6.3.2. Moreover, the influence of stress amplitude as well as temperature on the beneficial effects of deep rolling will also be presented. Eventually, effective borderlines of deep rolling for the AA5083 and differently aged AA6110 were established in this section. Consequently, in section 6.3.4, residual stress stability was discussed and used to analyze/explain the deterioration of the beneficial effects of deep rolling during cyclic and/or thermal loading. In the last two sections (§ 6.3.5 and 6.3.6), modified deep rolling treatments, e.g. deep rolling followed by ageing and deep rolling at elevated temperature will be discussed as compared to conventional deep rolling.

6.2 Quasistatic deformation behavior

Influence of precipitation: The aluminium alloy AA5083 is a non-precipitate-hardenable alloy which can be strengthened by work hardening (increasing dislocation densities) and/or strain fields induced by substitutional solute atoms. Therefore, the discussion will be focused on the precipitation-hardenable aluminium alloy AA6110 in this section. As mentioned and discussed already in section 5.2.1, mechanical properties, i.e. hardnesses, 0.2% yield as well as ultimate tensile strengths increased after an ageing treatment at a temperature of 160°C (see Figs. 5.10 and 5.11) due to finely distributed precipitates (see Figs. 5.14 (a)-(c)). From Fig. 5.11, the 0.2% yield and ultimate tensile strengths for the differently aged AA6110 were summarized in Fig. 6.1. For as-quenched condition, no effective precipitates in the aluminium matrix are assumed. Its strengthening is normally dominated by strain fields of (substitutional) solute atoms, similar to the aluminium alloy AA5083. Thus, the dislocations can move easier in the activated slip planes, consequently relatively low 0.2% yield and ultimate tensile strengths were measured. After the ageing treatment, coherent β´´ precipitates were observed (see Fig. 5.14) and they play an important role in impeding dislocation movement. Consequently, a significant increase of the 0.2% yield and ultimate tensile strengths can be seen for the under-, peak- and over-aged conditions. For the over-aged condition, coherent, semi-coherent precipitates β´´, β´ as well as Q´ which are relatively coarse were detected within the aluminium matrix (see Fig. 5.14 (c)). Consequently, mechanical properties, such as hardness, 0.2% yield and ultimate tensile strengths decreased as compared to the peak-aged condition. Precipitates not only affected on the 0.2% yield and ultimate tensile strengths, but also the work hardening rate ($d\sigma/d\varepsilon$). In fact, pure aluminium has high stacking fault energy (SFE), therefore easy glide and cross slip of edge and screw dislocations can be expected. Consequently, a relatively low work hardening rate was reported [30,67,115]. An addition of solute atoms/elements in aluminium normally decrease the stacking fault energy of the system, hence a relatively high work hardening rate can be expected in the aluminium alloy AA5083 as well as as-quenched AA6110 as shown in Fig. 6.2 which depicted the work hardening rate of AA5083 and AA6110 at a plastic strain of 3% for a test temperature of 20°C as a function of ageing time at an ageing temperature of 160°C. The work hardening

rates of the as-quenched AA6110 as well as AA5083 are relatively high. After the ageing treatment, the work hardening rate decreases with increasing ageing time. This behavior is typically observed in aluminium alloys containing shear/deformable precipitates. The peak- and over-aged AA6110 exhibit low work hardening rates. It confirms once more that precipitates in the peak- and over-aged conditions are coherent as well as semi-coherent with the matrix and dislocations move continuously through the precipitates [115,116].

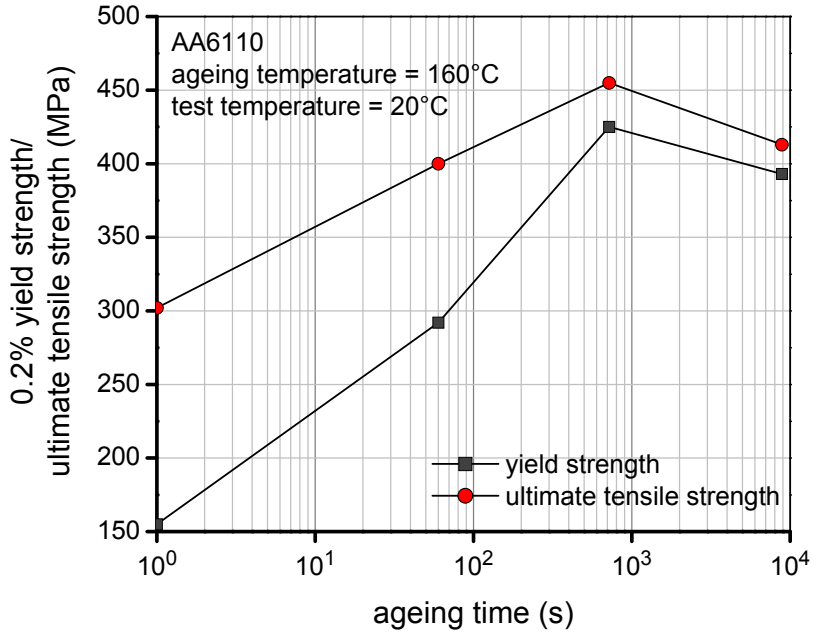

Figure 6.1: 0.2% yield and ultimate tensile strengths of differently aged AA6110 as a function of ageing time at an ageing temperature of 160°C.

Influence of temperature: In general, in the absence of strain ageing, the strength of metallic materials decreases with increasing temperature. Aluminium alloys also exhibit a similar behavior. The 0.2% yield as well as ultimate tensile strengths of AA5083, under-, peak- and over-aged AA6110 decreased considerably with increasing test temperature (see Figs. 5.1, 5.27, 5.41 and 5.57, respectively). However, an increase of the 0.2% yield strengths was detected in the as-quenched AA6110 with increasing test temperature up to 200°C, presumably due to static/dynamic precipitation (see Fig. 6.3).

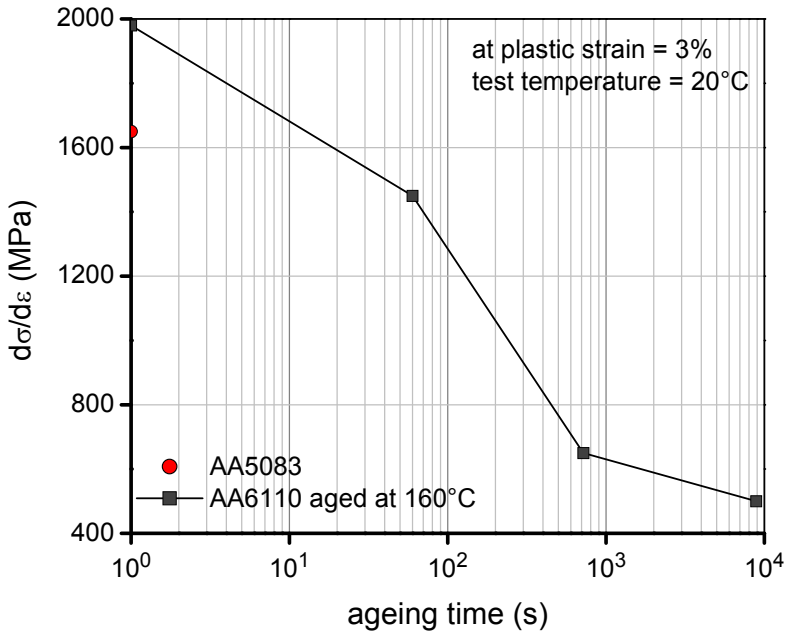

Figure 6.2: Work hardening rate of differently aged AA6110 as well as AA5083 as a function of ageing time at an ageing temperature of 160°C.

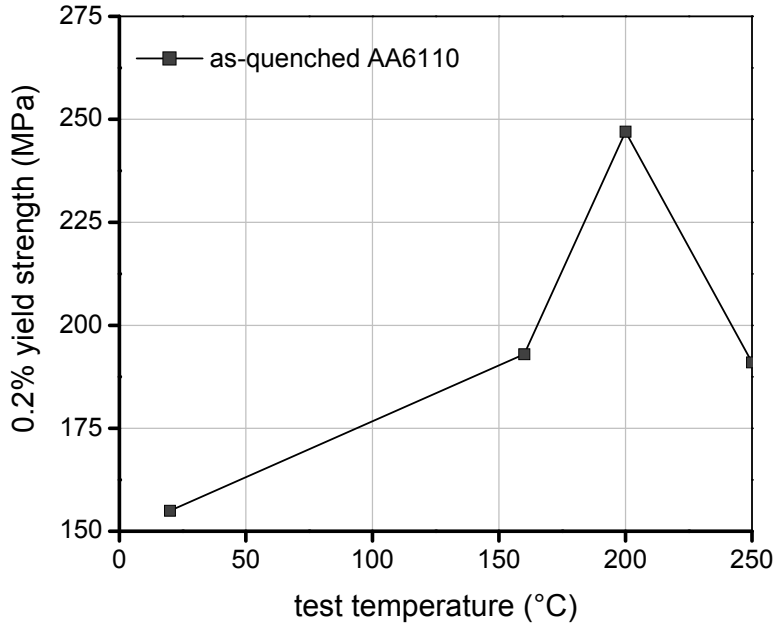

Figure 6.3: Change of 0.2% yield strength of as-quenched AA6110 during tensile tests for different test temperatures.

6.3 Cyclic deformation behavior

6.3.1 Polished condition

The cyclic deformation behavior of the polished condition is an essential information to analyze the effect of deep rolling in the following section. Therefore, in this section, the cyclic deformation behavior at room and elevated temperatures of the polished AA5083 and AA6110 (the letter one in differently aged conditions) will be intensively analyzed and its effect on fatigue lifetime will be discussed.

6.3.1.1 Fatigue lifetime

Influence of precipitation: To investigate the influence of precipitation on the fatigue lifetime of AA6110, s/n-curves of differently aged AA6110 are summarized and plotted in one diagram, as depicted in Fig. 6.4. No significant differences in fatigue lifetimes of the polished under-, peak- and over-aged AA6110 at room temperature are seen for these investigations. An analogous behavior was also documented for the alloy Al-5Mg-0.5Ag [1]. The quite similar hardnesses of the under-, peak- and over-aged AA6110 in table 5.1 can be perhaps attributed to this behavior. Obviously, for these investigations of AA6110, if the hardness is significantly lower as in the as-quenched condition, fatigue lifetimes are considerably lower when compared to other aged conditions in the low cycle fatigue regime. Usually, the influence of precipitations on the fatigue lifetime as well as strength is more obviously manifested in the high cycle fatigue regime (10^7-10^8 cycles) [1].

Influence of stress amplitude: The s/n-curve is the classical and simple method to describe the effect of stress amplitude on the fatigue lifetime especially for stress-controlled fatigue test. In general, fatigue lifetimes at room temperature decrease with increasing stress amplitude. The logical and typical s/n-curves of the polished AA5083 and differently aged AA6110 at room temperature are seen in Figs. 5.2 and 6.4. At room temperature, s/n-curves can be regularly described by a Basquin equation [30,32,34].

$$\sigma_a = aN_f^b \tag{4}$$

where *a* and *b* are materials constants, positive and negative values, respectively. From s/n-curves at room temperature of the polished AA5083 and different aged AA6110 in Figs 5.2 and 6.4, the materials constants *a* and *b* can be determined and are summarized in table 6.1.

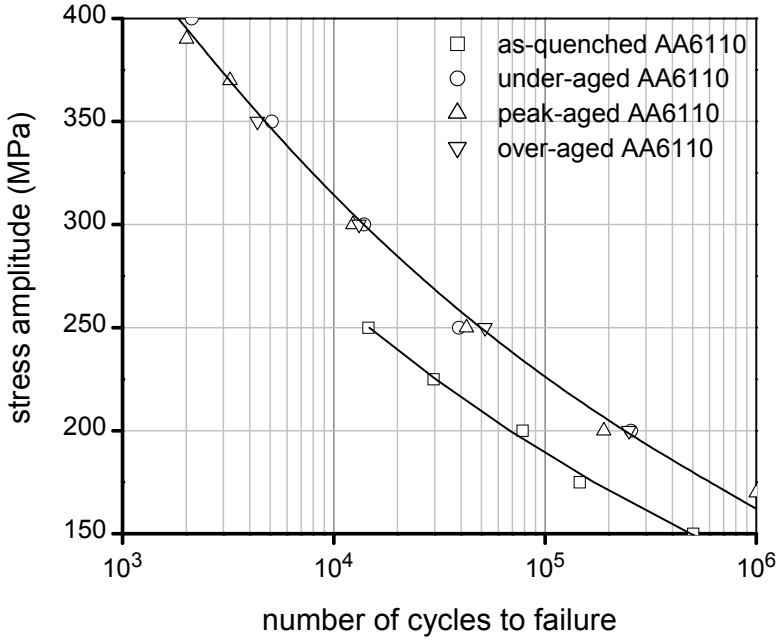

Figure 6.4: Non-statistically evaluated s/n-curves of polished differently aged AA6110 at room temperature.

Table 6.1: Determined materials constants *a* and *b* of the Basquin equation for polished AA5083 and differently aged AA6110 at room-temperature fatigue tests.

Polished condition	**Materials constant *a***	**Materials constant *b***
AA5083	696.65	-0.117
As-quenched AA6110	1014.2	-0.146
Under-aged AA6110	1185.7	-0.145
Peak-aged AA6110	1185.7	-0.145
Over-aged AA6110	1185.7	-0.145

Influence of temperature: From the results of elevated-temperature fatigue tests of the polished AA5083 and differently aged AA6110 in Figs. 5.2, 5.16, 5.28, 5.42 and 5.58, the effect of test temperature on the fatigue lifetime are clearly seen. Fatigue lifetimes of the polished AA5083 and AA6110 usually decreased with increasing test temperature. However, for the polished as-quenched and under-aged AA6110, static/dynamic precipitates occurred during high temperature exposure and hence affected more or less the fatigue lifetime at elevated temperatures. Therefore, the fatigue behavior at elevated temperature of the polished differently aged AA6110 is meaningful and ought to be analyzed in more details. For elevated temperature, if log-log scales and Kelvin temperature are used, the Basquin equation can be generalized to the following form [117].

$$\sigma_a = a^* N_f^b T^c \tag{5}$$

where a^* is a materials constant which differs from the constant a in equation (4), c is also a materials constant, named *the temperature sensitivity parameter* and can be defined by the equation

$$c = \left.\frac{\partial \log \sigma_a}{\partial \log T}\right|_{N_f = const.} \tag{6}$$

From equation (6), the temperature dependence of stress amplitude was plotted in a bi-logarithmic scale for a given number of cycles to failure ($3x10^3$, 10^4, $3x10^4$, 10^5 and $3x10^5$) of the polished differently aged AA6110 in Figs. 6.5 (a)-(d). Since experimental data for the above cycles to failure were not available, values obtained by separate fits for each temperatures using equation (4) were used. In Fig. 6.5 (a), stress amplitudes for given numbers of cycles increase at a test temperature of 100°C and then slightly decrease with increasing test temperature up to approximately 200°C. It can be attributed to the effect of static/dynamic precipitates on the fatigue lifetimes of the polished as-quenched AA6110 at elevated temperatures. Consequently, a materials constant c of the polished as-quenched AA6110 for fatigue tests at elevated temperatures can not be determined using equation (6). On the other hand, for the polished under-, peak- and over-aged AA6110 in Figs. 6.5 (b)-(d), two important aspects were detected: firstly, the experimental results can be fitted by equation (6) for test temperatures

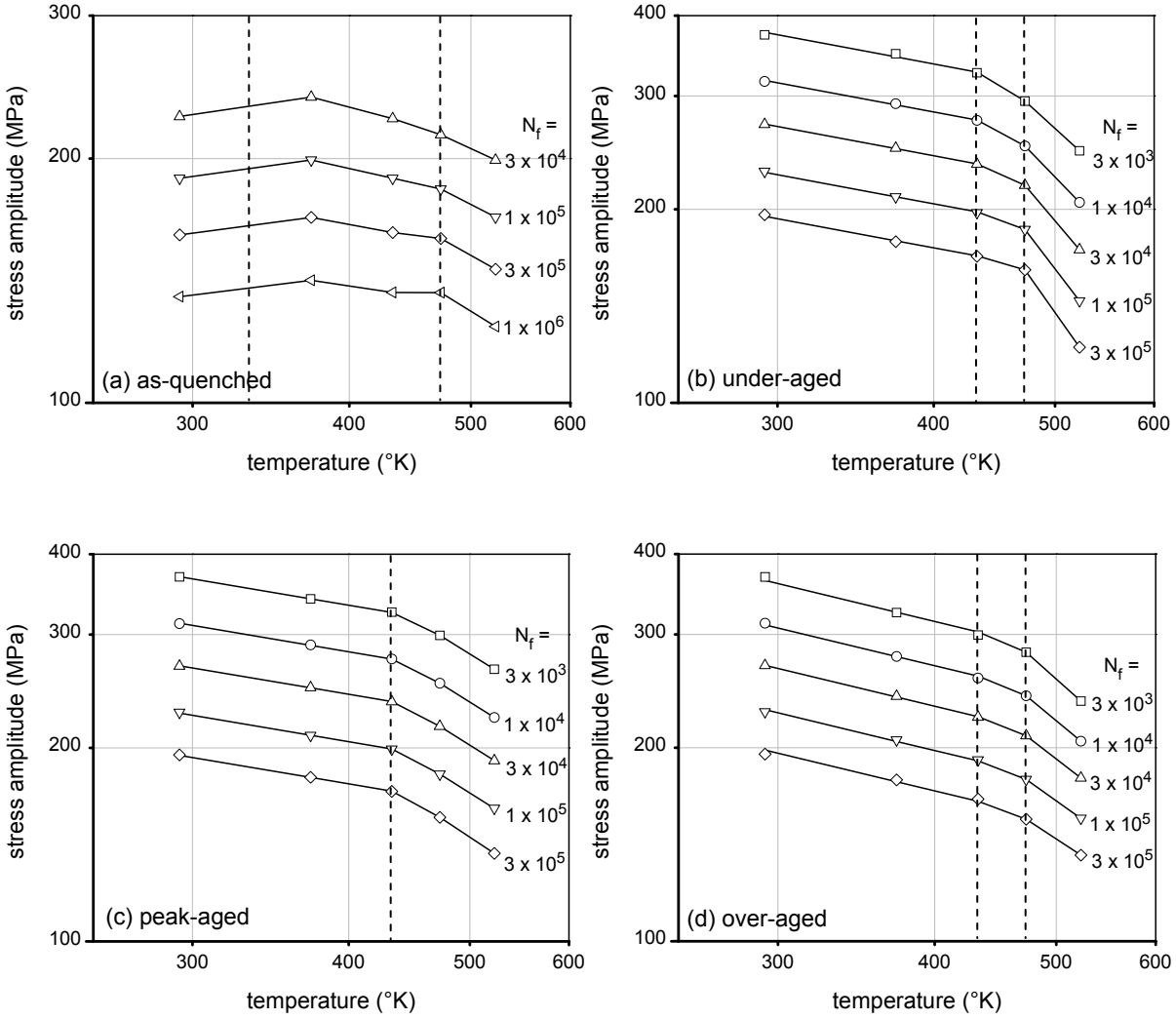

Figure 6.5: Temperature dependence of stress amplitudes in a bi-logarithmic scale of polished differently aged AA6110.

Table 6.2: Determined materials constants *c* and transition temperatures of polished differently aged AA6110.

Polished condition	Materials constant *c*	Transition temperature (°C)
As-quenched AA6110	-	200 (473°K)
Under-aged AA6110	-0.33	160-200 (433-473°K)
Peak-aged AA6110	-0.37	160 (433°K)
Over-aged AA6110	-0.47	160-200 (433-473°K)

lower than about 160-200°C; secondly, the decrease in stress amplitude as well as fatigue strength at temperatures of 200 and particularly 250°C indicates that creep probably begins to play a dominant role at these temperatures. Cyclic creep can be described by monitoring positive mean strains during stress-controlled fatigue test. Therefore, mean strains during fatigue tests were measured and plotted for different test temperatures in Fig. 6.6 which depicts values of mean strains during fatigue tests of the polished peak-aged AA6110 at an applied stress amplitude of 300 MPa for different test temperatures as an example (see Fig. 5.44 for plastic strain amplitudes). Obviously, for test temperatures less than 160°C, no significant mean strains during fatigue tests of the polished peak-aged AA6110 were observed. Whereas at a test temperature of 200°C at a similar applied stress amplitude of 300 MPa, positive mean strains were detected during fatigue test. Moreover, these mean strains became more and more pronounced with increasing number of cycles. The materials constants *c* and the transition temperatures of the polished differently aged AA6110 are summarized and shown in table 6.2. For the polished under-aged AA6110 in Fig. 6.5 (b), the effect of static/dynamic precipitates is still visible in the temperature range 160-200°C. The stress amplitude for a given number of cycles of $3x10^5$ (duration about 17 hours) at a test temperature of 200°C tends to be slightly recovered due to static/dynamic precipitates (see Fig. 5.28 for s/n-curves), since the exposure to high temperature was quite long. The materials constant *c* of the polished under-aged AA6110 was found to be quite similar to the polished peak-aged AA6110 (see table 6.2). It probably indicates that the effects of static/dynamic precipitates still play a beneficial role on the fatigue lifetimes of the polished peak-aged AA6110 at test temperatures up to 160°C. In contrast, if the beneficial effects of static/dynamic precipitates on the fatigue lifetime as well as strength quasi disappear like in the polished over-aged AA6110, the hardness tends to be only considerably decreased after continuous exposure to elevated temperatures during fatigue tests. Therefore, lower materials constant *c* of the polished over-aged AA6110 was detected as compared to the polished under- as well as peak-aged AA6110 (see table 6.2). However, stress amplitudes for a given number of cycles of the polished over-aged AA6110 decreased slightly in the temperature range 160-200°C. That might be due to the fact that the particles/precipitates which are sufficiently stable with respect to coalescence that their dimensions and/or the spacing between

them do not increase, or increase only very slowly, during loading at elevated temperature are preferential for the creep resistance [118].

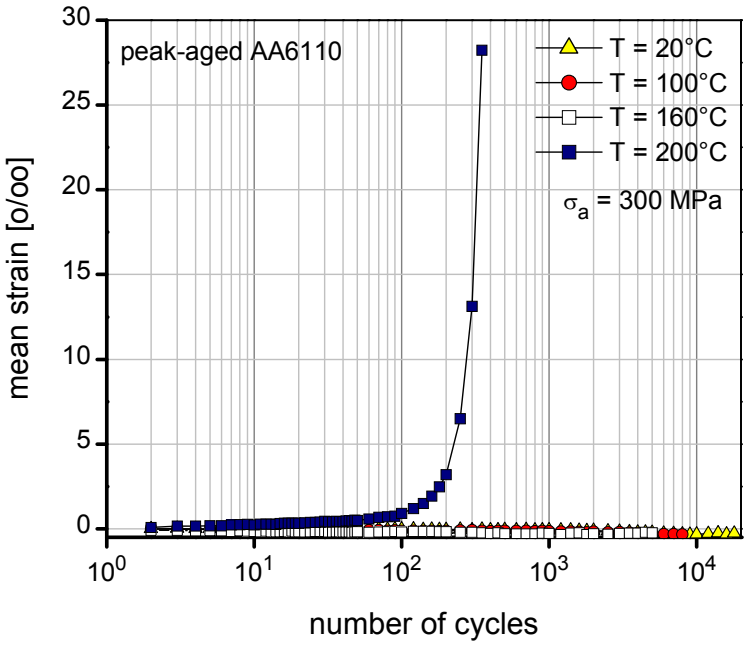

Figure 6.6: Mean strains during fatigue tests of polished peak-aged AA6110 at a stress amplitude of 300 MPa for different test temperatures.

6.3.1.2 Cyclic deformation curve

Influence of precipitation: The cyclic deformation curves during fatigue tests at room temperature of the polished AA5083 and as-quenched AA6110 containing mainly solute atoms (no effective precipitates are assumed) will be firstly discussed. Then, the focus will be on cyclic deformation curves during fatigue tests at room temperature of the polished differently aged AA6110 containing effective precipitates. For the polished AA5083 and as-quenched AA6110, cyclic hardening was observed at room temperature (see Figs. 5.3 and 5.17) due to the presence of solute atoms or atomic clusters, increasing dislocation densities and dislocation-dislocation interactions during cyclic deformation. Although fatigue lifetimes of under-, peak- and over-aged AA6110 show no significant differences at room temperature (see Fig. 6.4), their cyclic deformation behavior at room temperature was distinctly different (see Figs. 5.29, 5.43, and 5.59) because of the different

size and structure of precipitates within the aluminium matrix. The differences between the cyclic deformation curves are assumed to be associated with dislocation-precipitate and dislocation-dislocation interactions during cyclic deformation. Cyclic hardening was also detected in the polished under-aged AA6110 during fatigue tests at room temperature. It indicates that during fatigue tests at room temperature, dislocation densities increased and dislocation-dislocation interactions occurred in the polished under-aged AA6110, similarly as in the polished AA5083 and as-quenched AA6110. That means, that the precipitates of the polished under-aged AA6110 were so small and not fully effective (see Fig. 5.14 (a)). Consequently, for impeding dislocation movement, dislocations could still move easier through the precipitates as well as strain fields induced by remained solute atoms or atomic clusters and then dislocation-dislocation interactions occurred during cyclic deformation. On the other hand, if the major precipitates β´´ in AA6110 alloy are ordered, coherent and effective in size within the aluminium matrix (see Fig. 5.14 (b)), the to-and-fro motion of dislocations during cyclic deformation through the ordered precipitates causes a mechanical local disordering or scrambling of the atoms in the precipitates. The structure of the precipitates becomes disordered and degraded. The hardening due to ordering is lost, therefore cyclic softening is observed in the peak-aged AA6110. From DSC and TEM results (see Figs. 5.12 and 5.14 (c)), it can be concluded that semi-coherent precipitates β´ are the major precipitates of the over-aged AA6110. The to-and-fro motion of dislocations through the semi-coherent precipitates also causes cyclic softening in the over-aged condition. The analogous cyclic hardening and cyclic softening mechanisms of precipitation-hardened aluminium alloys were also reported in [101,102].

Influence of stress amplitude: In many cases, the stress amplitude does not strongly affect the shape of the cyclic deformation curve, i.e. the polished AA5083, as-quenched and under-aged AA6110 exhibit still cyclic hardening and the polished peak- and over-aged AA6110 show cyclic softening. However, an increase of plastic strain amplitudes during fatigue tests at room temperature was measured with increasing stress amplitude (see Figs. 5.43 and 5.59 as examples), consequently, fatigue lifetimes of the polished AA5083 and differently aged AA6110 decreased as discussed in section 6.3.1.1. A decrease of fatigue lifetimes

can be attributed to the higher plastic strain amplitudes during fatigue tests due to increasing stress amplitudes. This is in agreement with the Coffin-Manson law [49,50].

Influence of temperature: In general, at elevated temperature, easy glide, climb and cross slip of edge and screw dislocations can be expected. Therefore, an increase of plastic strain amplitudes during fatigue tests with increasing test temperature were detected if the effects of static/dynamic precipitation were negligible as in the polished AA5083 (see Fig. 5.3). However, for the precipitation-hardenable aluminium alloy AA6110, static/dynamic precipitation occurred during fatigue tests at elevated temperatures and affected the cyclic deformation curve. The polished as-quenched AA6110 exhibits cyclic hardening during fatigue tests at elevated temperature up to 250°C. It can be probably said that the static/dynamic precipitates of the polished as-quenched AA6110 were not fully effective during this investigation in spite of a relatively high temperature of 250°C (but relatively short investigated period). The results of the hardness measurements in Fig. 5.10 can be used to support this finding. Hence, dislocations could still move easier through the small precipitates as well as strain fields and then dislocation-dislocation interactions occurred during cyclic deformation. Cyclic deformation curves of the polished under-aged condition during fatigue tests at elevated temperature up to 200°C show an analogous behavior (see Fig. 5.29). Moreover, a change of cyclic deformation curve from cyclic hardening at test temperatures less than 200°C to cyclic softening at a test temperature of 250°C was observed (see Figs. 5.29 and 5.30). It indicates that during fatigue tests at a test temperature of 250°C, precipitates of the polished under-aged AA6110 were altered to be effective in size and coherent as well as semi-coherent with the aluminium matrix. Then, during cyclic deformation, dislocations moved to-and-fro through the coherent/semi-coherent precipitates causing a mechanical local disordering or scrambling of the atoms in the precipitates. The structure of the precipitates became disordered and degraded. The hardening due to ordering was lost, and consequently cyclic softening was observed for this situation. For the polished peak- and over-aged AA6110, cyclic softening still occurred during fatigue tests at test temperatures up to 250°C and their plastic strain amplitudes during fatigue tests increased with increasing test temperature (see Figs. 5.44 and 5.60).

6.3.2 Deep-rolled condition

In this section, only the deep-rolled condition will be discussed and analyzed before a comparison with the polished condition in the next section. The analysis methods and discussion direction are equivalent as used for the polished condition.

6.3.2.1 Fatigue lifetime

Important affecting factors on the fatigue lifetime of the polished condition have been considered and discussed, e.g. influence of precipitation, stress amplitude and temperature. However, for the deep-rolled condition, additional factors, such as macroscopic compressive residual stresses, work hardening states and increased near-surface hardnesses induced by deep rolling affect significantly the fatigue lifetimes of the deep-rolled condition. Thus, an assessment of the fatigue lifetime of the deep-rolled condition is more complex than the polished condition. As mentioned above, induced near-surface macroscopic compressive residual stresses and work hardening states of the deep-rolled condition are known to have major impact on the fatigue behavior. However, the induced macroscopic compressive residual stresses and work hardening states tend to decrease under cyclic and/or thermal loading. Consequently, the effect of decreasing macroscopic compressive residual stress on the fatigue lifetime of the deep-rolled condition can be expected. Therefore, in the next section the influence of stress amplitude and/or temperature on the fatigue lifetime will be explained in the light of near-surface macroscopic compressive residual stresses and work hardening states.

Influence of stress amplitude: First of all, the fatigue lifetimes of the deep-rolled differently aged AA6110 are compared together in one diagram (Fig. 6.7). Then, a Basquin function in equation (4) was used once more to describe the s/n-curves at room temperature of the deep-rolled AA5083 and deep-rolled differently aged AA6110 in Figs. 5.6 and 6.7, respectively. The materials constants *a* and *b* are determined and summarized in table 6.3. Interestingly, if s/n-curves of the deep-rolled under-, peak- and over-aged AA6110 in Fig. 6.7 are regarded, comparable fatigue lifetimes of the deep-rolled under- and peak-aged conditions are seen at room temperature, whereas fatigue lifetimes of the deep-rolled over-aged

condition are lower in the low as well as high cycle fatigue regime. An assessment of the mechanical residual stress relaxation might be a useful way to explain the causes. The initial macroscopic compressive residual stresses of the deep-rolled under-aged condition (-364 MPa at surface, see Fig. 5.31) were higher as compared to the deep-rolled peak-aged condition (-286 MPa at surface, see Fig. 5.45). After the strongly reduced macroscopic compressive residual stresses in

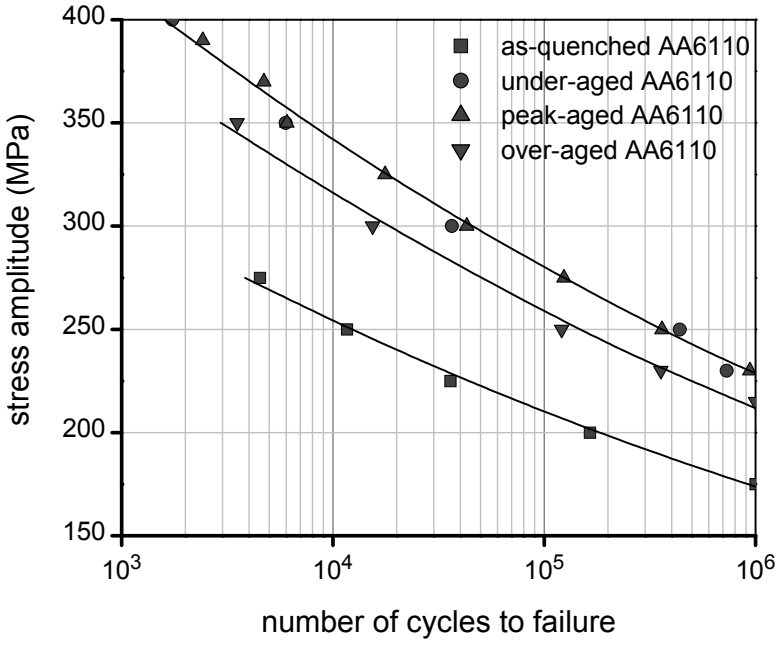

Figure 6.7: Non-statistically evaluated s/n-curves of deep-rolled differently aged AA6110 at room temperature.

Table 6.3: Determined materials constants *a* and *b* of the Basquin equation for deep-rolled AA5083 and differently aged AA6110 at room-temperature fatigue tests.

Deep-rolled condition	Materials constant *a*	Materials constant *b*
AA5083	365.93	-0.048
As-quenched AA6110	546.03	-0.083
Under-aged AA6110	761.01	-0.087
Peak-aged AA6110	761.01	-0.087
Over-aged AA6110	699.10	-0.086

the first cycle, no significant difference in the compressive residual stresses between the under- and peak-aged conditions was observed (see Figs. 5.36 and 5.50). Moreover, the residual stress relaxation rate during fatigue tests after the first cycle of the deep-rolled under- and peak-aged conditions was nearly similar, therefore no differences in the fatigue lifetime between the deep-rolled under- and peak-aged AA6110 were observed (see Fig. 6.7). Macroscopic compressive residual stresses of the deep-rolled over-aged condition relaxed more rapidly than in the deep-rolled peak- and under-aged conditions possibly leading to lower fatigue lifetimes, although the initial near-surface macroscopic compressive residual stresses of the deep-rolled over-aged condition before fatigue were not different from the deep-rolled peak-aged condition. To simplify the above mentioned findings, mechanical residual stress relaxation of the deep-rolled under-, peak-, and over-aged AA6110 at an applied stress amplitude of 350 MPa were compared in one diagram in an exemplary manner in Fig. 6.8. Additionally, instability of FWHM-values at the surface could be seen in the over-aged AA6110 at this applied stress amplitude.

Influence of temperature: The fatigue lifetimes as well as strengths of the deep-rolled AA5083 and differently aged AA6110 decreased undoubtedly under cyclic loading at elevated temperature (see Figs. 5.6, 5.20, 5.33, 5.47 and 5.63) due to the fact that dislocations can glide, climb as well as cross slip easier including high diffusion rates at elevated temperature. Consequently, residual stress relaxation is likely to be more pronounced for this loading situation which is controlled by thermomechanical residual stress relaxation. A more complicated situation can be expected for the deep-rolled as-quenched and under-aged AA6110, where occurring static/dynamic precipitation and thermomechanical residual stress relaxation took place simultaneously during elevated-temperature fatigue tests. The competition between occurring static/dynamic precipitates which enhance the fatigue lifetime (as discussed in section 6.3.1.1) and residual stress relaxation phenomena which normally deteriorate the fatigue lifetime of the deep-rolled condition is therefore the goal of discussion for this subsection. Equation (6) was used again to analyze the temperature sensitivity parameter, *c*. The temperature dependence of stress amplitude was plotted in a bi-logarithmic scale for a given number of cycles to failure ($3x10^3$, 10^4, $3x10^4$, 10^5 and $3x10^5$) of the deep-rolled

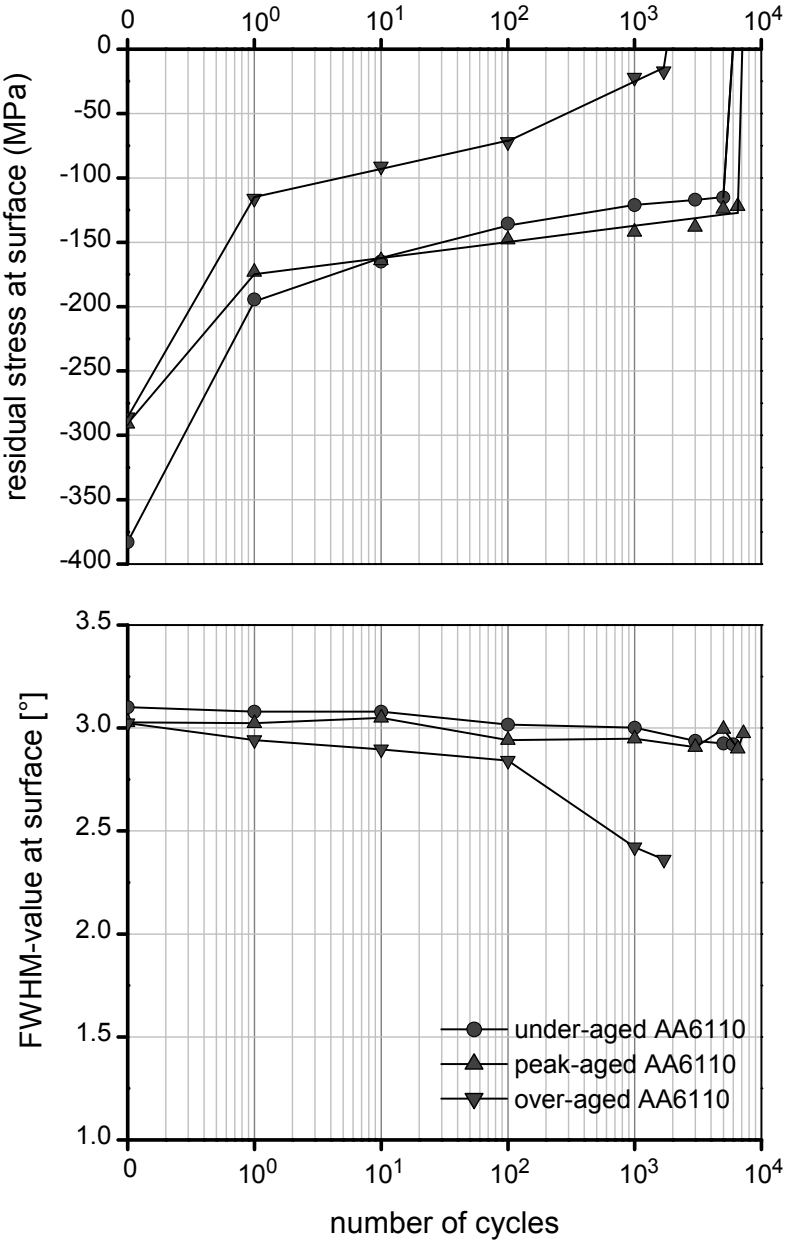

Figure 6.8: Residual stress and FWHM-value relaxation at the surface of deep-rolled under-, peak- and over-aged AA6110 during stress controlled fatigue at room temperature for an applied stress amplitude of 350 MPa

differently aged AA6110 in Figs. 6.9 (a)-(d). Since experimental data for the above cycles to failure were not available, values obtained by separate fits for each temperatures using equation (4) were used. The determined materials constants *c* and the transition temperatures from Figs. 6.9 (a)-(d) are summarized and shown in table 6.4 for the deep-rolled differently aged AA6110. Interestingly, for the deep-

rolled as-quenched AA6110 in Fig. 6.9 (a), the materials constant *c* can be unexpectedly determined although static/dynamic precipitation occurred during fatigue tests at elevated temperatures. It indicates that the fatigue lifetimes of the deep-rolled condition are dominated by the effects of the residual stress relaxation and not by the effects of static/dynamic precipitation for the deep-rolled as-quenched AA6110. However, the positive effects of static/dynamic precipitates on the fatigue lifetime of the deep-rolled as-quenched condition can be still observed, if the materials parameters *c* of the deep-rolled differently aged AA6110 are considered (see table 6.4). A higher materials constant *c* of the deep-rolled as-quenched condition was observed as compared to other deep-rolled conditions. It

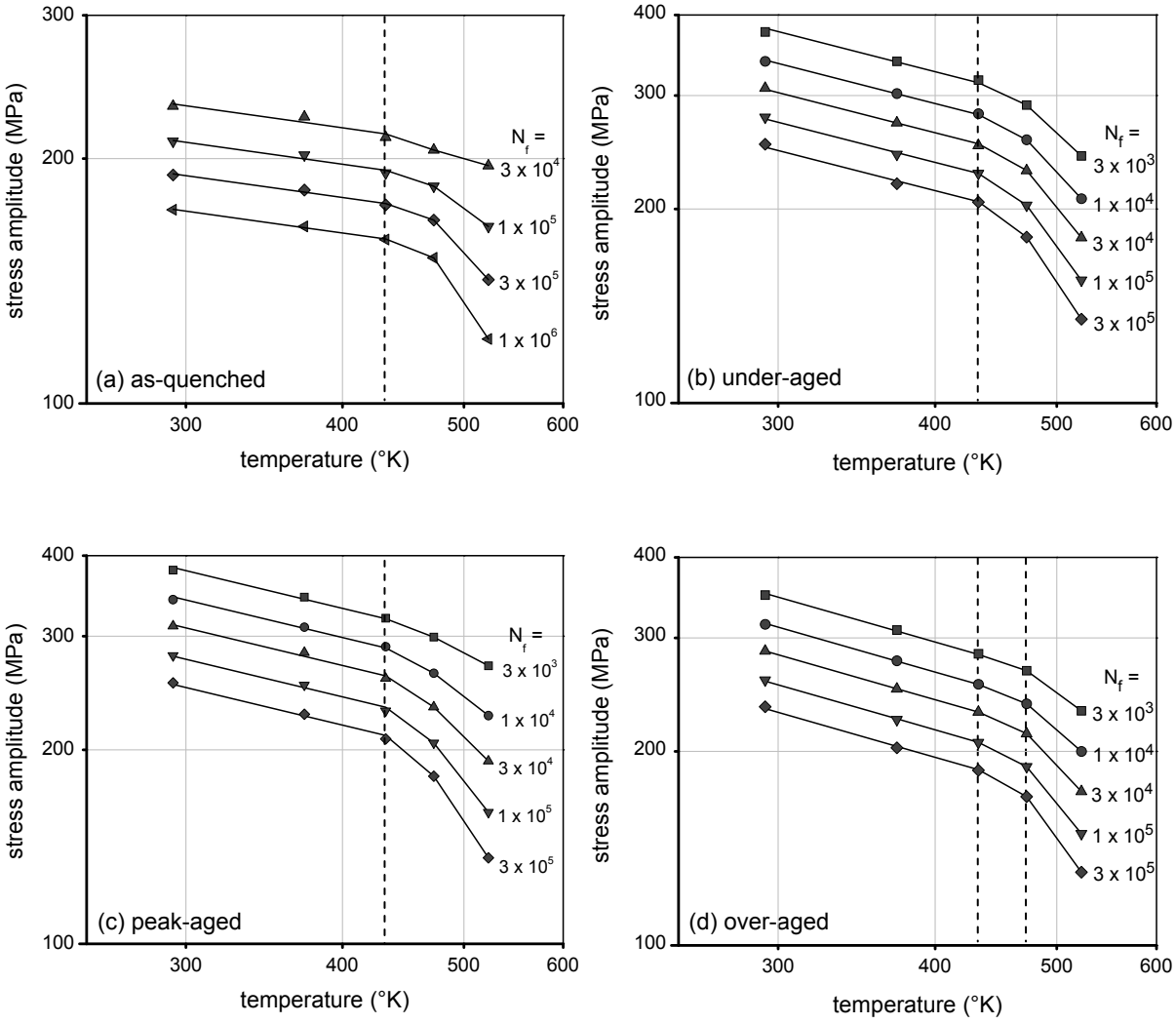

Figure 6.9: Temperature dependence of stress amplitudes in a bi-logarithmic scale of deep-rolled differently aged AA6110.

Table 6.4: Determined materials constants *c* and transition temperatures of deep-rolled differently aged AA6110.

Polished condition	Materials constant *c*	Transition temperature (°C)
As-quenched AA6110	-0.22	160 (433°K)
Under-aged AA6110	-0.50	160 (433°K)
Peak-aged AA6110	-0.50	160 (433°K)
Over-aged AA6110	-0.56	160-200 (433-473°K)

can be concluded that the fatigue lifetimes of the deep-rolled as-quenched condition might be more or less compensated by the effects of static/dynamic precipitation at elevated temperatures up to 160°C. For the deep-rolled under-, peak- and over-aged conditions, the materials constants *c* of the deep-rolled under- and peak-aged AA6110 are identical, whereas the materials constant *c* of the deep-rolled over-aged AA6110 is slightly lower. A transition temperature of 160°C was detected for the deep-rolled as-quenched, under- and peak-aged conditions, while the transition temperature of the deep-rolled over-aged condition is about 160-200°C.

6.3.2.2 Cyclic deformation curve

Influence of precipitation: As discussed, the shapes of cyclic deformation curves depend significantly on dislocation-dislocation as well as dislocation-precipitation interactions during fatigue tests (see table 3.3). The shape of the cyclic deformation curve of the deep-rolled condition should be normally not disturbed by the induced macroscopic compressive residual stresses as well as work hardening states, i.e. the deep-rolled AA5083, as-quenched and under-aged AA6110 generally exhibit cyclic hardening (see Figs. 5.8, 5.22 and 5.35), whereas the deep-rolled peak- and over-aged AA6110 show cyclic softening (see Figs. 5.49 and 5.65) during fatigue tests at room and elevated temperatures. Moreover, lower plastic strain amplitudes of the deep-rolled condition were normally observed during fatigue tests at room and elevated temperatures as compared to the polished condition (see Figs. 5.8, 5.22, 5.35, 5.49 and 5.65). However, in some

cases, higher plastic strain amplitudes of the deep-rolled condition were also detected if deep rolling became ineffective (see Fig. 5.35 as an example).

Influence of stress amplitude: In general, stress amplitudes do not affect the shape of cyclic deformation curves significantly, i.e. the deep-rolled AA5083, as-quenched and under-aged AA6110 exhibit normally still cyclic hardening and the deep-rolled peak- and over-aged AA6110 show cyclic softening. An analogous influence of stress amplitude as in the polished condition was observed. In other words, the plastic strain amplitudes of the deep-rolled condition during fatigue tests increased with increasing stress amplitude at the same test temperatures. Consequently, fatigue lifetimes of the deep-rolled AA5083 and differently aged AA6110 decreased (see section 6.3.2.1) according to the Coffin-Manson law [49,50].

Influence of temperature: Generally, an increase of plastic strain amplitudes of cyclic deformation curves were measured with increasing test temperature (at the same stress amplitude) due to easy glide, climb and cross slip of edge and screw dislocations. The influences of test temperatures on the shapes of cyclic deformation curves, e.g. cyclic hardening/softening of the deep-rolled condition are comparable to the polished condition which was discussed previously in section 6.3.1.2.

6.3.3 Comparison between polished and deep-rolled condition

In the previous sections 6.3.1 and 6.3.2, the important aspects of cyclic deformation behavior of the polished and deep-rolled conditions were separately analyzed and discussed. Subsequently, in this section, the effects of deep rolling on the cyclic deformation behavior will be discussed as compared to the polished condition using the obtained information in the sections 6.3.1 and 6.3.2. The important factors which may be detrimental for the deep rolling will be mentioned. Finally, effective borderlines of deep rolling for the AA5083 and differently aged AA6110 in stress amplitude-temperature diagrams will be established in this section.

6.3.3.1 Influence of deep rolling on fatigue lifetime

First of all, the altered near-surface properties after deep rolling treatment should be attributed and mentioned because they are the basic and important information to analyze/discuss the beneficial effects of deep rolling on the fatigue behavior of deep-rolled aluminium alloys. As mentioned, the concept of deep rolling is a localized (inhomogeneous) near-surface plastic deformation. Therefore, when the yield strength is exceeded, local plastic deformations occur, creating macroscopic compressive residual stresses and associated microstructural work hardening effects [40]. From experimental results, it is clearly that deep rolling induced macroscopic compressive residual stresses, work hardening states (see Figs. 5.4, 5.18, 5.31, 5.45 and 5.61) and increased hardnesses (see Figs. 5.5, 5.19, 5.32, 5.46 and 5.62) at the surface and in near-surface regions of all deep-rolled AA5083 and AA6110. Fatigue lifetime enhancement through deep rolling was observed for all low and intermediate applied stress amplitudes for given test temperatures. Nevertheless, at relatively high stress amplitudes for given test temperatures, deep rolling becomes ineffective. To simplify this state, s/n-curves at test temperatures of 20 and 160°C of the polished and deep-rolled peak-aged AA6110 were plotted again in one diagram as an example in Fig. 6.10. For AA5083 and other differently aged AA6110, analogous diagrams were found also. Residual stress as well as work hardening state relaxation/stability during fatigue tests at room and elevated temperatures may be a cause for the different effectiveness of deep rolling and will be intensively discussed in following sections.

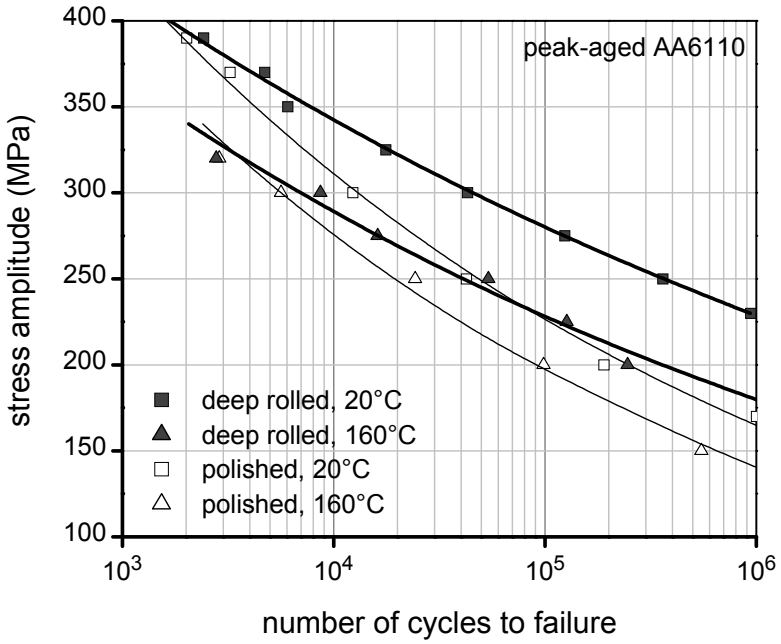

Figure 6.10: Non-statistically evaluated s/n-curves of polished and deep-rolled peak-aged AA6110 for test temperatures of 20 and 160°C.

6.3.3.2 Influence of deep rolling on cyclic deformation curve

Generally, due to the beneficial effects of deep rolling, such as near-surface macroscopic compressive residual stresses, work hardening states as well as increased hardnesses, plastic strain amplitudes during fatigue tests at given test temperatures of the deep-rolled AA5083 and AA6110 decreased obviously as depicted in Figs. 5.8, 5.22, 5.35, 5.49 and 5.65. However, in contrast, if the deep rolling became ineffective at given stress amplitudes and test temperatures, a decrease of plastic strain amplitudes was not observed, moreover in some cases, higher plastic strain amplitudes of the deep-rolled condition were measured during fatigue tests. As an example for these two principal extreme cases, cyclic deformation curves of the polished and deep-rolled under-aged AA6110 at applied stress amplitudes of 250 and 320 MPa for a test temperature of 160°C were compared in Fig. 6.11. Obviously, at an applied stress amplitude of 250 MPa, plastic strain amplitudes during cyclic loading of the deep-rolled under-aged condition are lower than the polished under-aged condition, consequently for this test condition, greater fatigue lifetimes of the deep-rolled under-aged condition can

be expected according to the Coffin-Manson law taking the lower plastic strain amplitudes into account [49,50]. The opposite effect was observed when a stress amplitude of 320 MPa was applied at a test temperature of 160°C. Higher plastic strain amplitudes of the deep-rolled under-aged condition were more or less observed, thus deep rolling became ineffective for this case. An analogous manner as in Fig. 6.11 was also detected although specimens were fatigued at a relatively high test temperature of 250°C and cyclic deformation curves of the under-aged AA6110 converted from cyclic hardening to cyclic softening due to altered precipitate states (see details in section 6.3.1.2). Fig. 6.12 depicts cyclic deformation curves of the polished and deep-rolled under-aged AA6110 at a test temperature of 250°C for applied stress amplitudes of 200 and 250MPa. At a relatively high test temperature of 250°C, the beneficial effects of macroscopic compressive residual stresses should not be expected. However, the remained work hardening states and increased hardnesses induced by deep rolling might be attributed for the beneficial lifetime enhancing effect. Hitherto, it can be summarized that deep rolling can more or less enhance the fatigue lifetime of aluminium alloys, however, under only below critical certain applied stress amplitudes for a given temperature. That means, stress amplitude and

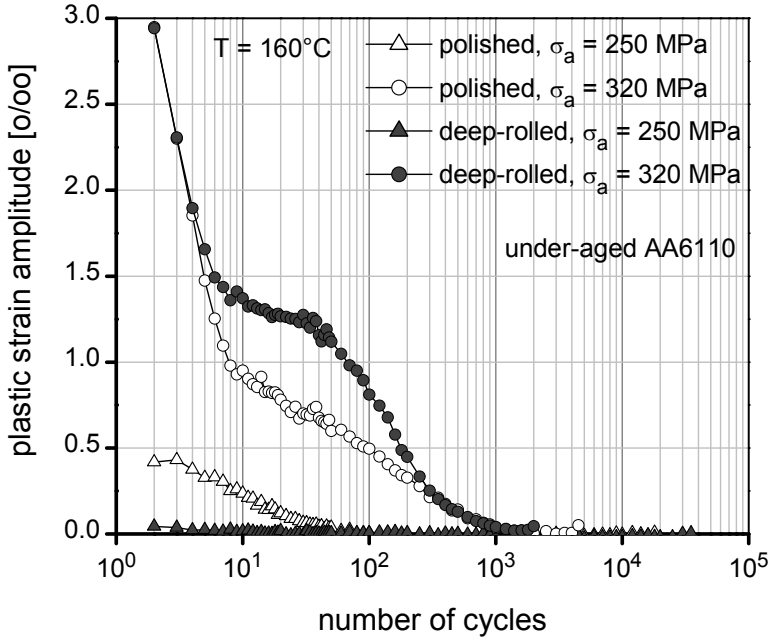

Figure 6.11: Cyclic deformation curves of polished and deep-rolled under-aged AA6110 at a test temperature of 160°C for applied stress amplitudes of 250 and 320 MPa.

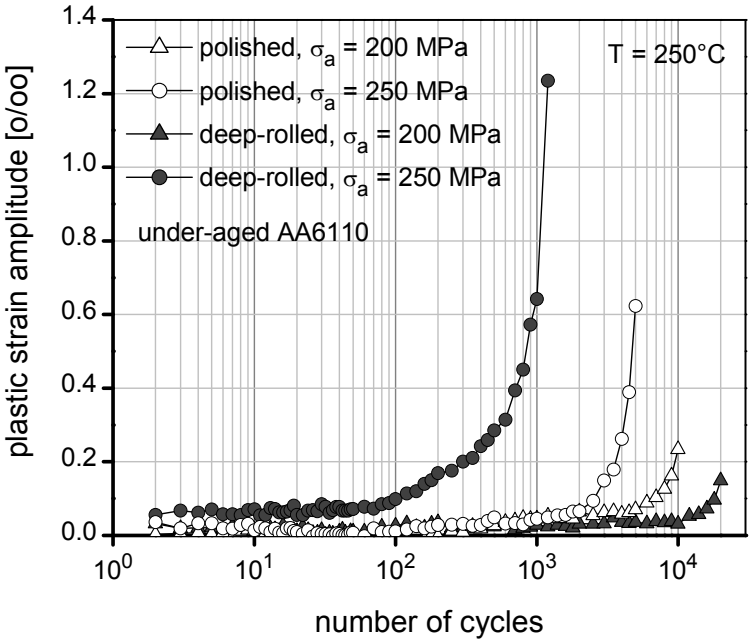

Figure 6.12: Cyclic deformation curves of polished and deep-rolled under-aged AA6110 at a test temperature of 250°C for applied stress amplitudes of 200 and 250 MPa.

temperature are the most important factors affecting the beneficial effects of deep rolling. Therefore, the influence of stress amplitude and temperature on the beneficial effects of deep rolling will be intensively discussed in the following section.

6.3.3.3 Influence factors on the effectiveness of deep rolling

Obviously, from Fig. 6.10, the beneficial effects of deep rolling decrease with increasing stress amplitude and/or test temperature. The analyzed information of the polished and deep-rolled conditions in sections 6.3.1 and 6.3.2 will be compared and discussed in these subsections.

Stress amplitude: The materials constant *b*, which can indicate the stress amplitude sensitivity of materials, was firstly considered. Apparently, from tables 6.1 and 6.3, the materials constant *b* of the deep-rolled condition is higher than the polished condition. It indicates that the fatigue lifetimes of the deep-rolled condition are more significantly affected by the stress amplitude as compared to the

polished condition. That might be due to the fact that the fatigue lifetime of the deep-rolled condition depends strongly on induced near-surface macroscopic compressive residual stresses as well as work hardening states which can continuously decline by relaxation phenomena during cyclic loading at room temperature (see Figs. 5.36, 5.50 and 5.66).

Temperature: An analogous behavior was detected when the materials constant *c*, the temperature sensitivity parameter of the polished and deep-rolled conditions in tables 6.2 and 6.4 were considered. Obviously, the materials constant c of the deep-rolled conditions are less than of the polished condition. It indicates that the fatigue lifetimes of the deep-rolled condition are more sensitive to test temperature than the polished condition. From these analyzed information, it can be strongly claimed that fatigue lifetimes of the deep-rolled condition depend significantly on the near-surface properties. During fatigue tests at elevated temperatures, thermomechanical residual stress relaxation occurred and affected the fatigue lifetimes of the deep-rolled condition detrimentally.

Up to now, it can be concluded that too high stress amplitudes and temperatures are certainly the main detrimental effects on the fatigue lifetime of deep-rolled aluminium alloys. This implies that at a certain (very high) stress amplitude for a given (very high) temperature, deep rolling becomes ineffective (see Fig. 6.10).

6.3.3.4 Effective boundary of deep rolling

The effectiveness and ineffectiveness of deep rolling can be analyzed by comparing s/n-curves of the polished and deep-rolled conditions as shown in Fig. 6.10, where intersection points between s/n-curves of the polished and deep-rolled conditions for each test temperatures were observed. Aluminium alloys AA5083 and other differently aged AA6110 exhibit also a similar manner. Therefore, all intersection points were summarized and plotted in stress amplitude-temperature diagrams for AA5083 and different aged AA6110 as shown in Figs. 6.13 (a)-(e). Below an obtained borderline deep rolling effectively enhances fatigue lifetime, whereas above this borderline deep rolling becomes ineffective. It still has to be clarified, however, macroscopic compressive residual stresses or work hardening states (FWHM-values) of the deep-rolled specimens, which were fatigued below

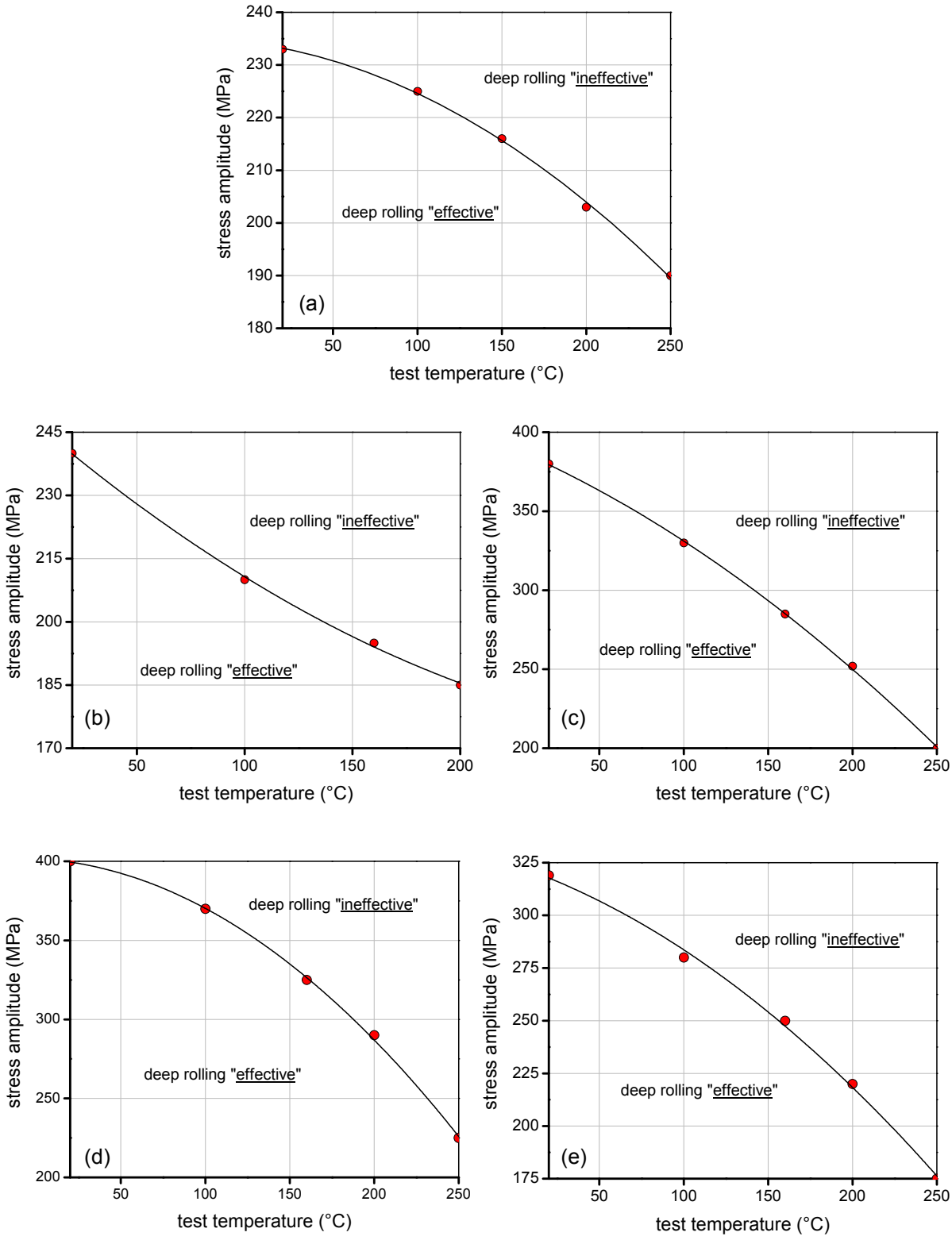

Figure 6.13: Effective borderlines of deep rolling treatment for (a) AA5083, (b) as-quenched AA6110, (c) under-aged AA6110, (d) peak-aged AA6110 and (e) over-aged AA6110 plots as a function of stress amplitude and test temperature.

and above the effective borderline correlate somehow with this behavior. From results of macroscopic compressive residual stress- as well as FWHM-value-depth profiles in Figs. 5.9, 5.26, 5.40, 5.56 and 5.70, a table was conceived where stability/instability of macroscopic compressive residual stresses and FWHM-values are summarized in table 6.5. Obviously, for all investigated conditions whether deep rolling is effective or ineffective, macroscopic compressive residual stresses are always unstable. On the other hand, deep rolling is still effective if FWHM-values are stable during fatigue tests at room or elevated temperatures. However, instability of FWHM-values can also be seen for severe test conditions and rendering the deep rolling treatment ineffective in terms of fatigue lifetime enhancement.

Table 6.5: Status of macroscopic compressive residual stresses, work hardening states and deep rolling for various test conditions.

	Applied stress amplitude (MPa)	Test temperature (°C)	Residual stresses*	FWHM-values*	Deep rolling
AA5083	205	20	unstable	stable	effective
	240	20	unstable	unstable	ineffective
As-quenched AA6110	150	160	unstable	stable	effective
	250	160	unstable	unstable	ineffective
Under-aged AA6110	175	200	unstable	stable	effective
	300	200	unstable	unstable	ineffective
Peak-aged AA6110	200	160	unstable	stable	effective
	350	160	unstable	unstable	ineffective
Over-aged AA6110	200	160	unstable	stable	effective
	290	160	unstable	unstable	ineffective

*as compared to the reference which was heated for 10 minutes at a given test temperature without any applied stress amplitude.

*Reduction of residual stresses as well as FWHM-values less than of approximately 5 % is considered as a stable condition.

6.3.4 Residual stress stability

Several examples have been demonstrated that the induced macroscopic compressive residual stresses as well as work hardening states at the surface and in near-surface regions play a dominant role on the fatigue lifetime of the deep-rolled aluminium alloys. However, unfortunately, they decrease more or less during cyclic and/or thermal loading. In this section, phenomena of residual stress relaxation/stability will be emphasized. Mechanical, thermal as well as thermomechanical residual stress relaxation will be firstly analyzed and then discussed. Additionally, their effects on the fatigue lifetime of the deep-rolled condition will be also presented.

6.3.4.1 Mechanical residual stress relaxation

From results of mechanical residual stress relaxation in Figs. 5.36, 5.50 and 5.66, three phases of change in the surface states of deep-rolled condition due to cyclic loading were observed, similarly as for other mechanically surface treated materials [51-56]. Firstly, the near-surface macroscopic compressive residual stresses are strongly reduced in the first cycle due to quasistatic loading. Secondly, a linear dependence of the residual stresses with the logarithm of number of cycles occurs according to a logarithmic creep law in equation (1). Finally, macroscopic compressive residual stresses as well as FWHM-values decrease drastically after crack initiation [53,55]. It is possible due to local microscopic cracks at an interface of precipitate and matrix. As known, macroscopic compressive residual stresses can be reduced or completely relaxed by the application of mechanical energy when the elastic residual strains can be converted into microscopic plastic strains (dislocation movement as well as rearrangement) by suitable deformation processes [51,52]. Therefore, the residual stress stability is correlated strongly to the plastic strain amplitude. Some of archival literature sources reported about the correlation of plastic strain amplitudes and residual stress relaxation. An increase of residual stress relaxation was observed with increasing plastic strain amplitude [40,43,62]. However, for the deep-rolled AA5083 and differently aged AA6110, some interesting observations should be noted: firstly, mechanical residual stress relaxation of the deep-rolled differently aged AA6110 occurred although insignificant or no plastic strain

amplitudes during fatigue tests at room temperature were observed. Since small local dislocation movements may be sufficient for inducing relaxation of macroscopic compressive residual stresses [40,51,52,119], local microscopic plastic strains during room-temperature fatigue tests at relatively low applied stress amplitudes should be made responsible for the mechanical residual stress relaxation. Secondly, the deep-rolled AA5083 and differently aged AA6110 exhibit a threshold stress amplitude below which the work hardening states (as expressed by FWHM-values) are unaltered and remained essentially constant, whereas macroscopic compressive residual stress relaxed substantially during fatigue loading. Moreover, threshold stress amplitudes render obviously the deep rolling ineffective as shown in table 6.6. If instability of the near-surface work hardening occurred at room temperature due to mechanical/cyclic loading, deep rolling can not enhance the fatigue lifetime of aluminium alloys. Instability of FWHM-values of the deep rolling aluminium alloys might indicate that microscopic crack initiation at the deep-rolled regions of the specimens occurred during cyclic loading at very high stress amplitude at room temperature (see Fig. 2.7). When microscopic cracks were initiated in the deep-rolled regions, unfortunately, crack propagation in these regions should be more rapidly as compared to the polished condition due to crack propagation can be accelerated by increasing work hardening [13]. As a consequence, for these situations, the fatigue lifetimes of the deep-rolled condition are more or less lower than the polished condition.

6.3.4.2 Thermal residual stress relaxation

Also without any applied stress amplitude, macroscopic compressive residual stresses and work hardening states decreased during exposure at elevated temperature, as demonstrated in Figs. 5.25, 5.39, 5.53 and 5.69. Obviously, the Zener-Wert-Avrami function in equation (2) can pleasingly describe the relaxation behavior. A very good correlation between the calculations and the experimental values was established. The materials constant *m* of residual stress as well as FWHM-value relaxation of the deep-rolled under-, peak-, and over-aged AA6110 do not show any significant differences and are about 0.20-0.22, except for the materials constant *m* of the deep-rolled as-quenched AA6110, which was in the

Table 6.6: Status of work hardening states and deep rolling at applied stress amplitudes below and above the threshold stress amplitudes.

	Threshold stress amplitude* (MPa)	Applied stress amplitude* (MPa)	Residual stresses**	FWHM-values**	Deep rolling
AA5083	230	205	unstable	stable	effective
		240	unstable	unstable	ineffective
Under-aged AA6110	380	350	unstable	stable	effective
		400	unstable	unstable	ineffective
Peak-aged AA6110	395	350	unstable	stable	effective
		400	unstable	unstable	ineffective
Over-aged AA6110	320	300	unstable	stable	effective
		350	unstable	unstable	ineffective

*at a test temperature of 20°C

**Reduction of residual stresses as well as FWHM-values less than of approximately 5 % is considered as a stable condition.

range of 0.12-0.17 (see tables 5.2, 5.3, 5.4 and 5.5). To obtain more information about the microstructural mechanism for residual stress relaxation, the activation enthalpy values of residual stress and FWHM-value relaxation of the deep-rolled differently aged AA6110 were summarized and depicted in Fig. 6.14. An analogous behavior was also observed for the activation enthalpy (ΔH) of the relaxation process. The activation enthalpy values of the deep-rolled under-, peak- and over-aged AA6110 are close to the activation enthalpy of self diffusion of aluminium ($\Delta H_{s,\,Al}$ = 1.47 eV [120]), whereas the activation enthalpy values of the deep-rolled as-quenched AA6110 are higher ($\Delta H_{RS,\,aq}$ = 1.63 eV and $\Delta H_{FWHM,\,aq}$ = 2.48 eV). From the above information, it can be derived that the relaxation mechanism of the deep-rolled as-quenched AA6110 is different from the deep-rolled under-, peak-, as well as over-aged AA6110. A lower residual stress relaxation rate could be expected in the deep-rolled as-quenched condition due to lower materials constant *m* and higher activation enthalpy of the relaxation process. The higher activation enthalpy of the deep-rolled as quenched condition as compared to the activation enthalpy of the self diffusion, particularly for the activation enthalpy of the FWHM-value relaxation (see Fig. 6.14) may indicate that

this relaxation mechanism is controlled by thermally activated glide of dislocations which depend strongly on the stacking fault energy [120]. The as-quenched AA6110 containing major substitutional solute atoms normally has a lower stacking fault energy as compared to pure aluminium. Consequently, cross slip of dislocations is rather difficult, thus the relaxation process is suppressed, especially for the relaxation of work hardening states which requires dislocation annihilations, whereas dislocation movement may be sufficient for a relaxation of macroscopic compressive residual stresses [40,51]. Occurring precipitates during exposure at elevated temperature of the deep-rolled as-quenched condition might be also one possible cause for impeding the dislocation movement and increasing microscopic residual stresses. Thermal residual stress as well as work hardening relaxation of the deep-rolled under-, peak- and over-aged AA6110 are controlled principally by volume diffusion. Predominantly volume diffusion occurred also in other investigated non-ferrous alloys, such as shot peened Al-Mg as well as Ti-6Al-4V [40,51,52,54,56]. However, actually, there are always two recovery mechanisms, volume diffusion and dislocation-core diffusion, operating simultaneously but in different degrees [56,120].

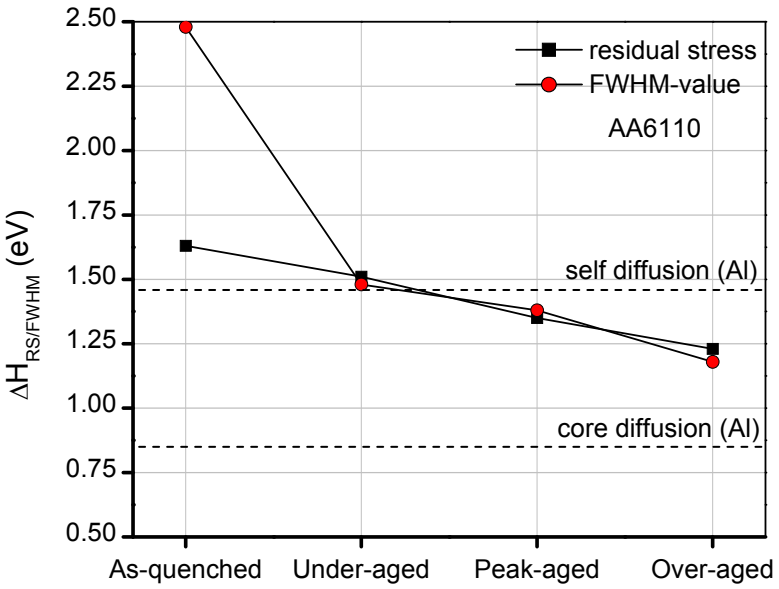

Figure 6.14: Activation enthalpy of residual stress and FWHM-value relaxation of deep-rolled differently aged AA6110.

6.3.4.3 Thermomechanical residual stress relaxation

After a separate consideration and discussion of mechanical and thermal residual stress relaxation, the more complicated mechanism, thermomechanical residual stress relaxation relating both mechanical and thermal residual stress relaxation at the same time will be discussed. Naturally, the residual stress decrease during cyclic loading at elevated temperature is always higher than only mechanical or thermal relaxation, unless special mechanisms, such as dynamic strain ageing occur. Thermomechanical residual stress (as well as work hardening) relaxation is assumed to be combination a simple additive of both mechanical and thermal residual stress relaxation as shown in equation (7):

$$\sigma_{TM,Ta}^{RS} = \sigma_{T,Ta}^{RS} + \sigma_{M,Ta}^{RS} \tag{7}$$

$\sigma_{TM,Ta}^{RS}$ = Thermomechanical residual stress relaxation at temperature T_a

$\sigma_{T,Ta}^{RS}$ = Thermal residual stress relaxation fraction at temperature T_a

$\sigma_{M,Ta}^{RS}$ = Mechanical residual stress relaxation fraction at temperature T_a

This equation is of course a very crude simplification. However, it is difficult to analyze the thermomechanical residual stress relaxation because in practice, the fractions of the mechanical and thermal relaxation cannot be separately measured during fatigue tests at elevated temperatures. It should also be noted that the mechanical relaxation fraction at elevated temperature should be higher than the mechanical relaxation at room temperature (for the same applied stress amplitude) due to easier dislocation movement at elevated temperature. The thermal relaxation fraction is also analogous; the thermal relaxation fraction with applied stress should be higher than thermal relaxation fraction without any applied stress (for the same test temperature). So, strictly speaking, the two fractions of equation (7) are not independent of each other. However, to make an attempt to evaluate the thermomechanical residual stress relaxation, the Zener-Wert-Avrami function with the respective material properties from the thermal relaxation investigations was used to calculate the thermal residual stress as well as FWHM-value relaxation during fatigue tests as shown in Fig. 6.15. Interesting characteristics were found. Residual stresses as well as FWHM-values relaxed from the initial

value during holding at a test temperature for 10 minutes prior to the start of the actual fatigue tests. Obviously, after starting of the fatigue test, the effects of thermal relaxation are negligible during the fatigue test until approximately 1,000 cycles (for a chosen test frequency of 5 Hz). From this diagram, it can be said that the residual stress as well as FWHM-value relaxation during fatigue tests at

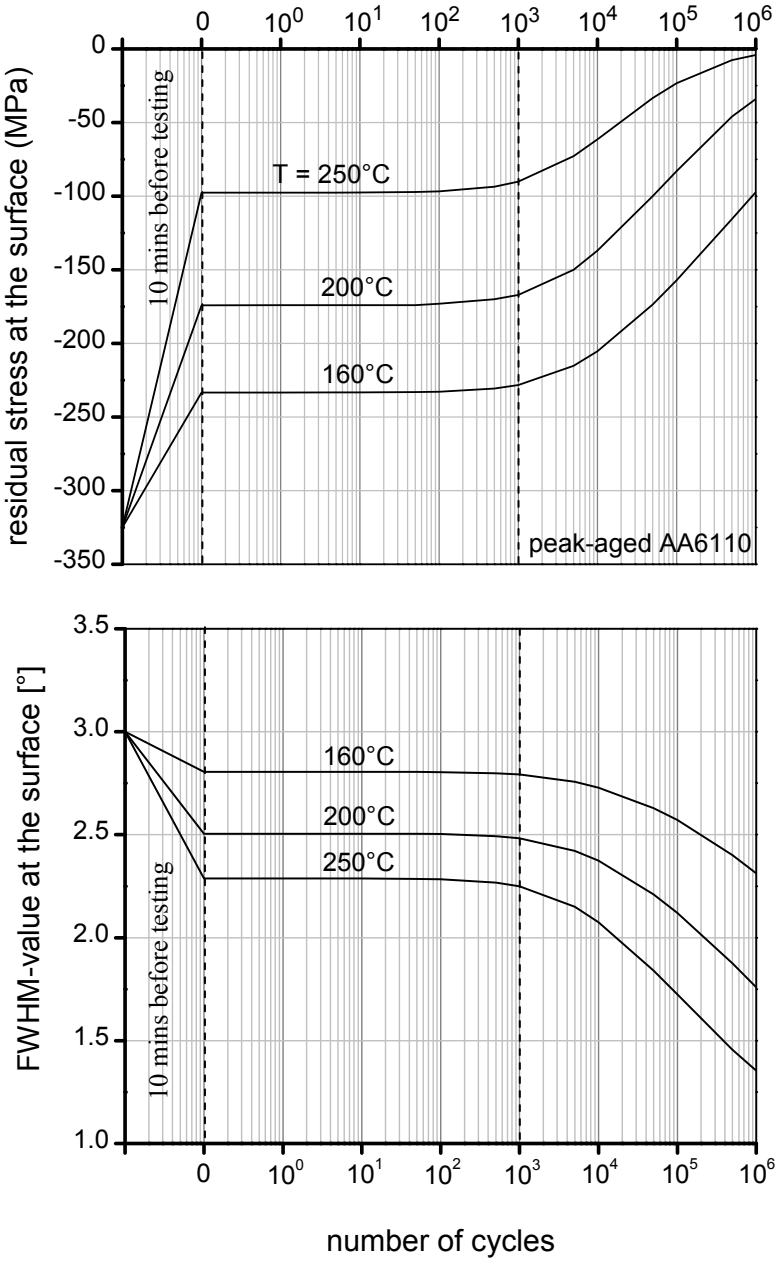

Figure 6.15: Thermal relaxation of residual stresses and FWHM-values at the surface of deep-rolled peak-aged AA6110 as a function of a number of cycles for a test frequency of 5 Hz (calculated from Zener-Wert-Avrami function in equation (2)).

elevated temperature up to 1,000 cycles are controlled by the mechanical relaxation fraction. Therefore, the measured thermomechanical relaxation in these regions, a linear dependence of the residual stresses with the logarithm of number of cycles should be observed. The results in Figs. 5.54 and 5.55 indeed confirm correctly this assumption. The residual stress relaxation during fatigue loading at elevated temperatures appears to be a linear according to a logarithmic creep law during fatigue tests until approximately 1,000 cycles. From Fig. 5.55, the materials constant *A* and *m* of the mechanical relaxation fraction at elevated temperatures were determined using equation (1) and summarized as compared to the values for room temperature in table 6.7. Higher values of materials constant *A* and *m* of the mechanical relaxation fraction at elevated temperature were detected due to the fact that dislocation movement, rearrangement as well as micro/macroscopic cracks can occur easier during fatigue tests at elevated temperature. The instability of the FWHM-value in the mechanically controlled region can be also observed at an applied stress amplitude of 300 MPa and at a test temperature of 200°C (see Fig. 5.55). As mentioned in the subsection of mechanical residual stress relaxation, instability of FWHM-values of the deep-rolled condition occurred due to mechanical loading/fraction might indicate that microscopic cracks were initiated in the deep-rolled regions of the specimens during cyclic loading at relatively high stress amplitude at a given test temperature. Crack propagation in these regions should be more rapidly as compared to the polished condition due to crack propagation can be accelerated by increasing work hardening [13]. As a consequence, the deep rolling treatment is ineffective for this test condition (see Figs 5.55 and 6.13 (d)). It can be said that for the effectiveness of deep rolling of aluminium alloys, stability of the work hardening (as expressed by stable FWHM-values) is mandatory in the cyclic loading at room and elevated temperatures. Until now, it can be noted that the stability/instability of work hardening states during cyclic loading at room and elevated temperatures is the most useful tool to characterize the effectiveness of deep rolling of deep-rolled aluminium alloys AA5083 and differently aged AA6110 (see tables 6.5, 6.6 and 6.7).

Table 6.7: Determined materials constant *A* and *m* of the mechanical relaxation fraction as well as stability and effectiveness of work hardening and deep rolling, respectively.

Test temperature (°C)	**Materials constant *A***	**Materials constant *m***	**FWHM-value***	**Deep rolling**
20	0.28	0.03	stable	effective
160	0.29	0.07	stable	effective
200	0.31	0.08	unstable	ineffective

*as compared to the reference which was heated for 10 minutes at a given test temperature without any applied stress amplitude.

*Reduction of residual stresses as well as FWHM-values less than of approximately 5 % is considered as a stable condition.

6.3.5 Deep rolling followed by ageing treatment

In this section (6.3.5) and following section (6.3.6), modified deep rolling treatments, e.g. deep rolling followed by ageing and elevated-temperature deep rolling will be analyzed and discussed, respectively. Finally, a comparison of modified and conventional deep rolling treatments will be shown.

6.3.5.1 Near-surface properties

After ageing treatments in the temperature range 160-250°C, hardnesses at the surface and in near-surface regions of the deep-rolled as-quenched AA6110 increased with increasing ageing time until reaching a maximum value (see Fig. 5.71). The precipitated phases, β'' as well as Q' lead to the increased hardness of copper-containing Al-Mg-Si aluminium alloys [1]. The maximum hardness of the deep-rolled as-quenched AA6110 can be found after an ageing treatment at a temperature of 160°C and an ageing time of 12 hours. For prolonged ageing treatments in the temperature range of 160-250°C, the hardness at the surface of deep-rolled as-quenched specimens declined after having reached the peak hardness. The formation of coarse, semi-coherent, β' and/or Q' as well as incoherent precipitates, β and/or Q at the surface as well as in near-surface regions is the reason for this observation. Conversely, for an ageing treatment at a temperature of 300°C with a short ageing time, an increase of hardness was not observed. It might be due to the dominant recrystallization process taking place before occurring precipitation process [120]. Near-surface microstructures before and after the ageing treatment at a temperature of 300°C for an ageing time of 1,000 seconds were investigated to support this assumption as shown in Figs. 6.16 (a) and (b). Compressed grains at the surface and in near-surface regions up to a depth of approximately 0.6 mm of the deep-rolled as-quenched AA6110 were observed before the ageing treatment. However, after the ageing treatment at the ageing temperature of 300°C for about 1,000 seconds, fine globular recrystallized grains in the deep-rolled regions were seen. As a consequence, very low macroscopic compressive residual stresses as well as work hardening states took place immediately at this ageing temperature (see Fig. 5.25).

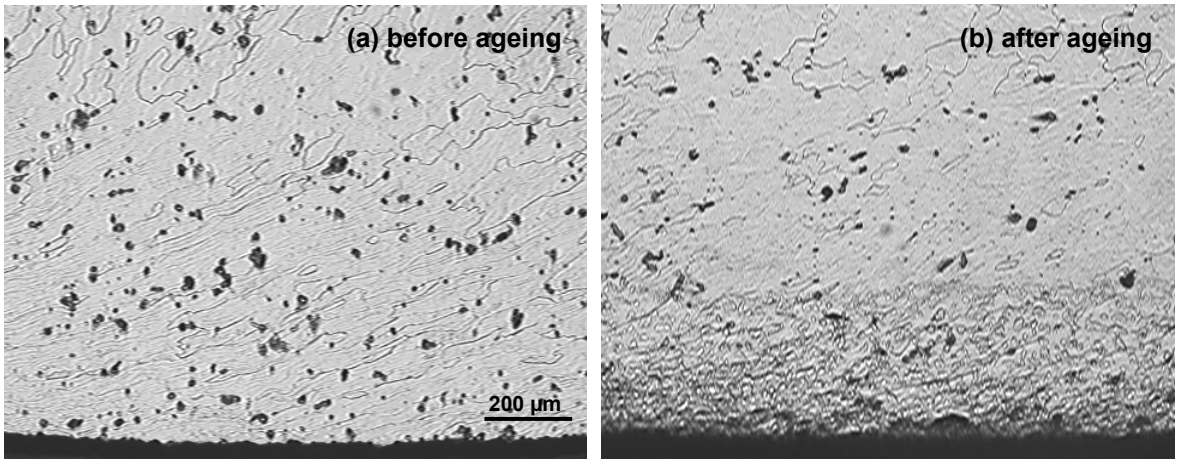

Figure 6.16: Microstructures of deep-rolled as-quenched AA6110 (a) before and (b) after an ageing treatment at a temperature of 300°C for about 1,000 seconds.

6.3.5.2 Fatigue lifetime

After ageing treatments in a temperature range of 160-250°C, the fatigue lifetime increased continuously with increasing ageing time until reaching a maximum fatigue lifetime (see Fig. 5.72). As expected, the increase of near-surface hardness after the ageing treatments resulted in fatigue lifetime enhancement. Figs. 5.71 and 5.72 show that there is a clear correlation between hardnesses and fatigue lifetimes of the deep-rolled as-quenched AA6110 after ageing treatments. To clarify this correlation, a diagram of fatigue lifetime improvement versus increase of hardness at the surface was constructed as shown in Fig. 6.17. The maximum fatigue lifetime of the deep-rolled as-quenched AA6110 can be found after an ageing treatment at a temperature of 160°C for 12 hours which is the optimized ageing parameter for hardness as mentioned above. Moreover, these optimized ageing parameters are also identical to the ageing parameters of the peak-aged condition (see Fig. 4.3). Fatigue lifetimes of the deep-rolled as-quenched condition were improved especially in the low cycle fatigue regime after the optimized ageing treatment (see Fig. 5.77) due to increased hardnesses at the surface and in near-surface regions as well as in the bulk. However, the induced macroscopic compressive residual stresses as well as work hardening states seem to be essential in the high cycle fatigue regime, where relatively low stress

amplitudes were applied and mechanical residual stress relaxation was not significantly pronounced during cyclic loading at room temperature.

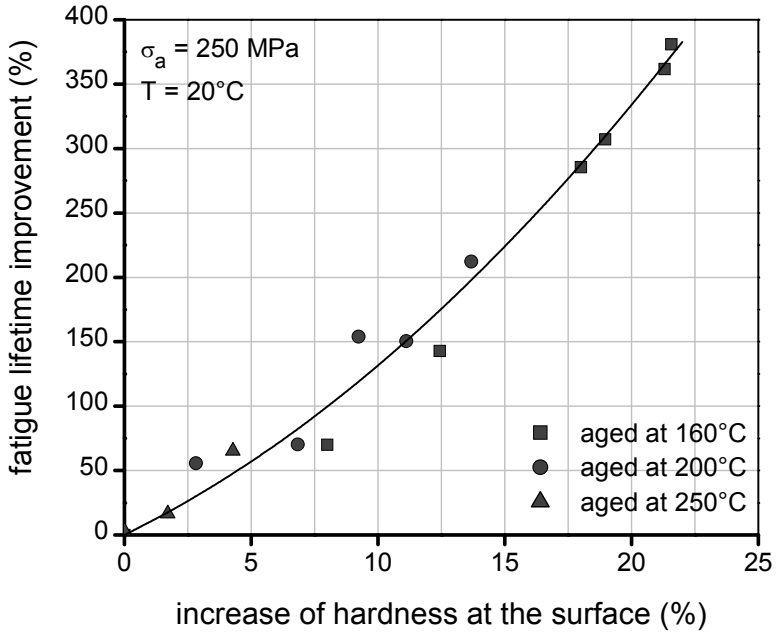

Figure 6.17: Fatigue lifetime improvement as a function of hardness increase at the surface of deep-rolled as-quenched AA6110 after ageing treatments at 160-250°C.

6.3.5.3 Cyclic deformation curve

The effect of ageing treatment on the cyclic deformation curve was evaluated by registrating the plastic strain amplitude during stress-controlled fatigue tests of the differently aged specimens. Cyclic hardening was observed in the deep-rolled as-quenched condition due to the presence of solute atoms or clusters as well as increasing dislocation densities and dislocation-dislocation interactions during cyclic deformation. After ageing treatments at elevated temperatures lower than 300°C, lower plastic strain amplitudes were measured (see Fig. 5.73) due to increased near-surface hardnesses and precipitates. The plastic strain amplitude decreased continuously with increasing ageing time, thus the fatigue lifetimes increased also continuously, since it can be correlated to the near-surface

hardness (see Fig. 6.17). After prolonged ageing treatments at elevated temperature, the hardness at the surface as well as in near-surface regions decreased and over-ageing took place (see Fig. 5.71). This decrease of near-surface hardness causes a corresponding reduction of fatigue lifetime and affects also the shape of the cyclic deformation curve. As mentioned in section 6.3.1.2, during cyclic deformation, the to-and-fro motion of dislocations through the small partially coherent precipitates causes a mechanical local disordering or scrambling of the atoms in the precipitates. Any ordering contribution to hardening of the over-aged condition is lost and therefore cyclic softening curves are seen in Fig. 5.74. For ageing treatments at 300°C, cyclic hardening was observed and the plastic strain amplitudes increased with increased ageing time (see Fig. 5.73) because of decreased hardnesses and domination of recrystallization at the surface and in near-surface regions (see Fig. 6.16).

6.3.5.4 Comparison of conventional and modified deep rolling

The most important and interesting issue of the modified mechanical surface treatment (deep rolling followed by optimized ageing treatment) is the comparison with the conventional mechanical surface treatment (optimized ageing followed by deep rolling). As mentioned, the optimized ageing parameters are identical to the ageing parameters of the peak-aged condition, therefore the modified deep-rolled (optimized-aged deep-rolled) as-quenched condition will be compared to the deep-rolled optimized/peak-aged condition in this section. First of all, important information of surface properties of the optimized-aged deep-rolled as-quenched and deep-rolled optimized/peak-aged condition were collected from Figs. 5.45, 5.46, 5.75 and 5.76 as shown in table 6.8. Noticeably, all important properties which are beneficial effects for fatigue lifetime enhancement, such as hardness, macroscopic compressive residual stress as well as the work hardening state of the optimized-aged deep-rolled as-quenched condition are significantly less than of the deep-rolled optimized/peak-aged condition. The greater near-surface macroscopic compressive residual stresses, FWHM-values as well as hardnesses the deep-rolled optimized/peak-aged condition indicate that the deep rolling after an optimized ageing treatment results in an excellent combination of work and precipitation hardening and thus excellent fatigue lifetime could be expected for

the deep-rolled optimized/peak-aged AA6110. To confirm this assumption, s/n-curve of the optimized-aged deep-rolled as-quenched condition was plotted and compared to the deep-rolled optimized/peak-aged condition in one diagram in Fig. 6.18. Obviously, the fatigue lifetime and strength of the deep-rolled optimized/peak-aged condition are superior to the optimized-aged deep-rolled as-quenched condition. It can be concluded that both hardening effects, work and precipitation hardening are required to yield the best fatigue lifetime of AA6110. As known, the deep rolling treatment serves principally to induce near-surface work hardening and macroscopic compressive residual stresses. For the ageing treatment after deep rolling, unfortunately, the work hardening and macroscopic compressive residual stresses were partially annealed out rapidly during the ageing treatment due to the relaxation process (mainly self diffusion). Therefore it can reasonably be assumed that fatigue lifetimes of the optimized-aged deep-rolled as-quenched AA6110 were governed by the precipitation hardening and residually effective work hardening as well as macroscopic compressive residual stresses at the surface and in near-surface regions. Therefore, the fatigue lifetime of the optimized-aged deep-rolled as-quenched AA6110 is better than the deep-rolled as-quenched AA6110 in the low cycle fatigue regime (see Fig. 6.18). However, the deep rolling after a suitable/optimized ageing treatment can completely combine the work and precipitation hardening in near-surface regions of AA6110 into an optimized microstructure and thus result in the best surface properties and fatigue lifetime of the investigated AA6110.

Table 6.8: Comparison of near-surface properties of conventional and modified deep rolling treatment.

	Hardness at the surface (HV0.05)	**Residual stress at the surface (MPa)**	**FWHM-value at the surface [°]**
Deep rolling followed by optimized ageing	137	-102	1.99
Optimized/peak ageing followed by deep rolling	161	-286	3.08

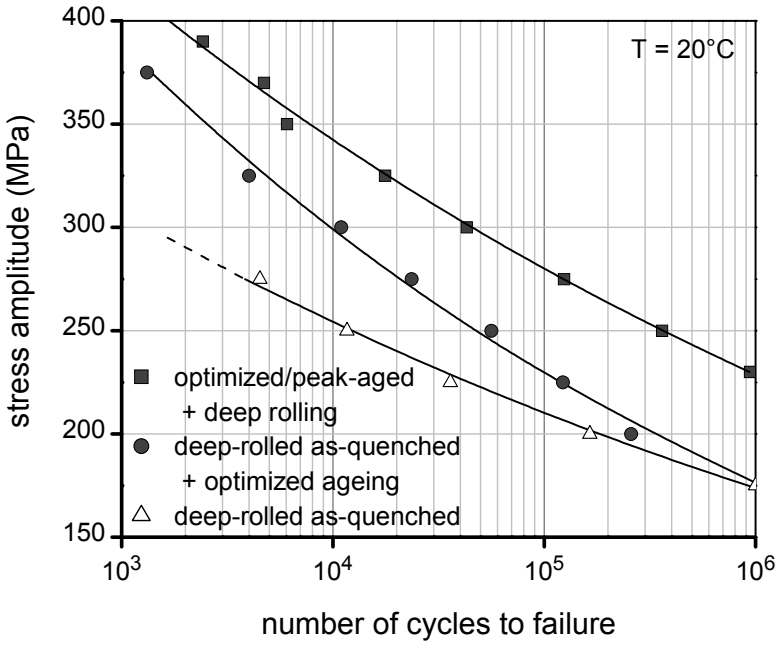

Figure 6.18: Non-statistically evaluated s/n-curves of optimized-aged deep-rolled as-quenched AA6110 as compared to deep-rolled optimized-aged AA6110 as well as deep-rolled as-quenched AA6110.

6.3.6 Deep rolling at elevated temperature

For steels, high-temperature deep rolling treatments have been successfully established with pleasingly improved fatigue performance due to dynamic strain ageing effects as reported in [20-24]. However, their effects on fatigue lifetimes of precipitation-hardenable aluminium alloy AA6110 performed disappointingly as seen in section 5.2.7. Nevertheless, important aspects of high-temperature deep rolling on precipitation-hardenable aluminium alloy AA6110 should be clarified and discussed.

6.3.6.1 Near-surface properties

Due to occurring static/dynamic precipitation during deep rolling at elevated temperatures, near-surface hardnesses after high-temperature deep rolling (160-200°C) increased as compared to the room-temperature deep-rolled as-quenched AA6110 (see Fig. 5.80). On the other hand, lower macroscopic compressive residual stresses and work hardening states were measured as compared to the room-temperature deep-rolled as-quenched condition (see Fig. 5.79) because static/dynamic recovery processes, which bring about relaxation phenomena, took place during deep rolling at elevated temperatures. The deep rolling treatment at a temperature of 250°C produced detrimental effects on the near-surface properties, i.e. near-surface macroscopic compressive residual stresses, work hardening states and hardnesses are considerably lower than of the room-temperature deep-rolled as-quenched condition. That might be due to the fact that this temperature too high for the aluminium alloy AA6110 and leads to serve over-ageing effects and a high-rate static/dynamic recovery for this situation.

6.3.6.2 Fatigue lifetime

The improvement of fatigue lifetimes at room temperature of the high-temperature deep-rolled as-quenched AA6110 is not obvious as compared to the room-temperature deep-rolled as-quenched AA6110. However, increased near-surface hardnesses after deep rolling at a temperature of 200°C slightly enhance fatigue lifetimes at room temperature in the low cycle fatigue regime. On the other hand, in the high cycle fatigue regime, the specimens deep rolled at a temperature of 200°C show slightly lower fatigue lifetimes as compared to the room-temperature

deep-rolled as-quenched condition (see Fig. 5.81). This can be attributed to the lower near-surface macroscopic compressive residual stresses as well as work hardening states after deep rolling at a temperature of 200°C (see Fig. 5.79). In spite of insignificant improvement of fatigue lifetimes at room temperature, fatigue tests of the high-temperature deep-rolled as-quenched condition revealed that high-temperature deep rolling induces beneficial effects on the fatigue lifetimes in the temperature range of 100-200°C (see Fig. 5.82). Initially, the higher near-surface hardnesses after deep rolling at elevated temperatures of 160 and 200°C as compared to the deep-rolled as-quenched condition (see Fig. 5.80) could be made responsible for these observations. Due to inferior near-surface properties after deep rolling at a temperature of 250°C (e.g. lower hardnesses, macroscopic compressive residual stresses and work hardening), low fatigue lifetimes at room temperature are undoubtedly seen in Fig. 5.81.

6.3.6.3 Cyclic deformation curve

After deep rolling at temperatures of 160 and 200°C, cyclic hardening during fatigue tests at room temperature was observed. It can be assumed that the precipitates occurring during deep rolling at elevated temperature are still too small size and not fully effective. Consequently, dislocations could still relatively easy move through precipitates and increasing dislocation densities and dislocation-dislocation interactions during cyclic deformation occurred. It indicates that precipitates occurring during high-temperature deep rolling were not fully optimized/effective in both near-surface regions and bulk due to the short duration of the deep rolling treatment at a given temperature (about only 2-3 minutes). Therefore, it can be conclude that suitable ageing temperature and sufficient ageing time are always essential for the precipitation process. To obtain the optimized/peak-aged condition, as-quenched specimens have to be aged at a temperature of 160°C for about 12 hours as described in section 5.2.1. For deep rolling at a temperature of 250°C, lower near-surface hardnesses were detected due to over-ageing effects, consequently cyclic softening during fatigue tests at room temperature was seen as describe in section 6.3.1.2.

6.3.6.4 Comparison of conventional and high-temperature deep rolling

Fatigue lifetimes of the high-temperature deep-rolled as-quenched condition will be compared to two conventional deep-rolled conditions; the room-temperature deep-rolled as-quenched condition and the room-temperature deep-rolled peak-aged condition. Non-statistically evaluated s/n-curves of all considered conditions were summarized in one diagram in Fig. 6.19. From this diagram, especially when taking into account near-surface properties in Figs. 5.45, 5.46, 5.79 and 5.80, superior fatigue lifetimes can be seen obviously when precipitation and work hardening were completely combined together as in the deep-rolled peak-aged condition. During deep rolling at elevated temperature, static/dynamic precipitation certainly occurred. However, these effects were not fully effective because of a too short period of deep rolling process. Moreover, static/dynamic recovery processes decreased macroscopic compressive residual stresses and work hardening states during deep rolling at elevated temperature. As a consequence, fatigue lifetime enhancement using high-temperature deep rolling for the as-quenched AA6110 was only small.

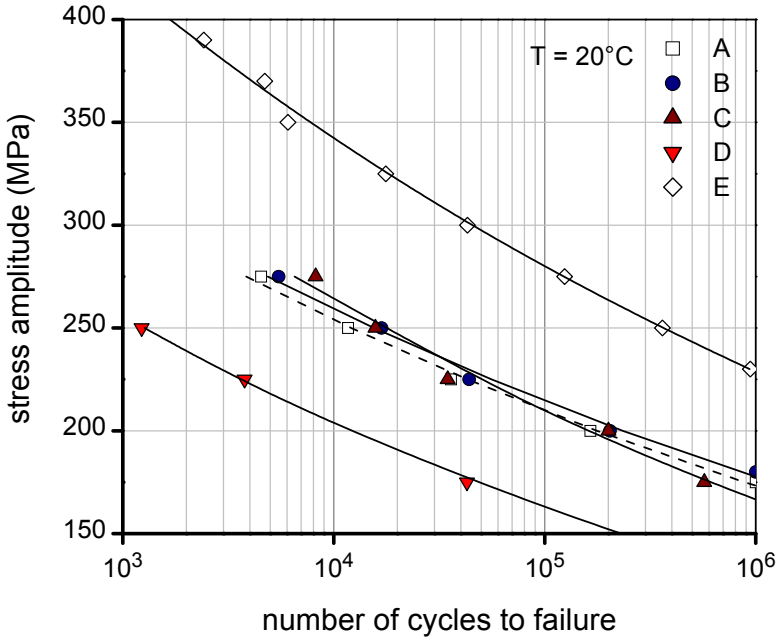

Figure 6.19: Non-statistically evaluated s/n-curves at room temperature of (A) as-quenched + deep-rolled at 20°C, (B) as-quenched + deep-rolled at 160°C, (C) as-quenched + deep-rolled at 200°C, (D) as-quenched + deep-rolled at 250°C and (E) peak-aged + deep-rolled at 20°C.

Chapter 7

Summary and conclusions

The cyclic deformation behavior of aluminium alloys AA5083 and differently aged AA6110 at room and elevated temperature under stress control has been investigated and discussed. The effects of deep rolling on cyclic deformation behavior have been systematically studied and clarified both at room and elevated temperatures as compared to the polished condition as a reference. Residual stress and work hardening stability have been investigated. Thermal, mechanical and thermomechanical residual stress relaxation and their effects on the cyclic deformation behavior of deep-rolled aluminium alloys AA5083 and AA6110 were analyzed. Finally, investigations about modified deep rolling treatments, e.g. deep rolling followed by ageing treatment and high-temperature deep rolling of as-quenched AA6110 have also been accomplished and assessed. From this research, following conclusions can be drawn:

Cyclic deformation behavior:

- Fatigue lifetimes of the polished and deep-rolled conditions depend strongly on stress amplitude and temperature. With increasing stress amplitude and/or temperature, their fatigue lifetimes decrease. However, an exception was found for polished as-quenched AA6110, where a slight increase of fatigue lifetime at a test temperature of 100°C was observed due to static/dynamic precipitation during investigations.
- The Basquin equation and its generalized form can be used in a conventional way to describe fatigue lifetimes of both polished and deep-rolled conditions at room and elevated temperature, respectively when the effects of static/dynamic precipitation are not very pronounced during elevated temperature fatigue. Lifetimes of deep-rolled conditions are more sensitive to stress amplitude and temperature than the polished condition since their fatigue life depends significantly on the induced near-surface

macroscopic compressive residual stresses as well as work hardening states which can relax during cyclic and/or thermal loading.

- The shapes of cyclic deformation curves of both polished and deep-rolled AA5083 and AA6110 are governed by dislocation-dislocation and dislocation-precipitation interactions during cyclic loading. Aluminium alloys AA5083 as well as as-quenched and under-aged AA6110 exhibit cyclic hardening due to increasing dislocation and dislocation-dislocation interactions during cyclic loading, whereas peak- and over-aged AA6110 show cyclic softening due to the to-and-fro motion of dislocations through the ordered precipitates during cyclic deformation causing a mechanical local disordering or scrambling of the atoms in the precipitates, leading to a loss of hardening [101,102].
- Deep rolling enhances fatigue lifetimes of aluminium alloys AA5083 and differently aged AA6110 efficiently for stress amplitudes lower than a specific threshold stress amplitude at a given temperature where the near-surface work hardening states are unaltered and remain essentially constant, whereas macroscopic compressive residual stress relax substantially during fatigue loading. On the other hand, above this threshold stress amplitude at a given temperature, deep rolling has no beneficial effect on the fatigue behavior of AA5083 and AA6110. This is a consequence of unstable near-surface work hardening states.
- A reduction of the plastic strain amplitude due to cyclic stability of deep rolling-induced near-surface work hardening states was observed when specimen were fatigued below the threshold stress amplitude at a given temperature. This reduction in plastic strain amplitude is associated with enhanced fatigue lifetimes.

Residual stress stability:

- Macroscopic compressive residual stresses of deep-rolled AA5083 and differently aged AA6110 decreased during cyclic and/or thermal loading due to mechanical and/or thermal relaxation processes which can be accurately described using a logarithmic creep law and a Zener-Wert-Avrami function, respectively.

- Deep-rolled AA5083 and differently aged AA6110 exhibit a threshold stress amplitude below which induced near-surface work hardening states are stable during fatigue loading at room temperature. Above this threshold stress amplitude, the induced near-surface work hardening states decreased significantly, consequently deep rolling became ineffective.
- Thermal residual stress and work hardening relaxation processes of the deep-rolled AA6110 are controlled principally by volume diffusion. Their activation enthalpy values are quite identical to the activation enthalpy of self diffusion of aluminium. However, the activation enthalpy value for the thermal work hardening relaxation of the deep-rolled as-quenched AA6110 is higher than the activation enthalpy of self diffusion of aluminium and possibly controlled by thermally activated glide of dislocations.
- Thermomechanical residual stress relaxation consists of two major parts: a mechanical relaxation fraction and a thermal relaxation fraction which can be characterized using a plot of calculated thermal relaxation as a function of number of cycles (see Fig. 6.15).
- The effectiveness of the deep rolling treatment for aluminium alloys AA5083 and differently aged AA6110 can be characterized using the stability/instability of work hardening states during cyclic loading at room and elevated temperatures. Instability of near-surface work hardening state caused by mechanical relaxation fraction during fatigue loading at room as well as elevated temperatures indicates microstructure alterations (e.g. rearrangement of dislocations), possibly also microscopic cracks at interfaces between matrix and precipitates in the deep-rolled regions. As a consequence the deep rolling treatment becomes ineffective.

Modified deep rolling treatment:

- Deep rolling followed by an ageing treatment of as-quenched AA6110 resulted in an increase of near-surface hardnesses. At the same time, a reduction of near-surface macroscopic compressive residual stresses and work hardening states took place. The optimized ageing condition is an ageing temperature of 160°C for about 12 hours.

- Increased near-surface hardnesses after the optimized ageing treatment are very beneficial for fatigue lifetimes in the low cycle fatigue regime, whereas in the high cycle fatigue regime, macroscopic compressive residual stresses are additionally important.
- Deep rolling at elevated temperatures up to approximately 200°C of the as-quenched condition resulted in an increase of near-surface hardnesses, whereas lower macroscopic compressive residual stresses and work hardening states were observed because of static/dynamic recovery processes. Deep rolling at a temperature of 250°C is detrimental for near-surface properties due to over-ageing effects and high-rate static/dynamic recovery at this temperature.
- Deep rolling at elevated temperatures up to approximately 200°C enhances fatigue lifetimes of as-quenched AA6110 in high-temperature fatigue tests up to temperatures of approximately 200°C. The higher near-surface hardnesses after deep rolling at elevated temperatures of 160 and 200°C as compared to the room-temperature deep-rolled state is responsible for these observations.
- An optimized/peak ageing treatment followed by a conventional deep rolling treatment, in the best way combines precipitation hardening and work hardening in near-surface regions of AA6110 and leads to an optimized microstructure and residual stress state. Thus it results in the best surface properties and fatigue lifetime of the investigated AA6110.

Chapter 8

Zusammenfassung

In der vorliegenden Arbeit wurde das Ermüdungsverhalten der Aluminium-legierung AA5083 und der unterschiedlich ausgehärteten Legierungen AA6110 unter Nennspannungsregelung bei Raumtemperatur und erhöhten Temperaturen untersucht und diskutiert. Hierbei wurden insbesondere die Auswirkungen des Festwalzens auf das Ermüdungsverhalten systematisch bei Raumtemperatur und erhöhten Temperaturen untersucht, wobei als Referenzzustand ein polierter, unverfestigter Zustand verwendet wurde. Insbesondere wurden sowohl die Stabilität des Eigenspannungszustands als auch der Randschichtverfestigung analysiert. Hierbei wurde sowohl der thermische und mechanische als auch der thermomechanische Eigenspannungsabbau studiert und ihre Auswirkungen auf das Wechselverformungsverhalten der Legierungen AA5083 und 6110 analysiert. Schließlich wurden alternative, kombinierte Oberflächenbehandlungsverfahren untersucht, wozu das Festwalzen mit anschließendem Auslagern und das Hochtemperaturfestwalzen des lösungsgeglühten Zustands gehören. Aus den durchgeführten Untersuchungen können folgende Schlussfolgerungen gezogen werden:

Wechselverformungsverhalten:

- Die Bruchlastspielzahlen der polierten und festgewalzten Zustände hängen sehr stark von Temperatur und Spannungsamplitude ab. Mit zunehmender Spannungsamplitude und Temperatur sinkt die Bruchlastspielzahl bei allen Zuständen mit Ausnahme des polierten, lösungsgeglühten Zustandes, welcher bei 100°C ermüdet wurde. Es ist anzunehmen, dass dieses abweichende Verhalten auf dynamische und statische Ausscheidungs-vorgänge zurückzuführen sind.
- Die Basquin-Gleichung in ihrer verallgemeinerten Form beschreibt sowohl die Lebendauer des polierten als auch die des festgewalzten Zustands im gesamten untersuchten Temperaturbereich hinreichend genau, sofern nicht

statische und dynamische Ausscheidungsvorgänge bei Hochtemperaturermüdung eine signifikante Rolle spielen. Der festgewalzte Zustand ist im Vergleich zum polierten Zustand empfindlicher gegenüber einer Änderung der Spannungsamplitude und Temperatur. Dies ist darauf zurückzuführen, dass das Ermüdungsverhalten des festgewalzten Zustandes stark vom Randschichtzustand (Eigenspannungen und Verfestigungen) abhängt, welcher sich belastungsinduziert ändert.

- Die Form der Wechselverformungskurve des festgewalzten und polierten Zustandes der beiden Legierungen wird bestimmt durch Versetzungs-Versetzungs- und Versetzungs-Ausscheidungs-Wechselwirkungen während der zyklischen Belastung. Die mischkristallgehärtete Aluminiumlegierung AA5083 und die lösungsgeglühten und unteralterten Zustände der Legierung AA6110 zeigten zyklische Verfestigung aufgrund von Versetzungs-Versetzungs-Wechselwirkungen während der Ermüdung, während die maximal ausgehärteten und überalterten Zustände zyklische Entfestigung durch Versetzungsschneidprozesse sowie Schneidprozesse der Ausscheidungen zeigen [101,102].
- Das Festwalzen verbessert die Lebensdauer der Aluminiumlegierungen AA5083 und AA6110 in unterschiedlichen Aushärtungszuständen signifikant unterhalb eines Schwellenwerts der Spannungsamplitude für eine vorgegebene Temperatur. Unterhalb dieses Schwellenwerts sind die randnahen Verfestigungszustände während der Ermüdungsbelastung stabil, während sich die Eigenspannungen 1. Art nahezu komplett abbauen. Hingegen hat das Festwalzen oberhalb dieses Schwellenwerts der Spannungsamplitude für eine vorgegebene Temperatur keine positiven Auswirkungen auf die Bruchlastspielzahl von AA5083 und AA6110. Dies ist eine Folge der zyklisch mechanisch und thermisch instabilen randnahen Verfestigung.
- Eine Verminderung der plastischen Dehnungsamplitude durch zyklisch stabile randnahe Verfestigungen wurde unterhalb der Schwellenamplitude für eine vorgegebene Temperatur beobachtet. Diese Verminderung der plastischen Dehnungsamplitude ist verbunden mit erhöhten Ermüdungslebensdauern.

Eigenspannungsstabilität:

- Die randnahen Eigenspannungen in festgewalztem AA5083 und AA6110 werden während zyklischer mechanischer und/oder thermischer Belastung durch mechanische und/oder thermische Relaxation abgebaut, welche durch ein logarithmisches Kriechgesetz bzw. durch eine Zener-Wert-Avrami-Funktion beschrieben werden können.
- Festgewalzte Proben der Legierungen AA5083 und AA6110 weisen eine Schwellenspannungsamplitude auf, unterhalb welcher die randnahen Verfestigungen während der Raumtemperaturermüdung stabil sind. Oberhalb dieser Schwellenamplitude sind die randnahen Verfestigungen zyklisch instabil, wodurch das Festwalzen uneffektiv wird und Lebensdauerverlängerungen nicht möglich sind.
- Der thermische Abbau von Makro- und Mikroeigenspannungen in festgewalztem AA6110 wird prinzipiell durch Volumendiffusion kontrolliert. Ihre Aktivierungsenthalpien sind identisch mit der Aktivierungsenthalpie der Selbstdiffusion in Aluminium. Die Aktivierungsenthalpie des Mikroeigenspannungsabbaus des festgewalzten lösungsgeglühten AA6110 ist wesentlich höher als die Aktivierungsenthalpie für Selbstdiffusion von Aluminium und scheint durch thermisch aktiviertes Versetzungsgleiten kontrolliert zu sein.
- Der thermomechanische Eigenspannungsabbau lässt sich in zwei Untermechanismen einteilen: Einen mechanischen Anteil und einen thermischen Anteil. Die Auftragung des thermischen Eigenspannungsabbaus über der Zyklenzahl lässt eine Charakterisierung des mechanischen und thermischen Anteils zu.
- Die Wirksamkeit des Festwalzens der Legierungen AA5083 und AA6110 wird wesentlich durch die Stabilität der randnahen Verfestigungen während der Raum- und Hochtemperaturermüdung bestimmt. Die Instabilität der randnahen Verfestigungen während der Raum- und Hochtemperaturermüdung (angezeigt durch Halbwertsbreitenänderungen der Röntgeninterferenzlinien) deutet auf mikrostrukturelle Änderungen (z.B. Umordnung von Versetzungen) als auch möglicherweise auf Rissbildung an der

Grenzfläche Ausscheidungen-Matrix hin. Insgesamt wird das Festwalzen hierdurch unwirksam.

Alternative Oberflächenbehandlungen:

- Festwalzen in Kombination mit nachfolgender Warmauslagerung des lösungsgeglühten AA6110-Zustandes führte zu einer signifikanten Härtesteigerung in der Randschicht. Gleichzeitig bauten sich die Makrodruckeigenspannungen und Verfestigungen ab. Die optimierte Auslagerungsbehandlung besteht aus einer 12-stündigen Glühbehandlung bei 160°C.
- Die erhöhten oberflächennahen Härtewerte nach der optimierten Auslagerungsbehandlung scheinen für die Lebensdauererhöhung im LCF-Bereich sehr nützlich zu sein, während im HCF-Bereich zusätzlich Makrodruckeigenspannungen eine Rolle spielen.
- Festwalzen bei erhöhten Temperaturen bis 200°C führt zu einer Erhöhung der Oberflächenhärte im lösungsgeglühen Zustand, wogegen kleinere Makro- und Mikroeigenspannungen im Vergleich zum Raumtemperatur-zustand beobachtet werden. Festwalzen bei 250°C führt hingegen zu schädlichen Effekten auf die Schwingfestigkeit aufgrund von Überalterungs-effekten und statischer/dynamischer Erholung.
- Festwalzen bei erhöhten Temperaturen bis ca. 200°C verbessert die Ermüdungslebensdauer des lösungsgeglühten AA6110 in Hochtemperatur-ermüdungsversuchen bis ca. 200°C. Die erhöhte Oberflächenhärte nach Hochtemperaturfestwalzen bei 160°C und 200°C im Vergleich zum Raumtemperaturfestwalzen kann hierfür verantwortlich gemacht werden.
- Eine optimierte Auslagerungsbehandlung und ein anschliessendes konventionellen Festwalzen kann durch eine Kombination aus Ausscheidungshärtung und Kaltverfestigung in oberflächennahen Bereichen optimierte Mikrostrukturen und Eigenspannungszustände erzeugen und somit optimierte Schwingfestigkeiten hervorbringen.

References

[1] I.J. Polmear, Light Alloys: Metallurgy of the Light Metals, Halsted Press, London, 1996.

[2] ASM Metal Handbook: vol. 2, Properties and Selection: Nonferrous Alloys and Special-Purpose Materials, ASM International, Ohio, 1993.

[3] D. Altenpohl, Aluminium Viewed from Within, Aluminium-Verlag, Düsseldorf, 1982.

[4] K.R. Van Horn, Aluminum: vol. 1, Properties, Physical Metallurgy and Phase Diagrams, ASM International, Ohio, 1967.

[5] W. Hufnagel, Aluminium-Taschenbuch 14 Auflage, Aluminium-Verlag, Düsseldorf, 1988.

[6] W.S. Miller, L. Zhuang, J. Bottema, A.J. Wittebrood, P. De Smet, A. Haszler, A. Vieregge, Recent development in aluminium alloys for the automotive industry, Mater. Sci. Eng. A 280 (2000) 37.

[7] Z.B. Wang, N.R. Tao, S. Li, W. Wang, G. Liu, J. Lu, K. Lu, Effect of surface nanocystallization on friction and wear properties in low carbon steel, Mater. Sci. Eng. A 352 (2003) 144.

[8] V. Schulze and A. Niku-Lari (Ed.), Shot Peening and other Mechanical Surface Treatments, IITT-International, Marne la Vallee, 2005.

[9] S.K. Cheong, J.H. Nam, J.H. Lee, T.H. Kim, Effect of shot peening on the corrosion fatigue life of Al 7075-T6, in: Ref [8], p. 338.

[10] P.S. Prevéy, J.T. Cammett, The influence of surface enhancement by low plasticity burnishing on the corrosion fatigue performance of AA7075-T6, Int J Fatigue 26 (2004) 975.

[11] A. Niku-Lari (Ed.), Advances in Surface Treatments, Pergamon Press, Oxford, 1987.

[12] B. Scholtes, Assessment of residual stresses, in: V. Hauk (Ed.), Structural and Residual Stress Analysis by Nondestructive Methods, Elsevier, Amsterdam, 1997.

[13] L. Wagner, Mechanical surface treatments on titanium, aluminum and magnesium alloys, Mater. Sci. Eng. A 263 (1999) 210.

[14] I. Altenberger, B. Scholtes, Improvement of fatigue behavior of mechanically surface treated materials by annealing, Scrip. Mater. 41 (1999) 873.

[15] U. Noster, I. Altenberger, B. Scholtes, Combined mechanical and thermal surface treatment of magnesium wrought alloy AZ31, in: C.A. Brebbia (Ed.), Surface treatment V, WIT Press, Southampton, 2001, p. 3.

[16] P. Juijerm, I. Altenberger, B. Scholtes, Influence of ageing on cyclic deformation and residual stress relaxation of deep-rolled as-quenched aluminium alloy AA6110, Int J Fatigue, in print.

[17] J.K. Gregory, C. Müller, L. Wagner, Bevorzugte Randschichtaushärtung: Neue Verfahren zur Verbesserung des Dauerschwingverhaltens mechanisch belasteter Bauteile, Metall 47 (1993) 915.

[18] L. Wagner, A. Berg, T. Dörr, M. Hilpert, Kugelstrahlen und Festwalzen von Titan-, Auminium-, und Magnesiumlegierungen, in: H. Wohlfahrt and P. Krull (Eds.), Mechanische Oberflächenbehandlungen, Wiley-VCH, Weinheim, 2000.

[19] A. Berg, J. Kiese, L. Wagner, Microstructural gradients in Ti–3Al–8V–6Cr–4Zr–4Mo for excellent HCF strength and toughness, Mater. Sci. Eng. A 243 (1998) 146.

[20] I. Altenberger, I. Nikitin, Alternative mechanische Oberflächenbehandlungsverfahren zur Schwingfestigkeitssteigerung, HTM 59 (2004) 4.

[21] I. Altenberger, Deep rolling – the past, the present and the future, in: Ref [8], p. 144.

[22] I. Altenberger, I. Nikitin, B. Scholtes, Static and dynamic strain ageing of deep-rolled plain carbon steel SAE 1045 for optimized fatigue strength, in: Ref [8], p. 253.

[23] I. Nikitin, I. Altenberger, B. Scholtes, Effect of deep rolling at elevated and low temperatures on the isothermal fatigue behavior of AISI 304, in: Ref [8], p. 185.

[24] I. Altenberger, Alternative mechanical surface treatments: microstructures, residual stresses and fatigue behavior, in: L. Wagner (Ed.), Shot Peening, Wiley-VCH, Weinheim, 2003, p. 421.

[25] P. Juijerm, U. Noster, I. Altenberger, B. Scholtes, Fatigue of deep-rolled AlMg4.5Mn (AA5083) in the temperature range 20-300°C, Mater. Sci. Eng. A 379 (2004) 286.

[26] P. Juijerm, I. Altenberger, U. Noster, B. Scholtes, Residual stress relaxation and cyclic deformation behavior of deep-rolled AlMg4.5Mn (AA5083) at elevated temperatures, Mater. Sci. Forum 490-491 (2005) 436.

[27] P. Juijerm, I. Altenberger, B. Scholtes, Effect of deep rolling on the fatigue behavior of under-, peak- and over-aged AA6110 at room temperature, in: Ref [8], p. 302.

[28] P. Juijerm, I. Altenberger, B. Scholtes, Fatigue and residual stress relaxation of deep-rolled differently aged aluminium alloy AA6110, Mater. Sci. Eng. A 426 (2006) 4.

[29] P. Juijerm, I. Altenberger, Fatigue behavior of deep-rolled Al-Mg-Si-Cu alloy at elevated temperature, Script. Mater. 55 (2006) 943.

[30] G.E. Dieter, Mechanical Metallurgy, McGraw-Hill, New York, 1988.

[31] H.-J. Christ, Ermüdungsverhalten metallischer Werkstoffe, Werkstoff-Informationsgesellschaft mbH, Frankfurt, 1998.

[32] S. Suresh, Fatigue of Materials, Cambridge university press, Cambridge, 1998.

[33] M. Klesnil, P. Lukáš, Fatigue of metallic materials, Elsevier, Amsterdam, 1980.

[34] ASM Metal Handbook: vol. 19, Fatigue and Fracture, ASM International, Ohio, 1996.

[35] D. Löhe, K.-H. Lang, O. Vöhringer, Residual Stresses and Fatigue Behavior, in: G. Totten, M. Howes and T. Inoue (Ed.), ASM International Handbook of Residual stress and Deformation of Steel, 2002.

[36] J. Polák, Cyclic plasticity and low cycle fatigue of metals, Elsevier, Amsterdam, 1991.

[37] P. Mayr, in: W. Dahl (Ed.), Verhalten von Stahl bei schwingender Beanspruchung, Verlag Stahleisen, Düsseldorf, 1978, p. 82.

[38] U. Noster, Zum Verformungsverhalten der Magnesiumbasislegierungen AZ31 und AZ91 bei zyklishen und quasi-statischen Beanspruchungen im Temperaturbereich 20-300°C, Dissrtation, University of Kassel, 2003.

[39] U. Noster, B. Scholtes, Stress-controlled fatigue of magnesium wrought alloy AZ31 in the temperature range 20-300°C, Z. Metallkd. 92 (2001) 260.

[40] V. Schulze, Modern Mechanical Surface Treatment, Wiley-VCH, Weinheim, 2005.

[41] H. Wohlfahrt und P. Krull (Eds.), Mechanische Oberflächenbehandlung, WILEY-VCH, Weinheim, 2000.

[42] V. Schulze, Characteristics of surface layers produced by shot peening, in: L. Wagner (Ed.), Shot Peening, Wiley-VCH, Weinheim, 2003, p. 145.

[43] I. Altenberger, B. Scholtes, Improvement of fatigue lifetime of mechanically surface treated materials in the low cycle fatigue regime, in: C.A. Brebbia and J.M. Kenny (Eds.), Surface treatment IV, WIT Press, Southampton, 1999, p. 281.

[44] A. Eftekhari, J.E. Talia, P.K. Mazumda, Influence of surface condition on the fatigue of an aluminium-lithium alloy (2090-T3), Mater. Sci. Eng. A 199 (1995) L3.

[45] C.S. Montross, T. Wei, L. Ye, G. Clark, Y.W. Mai, Laser shock processing and its effects on microstructure and properties of metal alloys: a review, Int J Fatigue 24 (2002) 1021.

[46] O. Higounenc, Correlation of shot peening parameters to surface characteristic, in: Ref [8], p. 28.

[47] K.H. Kloos, B. Fuchsbauer, J. Adelmann, Fatigue properties of specimens similar to components deep-rolled under optimized condition, Int J Fatigue. 9 (1987) 35.

[48] I. Nikitin, I. Altenberger, University of Kassel, unpublished, 2005.

[49] S. S. Manson, Thermal stress and low cycle fatigue, McGraw-Hill, New York, 1966.

[50] L.F. Coffin, A study of the effects of cyclic thermal stresses on a ductile metal, Trans ASME 76, 1954, p. 931.

[51] D. Löhe and O. Vöhringer, Stability of Residual Stresses, in: G. Totten, M. Howes and T. Inoue (Ed.), ASM International Handbook of Residual stress and Deformation of Steel, 2002.

[52] O. Vöhringer, Auswirkungen der mechanischen Oberflächenbehandlungen bei thermischer und bei mechanischer Beanspruchung, in Ref. [41], p. 29.

[53] B.L. Boyce, X. Chen, J.O. Peters, J.W. Hutchinson, R.O. Ritchie, Mechanical relaxation of localized residual stresses associated with foreign object damage, Mater. Sci. Eng. A 349 (2003) 48.

[54] B. Scholtes, Eigenspannungen in mechanish randschichtverformten Werkstoffzuständen, Ursachen-Ermittlung-Bewertung, DGM-Informations-gesellschaft, Oberursel, 1990.

[55] H. Holzapel, V. Schulze, O. Vöhringer, E. Macherauch, Residual stress relaxation in an AISI 4140 steel due to quasistatic and cyclic loading at higher temperatures, Mater. Sci. Eng. A 248 (1998) 9.

[56] O. Vöhringer, Relaxation of Residual Stresses, in: E. Macherauch, V. Hauk (Eds.), Residual Stresses, DGM-Informationsgesellschaft, Oberursel, 1986

[57] I. Altenberger, U. Noster, B. Scholtes, R.O. Ritchie, High temperature fatigue of mechanically surface treated materials, in: L. Wagner (Ed.), Shot Peening, Wiley-VCH, Weinheim, 2003, p. 483.

[58] I. Nikitin, I. Altenberger, B. Scholtes, Residual stress state and cyclic deformation behavior of deep-rolled and laser-shock peened AISI 304 at elevated temperatures, Mater. Sci. Forum 490-191 (2005) 376.

[59] A. Wick, V. Schulze, O. Vöhringer, Effects of warm peening on fatigue life and relaxation behavior of residual stresses in AISI 4140 steel, Mater. Sci. Eng. A 293 (2000) 191.

[60] R. Menig, V. Schulze, O. Vöhringer, Optimized warm peening of the quenched and tempered steel AISI 4140, Mater. Sci. Eng. A 335 (2002) 198.

[61] H. Mughrabi, On the dislocation mechanisms of dynamic strain ageing in fatigued plain carbon steels, Z. Metallkd. 94 (2003) 5.

[62] I. Altenberger, B. Scholtes, Recent developments in mechanical surface optimization, Mater. Sci. Forum 347-349 (2000) 382.

[63] A. Grüning, Einfluss unterschiedlicher Festwalztemperaturen während des Festwalzens des Werkstoffs X5 CrNi 18-10, Student Project, University of Kassel, 2005

[64] R. Menig, V. Schulze, O. Vöhringer, Effects of static strain ageing on residual stress stability and alternating bending strength of shot peened AISI 4140, Z. Metallkd. 93 (2002) 7.

[65] J.K. Gregory, L. Wagner, Selective surface ageing to improve fatigue behaviour in a high-strength beta titanium alloy, in: J.-P. Bailon and J.I.Dickson (Eds), Fatigue ´93, Montreal, 1993, p. 177.

[66] J.K. Gregory, L. Wagner, Property improvement in light metals using shot peening, in: L. Wagner (Ed.), Shot Peening, Wiley-VCH, Weinheim, 2003, p. 349.

[67] R.E. Reed-Hill, R. Abbaschian, Physical metallurgy principles, PWS Publishing, Boston, 1994.

[68] D.A. Porter, K.E. Easterling, Phase transformations in metals and alloys, Nelson Thornes, Cheltenham, 2001

[69] E.A. Starke, Jr, Aluminium alloys-Contemporary Research and Applications, Academic Press, 1989, p. 35

[70] T. Kobayashi, Strength and toughness of materials, Springer-Verlag, Tokyo, 2004, p. 111

[71] ASM Metal Handbook: vol. 10, Materials Characterization, ASM International, Ohio, 1986.

[72] B.D. Cullity, S.R. Stock, Elements of X-ray diffraction, Prentice Hall, New Jersey, 2001.

[73] R.F. Speyer, Thermal analysis of materials, Marcel Dekker, New York, 1994.

[74] M. Takeda, S. Suhmen, A. Yoshida, T. Kurosawa, Y. Nagura, T. Kurumizawa, DSC (Differential Scanning Calorimetry) study on precipitation behaviour in aluminium alloys, International conference on processing and manufacturing of advanced materials, Las Vegus, 2000.

[75] L. Zhen, S.B. Kang, DSC analyses of the precipitation behaviour of two Al-Mg-Si alloys naturally aged for different times, Mater. Letters 37 (1998) 349.

[76] P. Archambault, D. Godard, High temperature precipitation kinetics and TTT curve of a 7xxx alloy by in-situ electrical resistivity measurements and differential calorimetry, Scrip. Mater. 42 (2000) 675.

[77] R. Ferragut, A. Somoza, I. Torriani, Pre-precipitation study in the 7012 Al-Zn-Mg-Cu alloy by electrical resistivity, Mater. Sci. Eng. A 334 (2002) 1.

[78] S. Esmaeili, D.J. Lloyd, W.J. Poole, Effect of natural ageing on the resistivity evolution during artificial ageing of the aluminium alloy AA6111, Mater. Letters 59 (2005) 575.

[79] G.A. Edwards, K. Stiller, G.L. Dunlop, M.J. Couper, The precipitation sequence in Al-Mg-Si alloys, Acta. Mater. 46 (1998) 3893.

[80] W.F. Miao, D.E. Laughlin, Precipitation hardening in aluminium alloy 6022, Scrip. Mater. 40 (1999) 873.

[81] Y. Song, T.N. Baker, A calorimetric and metallographic study of precipitation process in AA6061 and its composites, Mater. Sci. Eng. A 201 (1995) 251.

[82] J.Y. Yao, D.A. Graham, B. Rinderer, M.J. Couper, A TEM study of precipitation in Al-Mg-Si alloys, Microns 32 (2001) 865.

[83] M. Takeda, F. Ohkuro, T. Shirai, K. Fukui, Stability of metastable phases and microstructures in the ageing process of Al-Mg-Si ternary alloys, J Mater. Sci 33 (1998) 2385.

[84] Q. Li, R.N. Shenoy, DSC and TEM characterizations of thermal stability of an Al-Cu-Mg-Ag alloy, J Mater. Sci 32 (1997) 3401.

[85] M. Takeda, T. Kurumizawa, S. Sumen, K. Fukui, T. Endo, Atomic composition of the metastable β´´ phase precipitate in an Al-Mg-Si alloy, Z. Metallkd, 93 (2006) 523.

[86] J. Dutkiewicz, L. Litynska, The effect of plastic deformation on structure and properties of chosen 6000 series aluminium alloys, Mater. Sci. Eng. A 324 (2002) 239.

[87] C.D. Marioara, S.J. Andersen, J. Jansen, H.W. Zandbergen, The influence of temperature and storge time at RT on nucleation of the β´´ phase in a 6082 Al-Mg-Si alloy, Acta. Mater. 51 (2003) 789.

[88] A. Deschamps, F. Livet, Y. Bréchet, Influence of predeformation on ageing in an Al-Zn-Mg alloy -I. Microstructure evolution and mechanical properties, Acta. Mater. 47 (1999) 281.

[89] J.D. Embury, A. Deschamps, Y. Brechet, The interaction of plasticity and diffusion controlled precipitation reactions, Scrip. Mater. 49 (2003) 927.

[90] R.S. Yassar, D.P. Field, H. Weiland, The effect of cold deformation on the kinetics of the β´´ precipitates in an Al-Mg-Si alloy, Metall. Mater. Trans. A 36 (2005) 2059.

[91] C. Prinz, O. Keßler, F. Hoffmann, P. Mayr, Verkürzung der Auslagerungsdauer von Al- und Cu-Legierungen durch die Kombination Kaltverformen und nicht-isothermes Warmauslagern, HTM 58 (2003) 1.

[92] http://www.alcoa.com/gcfp/en/product_category.asp?cat_id=969

[93] D. Henneberg, Einfluss von Vorerformung und Voralterung auf das Aushärtungsverhalten der ausscheidungsgehärteten Aluminiumlegierung AA6110, Bachelor thesis, University of Kassel, 2005

[94] P. Ratchev, B. Verlinden, P. De Smet, P. Van Houtte, Effect of cooling rate and predeformation on the precipitation hardening of an Al-4.2wt%Mg-0.6wt%Cu alloy, Scrip. Mater. 38 (1998) 1195.

[95] G.K. Quainoo, S. Yannacopoulos, The effect of cold work on the precipitation kinetics of AA6111 aluminium, J Mater. Sci. 39 (2004) 6495.

[96] Y. Birol, Pre-straining to improve the bake hardening response of a twin-roll cast Al-Mg-Si alloy, Scrip. Mater. 52 (2005) 169

[97] M. Jahn, TAHA processing of a 6201 aluminium alloy, Int. J. Prod. Res. 26 (1988) 1651.

[98] L. Zhen, S.B. Kang, The effect of pre-ageing on microstructure and tensile properties of Al-Mg-Si alloys, Scrip. Mater. 36 (1997) 1089.

[99] Y. Birol, Gebze, Kocaeli, Improvement in bake hardening response of a twin-cast Al-Mg-Si alloy, Auminium 80 (2004) 80.

[100] Y. Birol, Effect of natural ageing on the performance of pre-ageing to improve bake-hardening response of a twin-roll cast Al-Mg-Si alloy, Z. Metallkd. 96 (2005) 380.

[101] T. S. Srivatsan, E. J. Coyne, Jr, Cyclic stress response and deformation behavior of precipitation-hardened aluminium-lithium alloys, Int J Fatigue 8 (1986) 201.

[102] T. S. Srivatsan, The low-cycle fatigue and cyclic fracture behaviour of 7150 aluminium alloy, Int J Fatigue 13 (1991) 313.

[103] T. Hirsch, O. Vöhringer, E. Macherauch, Bending fatigue behavior of differently heat-treated and shot peened AlCu5Mg2, in: G. P. Balcar and H. Fuchs (Eds), International conferences on shot peening 2, Chicago, 1984, p. 90.

[104] M. Benedetti, T. Bortolamedi, V. Fontanari, F. Frendo, Bending fatigue behavior of differently shot peened Al 6082 T5 alloy, Int J Fatigue 26 (2004) 889.

[105] C.A. Rodopoulos, S.A. Curtis, E.R. de los Rios, J. SolisRomero, Optimization of the fatigue resistance of 2024-T351 aluminium alloys by

controlled shot peening-methodology, results and analysis, Int J Fatigue 26 (2004) 849.

[106] P. Peyre, R. Fabbro, P. Merrien, H.P. Lieurade, Laser shock processing of aluminium alloys. Application to high cycle fatigue behavior, Mater. Sci. Eng. A 210 (1996) 102.

[107] M.R. Hill, T.E. Pistochini, A.T. DeWald, Optimization of residual stress and fatigue life in laser peened components, in: Ref. [8], p. 156.

[108] L. Wagner, C. Müller, J.K. Gregory, Influence of surface rolling on notched fatigue strength of Al 2024 in two age-hardening conditions, in: J.-P. Bailon and J.I.Dickson (Eds), Fatigue ´93, Montreal, 1993, p. 471.

[109] X.L. Yue, S. Nishida, N. Hattori, Fatigue properties of notched aluminium specimens after hard rolling, Mater. Sci. Res. Int. 8 (2002) 53.

[110] F. Ludwig, M Lorenz, Untersuchungen zur Eigenspannungsstabilität kugelgestrahler Aluminiumbasislegierungen, Student project, University of Kassel, 1995.

[111] M. Grüber, Einfluss der Ausscheidungshärtung auf die Eigenspannungsstabilität und das Ermüdungsverhalten der festgewalzten Aluminiumlegierung AA6110, Master thesis, Universiy of Kassel, 2005.

[112] C. Barbosa, J. M. A. Rebello, O. Acselrad, J. Dille and J.-L. Delplancke, Identification of precipitates in 6013 aluminium alloy (Al-Mg-Si-Cu), Z. Metallkd. 93 (2002) 208.

[113] E. Zschech, Metallkundliche Prozesse bei der Wärmebehandlung aushärtbarer Aluminiumlegierungen, HTM 51 (1996) 3.

[114] V. Hauk, E. Macherauch, Eigenspannungen und Lastspannungen: Moderne Ermittlung-Ergebnisse-Bewertung, HTM, Carl Hanser Verlag, München.

[115] T.H. Courtney, Mechanical behavior of materials, McGraw-Hill, New York, 1990, p. 199.

[116] C.H. Cáceres, J.H. Sokolowski, P. Gallo, Effect of ageing and Mg content on the quality index of two model Al-Cu-Si-Mg alloys, Mater. Sci. Eng. A 271 (1999) 53.

[117] J. Kohout, Temperature dependence of stress-lifetime fatigue curves, Fatigue Fract Engng Mater Struct 23 (2000) 969.

[118] J. Čadek, Creep in metallic materials, Elsevier, Amsterdam, 1988.

[119] I. Altenberger, Mikrostrukturelle Untersuchungen mechanish randschicht-verfestigter Bereiche schwingend beanspruchter metallischer Werkstoffe, Dissertation, Univerity of Kassel, 1999.

[120] F.J. Hamphreys, M. Haltherly, Recrystallization and Related Annealing Phenomena, Pergamon, Oxford, 1995.

Acknowledgements

This dissertation would not be possible at all without the support of many people. First of all, I would like to sincerely thank my „Doktorvater" Prof.-Dr.-Ing. habil B. Scholtes, for giving me an incomparable opportunity to pursue my doctoral work in his institute. He spent tremendous time and effort on me and was always ready to help and discuss my difficulties, particularly during set-up period in Germany. It was a great pleasure working with him.

Next, I would like to give my deep debt to my primary guide, Dr.-Ing. I. Altenberger (leader of the Emmy Noether Group) for his valuable advice and for giving me valuable opportunity to work with him in Emmy Noether Group, especially a new project on a Laser Shock Peening. He spent also magnificent time and effort on correcting my English of all my publications as well as this manuscript.

My gratitude is also due to Prof. Dr. rer. nat. A. Brückner-Foit and Asst. Prof. Dr. Ch. Limmaneevichitr (from King Mongkut's University of Technology Thonburi, Thailand), committee of my disputation, for valuable discussion.

An extra paragraph has to be reserved for Dr.- Ing. U. Noster and Dipl.- Ing. T. Ratanasumawong. They helped me to clear many tasks during my first year in Germany. Without them, living in Germany would have been more difficult.

Thanks are also due to my undergraduate and graduate students, Dipl.-Ing. M. Grüber, Dipl.-Ing. S. Primee and Dipl.-Ing. D. Henneberg, as well as our institute secretariat and technicians, Ms. D. Thumser, Mr. C. Franz, Dipl.-Ing. G. Fehrl, Dipl.-Ing. R. Diederich and Mr. M. Rehbaum for their warm and friendly support.

I must take the opportunity to thank all my friends and colleagues from outside and inside of IfW, for their help and kindness contributing to a fascinating atmosphere during working and living in Germany. Special thanks go to Dipl.-Ing. I. Nikitin, my office mate, for his useful discussion and warm help in every theme.

The financial support obtained from the Faculty of Engineering, Kasetsart University, Thailand and the German Science Foundation (DFG) under grant no. AL-558/1-4 is gratefully acknowledged.

Last but not least, my parents deserve special thanks for their love, support and participation in every stage of my education. During the fantastic and very happy time in Germany, the biggest thanks are extended to my wonderful family, Jing and Zen for their endless love, support, encouragement, patience and for forgiving me spending so much time in the Laboratory as well as in the front of a computer screen during writing many publications and this dissertation.

Kassel, in May 2006

Dipl.-Ing. Patiphan Juijerm

from Suankularb (OSK109), Thailand.

Address in Thailand:

Department of Materials Engineering
Faculty of Engineering, Kasetsart University
50 Phahonyothin Rd, Jatujak
Bangkok 10900, Thailand

Email: fengppj@ku.ac.th